A Study of a Quarter-Car Active Suspension System Adaptable to Road Conditions

A THESIS

SUBMITTED TO THE COLLEGE OF ENGINEERING

UNIVERSITY OF BASRAH IN PARTIAL FULFILMENT

OF

THE REQUIREMENTS FOR THE DEGREE OF

DOCTOR OF PHILOSOPHY

IN

MECHANICAL ENGINEERING

By

Mahmood Shacker Mahmood

(M.Sc. Mech. Engineering)

January 2023

Acknowledgements

First and foremost, I give praise and thanks to ALLAH, for his assistance and generosity.

Second, I would like to express my gratitude to my supervisors Prof. Ameen A. Nassar and Assist.Prof.Dr. Haider M. Mohammad. For their guidance, assistance and encouragement offered continually during the stages of this work.

I would like also to thank Prof. Dr. Ramzi S. Ali, dean of the College of Engineering, Dr. Hassanein Ibraheem Khalaf, head of the Department of Mechanical Engineering, and all staff of Collage of Engineering especially the staff of mechanical engineering department for achievement this work.

I would like to express my sincere gratitude to Assist. Prof. Dr. Abdul-Baki Khalaf Ali, for his generous help during the various stages of this work.

I am indebted to Prof. Dr. Ahmed Kadhim Alshara, Assist.Prof. Ameer Latef, Prof. Dr. Ammar A. Aldair, Dr. Yahya Muhammad, Dr. Atheel K. Abdulzahra, Mr**.** Hayder Kareem and all friends for their help to finish this work.

Last but not the least, I thank my family, most of all my parents, who have made a number of sacrifices to support me throughout the past years. This accomplishment would not have been possible without them.

CERTIFICATION

We certify that this thesis titled " **A Study of a Quarter-Car Active Suspension System Adaptable to Road Conditions**" which is being submitted by **Mahmood Shacker Mahmood** was prepared under my supervision at the University of Basrah as partial fulfillment of the requirements for the degree of Doctor of Philosophy in Mechanical Engineering.

Signature:
Prof. Dr. Ameen A. Nassar
(Supervisor)
Date: / /

Signature:
Assist.Prof.Dr. Haider M. Mohammad
(Supervisor)
Date: / /

In view of the available recommendation, I forward this thesis for debate by the examining committee.

Signature:
Assist. Prof. Dr. Hassanein I. Khalaf
(Head of Mechanical Engineering Department)
Date: / /

COMMITTEE REPORT

We certify that we have read this thesis titled " **A Study of a Quarter-Car Active Suspension System Adaptable to Road Conditions**" which is being submitted by **Mahmood Shacker Mahmood** and as examining committee, examined the student in its contents. In our opinion, the thesis is adequate for award of Doctor of Philosophy degree in Science of Mechanical Engineering.

Signature:
Name: Assist. Prof.Dr. Haider M. Mohammad
(Supervisor, Member)
Date: / / 2023

Signature:
Name: Prof. Dr. Ameen A. Nassar.
(Supervisor, Member)
Date: / / 2023

Signature:
Name:Assist. Prof. Dr.Hassanein I. Khlaf
(Member)
Date: / / 2023

Signature:
Name: Assist. Prof. Dr. Haider Khazal
(Member)
Date: / / 2023

Signature:
Name: Assist. Prof. Dr. Jaafar K. Ali
(Member)
Date: / / 2023

Signature
Name: Prof. Dr. Jawad K. Oleiwi
(Member)
Date: / / 2023

Signature:
Name: Prof. Dr. Abdul Kareem F. Hassan
(Chairman)
Date: / / 2023

Approval of the College of Engineering

Signature:
Prof. Dr. Ramzy S. Ali
Dean of Engineering College
Date: / / 2023

ABSTRACT

The safety and comfort of the occupants and the stability of the vehicle are affected by the vehicle's vibration, the main goal of designing the vehicle's suspension control device is to reduce the discomfort that occupants feel due to the roughness of the road. Numerous studies used quarter vehicles with various types of stimulation to study and assess the vibration of automobiles. Through modeling, simulation, and control scheme, this thesis examines the characteristics and effectiveness of a novel type of active suspension for vehicle (integrating an air suspension with a hydraulic actuator to create an additional force that withstands the incoming vibration from the road).

In this study, a mathematical model of the nonlinear pneumatic suspension system for a quarter vehicle using the hydraulic actuator was constructed and the pneumatic suspension system parameters, such as vertical acceleration, road holding, and vertical displacement are improved continuously based on the controllers which have been used for nonlinear pneumatic suspension systems.

Six distinct control types are created, and to choose the best controller among them, comparisons between them versus various disturbance types are looked at. The genetic algorithm is utilized to tune the controller's parameters to the nonlinear active pneumatic system's 3-DOF. The proposed controllers are simulated with using the MATLAB/SIMULINK program, and the responses of the controlled models to various disturbances are shown in the time domain.

For the model of the air suspension system, the controllers are employed to control the force of the hydraulic actuator. The outcomes demonstrated that the Active Force Fuzzy Logic Controller outperforms the other controller types in terms of efficiency and robustness in the reduction of the vertical displacement of sprung mass, vertical acceleration of sprung mass, road holding, and dynamic load coefficient respectively by 88.5%, 95%, 33.2%, and 33.6% in

comparison with other controllers for rough road class B. The non-linear quarter vehicle suspension modeling and simulation of the two air spring models (the conventional and Gensys air spring) were also compared in terms of sprung mass acceleration (RMS), dynamic load factor and vertical displacement. The results obtained by comparison it indicate that Gensys type is more efficient than the traditional type.

Contents

Nomenclature

Symbol	Description	Unit
A_e	The effective area of the air bag	m^2
A_p	The cross-sectional area of piston	m^2
A_s	The cross-section area of the surge pipe	m^2
C_a	Nonlinear air damping	N.s/m
C_s	The damping coefficient of damper	N.s/m
C_t	The damping coefficient of tire	N.s/m
d_p	The diameter of the surge pipe	m
f	The coefficient of friction	-
F_h	Hydraulic force	N
F_z	The vertical force affected on air spring	N
K_c	Servo valve gain	m/v
K_e	The main spring of air spring	N/m
K_v	The auxiliary spring of air spring	N/m
K_t	The stiffness of tire	N/m
m_a	Air mass in surge pipe	Kg
m_s	Sprung mass	Kg
$\dot{m}_b$	Flow rate of gas air bag	Kg
$\dot{m}_r$	Flow rate of gas reservoir	Kg
m_s	Sprung mass	Kg
m_{us}	Unsprung mass	Kg
$\dot{m}_u$	Mass flow rate of upstream	Kg
n	The polytropic index	-
p_a	The atmospheric pressure	Pa
p_b	The pressure of the air bag	Pa
p_o	The initial pressure	Pa

Symbol	Description	Unit
p_r	The pressure of the reservoir	Pa
P_s	Pressure supply	Pa
T_{bo}	The initial temperature of air bag	C^o
T_{ro}	The initial temperature of reservoir	C^o
V_b	The volume of air bag after deflection	m^3
V_{bo}	The initial volume of the air bag spring	m^3
V_r	The volume of reservoir	m^3
V_{ro}	The initial volume of reservoir	m^3
W_f	The work done in surge pipe	N.m
w_s	The displacement of air in surge pipe	m
Z_s	Vertical displacement for sprung mass	
Z_{us}	Vertical displacement for sprung mass	
$\dot{z}_p$	surge pipe's average speed	m/s

Abbreviations

Symbol	Description
ARBFNN	Adaptive Radial Basis Function Neural Network
DLC	Dynamic Load Coefficient
FLAFC	Fuzzy Logic Active Force Control
FLC	Fuzzy Logic Control
FOSMC	First-Order Sliding Mode Control
ITAE	Integral of Time Absolute Error
LQR	Integral Sliding Mode Control
NL	Negative Large
NM	Negative Medium
NS	Negative Small
PACSA	Parallel Adaptive Clonal Selection Algorithm
PID	Proportional Integral Derivative
RH	Road Holding
SMC	Sliding Mode Control
STA	Super Twisting Algorithm
VVSM	Vertical Velocity Sprung Mass
VASM	Vertical acceleration sprung mass
VFD	Vertical Force Dynamic

Greek Symbol

Symbol	Description	Unit
λ	real order of FOPID	-
δ	real order of FOPID	-
β	The viscous damping parameter.	-
$\sigma, \beta_e, \gamma_s$	Actuator parameters	-
β	The viscous damping parameter	-
τ	Time constant	second
ω	Displacement of air mass	m
ρ	The fluid density	Kg/ m^3
μ	Viscosity	N.S/ m^2
γ	Specific heat for an ideal gas	-

Chapter One

Introduction

CHAPTER ONE

Introduction

1.1 Vehicle Suspension

A few years ago, there has been significant interest in suspension systems, especially air suspension systems in modern vehicles. The necessity of having this vital part in the vehicle to keep vibrations out, separate it from the uneven roads, and provide comfort to passengers. In order to achieve adequate vehicle stability when driving, the suspension system must also maintain continual contact between the tires and the road surface. This capability is crucial when turning, accelerating, or braking for a brief period of time. This, in turn, would lead directly to safety, briefly the design of automotive suspension system involves compromise between the ride quality and driving stability. In general, sports cars have rigid, hard suspensions with low quality of driving while the better suspension is seen in luxury vehicles, but have a low potential for road handling. Fairly minimizing output disturbance is a priority in a good suspension design (e.g. vehicle height) and it needs to be "soft" against the road with adequate cushioning disruptions and "strong" against disturbances of load [1]. A suspension that is very dampened can produce good handling of the car, but will also move most of the road input to the body of the vehicle when it is on a low-speed ride on a rough road or in a straight line at high speed, this would be perceived as a rough journey and the passengers may find that the rough ride can be objectionable, or it can physically hurt a car, while a lightly damped suspension results in a more relaxed journey, but will greatly decrease vehicle stability at turns and maneuvers. A successful passive suspension design will work toward a certain scope to regard to improve riding comfort and road-holding capacity, however, this tradeoff cannot be avoided. There has been substantial interest in active vehicle suspensions used in recent years, this can get around certain passive suspension systems' restrictions. Many automobile

industries are considering the usage of active suspensions as a result of requests for better driving comfort and road management. Electronically, these active suspension systems that are regulated can ability enhance the ease of the trip and road handling of the simultaneously with a vehicle. The pneumatic vibration isolation technology for air-suspensions is increasingly improving. The use of pneumatic isolators has become more common as environmental vibroisolation standards on precision equipment and air suspensions become more stringent, and their performance needs to be further improved.

1.2 Mechanism of Vehicle Suspension

The unit of suspension is composed of two simple spring and damper suspension components, set in parallel. Spring absorb the shock-excitation that are due to the roughness of the road surface that is, the spring is compressed and stores shock energy when the suspension hits a bump. It then eventually expands and transfer the absorbed energy to the body of the vehicle.

However, on the other side, dissipating the energy of suspension vibrations is the feature of a damper. The damper explicitly dampens a portion of the shock energy when the suspension hits a bump. In addition, in the spring, it dissipates accumulated energy. It regulates the operation of the springs in this way. Similarly, the motion of the vehicle's body triggered by driving movements is controlled by springs and dampers.

1.3 Pneumatic suspension

Pneumatic suspensions can be passive, semi-active, or active, with air springs serving as the primary elastic component. The benefits of employing an air suspension come from the air springs, where ride height, comfort, and handling can all be adjusted and can be summed up:

1. The pneumatic suspension system is neither expensive nor messy, and it does not necessitate constant fluid pumping [2].

2. Air springs effectively shield the crew and passengers from wheel-rolling noise and vibration. This contributes to their comfort [3].
3. Air springs are known for their dynamic nature, which provides excellent road handling and comfort. Variable stiffness is provided by the air spring.
4. The resonance frequency of air suspension systems is lower. Because natural frequency is consistent, a better ride is provided under all loads.
5. Spring rate can be adjusted across a wide load range.
6. Because of the inherent limitations of passive suspension systems, have enabled modeling of the air suspension system.
7. Air suspension systems are used in both active and passive suspensions to meet the drawbacks of power consumption and design [4].
8. Air suspension reduces vehicle vibration, resulting in less wear and tear on truck or trailer components.

1.4 Ride Comfort

The primary goal of car suspension systems is to provide a comfortable ride. The term "ride comfort" refers to how comfortable passengers are when traveling in a vehicle. As well as comfort for passengers, which is related to the level of vibrations they feel while the vehicle is traveling on a bumpy road. On-board sources and road sources are the two broad categories of vibration sources that have an impact on ride comfort. The roughness of the road and the maneuvering fall under the second group of vehicle vibration sources, known as the road source. Because it influences how high the vehicle's center of gravity will be, the ride height is crucial. Since it affects how high the vehicle's center of gravity is, the ride height is critical (CG) so the CG must keep the as low as possible but at the same time lowering the ride height reduces the suspension movement and therefore a stiffer spring must be used which makes the ride less comfortable. Heave acceleration is utilized as a gauge of comfort and vibration levels, and the vertical motion of sprung mass is employed to assess the amount

of body control attained [5]. the tire forces and road surface are connected to road handling and relative motion, which is the movement of the sprung and unsprung masses in relation to one another, whereas the acceleration felt corresponds to ride comfort [6]. Stiff suspension is therefore necessary for high handling performance and derive stability, however, comfortable rides are not permitted [7]. In this study, weighted r-m-s measurements were used, which is described by[8]. and depends on ISO 2631-1 in 1997 to analyze vibration utilizing the fundamental way:

$$a_w = \left[\frac{1}{T}\int_0^T {a_w}^2\,(t)dt\right]^{1/2} \qquad (1.1)$$

The vehicle's vertical acceleration value would be compared to the readings in Table (1.1) to get an idea of what kinds of reactions to expect from different levels of overall vibration in vehicle [9].

Table (1.1) The comfort levels related to vertical acceleration[9].

a_w(m/s^2)	Comfort level
< 0.315	Not uncomfortable
0.135-0.63	A little uncomfortable
0.5-1	Fairly uncomfortable
0.8-1.6	Uncomfortable
1.25-2.5	Very uncomfortable
> 2	Extremely uncomfortable

1.5 Road Holding

It is a characteristic that establishes constant contact between the road's surface and the tires, ensuring safe and stable driving. Road holding is also referred to by various names in certain contexts, including handling, ride stability, and driving stability, all of which suggest the same concept. A vehicle's

comfort and road holding are both impacted by its capacity to smooth out road irregularities.

When making motions like turning, braking, or accelerating, a vehicle's road holding ability is crucial. The vehicle's capacity to regulate itself in the maneuvers is reduced by poor road holding, which may jeopardize the passengers' safety. The road-holding ability of the car is affected by an important part of the wheel which is the car's suspension. Wheel and vehicle body vibrations have an impact on the tire contact force, which in turn affects road holding. Road roughness mostly affects wheel vertical motion, and vehicle direction changes primarily cause body motion [10]. The shift of the load from one side to the other occurs due to the centrifugal force on the tires, this significantly reduces the tire contact forces and, as a result, results in poor road holding performance. Efficient suspension can limit the vertical wheels' vertical vibration, which is brought on by road roughness and directly affects tire contact strength and, consequently, vehicle handling.

handling objective consists [11]

$$min(z_{\mathrm{us}} - z_{\mathrm{r}}) \tag{1.2}$$

where the tire deflection $(z_{\mathrm{us}} - z_{\mathrm{r}})$

z_r: road reference.

z_{us} :displacement of unsprung mass.

1.6 Dynamic Load Coefficient

The tire load's vertical dynamic root-mean-square divided by the static load is known as the dynamic load coefficient (DLC) [12] which is used as an objective goal to perform the effectiveness of the suspension system, that is, the lower this ratio, the better the performance of the suspension of system towards stability and comfort of vehicle.

$$DCL = \frac{F_{t,rms}}{F_s} \tag{1.3}$$

Where $F_{t,rms}$ represent dynamic vertical wheel force and F_s represent the static tire force. DLC may be zero when traveling down a particular smooth road [13].

1.7 Models of Air Spring

The preload and the frequency and amplitude of dynamic displacements impact the air suspension systems' vertical behavior, whereas their horizontal behavior is influenced by the preload [14]. The models of vertical air springs are possible categorized into reward thermodynamic and mechanical models [15].

- The mechanical models that are equivalent, are dependent on the utilization of lumped parameters for dampers ,springs, and masses.
- All parameters in the air suspension system in thermodynamic models have a clear physical significance since they depict the real mechanical and thermodynamic processes taking place, such as many different types of air spring models; some of them are detailed in this section.

1.7.1 The Simple Model

In this model, two springs are parallels coupled to dampers as shown in Figure (1-1).

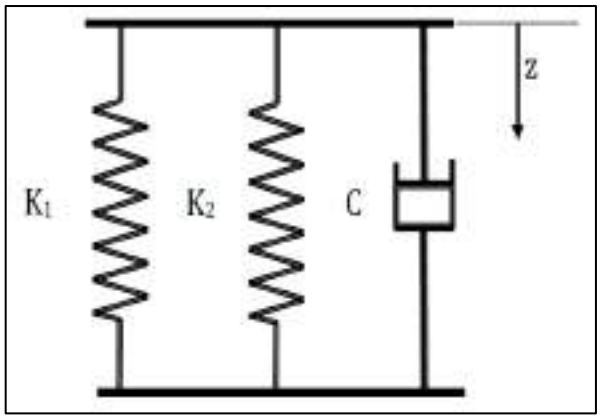

Figure (1-1) Simple air spring dynamics model [14].

The following are the stiffness constants:

$$K_1 = (p_o - p_a)\frac{dA_e}{dz}$$

$$K_2 = n(A_e)^2\frac{p_o}{V_i}$$

Where $K_1$is the stiffness of the area component's change(N.m^{-1}), K_2 is the gas compression's stiffness(N.m^{-1}), p_o is the system's initial pressure, Pa is the atmospheric pressure, A_e is airbag's effective area(m^2), V_i is the air bag's initial volume(m^3), Z is vehicle body displacement, n is index of thermal process, and "damping coefficient" is C indicate to the material in the spring and the air are both dampened.

1.7.2 Nishimura Model

A one-volume assumption does not apply to the Nishimura air spring and the orifice damping and flow resistance through the pipe may be modeled using this model.

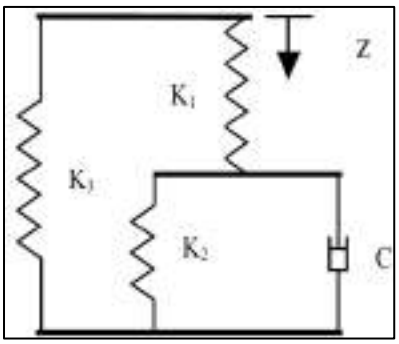

Figure (1-2) NISHIMURA model [14].

$$K_1 = n \cdot (A_e)^2 \cdot \frac{p_0}{V_r}$$

$$K_2 = n \cdot (A_e)^2 \cdot \frac{p_0}{V_b}$$

$$K_3 = p_{g0} \cdot \frac{dA_e}{dz} = (p_0 - p_a) \cdot \frac{dA_e}{dz}$$

$$C = R_f \cdot A_e^2 \cdot \rho_0 \cdot g = \frac{0.126}{d_s^3} \cdot A_e^2 \cdot \rho_0 \cdot g$$

The stiffness parameters are:

K_1: the stiffness of airbag (N/m), K_2: the stiffness of the reservoir (N/m). K_3: the stiffness of air spring due to change in the effective area(N/m),C: Coefficient of damper accounting for substantial losses in the surge pipe and moderate losses in fittings, ds: the surge pipe's diameter (m), g: acceleration due to gravity (m/s^2), A_e: effective area (m^2), V_b: air bag volume (m^3), V_r: reservoir volume (m^3), ρ_i: mean density of the air (kg/m^3), p_i: initial absolute pressure (Pa), p_a: Atmospheric pressure (Pa).

1.7.3 Vampire Model

This model consists of four types of springs and a mass M, which consists the air mass's inertia flowing in the tube connecting air bag and the reservoir. This model differs from the one before it (Nishimura) is the addition of an extra spring (K4) depicts the safety spring, while the damper coefficient is non-linear, and it differs from the model before it, as shown in the Figure(1-3)

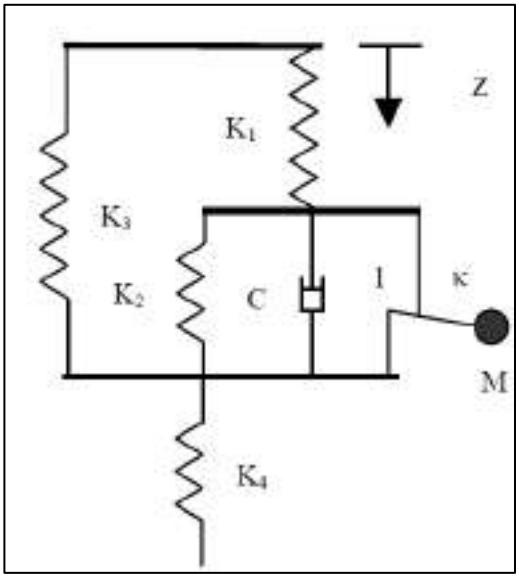

Figure (1-3) VAMPIRE model [14].

1.7.4 Simpac Model

This model of air spring includes four stiffness, K1 represents the air effect of the original air spring. K2 represents the stiffness of the air's effect on the additional volume, K3 is the stiffness that depicts the impact of the changing

air bag effective area, K4 refers to the rubber mounts' stiffness. The surge pipe is dampened by the damping coefficient C2, and the air bag is dampened by the damping coefficients C3 and C4, respectively as shown in Figure 1.4 [14].

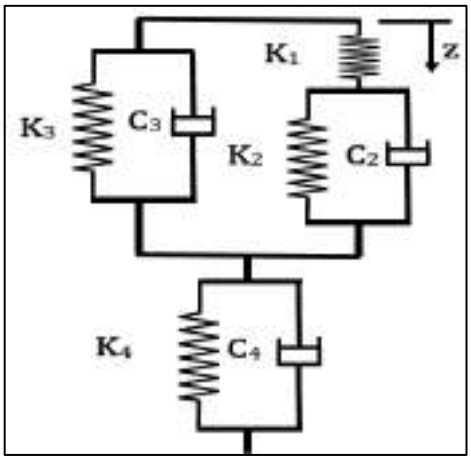

Figure (1-4) SIMPACK model [14].

Where

$$p_g = \frac{-F_Z}{A_e}$$

$$K_1 = n \cdot (p_g + p_a) \frac{A_e}{V_b}$$

$$K_2 = \frac{V_b}{V_r} \cdot K_1$$

$$K_3 = -p_g \frac{dA_e}{dz}$$

Where

$K_1$is the stiffness of air in air bag (N/m), K_2 is the stiffness of air in reservoir (N/m), K_3 is the stiffness of the air spring's changing effective area (N/m), K_4: Stiffness of the rubber (N/m), C_2 is damping coefficient of the surge pipe, C_3 and C_4 are damping coefficients of the air bag, F_z is Vertical force (N), Ae is Effective area of air spring (m^2), p_a is Atmospheric pressure (Pa),V_b is Volume of the air bag (m^3), and V_r is Volume of the reservoir (m^3).

1.7.5 Gensys Model

It represents the lateral, longitudinal, and vertical behavior of an air spring in three dimensions, as seen in Figure 1.5 [16]. a contribution from friction and one from viscosity [17]. We shall analyze the Gensys equations for vertical motion in section (3.1).

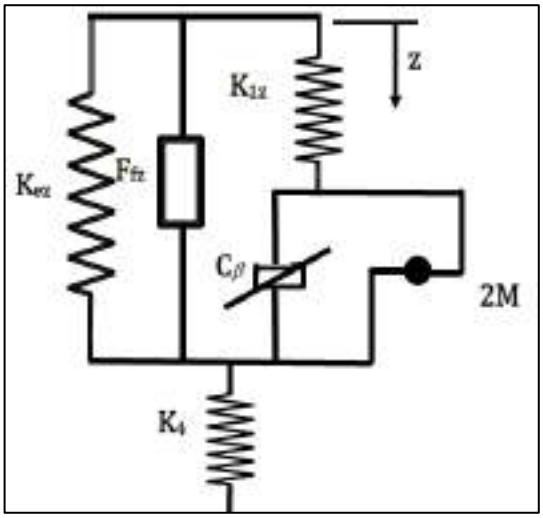

Figure (1-5) GENSYS model [17].

1.8 Control System

In the area of controlling oscillations, Many control laws are created to provide the necessary performance for any closed loop system to solve different problems. “FLC, FOPIDC, and SMC” are implemented in the current study.

1.8.1 Fractional Order-Proportional Integral Derivative

In order to overcome the shortcomings of the conventional controller a “Fractional Order Proportional Integral Derivative” controller was used. The following is a mathematical representation of the FOPID controller form [18].

$$u(t) = K_p \cdot e(t) + K_i \cdot D^{-\lambda} \cdot e(t) + K_D \cdot D^{\delta} \cdot e(t) \qquad (1.4)$$

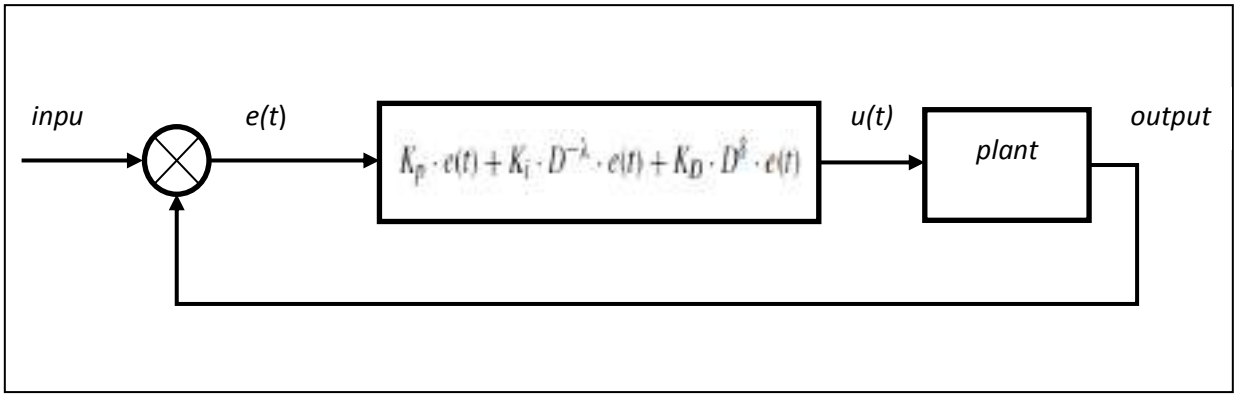

Figure (1-6) "Fractional Order PID" control system.

1.8.2 Fuzzy Logic Control

One of the most effective and well-liked control techniques available for controlling active suspensions is fuzzy logic control (FLC). A "Decision-making logic, a fuzzy rule base, a defuzzification interface, and a fuzzy interface " make up a standard FLC.

Using a fuzzy controller, a linguistic control method is converted into a program that intelligently controls nonlinearities with uncertainty. In spite of road disturbances, this control system aims to keep the sprung mass acceleration and displacement as near to zero as possible.

1.8.3 Sliding Mode Control

Slide mode control is one of the techniques which is used to control suspension systems due to the main characteristics, such as robustness and finite-time convergence compared to other linear controllers, it has a significantly more complex layout and control process.

1.9 Genetic Algorithm

Ordinary and dynamic programming is one of the classic types of optimization, in which it is not possible to deal with tasks that require complex solutions with constraints and nonlinear functions, it also cannot find an optimal solution or requires a longer processing time. Evolutionary algorithms (EAs), stochastic optimization approaches that function similarly to the biological

evolution of natural selection and/or the social behavior of species, are offered as a solution to these problems [19].

A set of optimization parameters has been used for the purpose of solving an engineering, scientific or economic problem, such as reducing losses in power networks by finding the best solutions in the distribution or training a neural network to identify a problem through training on a set of images [20].

The biological system and Darwinian Theory of natural evolution, which relies on the "survival of the fittest" tenet, served as inspiration for the concept of a genetic algorithm. Genetic algorithms for solving problems were developed and tested by John Holland, who put this algorithm into a theoretical form [21], on the basis of genetics, in addition to the laws of natural selection [22]. The genetic algorithm operates on three operators, selection, crossover, and mutation. The GA mechanism depends on diagnosing specific sets of solutions, called chromosomes, for a desired optimization problem called population, within the search space using the fitness function in each repetition case or iteration called generation [23]. Chromosomes consist of chains where each chain consists of genes. Genes represent a specific value, which can be a binary system, an alphabet, a specific value, or an integer.

Chromosomes are grouped together as a population. During each repetition or generation, the chromosomes are modified towards the optimal solution through the chromosomes that began to be generated randomly, as genetic factors (selection, crossover, mutation) are applied to this modification, as shown in the first factor responsible for transferring information from one generation to another through selecting the most chromosomes effectiveness which is based on improving the desired fitness function while neglecting others without affecting the population [24].The cross factor works to produce new chromosomes (operable solutions) from the selected solutions by cutting and switching these solutions between these genes [25]. The mutation factor creates new solutions by changing the value of the gene within the chromosome that is

randomly selected on the basis of the mutation rate to ensure population diversity, that is, GA does not depend on gradient information and thus enables it to deal with non-simple optimization problems that include non-linear functions or constraints [26]. This technique has been widely used in academia in a variety of research domains, including drones, seat suspension systems, and vehicle suspension systems [27, 28]. When using a large population and number of generations, the probability of achieving an optimal solution increases globally. However, this requires more time for calculations, especially for complex [19]. The survival of the fittest is applied by a genetic algorithm to a population of alternative solutions to create ever-improving estimates of the solution. By selecting individuals based on their level of fitness in the issue domain and breeding them together using natural genetics-inspired operators, a new set of approximations is produced at each generation. Similar to how natural adaptation occurs, this process causes groups of people to develop that are better adapted to their surroundings than the individuals from which they originated. A population of people is initialized at random at the start of the computation.

Then, for these people, the objective function is assessed. Produced is the first or initial generation. The start of a new generation occurs if the optimization conditions are not met. People are chosen based on how well they are able to produce progeny. Offspring are created by combining parents. There is a certain possibility that every offspring will have a mutation. Next, the fitness of the progeny is estimated. A new generation is created when the offspring are introduced into the population in place of the parents. Up till the optimization conditions are met, this cycle is repeated [29].

1.10 Road Profile Excitation

There are three road profile kinds that are utilized to test the models in this section using MATLAB-Simulink.

1. In this case, the road profile is taken from a simple sine bump and applied. A speed hump that was generated from an equation and used in this case for quarter-car model is depicted in Figures (1.7). Common humps come in recognizable shapes like circles, parabolas, and flat surfaces [30]. In this case, the circular type will be taken into account. The circular speed hump's parameters, as described in eq.(1.4) [31].

$$y = h\sin(\omega t) \tag{1.4}$$

Where:

$\omega = \frac{\pi V}{3.6L}$ rad/s, h is height of bump equal to 0.1 m, L is equal to 5.2 m, V is velocity of vehicle in km/h. The block simulation for this bump is presented in (Appendix-A).

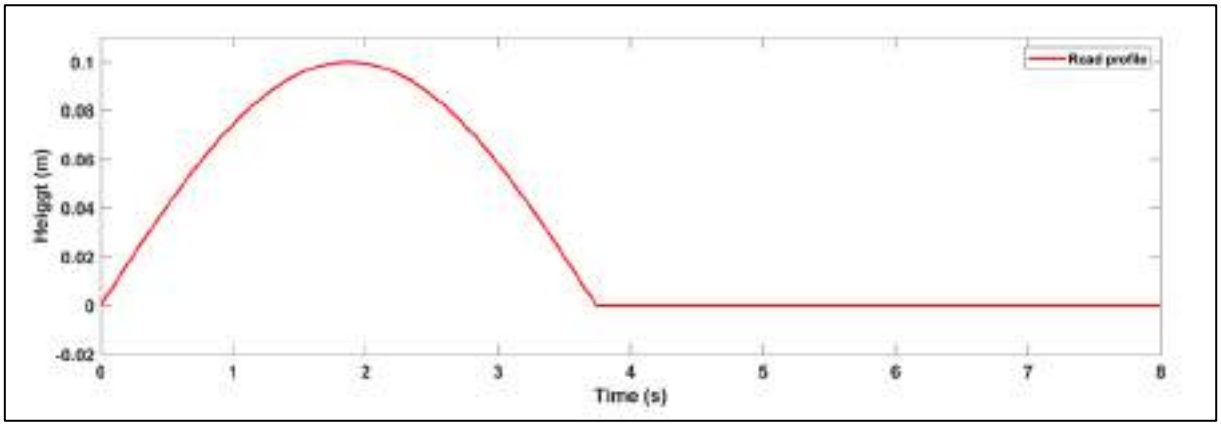

Figure (1-7) Road profile with 0.1-meter high bump.

2. A two-bump road disturbance of varying sizes, modeled utilizing the subsequent eq. (1.5) [32].

$$\mathrm{y}(t) = \begin{cases} \frac{A}{2}\left(1 - \cos\left(2\pi\left(\frac{t}{T_{b1}}\right)\right)\right), \text{for } T_{b1} \le t \le 2T_{b1} \\ \frac{B}{2}\left(1 - \cos\left(2\pi\left(\frac{t}{T_{b2}}\right)\right)\right), \text{for } 8T_{b2} \le t \le 9T_{b2} \\ 0 \text{ Otherwise} \end{cases} \tag{1.5}$$

Where:

A is the height of the first bump which is taken into account between the seconds T_{b1} and $2T_{b1}$, B is the height of the second bump which is taken into account between the seconds $8T_{b2}$ and $9T_{b2}$. The following Figure (1.8) depicts the two bump road disturbance. The (Appendix-A) contains the block simulation for this two-bump road.

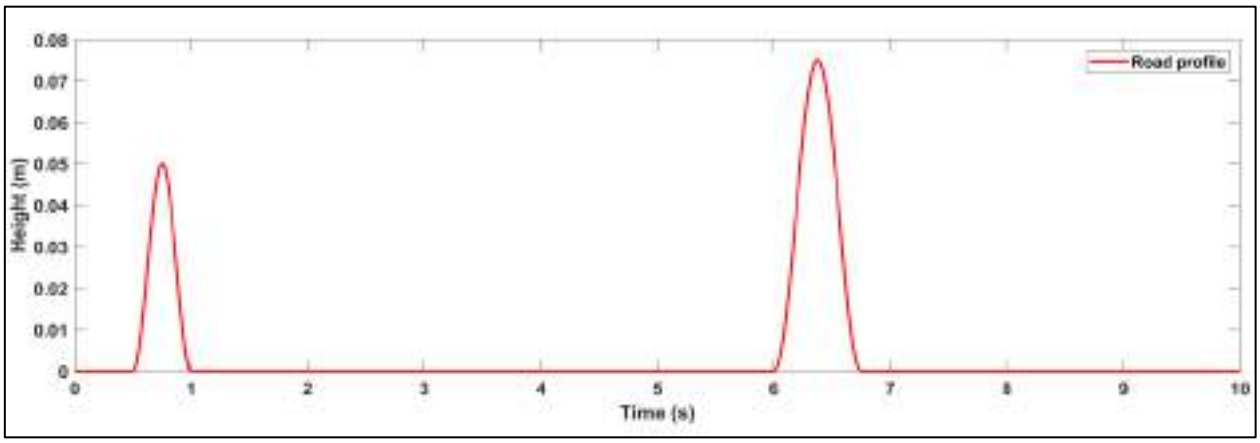

Figure (1-8) Road profile with two bumps.

3. A random road roughness is used to simulate the road profile using the MATLAB/Simulink platform according to ISO/TC108 as illustrated in Figures (1.9). using the Gq coefficient of roughness described in Table (1.2) for a level B rough road.

where q(t) represents the unevenness of the road surface, which can be calculated using the equation below [33].

$$\dot{q}(t) = -2\pi f_o v q(t) + 2\pi n_o \sqrt{v\, G_q(n_o)}\, w(t) \qquad (1.6)$$

Where:

f_o is a minimal boundary frequency and equal to 0.0628 Hz, v is the speed in ($m.s^{-1}$) which are various, n_o = 0.1($m^{-1)}$ represented a reference spatial frequency, w (t) : the Gaussian white noise, $G_q(n_o)$: the roughness coefficient (m^3). In (Appendix-A), the block simulation for random road roughness (level-B).

Table (1-2) Road classification levels[33].

Road Class	**A**	**B**	**C**	**D**
$G_q(n_o)(*10^{-6})$	16	64	256	1024

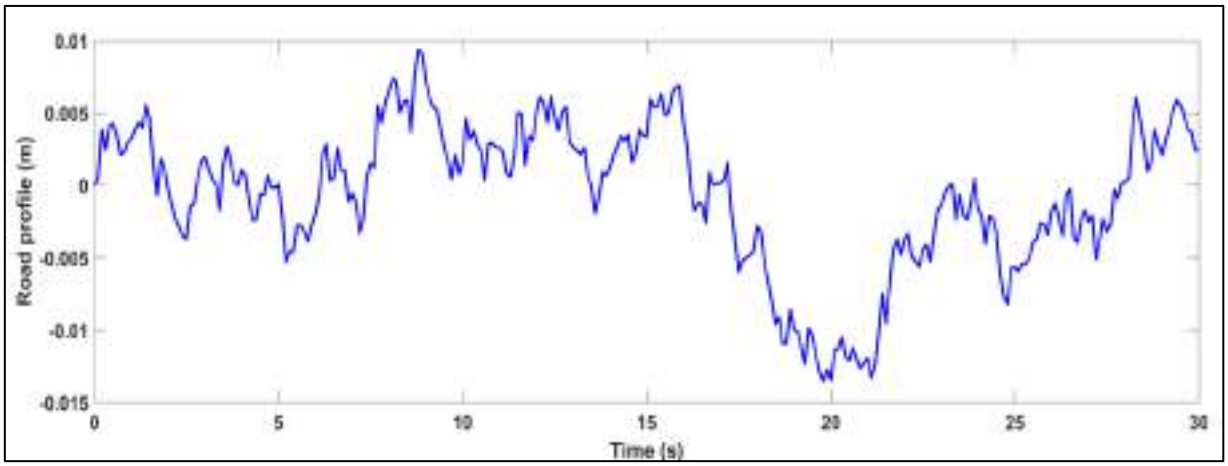

Figure (1-9) Road input for roughness road ISO class B.

1.11 Objectives of the Work

The fundamental aim of this study is to create an active air suspension integrated with hydraulic actuator for vehicle in order to improve their dynamic behavior. These particular objectives have been established in order to reach this goal:

- To research the history of air suspensions as well as their strategies of control.
- Evaluate a mathematical model of air suspension to quarter vehicle model.
- Establishing the air suspension system's parameters.
- Make a comparison between two models of the air spring, the traditional type with the Genesys type, to find out which one is better in the suspension system
- demonstrate the effectiveness of integration of the hydraulic actuators with pneumatic suspension system (build a model of an air suspension

system combined with a hydraulic actuator) and optimal control strategies by optimization and to know the effectiveness of this type of suspension system

- Validation of the simulation model by comparing simulation results with other studies.

1.12 Thesis Structure

This thesis is divided into seven further chapters, each of which is briefly described in this part.

The first chapter covers a wide a variety of subjects, including the background information about vehicle suspension systems, the models of air spring, Genetic algorithm, and the thesis' objectives.

The second chapter relates to review of the literature on air suspension systems and associated control methods.

The third chapter includes the designing, modeling the air spring and its parameters and hydraulic actuator of suspension system model

The fourth chapter includes the derivation of the air spring of the tradition type in addition to a simulation to compare two types of air springs in order to connect one of them with hydraulic actuator.

The fifth chapter, Model comparisons between their outputs are carried out (results and discussions).

The sixth chapter describes the conclusions of this study, and provide suggestions for further research.

Chapter Two

Literature Review

CHAPTER TWO

Literature Review

2.1 Introduction

The vehicle's suspension system is an essential component. This system aids in regulating and dampening vibrations that are transmitted from the road surface to the vehicle body. The stability and comfort of the vehicle depend on the operation of the suspension system. In order to increase the smoothness and comfort for passengers in the vehicle, the stiffness of the suspension system needs to be changed flexibly. The conventional pneumatic suspension system can partially meet these requirements. However, the change is not much [34].This chapter provides the technical background needed to understand active suspension and the behavior of the air spring.

The suspension system's electronic control might improve the trade-off between the stability and comfort that the vehicle's suspension scheme is designed to achieve. Car suspension systems may be divided into three parts semi-active, active, and passive suspension. The typical springs and damper are part of a system of passive suspension. That mechanism have the capability to accumulate energy using a spring and disperse it using a damper. A semi-active, the damping coefficient value is variable, while the ability of the active suspension to supply the system with energy between sprung and unsprung masses, the actuator is linked in parallel together with a shock absorber and the spring where desired force may be produced in any direction using the actuator. The car's active suspension is fitted with sensing devices that are connected to a reliable computer system that contains data on the vehicle and how it responds to various road conditions. Figure (2-1) shows the types of suspension

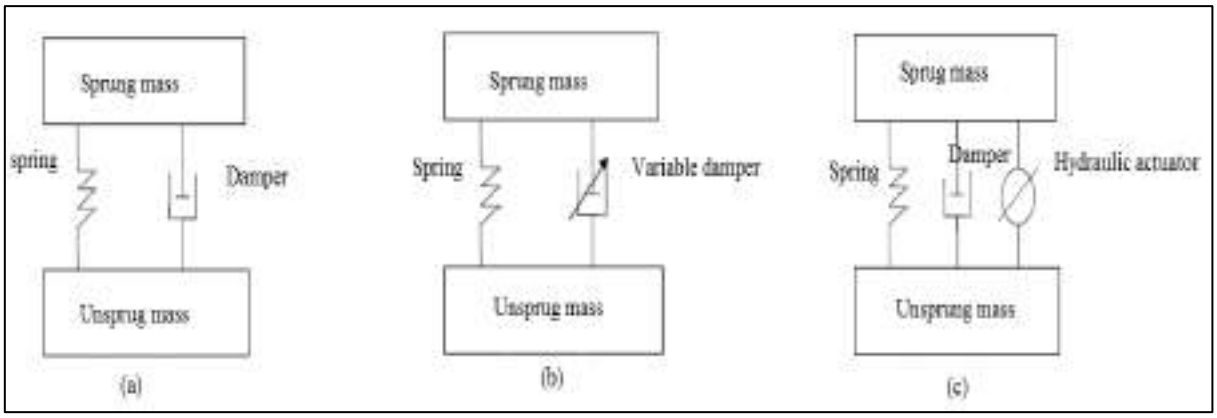

a) The passive system b) The semi-active system c) The active system

Figure (2-1) The types of suspension.

Many researchers added improvements to the pneumatic suspension system and studied the strategies through experimental work and simulation.

2.2 Air Spring

A general model of an air spring is very difficult to create due to the strong nonlinearities in the stiffness and the hysteresis effects, which are scarcely noticeable in normal coil springs. The design of vehicles using air springs can make use of them to improve the ride and handling while also including a number of functions for the comfort of the passengers.

Kim and Lee, (2011), [35] proposed a new algorithm of control (Fail-safe Algorithm) with (Fault Detection) for closed loop air suspension system. This algorithm was implemented and verified through the simulation and the vehicles test and then showed from this technique can evaluate the target height to accomplish different control objectives and adjust the height of vehicle to the desired height, even when using a time-varying model uncertainty.

Yin, et al., (2012), [7] proposed a new pneumatic air spring which includes a tuning subsystem, two accumulators, and a double-acting pneumatic cylinder., spring stiffness was derived according to the principles of fluid and

thermodynamics, the experiments were carried out with various chamber pressure settings and ride heights. The analytical and experimental findings studies demonstrated an ability of the improved air spring system to independently adjust the stiffness and ride height.

A. Kazemini et al., (2013), [36] designed a model for air suspension for a quarter car, where the model-based simulation and experimental testing were the two methodologies used in the test strategy for the suspension model. To enhance the isolation effectiveness in the minimal frequency range, an active control approach based on applying pressure to a pneumatic vibration isolator is developed. They validated the effectiveness of their strategy by comparing simulated results with experimental results through values, In modeling and experimental data, the body acceleration was improved by 17.92% and 11.51%, respectively, tire force was used to define handling performance, which improved 8.1% stimulatory and 3.04% experimentally.

N. Khettou et al., (2015), [37] modeled a semi-active control of a quarter vehicle using air spring. The air spring model was established by the dynamics of equation, MATLAB and the transfer function were used to implement the simulation model. Simulation results show that the valve diameter, air spring pressure, the mechanical stiffness and the dumping coefficient impact the system's dynamic responsiveness. The results showed a decrease in the amplitude of oscillation in around the system's natural frequency.

Masliiev et al., (2015), [3] improved the mathematical model around the damping of vibration considering the effect of pneumatic spring suspension system parameters, gas thermal and dynamic system characteristics, and the direction of airflow via the throttle orifice situated between the air spring and the extra reservoir. The findings of the search revealed that the mass's vibration

frequency was dependent on the throttle's cross section, the surface's area, and the additional reservoir's capacity, which gave rise to the need to include them in the expression for calculating the coefficient of damping, which also took the air spring's active capacity, the density of the air, and the frequency of the resonant vibration into account.

H. J. Abid et al., (2015), [38] investigated an equivalent model is one that uses the same road profile inputs and an pneumatic suspension system configuration to achieve a suspension system that performs similarly to a passive suspension system component through the use of Matlab-Simulink with (OptiY) optimization, as well as the air spring's characteristics as length of surge pipe, initial pressure, ,diameter of pipe, a bag's volume, and the reservoir's size are gained from optimization.

P. Karimi et al., (2016), [39] built a dynamic air suspension model with independent stiffness and height adjustment techniques by modifying the air pressure in the two air chambers of this air suspension, so that the ride height and stiffness of the vehicle is synchronously changed for different driving conditions. They used the maximum and least desirable natural frequencies when operating at maximum pressure to derive the equations for the optimum accumulator volume.

G. dalvi et al., (2017), [40] designed the mathematical model of air spring by MATLAB/Simulink and studied the character of the variation in stiffness with pressure for different loads, an adequate experimental setup was created, frequency dependency of stiffness consideration and presence of friction because of in connection pipeline the flow resistance was modeled according to approximation. The simulation and the experiment were compared and examined. As a result, the air spring's vibration settling time was reduced. They

also explained that an amount of damping and flexibility can be produced by the developed air spring.

Moheyeldein et al.,(2018), [33] evaluated the passenger's comfort and vehicle stability by conducting a time and frequency analysis of several parameters of the spring and their effects on the suspension vehicle at a speed of (20 $m.s^{-1}$) with the road level C and comparing it with, after that, both the passive suspension and the dynamic air spring suspension in RMS of dynamic tire force, suspension travel, and body acceleration. Results showed that these parameters improved by 27 percent, 10 percent, and 20 percent, respectively when compared to passive suspension, which offers more comfort and easier handling.

Wei Li et al., (2018), [41] developed a single degree of freedom air suspension mathematical model that is nonlinear and an additional chamber based on fluid dynamics and engineering thermodynamics theories. They showed that a tight relationship exists between the throttle orifice opening and the damping properties of an auxiliary chamber air suspension and concluded it has correlation of amplitude and has a close connection to the throttle's orifice opening valve and showed the maximum error for the ratio is 7.69 percentage, and the natural frequency of the system's maximum inaccuracy is 4.17 percent, this demonstrates the precision of the simulation analysis and mathematical model.

Mei Li et al., (2019), [42] showed that the performance of air suspension (shared chamber air suspension) with the Fuzzy-PID controller has explicit improvement in the vehicle body's acceleration differs from the effectiveness on dynamic tire load and suspension deflection. They concluded that a larger the combined chamber volume with the lower pressure contributes to the improvement of the acceleration of the body, while the dynamic tire load(DTL)

and the suspension's deflection cannot obtain optimum value simultaneously when these parameters are given weights.

K. A. Abd El-gwwad et al., (2020), [43] developed used to evaluate the performance of semi-active four state switchable damper suspension gadget with dynamic air spring then contrast the results with those provided by the passive dynamic air suspension system and the semi-active four state switchable damper device. The air spring size, air pressure, reservoir size, and tubing dimensions were included in this parametric analysis. Therefore, as compared to passive dynamic air suspension, the improved four state semi active suspension systems offer considerable improvements.

2.3 Control of Air Suspension System

Many methods of control are utilized to enhance the efficiency of the system of active suspension, such as:

M. Mailah and G. Priyandoko, (2007), [44] presented active force control (AFC) and used adaptive fuzzy (AF) logic techniques to build a model of control methodology which is applied to the suspension system of the quarter-active car. The main components of the overall control system are three feedback control loops: the inner control loop for PI, which tracks a force applied by the hydraulic actuator, the middle AFC control loops, which compensate for disruptions as well as the external AF control loop, which calculates the ideal target or commanded force. They observed that the performance of the active suspension system with Adaptive Fuzzy Active Force Control (AF-AFC) is superior to that of its passive and AF counterparts, which may thus improve the comfort of driving a car.

Pekgokgoz et al., (2010), [45] studied proportional- integral- derivative (PID) and the fuzzy logic controller methods on a sample quarter-car model, and genetic algorithm techniques are used to optimize the membership functions. Additionally, a comparison of the car's body deflections and force of control has been established and contrasted. This comparison represented the effeteness and convenience of the offered Fuzzy Logic Controller (FLC). They showed that the proposed approach can be efficiently used for active suspension control in vehicles.

J. Sun and Y. Sun, (2011), [46] studied three types of active suspension control strategies of random road signal and verified that a method of the least means squares (LMS) adaptive control which deprived from signal procession is applied on the active control of suspension and the outcomes are evident, the sky-hook and generalized adaptive controllers in 2D of freedom vehicle suspension . They conducted a LMS adaptive control method might significantly enhance the suspension system's performance (dynamic suspension deflection and the sprung mass's acceleration) when compared to passive suspension, in the frequency domain acceleration decreases by eight–ten times.

G. Yang and Y. Zhao, (2012), [47] proposed system of semi-active suspension to enhance riding comfort and a 2-DOF vehicle simulation system is designed to simulate the activities of the suspension system. They employed Fuzzy Logic technology to control the suspension's continuous damping to reduce vehicle acceleration when the vehicle is exposed to an irregular road and according to the findings of the simulation, the proposed fuzzy logic controller outperformed both a conventional passive suspension system and the linear quadratic regulator control approach.

M. Jamil et al., (2013), [48] developed controller by combining intelligent control and optimum control methods by fuzzy logic rules based to reduce the vertical displacement of the vehicle's body, through this integration,

the actuator control force is also decreased while comparing uncontrolled suspension. The system's vertical displacement was reduced by 62.5% after the implementation of the LQR controller, but produce high actuator force while, proposed control was minimized by 40% with the modest peak and stable magnitudes for actuator control forces, a more effective control strategy is offered by these actuator's force to enhance ride comfort and stability when coupled with active suspension.

C. V. Reddy et al., (2014), [49] modeled and analyzed hydro-pneumatic suspension system for passenger cars and they built a hydro pneumatic suspension of a quarter car using Matlab/Simulink with PID controller. By adjusting the pneumatic pressure inside the chamber, the suspension stiffness can be changed. In a hydropneumatic chamber, the pneumatic pressure can also be regulated by adjusting the hydraulic pressure on the opposite side of the diaphragm.The hydraulic cylinder, pump, valve, orifice, piston, and gas compression and expansion are all included in the suspension model, the valve is turned by a PID controller to produce the required suspension performance. The observed from the suspension model, the maximum sprung mass of the passive suspension system is approximately 1.11*10-3m while the maximum displacement of the hydro pneumatic suspension system is approximately 1.11*10-4m. That is, sprung mass displacement was reduced by 90%, also the sprung mass's acceleration is reduced by 79.5 percent as compared to conventional suspension systems. further demonstrated that the use of hydro pneumatic suspension model results in a reduction in the response time-length to return to the static equilibrium position, thereby enhancing the suspension system and passenger comfort.

A. Çakan et al., (2014), [50] suggested a linear actuator for active vibration control of quarter suspension system . Various controller kinds are

established under the influence of two road profiles by using ADAMS and MATLAB software and two types of controllers under the influence of two road profiles, Artificial Neural Network Based Fuzzy Logic (ANNFL) and PID as a tool for control of active vibration simulations of the suspension system. The used techniques and implementation are performed well according to molding and control performance. By employing simulations, the comparison between modalities of active and passive are established, and it is proven that the controllers that were built are effectiveness.

R. Rosli et al., (2014), [51] implemented a hybrid control approach for a vehicle suspension system utilizing a PID control system, iterative learning, and active force control, with performed on test rig for quarter car, also they suggested that PID and Iterative Learning algorithms for active force control are technically feasible and readily implemented in real-time. The testing findings showed that the AFCIL scheme's active suspension system outperformed its PID and passive counterparts. The obvious decrease in vertical body acceleration and displacements and that the suggested control strategy improved the system's ride comfort feature.

A. M. Shirahatti, (2015), [52] designed and simulated the Linear Quadratic Control (LQR) controller for full vehicle model based active suspension and eight-degree of freedom and used an input to the whole vehicle model, measured random road surface that fits within the poor category of roads according to ISO is utilized as input to the entire vehicle model. An optimization approach (stochastical technique) has been used for quantitative comparison the LQR controller design approach of active system with respect to a passive system. When compared to a passive suspension system, the active case's seat bounce and acceleration are reduced by 92 and 86 percent, respectively, while the active case's tire vertical displacement with suspension- travel lowered by 13.8 and 18.4 percent.

H. K. Tran et al., (2016), [27] proposed controller software showed a superior and the most efficient process trajectory, including fuzzy logic control for Unmanned Aerial Vehicles' flight motion control simulation. Fuzzy Scaling Factor was optimized using ITAE "the integral of time times absolute error" criterion using genetic algorithm optimization as the training software for the Tricopter of flight motion control system and the performance finding demonstrate the extremely dependable waypoint tracking and stable functioning as per Figure (2-3).

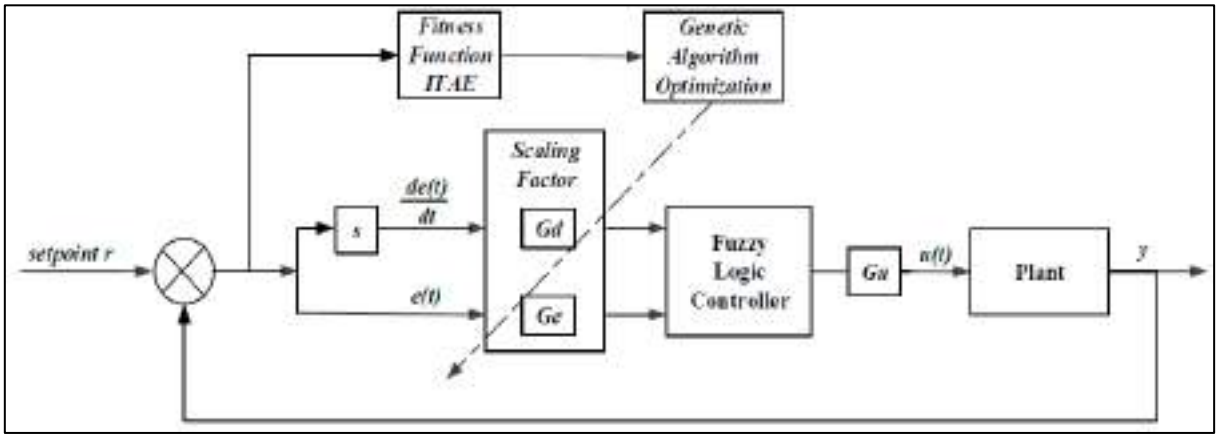

Figure (2-3) Diagram of the GA-FLC controller [27].

P. Karimi et al., (2016), [39] used a type of suspension in the chassis height in form of air suspension that can be controlled the airbag by further inflating, furthermore, the stiffness is not adjustable and is based on the airbag volume and chassis load, including two chambers for air (rubber airbags), which allow independent ride height and stiffness tuning. In this air suspension design, the vehicle's stiffness and ride height can be altered simultaneously by adjusting the air pressure in the two chambers for different driving conditions, allowing the height of the vehicle and the natural frequency must be adjusted for the charge situation and the road situation. They developed an optimal configuration

that has been found for this air suspension system and can be used for any vehicle model and air suspension geometry.

S. Palanisamy and S. Karuppan, (2016), [53] studied the effectiveness of an active suspension system employing FLC as the control strategy and suspension deflection of the vehicle body as the main control criterion. They carried out the simulation results by simulation/MATLAB using a quarter-car model with, two different road profiles and compared the analytical results of the model with a PID controller. Through the proposed model, they were able to significantly reduce both the acceleration of the car body and the vertical displacement in comparison to the PID controller's performance and the passive suspension. By lowering body acceleration with the use of a fuzzy control method, the comfort of the ride is increased.

X. Dong et al., (2016), [54] developed a nonlinear model for an electro-hydraulic servo actuator with active suspension system by designing a FOPID controller to control the displacement servo of the actuator. The optimizing the parameters are tuned using a parallel adaptive clonal selection algorithm (PACSA) by error integral criterion. They demonstrate that the performance of the system for suspension using the FOPID actuator is superior to both the passive suspension system and the active suspension system using the PID actuator.

M. H. Ab. Talib, (2017), [55] studied a magneto rheological (MR) damper for semi active controlled suspension. His study aim to investigate the development of vehicle suspension system intelligent controllers using magneto rheological damper, PID control and FL control tuned using PSO algorithm, algorithm firefly (FA), and sophisticated firefly algorithm. He proposed a parametric modeling technique known Spencer model and used for measuring MR damper. A semi-active simulation performed in the MATLAB/Simulink

environment. The efficiency of all control strategies was examined with regard to two key issues: the controller's capacity to reject the vehicle's undesirable motion and to overcome the damping limitation. PID-AFA's proposed control scheme has decreased the acceleration of the sprung mass and displacement of sprung mass up to 28.21 percent and 16.9 percent respectively over the FL - AFA and passive system.

Y. Taskin et al., (2017), [56] designed three inputs and one output fuzzy logic controller for suspension testing setup for quarter car. Comprehensive time and frequency responses are used to display and explain the outcomes of the experiment. For comparison, the traditional fuzzy logic controller is also used. Both passive systems and active controllers, sprung mass vertical accelerations, displacements , suspension travel, and forces of actuator are compared. According to comparison the passive and traditional fuzzy logic controlled systems, the results show that proposed controller worked well.

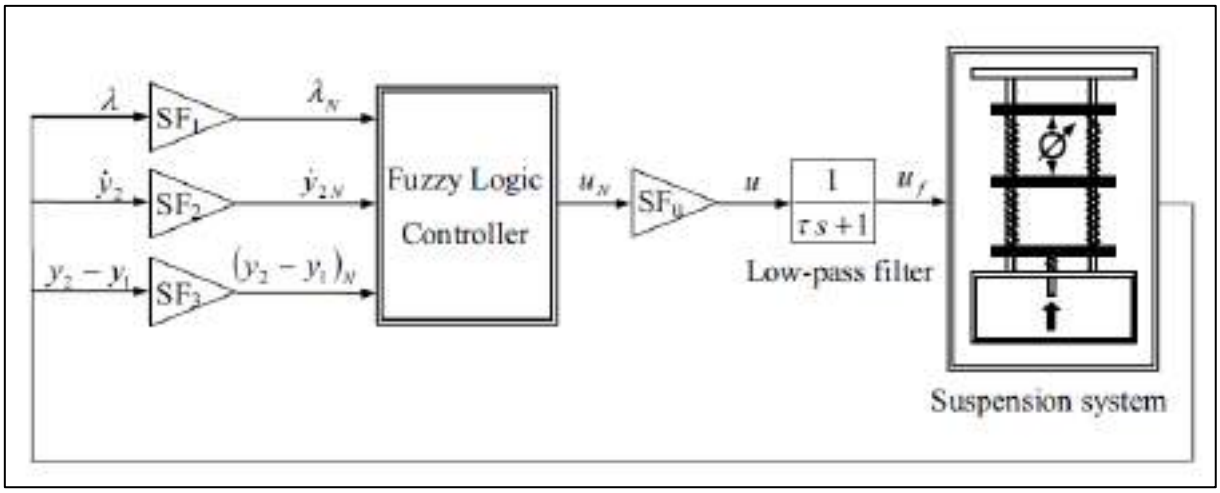

Figure (2-2) The FLC active suspension system's standard block diagram [56].

Z. Ding et al., (2017), [57] used an adaptive neural controller with a continuous damping controller damper (CDC) for the nonlinear suspension system to minimize the sprung mass from oscillating locally in the case of road

roughness, they employed an (ARBFNN) using online learning and skyhook controller, additionally, the controller's settings are determined and optimized using the PSO approach. They showed that the improvement in root-mean-square values by use of the controller is that the displacement is decreased compared to the control for a skyhook. The outcome demonstrated the effectiveness of the control unit to improve semi-active suspension systems' performance compared to passive suspension systems and Skyhook control structures.

Durairaj et al., (2018), [58] proposed a fractional order PID controller with five parameters (five gains), with harmony search acting as the stochastic optimizer to automatically tune the fractional order PID controller, utilizing the objective function of ITAE. The tuned controller provides the best tuning parameter that significantly decreases body displacement and ensures passenger comfort by correcting wheel deflection.

Salem, (2018), [59] studied a quarter car model with two degrees of freedom by designing a nonlinear spring and compared it with a linear spring. Results reveal that adding nonlinear stiffness reduces the sprung mass's vibration to satisfy ideal ride comfort standards and a nonlinear suspension that might offer performance gains over those made possible by passive, semi active, and active suspension. To achieve the required performance requirements, an automatic optimization of the suspension parameters was carried out using the Genetic algorithm. In comparison to a linear connection, the theory of energy transfer between a linear oscillator and an energy absorber has been studied and showed a significant energy transfer. According to the findings, adding the nonlinear spring to the suspension will reduce the sprung mass' amplitude by 50% to 60%. The amplitude would decrease to 60% to 90% with subsequent advancement employing the new genetic parameters.

Tran and Nguyen, (2018), [60] optimized the PID controller variables both for real-time quadcopter flying motion and simulation using genetic algorithms. They implemented the GA-optimized PID through criteria of ITAE with regard to a motion control system for quadcopters as shown in Figure (2-4), as well showed that the controller for PID controller works effectively in evaluation of tracking flight motion and waypoint, the consequence is an improvement in the operation time.

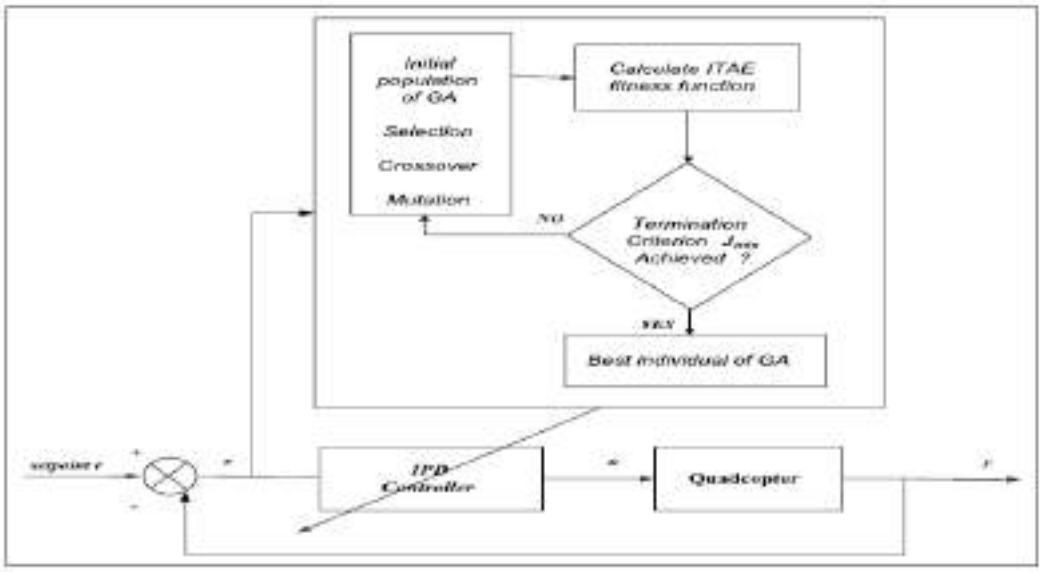

Figure (2-4) Diagram of the proposed controller [60].

Ammar and Ameen, (2018), [61] studied different control algorithms for modeling, simulating, and controlling a linear half-car for system of suspension using "Matlab/Simulink" for model which has 4 degrees; consisting of front and rear-axel heave movements, pitch and heave movements of the vehicle's unsprung mass, as well developed and implemented different control Fuzzy, PID, and Fuzzy-PID for linear half-car active suspension systems with a hydraulic actuator. Comparisons between active suspension using various control systems revealed that the fuzzy-PID controller and passive suspension indicated in the work performed better than the other controllers used in the

analysis, having shorter settling times, smaller overshoots, and rising steady precision, and better dynamic performance.

Ahmed A. Abougarair and Muawia M. A., (2019), [62] employed an active mathematical model suspension system for the quarter car system. They presented and used linear Quadratic Control, the proportional derivative (PD), and Fuzzy logic tune PD controllers, and then compared between these controllers to reduce the quarter-response car's to road disruptions model under the influence of two road profiles and variation of body mass. The outcome indicates that the usage of the three control strategies proposed is successful in controlling a vehicle but the fuzzy logic tune PD controller is more robust than the other two controllers.

C. Zhou et al., (2020), [63] researched a dynamic switch control technique that can switch between handling and comfort controllers when driving on various road surfaces. The load transfer ratio, which is determined using a six-degrees-of-freedom (6 DOF) model, is chosen as the switch performance index in accordance the sliding mode control strategy. Analytic hierarchy method is used to produce the sliding mode controller's objective functions, and the parallel adaptive clonal selection approach is then used to optimize the controller's parameters (PACSA). They conclude that, when compared to a traditional SMC controlled suspension system, the suggested key control technique simultaneously enhances ride comfort and maneuvering stability under a variety of maneuvers and road profiles.

Y. Shahid and M. Wei, (2020), [64] deal with the control of vibration for active a quarter-car system of suspension . They searched strategies of damping control , (HOSMC) according to a (STA), (ISMC), (FOSMC), (LQR), (PID), and passive system for suspension . Analysis is done on the performance

comparison of various active controls in form of vertical movement, wheel deflection, and suspension deflection . The theoretical and qualitative analysis verified the STA-based on HOSMC demonstrates better efficiency well as negates the undesired FOSMC, LQR, ISMC, PID and passive system, and then improves the ride comfort and vehicle stability.

G. W. Kim et al., (2020), [65] enhanced discrete Kalman filter for a car suspension control system's input of unknown road roughness and used it to estimate all state variables at once without any background knowledge of the suspension system for the vehicle. **U**tilizing the CarSim program, the performance of the estimator for the car suspension control system is validated in order to evaluate every variable state and rough input from an unknown surface for a car suspension control system that is important for performance of the vehicle's ride and handling while being driven. They prove an effectiveness of the proposed algorithm through simulation and experimentation with an in-vehicle test bed type with a laser profilmeter under different driving settings, such as changing vehicle speeds and road conditions.

Z. A. Karam and O. A. Awad, (2020), [66] proposed a robust controller, the Fractional Order PIDC for active quarter vehicle suspension and Particle Swarm Optimization PSO with Whales Optimization Algorithm WOA for tuning of parameters of the FOPID controller to minimize car body displacement and decrease oscillation time's damping frequency. The FOPID-based WOA controller appears to function significantly better than that reached by the PSO and conventional PID one, according to a simulation result. In comparison to the PID controller, the FOPID controller offers a faster speed response of the suspension system with a reduced overshoot, faster setting time, and faster rising time.

T. A. Nguyen,(2021), [67] used a system of nonlinear (single input–single output) for the sliding mode strategy to control a hydraulic actuator force that applies to the unsprung mass and the sprung mass for the active suspension system. They obtained results for the sprung mass's acceleration and the displacement of sprung mass much smaller than the passive suspension system when comparing the model with it, also showing that the sliding mode controller is extremely durable and robust versus road disturbance.

2.4 Concluding Remarks

Pneumatic vibration isolation technology for air suspension technique is steadily developing, since pneumatic isolators are used frequently, its performance needs to be further enhanced. The performance of comfort and handling at the same time in any vehicle is one of the challenges, here comes the role of active suspension as a key to solving this challenge, this is why there is a lot of research and study done on the active suspension. In this study, presents a new design and control pertaining to the active suspension system are incorporated the hydraulic actuator into a pneumatic suspension system, as the suspension system's stiffness must be flexibly altered on a regular basis to maintain the vehicle's stability and comfort during the ride.

Chapter three

Theoretical Analysis

CHAPTER THREE

Theoretical Analysis

3.1 Introduction

One of a vehicle's suspension system's primary purposes is to prevent road vibrations experienced by the tires from being communicated to the occupants; the creation of effects that stop rolling, squatting, and diving caused by dynamic load transfer, as well as the provision of the road holding. Passive suspensions have constant spring stiffness and damping coefficient limiting the suspension system’s unable to adapt to the dynamic conditions of a vehicle leading to the deterioration of the ride and handling performance of a vehicle. This necessitates the search for adaptive suspension technologies and at present pneumatic suspension technology is promising and becoming popular in high-end passenger cars.

3.2 Air Spring Model

The spring and damper stiffness are constant in a traditional passive suspension system. Perhaps that may bring the stability and comfort of the car to a lower level. In order to improve this case, the characteristics of the damper and spring, or both, must be modified. In this study, an air spring was used instead of a coil spring to get more comfort.

Nishimura, Vampire, Simpac, and Gensys are just a few of the many air spring models that are accessible as a simplified model for vertical air spring dynamics. The quarter vehicle air spring model, presented here with the airbag and reservoir which is connected by pipeline with valve, as shown in Figure (3-1).The leveling mechanism is not taken into account in the air spring modeling that is described here since these changes happen extremely slowly.

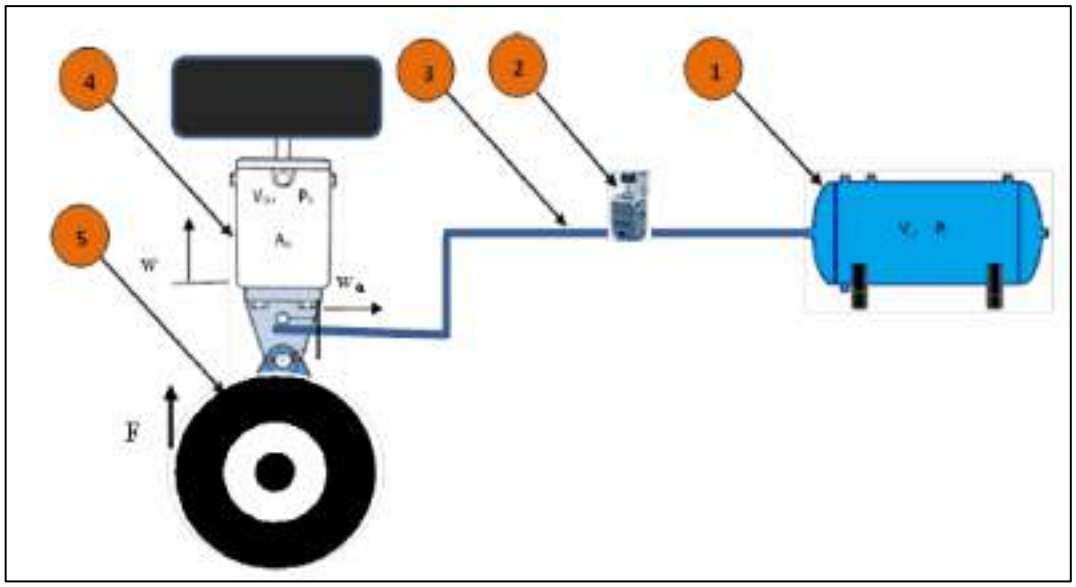

Figure (3-1) Pneumatic suspension system, (1) tank, (2) valve, (3) tube, (4) airbag (5) wheel [15].

It is possible to use air springs in a mechatronic method for suspension design the fact that it offers a simple regulated variable spring rate, low-cost, and leveling automatically.

For Gensys model to account for the difference in gas state between the volumes(air bag and reservoir), a mechanical barrier has already been added to the pipeline in the form of a fictive piston as shown in Figure(3.2). The structural barrier is assumed to neglect mass, and an additional liquid mass that oscillates along the pipeline is added to the barrier. The pressure difference between the two volumes is caused by the barrier displacement. A significant assumptions for minute changes in the gas state are made for the simplified air spring model, and suitable linearization is used [68]. The fundamentals of thermodynamics and fluid are the foundation for modeling an air spring, the change in gas state is polytrophic [69]. The nature of pneumatic processes makes the performance of the pneumatic suspension system inherently nonlinear and irreversible.

From Figure (3-2), the pressure between the two volumes changes as the bag(air spring) is subjected to a static load F_z, as well as a reduction in the

volume of the air bag. The following are the approximate pressures in the air bag and reservoir.

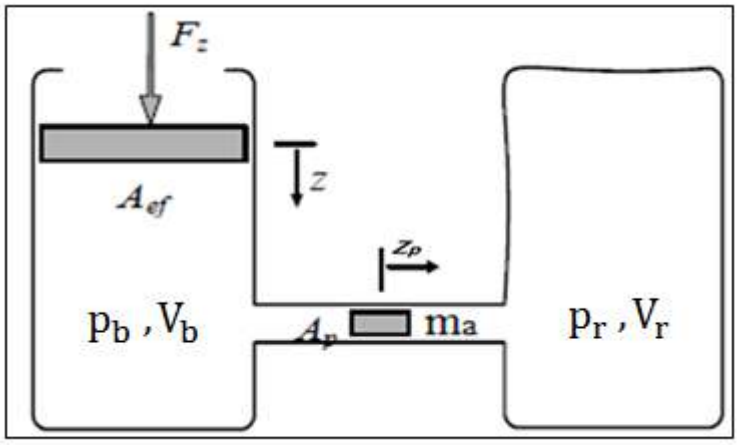

Figure (3-2) The physical representation of the air spring [68].

$$p_b = p_o + \Delta p_b \quad (3.1)$$

$$p_r = p_o + \Delta p_r \quad (3.2)$$

Where:

p_b : after deflection, the pressure of the air bag (Pa).

p_r: after deflection, the pressure of the reservoir (Pa).

p_o : the initial pressure(Pa).

Δ : the pressure change.

The new air bag volume after a deflection as well as the new reservoir volume.

$$V_b = V_{b0} - zA_e + z_pA_s \quad (3.3)$$

$$V_r = V_{r0} - z_pA_s \quad (3.4)$$

Where

V_b: After deflection, the volume of the air bag (m^3).

V_r: After deflection, the volume of the reservoir (m^3).

z : An air bag's piston displacement (m).

z_p: The air displacement in the surge pipe (m).

The relationship between volume and pressure in general after deflection is as follows:

$$p_1 V_1^n = p_2 V_2^n \tag{3.5}$$

Where n is the polytropic index.

Substitute equations (3.1) to (3.4) in equation (3.5) become:

$$(p_0 + \Delta p_b) \cdot \left(V_{b0} - zA_e + z_p A_s\right)^n = p_0 V_{b0}^n \tag{3.6}$$

$$(p_0 + \Delta p_r) \cdot \left(V_{r0} - z_p A_s\right)^n = p_0 V_{r0}^n \tag{3.7}$$

The binomial expansion is used to expand the equations [15].

$$(a+b)^n = a^n + nba^{n-1} + \frac{n(n-1)}{2!}a^{n-2}b^2 + \frac{n(n-1)(n-2)}{3!}a^{n-3}b^3 + \cdots \ldots + nab^{n-1} + b^n \tag{3.8}$$

from equation (3.7) and equation (3.8) respectively, assuming small linearized motions, the equations (3.7) and equation (3.8) become:

$$(p_o + \Delta p_b)\left({V_{bo}}^n + n\left(-zA_e + z_p A_s\right){V_{bo}}^{n-1}\right) = p_o V_{bo}^n \tag{3.9}$$

$$(p_o + \Delta p_r)\left({V_{ro}}^n + n\left(-z_p A_s\right){V^{n-1}}_{ro}\right) = p_o V_{ro}^n \tag{3.10}$$

When we rearrange equation (3.9), we get the following:

$$\frac{\Delta p_b}{p_o} + \left(\frac{\Delta p_b}{p_o} + 1\right)\left(\frac{n\left(-wA_e + z_p A_s\right)}{V_{bo}}\right) = 0 \tag{3.11}$$

To ensure that the air bag maintains the initial pressure for improved comfort and stability while riding.

$$\frac{\Delta p_b}{p_o} \ll 1, \text{ gives } \left(\frac{\Delta p_b}{p_o} + 1\right) \approx 1 \tag{3.12}$$

Then the equation (3.11) becomes

$$\frac{\Delta p_b}{p_o} \approx \frac{n\left(zA_e - z_p A_s\right)}{V_{bo}} \tag{3.13}$$

Also for equation (3.10):

$$\frac{\Delta p_r}{p_o} + \left(\frac{\Delta p_r}{p_o} + 1\right)\left(\frac{n\left(-z_p A_s\right)}{V_{ri}}\right) = 0 \tag{3.14}$$

Because there is a big reservoir volume, any small increase in pressure has no influence on the reservoir pressure $\frac{\Delta p_r}{p_o} \ll 1$. then equation (3.14) becomes

$$\frac{\Delta p_r}{p_o} \approx \left(\frac{n z_p A_s}{V_{ro}}\right) \tag{3.15}$$

It is possible to express the force balance for the piston.

$$F_z = A_e p_b - A_e p_a \tag{3.16}$$

With equation (3.13), it is possible to develop the pressure p_b.

$$p_b = p_0 + \frac{p_0 n\left(zA_e - z_p A_s\right)}{V_{b0}} = p_0\left(1 + \frac{n\left(zA_e - z_p A_s\right)}{V_{b0}}\right) \tag{3.17}$$

equation (3-16) with equation (3-17) become:

$$F_z = p_0 A_e\left(1 + z\frac{nA_e}{V_{b0}} - z_p\frac{nA_s}{V_{b0}}\right) - p_a A_e \tag{3.18}$$

A scaling of the air displacement in the pipe is required to get parameters for the new air spring model. The scaling constant k_{wz} is responsible for this [14], let

$$z_p = k_{wz} w_s \tag{3.19}$$

Substitute in equation(3.19)in (3.18) , add and subtract the $z\frac{nA_e}{V_{b0}}$ and give:

$$F_z = p_0 A_e \left(1 + (z - w_s)\frac{k_{wz} n A_s}{V_{b0}} + z\left(\frac{nA_e}{V_{b0}} - \frac{k_{wz} n A_s}{V_{b0}}\right)\right) - p_a A_e \tag{3.20}$$

The force balance in the pipe is calculated as [15]:

$$m_p \ddot{z}_p = (\Delta p_b - \Delta p_r) A_s - C_a \dot{z}_p^{\beta} \tag{3.21}$$

Where

β : The parameter for viscous damping ($1< \beta <2$).

m_p : The surge pipe's mass (kg).

$\ddot{z}_p$: a surge pipe, the air mass accelerates. (m/sec^2).

$\dot{z}_p$: The air mass velocity in the surge pipe ($m.sec^{-1}$).

Equations (3.13) and (3.15) should be used in place of (3.21):

$$m_p \ddot{z}_p = p_0 A_p n \left(\frac{zA_e - z_p A_s}{V_{b0}} - \frac{z_p A_s}{V_{r0}}\right) - C_a \dot{z}_p{}^{\beta} \tag{3.22}$$

Insert equation (3.19)to (3.22)and multiplying with (K).

$$K.m_p k_{wz} \ddot{w}_s = K p_0 A_s n \left(\frac{A_e}{V_{b0}}\left(z - \frac{V_{b0}}{A_e}\left(\frac{A_s k_{wz}}{V_{b0}} + \frac{A_s k_{wz}}{V_{r0}}\right) w_s\right)\right) - K C_a (k_{wz} \dot{w}_s)^{\beta} \tag{3.23}$$

Compare equation (3.20) with equation (3.23), we put the term which with z_s equal to (1) to compare the factors that with ($z- z_p$) [68].

$$\left.\begin{aligned} \frac{V_{b0}}{A_e}\left(\frac{A_s k_{wz}}{V_{b0}} + \frac{A_p k_{wz}}{V_{r0}}\right) &= 1 \\ p_0 A_e \frac{k_{wz} n A_p}{V_{b0}} &= K p_0 A_s \frac{nA_e}{V_{b0}} \end{aligned}\right\} \tag{3.24}$$

The answer to the above-mentioned equation system is

$$\left.\begin{aligned} K &= k_{wz} \\ k_{wz} &= \frac{A_e}{A_s}\frac{V_{r0}}{(V_{b0}+V_{r0})} \end{aligned}\right) \qquad (3.25)$$

Equation (3.23) can be written using the derived scaling.

$$m_p {k_{wz}}^2 \ddot{w}_s = \frac{p_0 n {A_e}^2}{V_{b0}+V_{r0}}\frac{V_{r0}}{V_{b0}}(z-w_s) - C_a\left(\frac{A_e}{A_s}\frac{V_{r0}}{(V_{b0}+V_{r0})}\right)^{1+\beta}\dot{w}_s^{\beta} \qquad (3.26)$$

Equation is produced when the k_{wz} formula is inserted (3.20)

$$F_z = (p_0 - p_a)A_e + z\left(\frac{p_0 A_e^2 n}{V_{b0}+V_{r0}}\right) + (z-w_s)\frac{p_0 A_e^2 n}{V_{b0}+V_{r0}}\frac{V_{r0}}{V_{b0}} \qquad (3.27)$$

The static load and stiffness constants, k_e and k_v, are identified in the equations above.

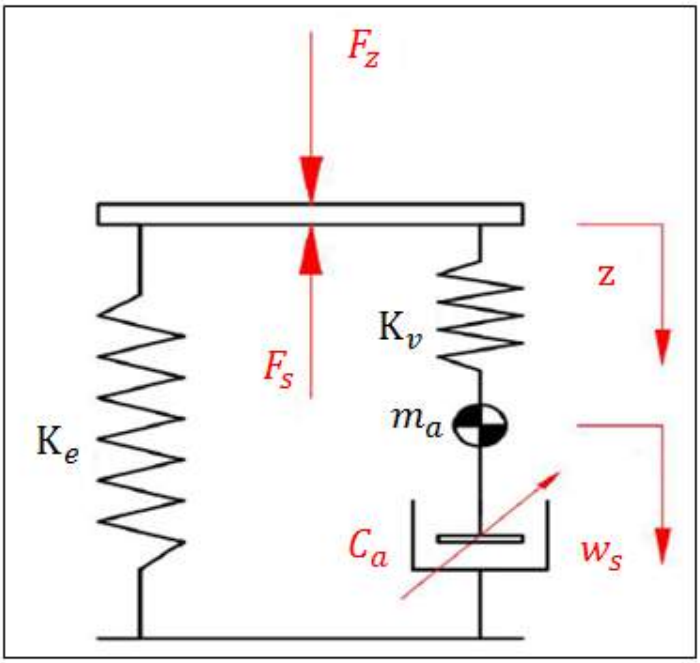

Figure (3-3) GENSYS model [70].

In Figure (3-3), the air spring is equivalent to the oscillation system. The system is made up from two linear springs: the main spring K_e and the auxiliary spring K_v.

$$\left.\begin{aligned} \mathrm{K}_e &= \frac{\mathrm{P_o} n\, \mathrm{A_e^2}}{\mathrm{V_{bo}} + \mathrm{V_{ro}}} \\ \mathrm{K}_v &= \frac{\mathrm{P_o n\, A_e^2}}{\mathrm{V_{bo}} + \mathrm{V_{ro}}} \frac{\mathrm{V_{ro}}}{\mathrm{V_{bo}}} \end{aligned}\right\} \quad (3.28)$$

Friction is created as air passes through the pipes. $\mathrm{C_a}$ nonlinear damping demonstrates this friction process. The initial absolute pressure $\mathrm{P_o}$, the effective area of the spring $\mathrm{A_e}$, the initial volumes of the bag and reservoir $\mathrm{V_{bo}}$ and $\mathrm{V_{ro}}$, and the multivariable coefficient n all influence the stiffness of the main spring K_e. By comparing the initial volume ratios, the stiffness of the auxiliary spring K_v is related to the main spring's stiffness K_e.

The mass m_a can be evaluated from the following :

$$m_a = m_s {k_{wz}}^2 = m_s \left(\frac{A_e}{A_s}\frac{V_{r0}}{V_{b0}+V_{r0}}\right)^2 = l_s A_s \rho \left(\frac{A_e}{A_s}\frac{V_{r0}}{V_{b0}+V_{r0}}\right)^2 \quad (3.29)$$

Instead of the 2D of freedom, this model employs 3D of freedom($\mathrm{Z_s}$, ω_s, and $\mathrm{Z_{us}}$) for three masses ($\mathrm{m_s}$, $\mathrm{m_a}$, and $\mathrm{m_{us}}$) and their directions are shown in the figure(1a) and agreement with[70]. The difficulties in a simulation caused by adopting 3DoF due to the nonlinear viscous damper Ca is linked to the velocity over the damper Ca and not linked to the velocity in the surge of pipe , the vertical viscous nonlinear force is denoted by [16].

$$F_{vz} = K_v(z - w_s) = C_a|\dot{w}_s|^{\beta}\,\mathrm{sign}(\dot{w}_s) + m_a\ddot{w}_s \quad (3.30)$$

The previous equation can be rewritten as:

$$m_a\ddot{w}_s = K_v(z - w_s) - C_a|\dot{w}_s|^{\beta}\,\mathrm{sign}(\dot{w}_s) \quad (3.31)$$

When comparing equation (3.31) to equation(3.26), it is possible to determine the link between the nonlinear damping C_{a} and C_{p}

$$m_a\ddot{w}_s = K_v(z - w_s) - C_a|\dot{w}_s|^{\beta}\mathrm{sign}(\dot{w}_s) = \frac{p_0 A_{\mathrm{p}} n A_e k_{wz}}{V_{b0}}(z - w_s)$$

$$- C_s {k_{wz}}^{1+\beta}|\dot{w}_s|^{\beta}\mathrm{sign}(\dot{w}_s) \quad (3.32)$$

This provides

$$C_{\mathrm{a}} = C_p {k_{wz}}^{1+\beta} = C_{\mathrm{p}} \left(\frac{A_e}{A_{\mathrm{s}}} \frac{V_{r0}}{V_{b0} + V_{r0}}\right)^{1+\beta} \quad (3.33)$$

β : The parameter for viscous damping (1< β<2).

Compressed air is turned to mass m_a in a similar way. Assumed $\beta = 2$.

where

A_e is the airbag's effective area, A_s The cross-section area of the surge pipe, V_{bo} and V_{ro} are the reservoir's and balloon's initial volumes, P_o is the air spring's absolute pressure, P_{at} ambient pressure outside, k_t is the connection pipes' total loss coefficient, l_p length of the connecting pipe and ρ_{air} represents the original density of the air.

The overall pressure loss in a conventional surge pipe results from the fluid's energy being lost as a result of friction with the pipe (major losses).

3.3 Configuration of the Air Suspension System Parameters

The pipe's air mass is propelled forward and backward by the variations between the pressure in the airbag and the reservoir according to the assumptions used in developing the governor equations of motion [2].

There are some presumptions, including:

1. Since there isn't enough time for heat transfer because of the rapid compression and expansion, it may be said that the gas process is isentropic, and airflow in a pipe is regarded to be adiabatic because no heat is added to or removed from the system.
2. The valve's input and output pressure-volume changes are thought to be adiabatic.
3. In a pipe, the air is moved as a single lump of mass.
4. In the reservoir and the air bag, the density value is considered to be average.

3.3.1 Air Flow Equations in the Bag

Figure (3-4) depicts a quarter-car model's schematic with the air spring (Gensys). Compared to traditional air springs, which have a working pressure that is dependent on the static load, the air spring's(Gensys) ability to independently regulate pressure to balance the static load at various heights. The piston can travel up and down, getting closer to the set riding height; the stiffness can then be adjusted at this ride height by adjusting the pressures in the airbag plus reservoir, in order to support the static load, while maintaining the pressure difference in constant.

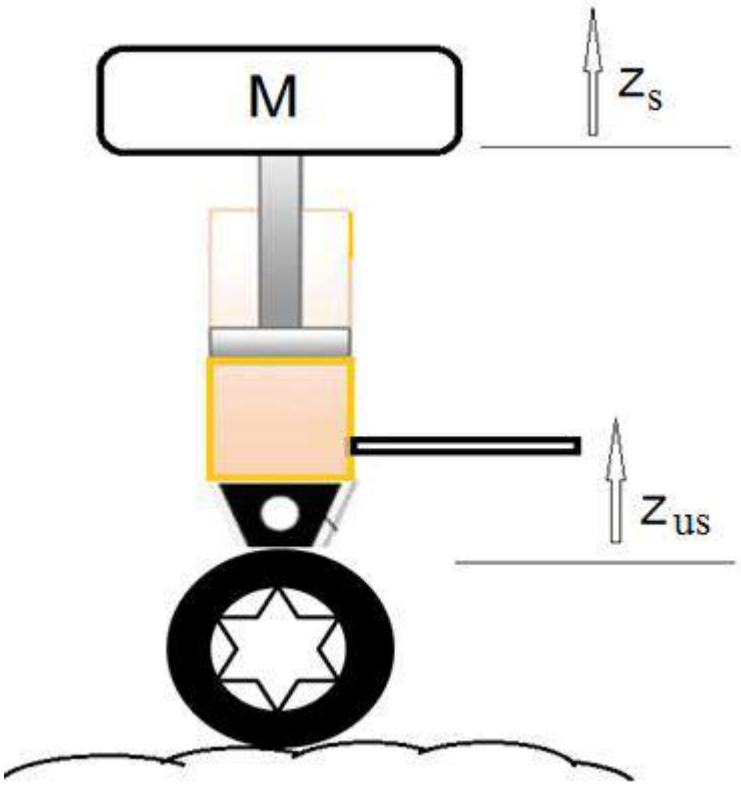

Figure(3-4) Diagram of a quarter-car model with the air spring.

Assuming an isentropic gas process in cylinder chamber, then

$$\frac{P_b}{\rho_b^{\gamma}} = \frac{P_{bo}}{\rho_{bo}^{\gamma}} \tag{3.34}$$

• P_b : The instantaneous gas is represented by the air spring pressure..

• p_{bo} : the initial pressure of the air spring.

• ρ_{bo} : an initial density of the air spring

• ρ : an air spring density represent the instantaneous gas

• γ specific heat for an ideal gas it is defined as (cp/cv);

Ideal gas state equation is

$$P_{bo}v_{bo} = mRT_{bo} \tag{3.35}$$

Where R is the gas constant (J/kg/K).

Combining Equations (3.34) and (3.35), the instantaneous air density is obtained as:

$$\rho_b = \frac{p_{bo}}{R\,T_{bo}}\left(\frac{P_b}{P_{bo}}\right)^{1/\gamma} \tag{3.36}$$

The equation of continuity and the air spring are applying :

$$dm/dt = \sum \dot{m}_i - \sum \dot{m}_e = -\dot{m} \tag{3.37}$$

Where:

$\dot{m}_i$: the airflow on the inlet.

$\dot{m}_e$: the airflow on the outlet.

The sign convension assumes a negative value, hence the negative sign corresponds to it.

$$\dot{m} = -\frac{d(\rho_b V_{b)}}{dt} = -V_b\frac{d\rho_b}{dt} - \rho_b\frac{dV_b}{dt} \tag{3.38}$$

where

$\dot{m}$ is mass flow rate and V_b: an instantaneous gas volume within the cylinder chamber.

Substituting equation (3.36) into Equation (3.38), the mass flow rate is written as:

$$\dot{m}_b = -\frac{1}{\gamma R\,T_{bo}}\left(\frac{P_1}{P_{bo}}\right)^{\left(\frac{1}{\gamma}\right)-1} V_b\dot{P}_b - \frac{P_{bo}}{RT_{bo}}\left(\frac{P_b}{P_{bo}}\right)^{\frac{1}{\gamma}}\dot{V}_b \tag{3.39}$$

Then, the pressure gradient in the chamber of pneumatic cylinder can be obtained from equation (3.39):

$$\dot{\mathrm{P}}_{\mathrm{b}} = -\frac{\gamma R \mathrm{T}_{\mathrm{bo}}}{\mathrm{V}_{\mathrm{b}}} \left(\frac{\mathrm{P}_{\mathrm{b}}}{\mathrm{P}_{\mathrm{bo}}}\right)^{\frac{(\gamma-1)}{\gamma}} \dot{m} - \frac{\gamma \mathrm{P}_{\mathrm{b}}}{\mathrm{V}_{\mathrm{b}}} \dot{\mathrm{V}}_{\mathrm{b}} \tag{3.40}$$

And,

$$\mathrm{T}_{\mathrm{b}} = \mathrm{T}_{\mathrm{bo}} \left(\frac{\mathrm{P}_{\mathrm{bO}}}{\mathrm{P}_{\mathrm{b}}}\right)^{\frac{\gamma-1}{\gamma}} \tag{3.41}$$

The instantaneous volume and volume variation of air bag [7].

$$V_b = V_{bo} + A_b \left(Z_s - Z_{\mathrm{us}}\right) \tag{3.42}$$

$$\dot{V}_b = A_b \left(\dot{Z}_s - \dot{Z}_{\mathrm{us}}\right) \tag{3.43}$$

Where:

Z_{us}: the unsprung mass's vertical displacement.

$\dot{Z}_{us}$: velocity vertical of the unsprung mass.

Z_s: vertical displacement for sprung mass.

$\dot{Z}_s$: the sprung mass's vertical velocity.

3.3.2 Auxiliary Reservoir

In this case the volume V_{ro} is constant, however, the equation of the pressure gradient P_{ro} is simplified and demonstrable. The reservoir model follows the same methodology as the air bag spring. The airflow expression using the continuity equation are write as:

$$\dot{\mathrm{m}} = \frac{\mathrm{d}\left(\rho_{\mathrm{r}} \mathrm{V}_{\mathrm{r}}\right)}{\mathrm{dt}} = \frac{\mathrm{d}\rho_{\mathrm{r}}}{\mathrm{dt}} \mathrm{V}_{\mathrm{r}} \tag{3.44}$$

In this case, positive airflow were noticed and it means that the air enters the auxiliary storage tank.The pressure gradient is indicated by the air density equation and its derivative:

$$\dot{\mathrm{P}}_r = \frac{\gamma \mathrm{R} \mathrm{T}_{\mathrm{ro}}}{\mathrm{V}_{\mathrm{r}}} \left(\frac{\mathrm{p}_{\mathrm{r}}}{\mathrm{p}_{\mathrm{ro}}}\right)^{\frac{\gamma-1}{\gamma}} \dot{\mathrm{m}}_r \tag{3.45}$$

3.3.3 The Orifice of Valve(Flow restriction of fixed area)

The mass flow rate into the valve through one port must thus match the mass flow rate out of the valve through the other port, according to the principle of mass conservation. To give damping to the air suspension system, a flexible area of orifice is employed to modulate the mass flow rate of air between the reservoir and the air bag when the fluid reaches a restriction in the opening because of the pressure differnce [2]. The orifice of air spring-to-auxiliary connection is modeled in accordance with ISO 6358-3[71] as a Constant Area Pneumatic Orifice, Considering an ideal gas flow rate through a sharp-edged orifice fixed-area.

The mass flow rate via the resistive element in a constricted flow is computed as:

Using total energy conservation (kinetic +potential+ pressure).

From equation(3.39) the mass flow rate of gas from the air bag to the reservoir is given by $\dot{m}_b$and equation (3.45) $\dot{m}_r$the mass flow rate of gas from the reservoir to air bag, i.e $\dot{m}_r = -\dot{m}_b$.

The temperature and pressure of the air within the spring chambers and the reservoir are initially similar, resulting in:

$T_{ro} = T_{bo} = T_o$.

$P_{ro} = P_{ro} = P_o$.

Figure(3-5) shows the air flow via the orifice from upstream into downstream. The orifice model is calculated using fluid dynamics theory [72],[73].

$$\dot{m}_u = -C_d\, A_o \emptyset\,(b) \sqrt{\frac{P_{uo}^{\frac{n-1}{n}}}{R\, T_{u0}}} \quad \sqrt{P_u^{\frac{n-1}{n}}} \qquad (3.46)$$

where

subscript (u) refers to upstream.

subscript (d) refers to downstream.

C_d: the discharge coefficient.

A_o: The effective orifice area.

b : the ratio of pressure, $b = \frac{P_d}{P_u}$.

If $P_b > P_r$, the cylinder chamber side is upstream, and the reservoir side is downstream, i.e $\dot{m}_u = \dot{m}_b$.

$P_u = P_b$, $P_d = P_r$, $P_{uo} = P_{bo}$ and $T_{uo} = T_{bo}$

If $P_b < P_r$, the cylinder chamber side is downstream, and the reservoir side is Upstream, i.e $\dot{m}_u = \dot{m}_r$.

$P_u = P_r$, $P_d = P_b$, $P_{uo} = P_{ro}$ and $T_{uo} = T_{ro}$.

Flow-in is represented by a positive sign, whereas flow-out is represented by a negative sign.

$\emptyset$(bi) is a flow function that is defined as [7].

$$\emptyset(bi) = \begin{cases} \sqrt{\left(\frac{2n}{n-1}\right)\left(b^{2/n} - b^{(n+1)/n}\right)} & for\ b \geq 0.528 \\ \sqrt{\frac{(2n)}{n+1}}\left(\frac{2}{n+1}\right)^{1/n-1} & for\ b < 0.528 \end{cases} \quad (3.47)$$

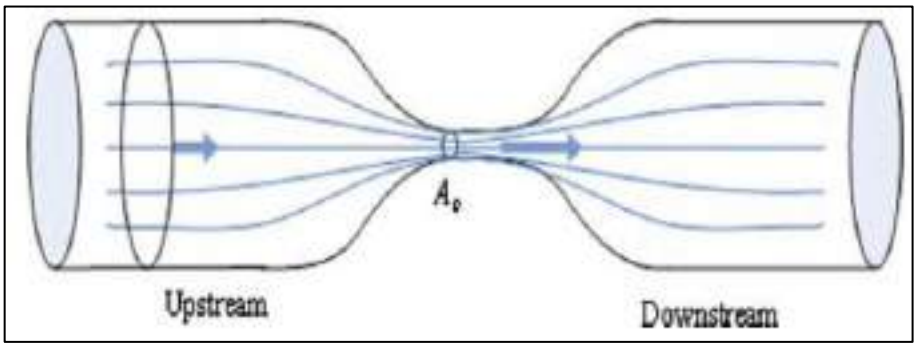

Figure (3-5).orifice air flow [7].

3.3.4 Determining the Damping Parameters

The fluid's loss of energy results in a typical pressure drop total connecting the pipeline induced by pipe friction, When there is a sudden change in section, the flow direction can alter, creating turbulent eddies. The rapid expansions and contractions that occur when the airbag and reservoir join the flow tube, tube friction and the number of tube bends are the sources of this wasted energy. The total loss coefficient so has the following components [14]:

Considering the surge pipe's flow to be steady and incompressible

$$\Delta p_b - \Delta p_r = \rho_0 w_f = \rho_0 \frac{1}{2} k_t \dot{z}_{\mathrm{p}}^2 \tag{3.48}$$

where

w_f : the work done due to pipe surge losses (J.kg^{-1}).

ρ_0 : the equilibrium air density (kg/m^3).

k_t : the total loss coefficients measured inside the surge pipe.

$\dot{z}_{\mathrm{p}}$: surge pipe's average speed in meter per second.

Along the pipe's length, there is a force of

$$\Delta F = A_{\mathrm{p}}(\Delta p_b - \Delta p_r) = \frac{1}{2} A_s \rho_o C_a \dot{z}_{\mathrm{p}}^2 \tag{3.49}$$

ρ_o : following deflection, air density is at equilibrium.

ΔF : the force variation along the pipe's length

The equation of state for an ideal gas can be used to obtain air density at equilibrium

$$\rho_0 = \frac{p_0}{RT} \tag{3.50}$$

The following components sum up the overall loss coefficient:

$$k_t = k_{fr} + k_c + k_b + k_{en} \tag{3.51}$$

where

k_{fr} : the frictional loss factor

k_c : the loss factor resulting from contraction

k_b : the loss factor resulting from pipe bends

k_{en}: the enlargement loss coefficient

The work done as a result of friction in the flow tube can be found [14].

$$W_f = \frac{1}{2}\frac{L_p f}{d_p}\dot{z}_p^2 \tag{3.52}$$

$$k_{fr} = \frac{L_s f}{d_p} \tag{3.53}$$

L_p : the length of the surge pipe (m)

f : the coefficient of friction

d_p : the diameter of the surge pipe (m)

Reynolds number influences the friction coefficient (Re), and the Moody diagram can be used to determine the relative roughness (r/d_p) from Appendix-B or simply from the following equation (3.54). Roughness value (r) for new steel pipes may be approximately 0.025 mm, pipe friction [14].

$$f = \frac{0.25}{\left(\log\left(\frac{r}{3.7d_p} + \frac{5.74}{Re^{0.9}}\right)\right)^2} \tag{3.54}$$

Where Reynolds number

$$R_e = \frac{\rho\, \dot{z}_p d_p}{\mu} \tag{3.55}$$

3.4 Active Suspension System with Hydraulic Actuators

Active suspension can be obtained by adding a part to the passive system, adding an actuator or controlling the air spring pressure. System hydraulics are commonly used in high-performance applications requiring quick reaction and tremendous power. High-bandwidth control of position and force is one of these applications. Actuators utilized in the active suspension system must fulfill certain performance requirements. Reasonable cost, excellent dependability, simple and inexpensive maintenance, strong input and output performance. Addition to, an actuators have a wide variety of applications in production systems, machines for material testing, machinery for injection molding, milling equipment for steel with aluminum, etc. Electric pumps do these tasks, but not at the level of the hydraulic servo system, because the latter offers greater forces and higher efficiency. Additionally, electrohydraulic servo actuators are frequently utilized in industrial applications since they have a high lifting force, a high power/volume ratio, and are resistant to environmental influences. The control valve and the spool shape, as well as their manufacturing tolerances, have a significant impact on hydraulic system performance [74].

3.4.1 Advantage and Disadvantage the Hydraulic Actuator Compared to the Pneumatic Actuator

1. The efficiency of the hydraulic actuator is higher than that of the pneumatic actuator because of the ability to control in a frequency range up to about (10Hz) compared to (2–3 Hz) for pneumatic actuator [75].
2. The possibility of oil leakage is the most significant disadvantage of hydraulic actuators.
3. Hydraulic systems include a number of non-linear effects that might make the control task more difficult.
4. Purchasing pneumatic actuators is less costly than purchasing hydraulic [75].

5. If the power required is considerable, it is advisable to utilize a hydraulic system when comparing pneumatic and hydraulic actuators.
6. Hydraulic cylinders require regular maintenance and care in order to function properly compared to the pneumatic actuator.
7. Hydraulics are stronger than pneumatics when it comes to durability.

3.4.2 Nonlinear Hydraulic Actuator Model

Hydraulic actuators are linked in parallel to the necessary suspension springs and dampers to produce a force and placed between the vehicle body and wheel assembly.

To get a better understanding of the suspension system's performance and to create a reliable controller for it, the development of an accurate dynamic model for the hydraulic servo system is essential, as a result, a description of the parts subsystem's dynamics is required. Due to the large reservoir of the fluid, the effects of temperature on the dynamic merits of the active system are neglected in fluid dynamics(the driving fluid functions as a cooling medium, moving heat away from the actuator and flow control components, making it self-cooling). An actuator force is generated by a pressure differential between the two chambers of the actuator cylinder.

As illustrated in Figure(3-6), a full hydraulic actuator set consists of five basic components: an electro hydraulic driven spool valve, a piston-cylinder, a reservoir, a hydraulic pump and a pipe system. A piston is controlled by a voltage signal supplied to the servo-valve in an electro-hydraulic system.
Figure (3-7) depicts a hydraulic actuator physical model with a nonlinear air spring model.

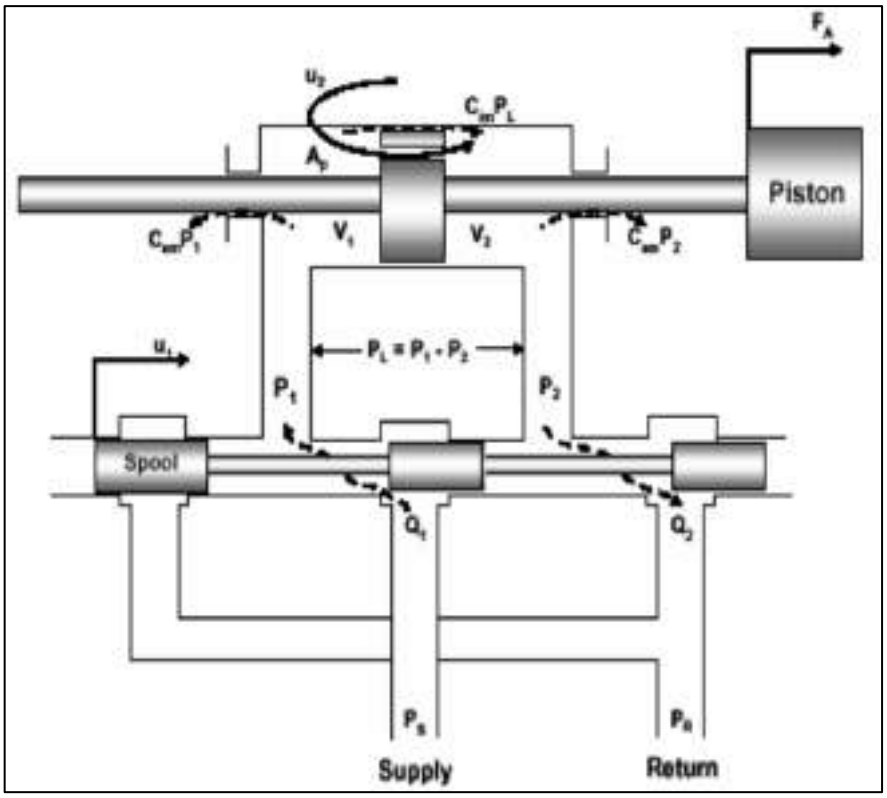

Figure (3-6) The hydraulic actuator's physical schematic and variables [76].

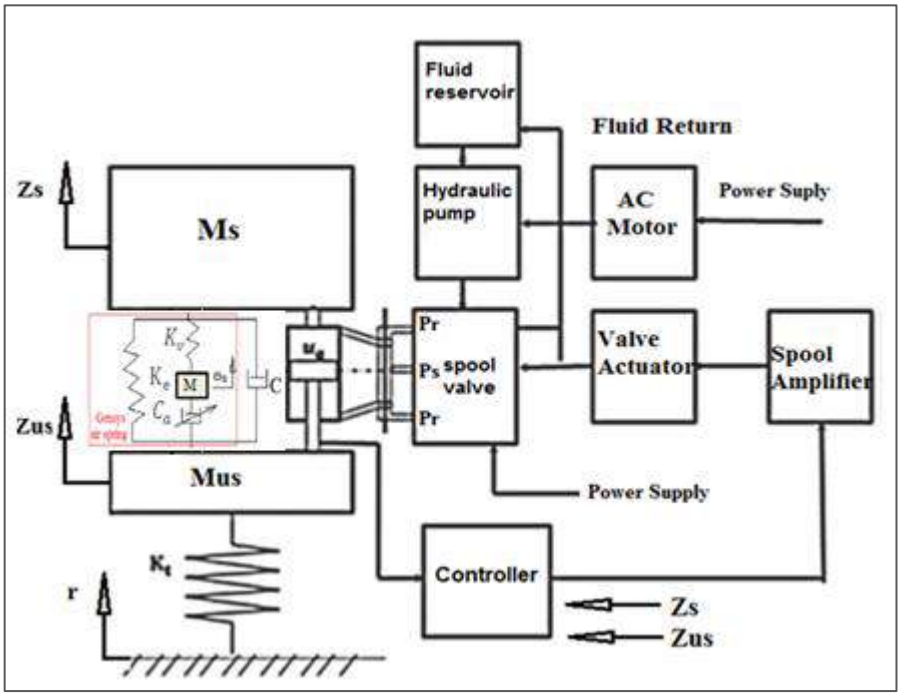

Figure (3-7) A physical model of hydraulic actuators as a whole set and a nonlinear suspension system.

The spool's principal function is to travel within the enclosed box and open and close these ports based on the spool's position. Spool valve can be driven by a solenoid and spool controlling position permits a flow of liquid to be sent from the source to any of the cylinder's chambers and removed from another chamber to the oil reservoir.

3.4.3 Turbulent Flow Orifice Equations

In order to derive the excitation equations, it is necessary to understand the flow effects via orifices in the control design of many hydraulic systems.

This region is crucial because most orifice flows happen at high Reynolds numbers. Orifices are simply holes which restrict the flow of fluid through variable or permanent region. The term "turbulent" is frequently used to describe such flows (Figure 3.2b),

Orifices are being used to reduce pressure or enhance the velocity of fluid flow. As shown in Figure, two types of flow systems. The flow through an orifice is shown in Figure (3-8) .

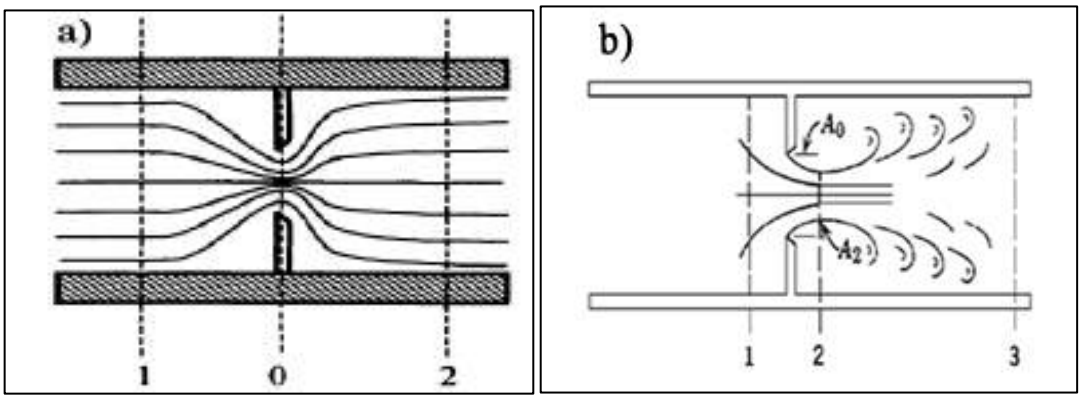

Figure (3-8) Fluid flows via orifice(a) laminar of flow; (b) turbulent of flow [77].

From Figure(3.2b) shown, sections 1and 2, the fluid's velocity is boosted from its upstream velocity to its jet velocity justified the utilize the Bernoulli's equation in this areas. The region of the jet is less than the region of the orifice because the fluid particles have inertia and move in a path curve at the orifice so

the particles of flow have inertia and proceed in a path curve at the orifice and the region (A_2) referred to as "the vena contracta" and (A_o) is orifice area [77].

$$A_2=C_cA_o \tag{3.56}$$

Where c_o is the coefficient of contraction.

In the case of incompressible fluids, ρ = const

The upstream velocity and jet velocity connection may be stated as follows using the continuity equation. ρ = const.

$$A_1V_1 = A_2V_2 \tag{3.57}$$

Generally

$$Q = VA = \text{constant (flow of volume)} \tag{3.58}$$

The difference in pressure necessary to accelerate fluid particles from upstream to jet pressure may be calculated as follows:

$$V_2^2 - V_1^2 = \frac{2}{\rho}(P_1 - P_2) \tag{3.59}$$

Substitute equation (3.4) in (3.2) and V_2 can be written in the following way:

$$V_2 = \left[1 - \left(\frac{A_2}{A_1}\right)^2\right]^{-1/2} \sqrt{\frac{2}{\rho}(P_1 - P_2)} \tag{3.60}$$

V_2 is somewhat less than that provided in equation (3.4) due to viscous friction. As a result, the velocity coefficient C_v can be taken into consideration.

By substituting eqs (3.1) and (3.5) in (3.3) The flow rate may be expressed in the following:

$$Q = \frac{C_vC_cA_0}{\sqrt{1 - \left(\frac{A_2}{A_1}\right)^2}} \sqrt{\frac{2}{\rho}(P_1 - P_2)} \tag{3.61}$$

$\frac{C_v C_c A_0}{\sqrt{1-\left(\frac{A_2}{A_1}\right)^2}}$ can be represent the coefficient of discharge (C_d)

Equation (3.61) can be write as

$$Q = C_d A_0 \sqrt{\frac{2}{\rho}(P_1 - P_2)} \tag{3.62}$$

3.4.4 Coefficient of Discharge for Turbulent Flow

Orifices (Sharp-edged) as shown in Figure(3.9) are preferred because of their known properties and temperature insensitivity. Cost typically prevents their employment, especially as permanent restrictors, and orifices of length Figure(3.3a) are used instead [78]. For short tube orifices, the average coefficient of discharge is as follow [77]

$$C_{\mathrm{d}} = \left(2.28 + 64\frac{2L}{d_0 d}\right)^{-1/2} \quad \text{for } \frac{d_0 d}{2L} \leq 50$$
$$C_{\mathrm{d}} = \left[1.5 + 13.74\left(\frac{2L}{d_0 d}\right)^{1/2}\right]^{-1/2} \quad \text{for } \frac{d_0 d}{2L} > 50 \tag{3.63}$$

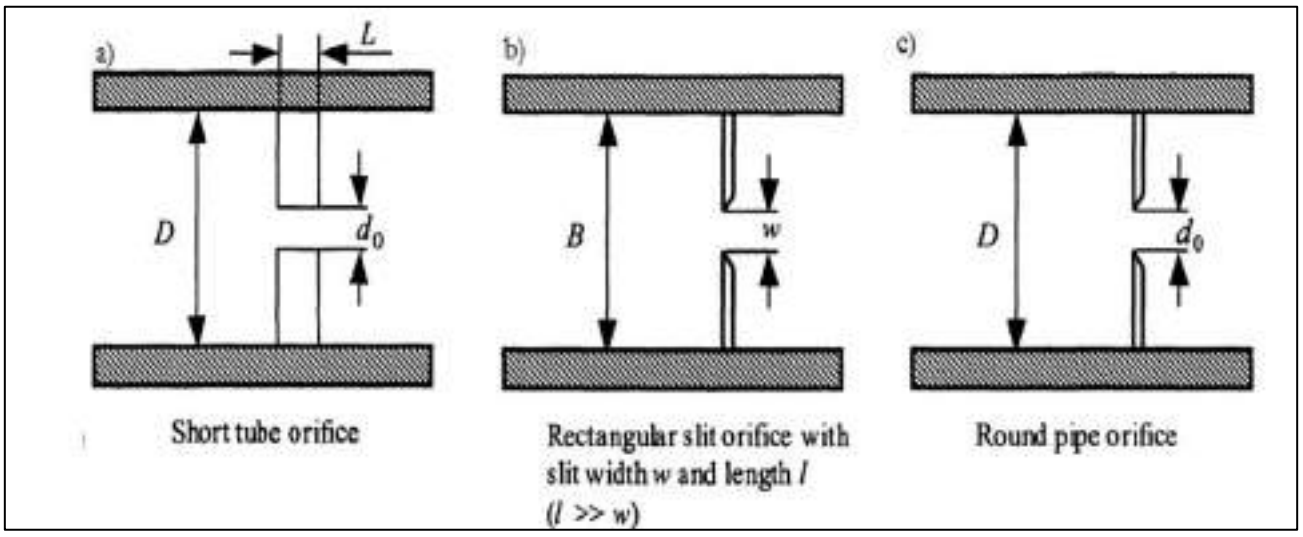

Figure (3-9) Short , slit-type and round tube orifices [77].

3.4.5 Analogy of Electro-Hydraulics

An electro-hydraulic analogy concepts are summarized in Figure (3.10)

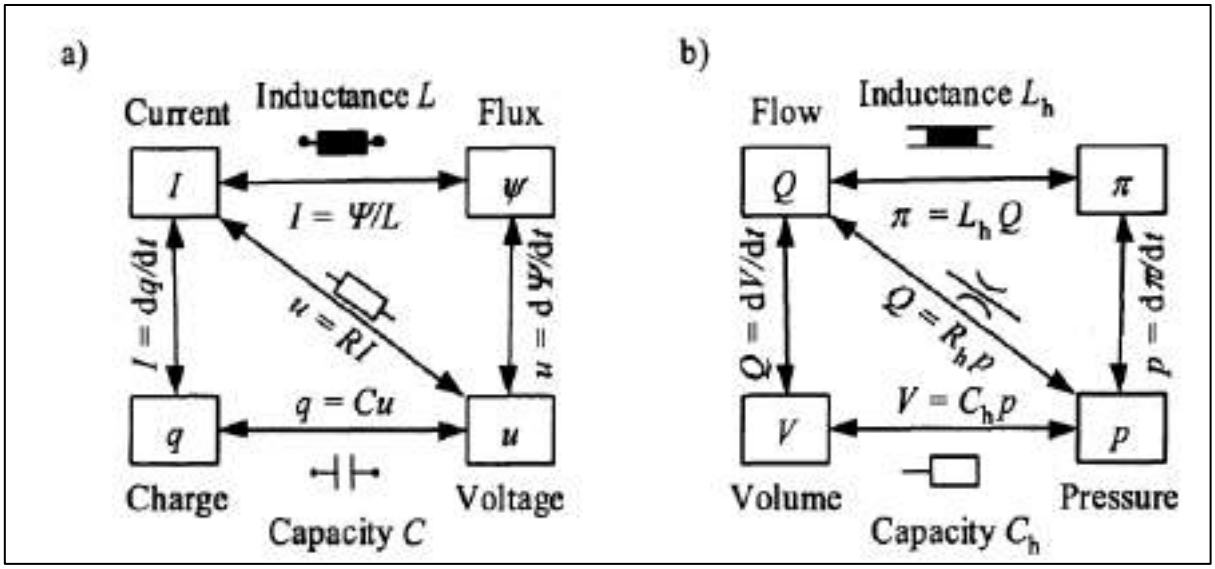

Figure (3-10) Variable relationship in (a) electrical, (b) hydraulic systems [79].

In this section the Analogy of electro-hydraulics (three land four-way spool) with Wheatstone bridge (four-armed) shown in Figure (3-11) [77]. This analogy is frequently used to visualize valve action. For the two valve chambers' continuity equations are:

$$Q_L = Q_1 - Q_4 \tag{3.64}$$

$$Q_L = Q_3 - Q_2 \tag{3.65}$$

And the pressure changes over the load are calculated using the equation below.

$$P_L = P_1 - P_2 \tag{3.66}$$

a)

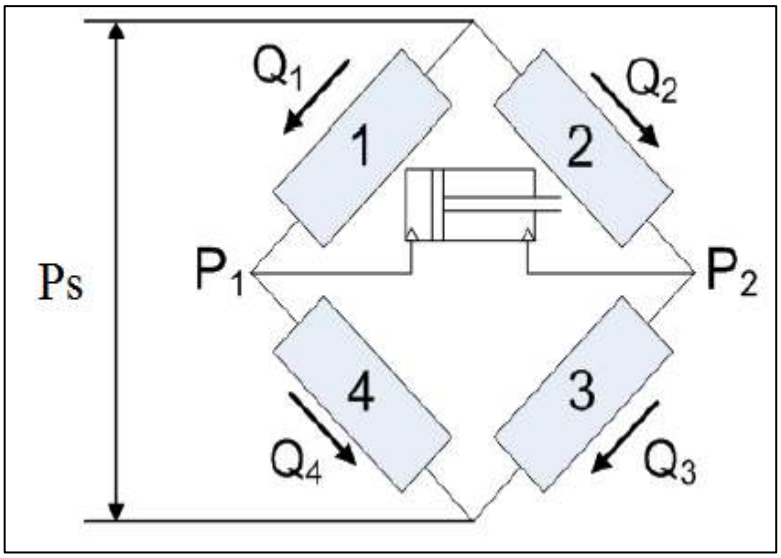

b)

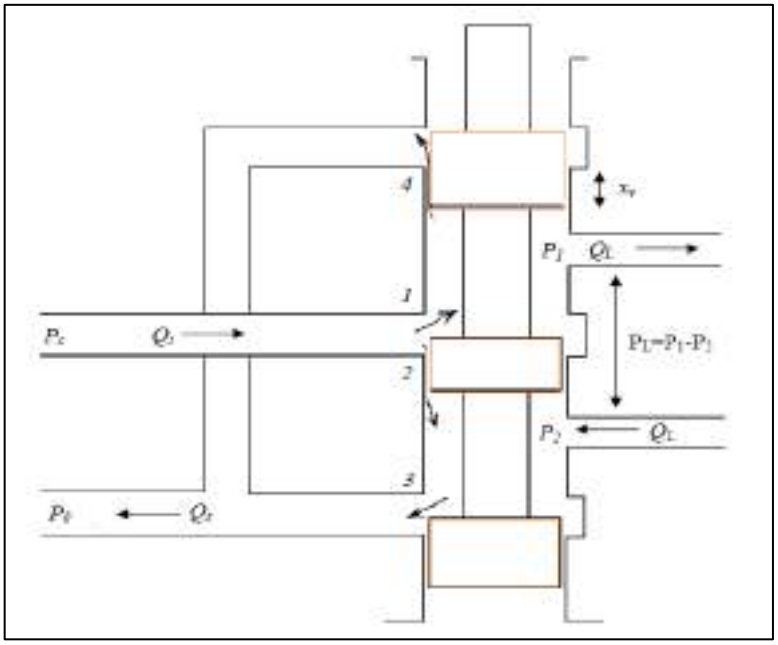

Figure (3-11) a)Wheatstone's bridge, b) Three-land-four-way, spool valve [80].

The arrows of the ports show the flow direction, while the numbers at the ports indicate the valve orifices. by Ignoring the valve's leaking, The following equations explain the flow via the valve orifices.

$$Q_1 = c_d A_1 \sqrt{\frac{2}{\rho}(P_s - P_1)} \tag{3.67}$$

$$Q_2 = c_d A_2 \sqrt{\frac{2}{\rho}(P_s - P_2)} \tag{3.68}$$

$$Q_3 = c_d A_3 \sqrt{\frac{2}{\rho}(P_2 - P_o)} \tag{3.69}$$

$$Q_4 = c_d A_4 \sqrt{\frac{2}{\rho}(P_1 - P_o)} \tag{3.70}$$

Where

P_o: the pressure of the return, and $P_o \approx 0$ due to much smaller.

P_s: the pressure of supply.

P_1: the chamber -one pressure.

P_2:the chamber -two pressure.

$A_{1,2,3,4}$: the orifice areas, It is a function of the spool valve's movement x_v.

In particular, The orifices of the valves are symmetrical and matched. Matching orifices necessitates:

$$A_1(x_v) = A_3(x_v)$$
$$A_2(x_v) = A_4(x_v) \tag{3.71}$$

Symmetrical orifices necessitate the use of :

$$A_1(x_v) = A_3(-x_v)$$
$$A_3(\mathrm{x}_v) = A_4(-\mathrm{x}_v) \tag{3.72}$$

The load flow a function that depends on the valve's position and the load's pressure as:

$$Q_L = Q_L(x_v, P_L) \tag{3.73}$$

The flow rates in the Wheatstone bridge's diagonally opposing arms are equal.

$$Q_1 = Q_3 \tag{3.74}$$

$$Q_2 = Q_4 \tag{3.75}$$

Equations (3.67),(3.69),(3.72) into (3.74), the supply line pressure is determined by the equation below.

$$P_S = P_1 + P_2 \tag{3.76}$$

Similarly, equations (3.66),(3.68),(3.72) into ($Q_2 = Q_4$), to obtain

$$\mathrm{P}_1 = \frac{P_S - \mathrm{P}_L}{2} \tag{3.77}$$

$$\mathrm{P}_2 = \frac{\mathrm{P}_S - \mathrm{P}_L}{2} \tag{3.78}$$

For symmetrical and matched valve and no load i.e., (P_L=0), the pressure in each motor line is (Ps/2).When the load is applied, the pressure in each line increases while the pressure in the other line decreases by an equal amount. Because the pressure drops via orifices 1 and 3 are comparable, and the areas are likewise the same, equation (3.74) is fulfilled. For the same approach may be used to prove the correctness of equation (3.75). Using the Figure as a guide (3-11):

$$Q_s = Q_1 + Q_2 \tag{3.79}$$

$$Q_s = Q_3 + Q_4 \tag{3.80}$$

In summary, the equations (3.64) and (3.65) combined may be used for the symmetrical and matching valve ((3.74), (3.75), (3.77), and (3.78).

$$Q_L = C_d A_1 \sqrt{\frac{1}{\rho}(P_s - P_L)} - C_d A_2 \sqrt{\frac{1}{\rho}(P_s + P_L)} \tag{3.81}$$

In the same way, for equations (3.79) and (3.80) :

$$Q_s = C_d A_1 \sqrt{\frac{1}{\rho}(P_s - P_L)} + C_d A_2 \sqrt{\frac{1}{\rho}(P_s + P_L)} \quad (3.82)$$

By making the assumption that the critical the geometry of the central valve is perfect, which means that the orifice's edges are exactly square and there is no rounding, as a result of the leakage flows at section 2 and section 4 (Q2 and Q4) are zero when x_v is positive, the flow of leakage at section 1 and section 3(Q1 and Q3) are zero when x_v is negative.

As a result, the new formulation for the equations can be obtained by the equations (3.64) and (3.67) into (3.77) to get

$$Q_L = C_d A_1 \sqrt{\frac{2}{\rho}\left(\frac{P_s - P_L}{2}\right)}, \text{ for } (x_v > 0) \quad (3.83)$$

For the valve's negative displacement (Q_L=−$Q4$), the equations ((3.70) and (3.77) into(3.65) give:

$$Q_L = -C_d A_1 \sqrt{\frac{2}{\rho}\left(\frac{P_S + P_L}{2}\right)} \text{ for } x_v < 0 \quad (3.84)$$

As a symmetrical valve, as seen below, the equations ((3.83) and (3.84) may be combined for a single equation:

$$Q_L = C_d |A_1| \frac{x_v}{|x_v|} \sqrt{\frac{1}{\rho}(P_S - \text{sgn}(x_v) P_L)} \quad (3.85)$$

A sigmoid function is referred to as $\text{sgn}(x_v) = \begin{cases} 1 & for\ x_v > 0 \\ -1 & for\ x_v < 0 \end{cases}$

$$Q_L = C_d x_v \omega \sqrt{\frac{1}{\rho}(P_s - \text{sgn}(x_v) P_L)} \quad (3.86)$$

Where $\omega = \left|\frac{A_1}{x_v}\right|$ indicates the gradient region.

3.4.6 The Valve-Piston Control System

The piston's up and down motions are determined by a solenoid connected to the electro valve, which dispenses the spool valve according to the control signal in voltage. By raising the electro valve's positive input voltage, the oil flowing from a pump to the cylinder's first chamber and the pressure level rises and guides the piston's upward movement as its velocity rises. When there is a negative voltage, the piston's downward movement is determined by the pressure increasing in the cylinder's second chamber [74].

The hydraulic actuator model. The orifices of the spool valve are considered to be matched and identical, therefore the continuity equation may be written as [81].

$$\sum Q_{\text{in}} - \sum Q_{\text{out}} = \frac{dV}{dt} + \frac{V}{\beta_e}\frac{dP}{dt} \tag{3.87}$$

When Eq. (3.32) is applied to each of the piston chambers, the conclusion is:

$$Q_1 - C_{ip}P_L - C_{ep}P_1 = \frac{dV_1}{dt} + \frac{V_1}{\beta_e}\frac{dP_1}{dt} \tag{3.88}$$

$$C_{ip}P_L - C_{ep}P_2 - Q_2 = \frac{dV_2}{dt} + \frac{V_2}{\beta_e}\frac{dP_2}{dt} \tag{3.89}$$

Where

V_1 : supply chamber volume.

V_2 : return chamber volume.

P_1 : supply chamber's pressure.

P_2 : return chamber pressure

C_{ip}: piston's interior leakage coefficient.

C_{ep}: piston's exterior leakage coefficient

β_e : system's effective bulk modulus.

The piston chamber volumes can be expressed as:

$$V_1 = V_{01} + A_p x_p \tag{3.90}$$

$$V_2 = V_{02} - A_p x_p \tag{3.91}$$

Where

A_p : piston's cross-sectional area.

x_p : the piston's inside-cylinder displacement.

V_{01} : supply chamber's initial volume.

V_{01} : initial return chamber volume.

The volumes in total remains constant regardless of the piston's position inside of the cylinder.

As a result, the total volume (V_t) of the fluid compressed in both chambers may be calculated as follows:

$$V_t = V_1 + V_2 = V_{01} + V_{02} \tag{3.92}$$

The following equation can be used to control the flow rate via the load (i.e. piston):

$$Q_L = \frac{Q_1 + Q_2}{2} \tag{3.93}$$

Substituting Eq. (3.90) in (3.88) yields:

$$Q_1 - C_{ip}P_L - C_{ep}P_1 = A_p\dot{x}_p + \frac{V_1}{\beta_e}\frac{dP_1}{dt} \tag{3.94}$$

In addition, substituting Eq. (3.91) into (3.89) produces

$$C_{ip}P_L - C_{ep}P_2 - Q_2 = \frac{V_2}{\beta_e}\frac{dP_2}{dt} - A_p\dot{x}_p \tag{3.95}$$

Eqs. (3.94) and (2.95) are substituted in (3.93) to produce:

$$2Q_L = 2A_p\dot{x}_p + 2C_{ip}P_L + \frac{V_1}{\beta_e}\frac{dP_1}{dt} - \frac{V_2}{\beta_e}\frac{dP_2}{dt} + C_{ep}P_1 - C_{ep}P_2 \tag{3.96}$$

By substituting Eq. (3.66) for (3.96), we get

$$Q_L = A_p\dot{x}_p + C_{tp}P_L + \frac{V_t}{4\beta_e}\dot{P}_L \tag{3.97}$$

Where $C_{tp} = C_p + \frac{C_{ep}}{2}$ the piston's overall leakage coefficient, and made assumptions consist of the following: $\sigma = \frac{4\beta_e}{V_t}$ and $\beta = \sigma C_{tp}$, It's possible to rewrite eq. (3.97) as:

$$\dot{P}_L = -\beta P_L - \sigma A_p \dot{x}_p + \sigma Q_L \quad (3.98)$$

The servo valve's spool displacement dynamic equation x_v, and the voltage signal (u_m) supplied to the servovalve controls it.

The equation of dynamic for the spool valve displacement , which is determined using a linear filter in a fixed time (τ), and the gain of conversion (K_c) is:

$$\dot{x}_v = \frac{1}{\tau}(K_c u_m - x_v) \quad (3.99)$$

$$F_h = A_p P_L \quad (3.100)$$

In this study, the nonlinear friction force resulting from the actuator's piston seals rubbing against the cylinder wall was taken into consideration. As a result, the force supplied by the hydraulic actuator not equal to the force actually created by the hydraulic actuator.

Fraction force F_f is the term given to the difference between these two forces [82].

$$F_f = \begin{cases} \kappa \mathrm{sgn}(\dot{z}_s - \dot{z}_{us}) & \text{if } |\dot{z}_s - \dot{z}_{us}| > 0.01 \\ \kappa \sin\left(\frac{\dot{z}_s - \dot{z}_{us}}{0.01}\frac{\pi}{2}\right) & \text{if } |\dot{z}_s - \dot{z}_{us}| < 0.01 \end{cases} \quad (3.101)$$

The hydraulic actuator's force can be expressed as

where F_h is the actuator's nonlinear hydraulic force and F_f is the force created when the piston seals inside the actuator rub against the cylinder wall. The relationship between the actuator's output force, F_h, and the spool valve velocity $\dot{x}_v$ exhibits a nonlinear dynamic behavior [77].

3.5 Mathematical Modeling of Active Suspension System for Quarter Car

A quarter-car active suspension system's primary parts are two masses (sprung mass and unsprung mass). Additionally, the hydraulic actuator, primary damper, and air spring are linked in parallel. When the suspension encounters a bump, the spring absorbs the shock and stores the shock's energy. The damper is utilized to release the vibration's energy (road profile), by supporting the whole suspension system, the hydraulic actuator is employed to control the suspension to improve riding comfort (by F_h is the force used in the suspension system to minimize the vertical motion brought on by the input of road roughness). The tire is modeled as a highly stiffness spring and a damper as depicted in Figure(3-12).

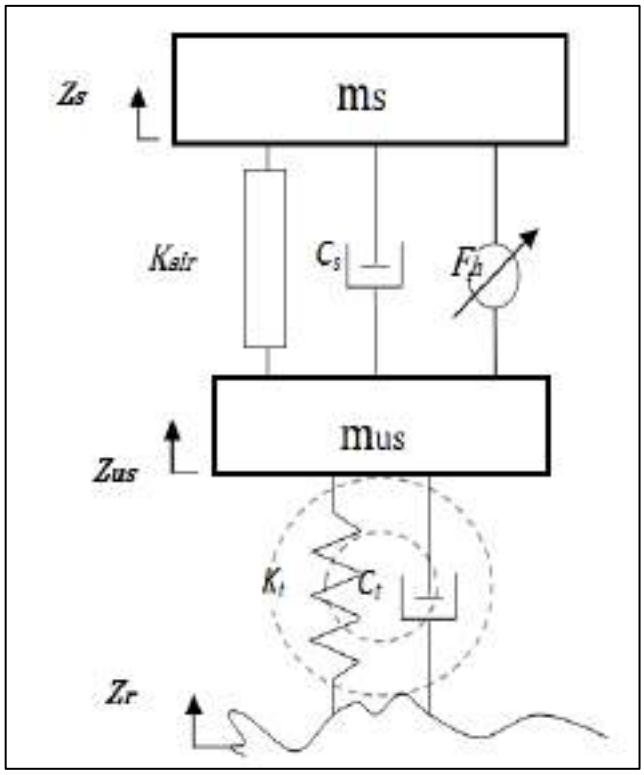

Figure(3-12) The Quarter-car pneumatic active suspension.

The formulation of the motion equations is:

$$m_s\ddot{Z}_s + K_{air}(Z_s - Z_{us}) + C_s(\dot{Z}_s - \dot{Z}_u) - F_h = 0 \qquad (3.102)$$

$$m_{us}\ddot{Z}_u + K_t(Z_u - Z_r) + C_t(\dot{Z}_u - \dot{Z}_r) - K_{air}(Z_s - Z_{us}) - C_s(\dot{Z}_s - \dot{Z_{us}}) + F_h = 0 \quad (3.103)$$

We obtain from equations (3.97) ,(3.98), and (3.100).

$$\dot{P}_L = -\beta P_L - \sigma A_p \dot{x_p} + \sigma C_d w x_v \sqrt{\frac{1}{\rho}(P_{sup} - sgn(x_v)P_L} \quad (3.104)$$

where $\gamma_s = \sigma C_{di} w$

where x_p depicts the difference in vertical displacement between sprung mass and unsprung mass and equal to $Z_s - Z_u$.

from equation (3.100), by making the following assumptions:

$x_1 = (Z_s - Z_u)$

$x_2 = \dot{Z}_s$

$x_3 = (Z_{us} - Z_r)$

$x_4 = \dot{Z_{us}}$

$x_5 = P_L$

$x_6 = x_v$

Taking the state variables utilizing the aforementioned assumptions:

$$\dot{x_1} = x_2 - x_4 \quad (3.105)$$

$$\dot{x_3} = x_4 - \dot{Z}_r \quad (3.106)$$

$$\dot{x_4} = \frac{K_{air}}{M_u}x_1 + \frac{C_s}{M_u}x_2 - \frac{K_t}{M_u}x_3 - \frac{C_t + C_s}{M_u}x_4 - \frac{A_p}{M_u}x_5 + \frac{C_t}{M_u}\dot{Z}_r \quad (3.107)$$

$$\dot{x_5} = -\sigma A_p x_2 + \sigma A_p x_4 - \beta x_5 + \gamma_s x_6 \sqrt{\frac{1}{\rho}(P_{sup} - x_5 sgn x_6)} \quad (3.108)$$

$$\dot{x_6} = -\frac{1}{\tau}x_6 + \frac{1}{\tau}u_m \quad (3.109)$$

For a quarter-car active suspension , the state space equations are [83, 84, 85, 86].

$$\dot{X} = AX + B\dot{r} + Cu_m$$

where:

$$A = \begin{bmatrix} 0 & 1 & 0 & -1 & 0 & 0 \\ -\frac{K_{air}}{M_s} & -\frac{C_s}{M_s} & 0 & \frac{C_s}{M_s} & \frac{A_p}{M_s} & 0 \\ 0 & 0 & 0 & 1 & 0 & 0 \\ \frac{K_{air}}{M_{us}} & -\frac{C_s}{M_u} & -\frac{K_t}{M_u} & -\frac{C_t+C_s}{M_u} & \frac{A_p}{M_u} & 0 \\ 0 & -\sigma A_p & 0 & \sigma A_p & \beta & \gamma_s\sqrt{(P_s - x_5 sgn x_6)} \\ 0 & 0 & 0 & 0 & 0 & \frac{1}{\tau} \end{bmatrix}$$

$$B = \begin{bmatrix} 0 \\ 0 \\ -1 \\ \frac{C_t}{M_u} \\ 0 \\ 0 \end{bmatrix}$$

$$C = \begin{bmatrix} 0 \\ 0 \\ 0 \\ 0 \\ 0 \\ \frac{1}{\tau} \end{bmatrix}$$

The two following tables provide a list of the parameters utilized in the simulation block [70, 84].

Table (3-1) The hydraulic actuator's physical parameters[80]

Symbol	**Description**	**Value**	**Unit**
σ	Actuator coefficient	4.515×10^{13}	N/m^5
β	effective bulk modulus of hydraulic system	1	Sec^{-1}
γ_s	Actuator coefficient	1.545×10^9	$N/m^{5/2}kg^{1/2}$
P_{sup}	Pressure supply	10.3425×10^6	Pa
A_p	Piston cross section	3.35×10^{-4}	m^2
τ	Time coefficient	1/30	sec
K_c	Servo valve gain	0.001	m/v

Table (3-2)the quarter vehicle's specific specifications[34].

Symbol	Description	Value	Unit
M_s	sprung mass	400	kg
M_{us}	unsprung mass	40	kg
C	Damping coefficient	3000	N_s/m
K_t	Tire stiffness	180000	N/m
A_e	Effective area of the airbag	0.002	m^2
A_s	Connecting pipe cross-section	3*10^-4	m^2
L_s	Connecting pipe length	2	m
V_{ro}	Initial volume of the reservoir	0.004	m^3
V_{bo}	Initial volume of the airbag	0.008	m^3
p_o	Initial pressure in air bag.	4*10^5	N/m^2

Chapter four

Modeling of Control Strategies

CHAPTER FOUR

Dynamic Analysis and Modeling of Control Strategies

4.1 Introduction

The vehicle suspension system is crucial for enhancing the vehicle's mobility, ride comfort, and stability, which extends the life of the vehicle. One of the most notable benefits of pneumatic suspension over metallic alternatives is the ability to make the system's primary natural frequency independent of sprung mass [87]. Additionally, air springs offer reliable protection versus wheel-rolling vibrations for the benefit of passengers. In order to the better performance of the air spring in obtaining more effective parameters of the suspension system, the tradition type was derived and established for simulation and compared with the Gensys type as shown in Figure (4-1), to reduce the effects resulting from the road surface while driving the vehicle on different types of roads.

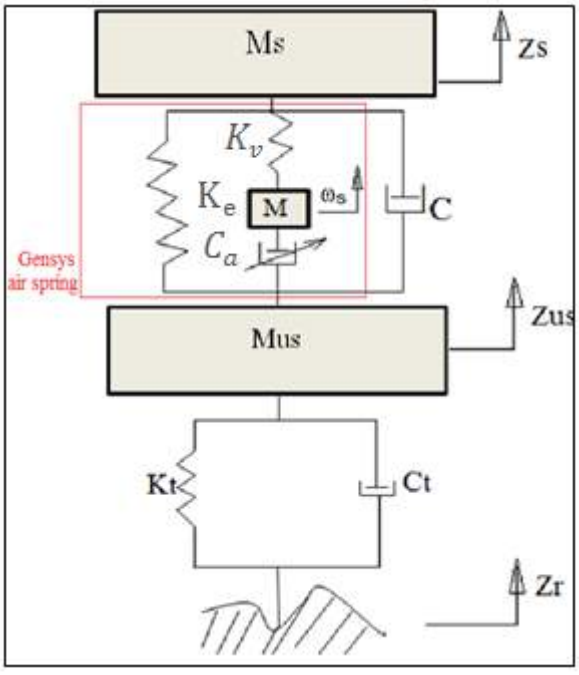

Figure (4-1) Air spring (Gensys).

4.2 Mathematical Model of the Traditional Air Suspension System

The system shown in Figure (4-2) is a quarter car dynamic model for air suspension system with two degree of freedom. The traditional rubber type of air spring employed in this section is typically non-linear. On the basis of the thermodynamic and fluid equations, a model of the quarter car-air spring is established under random road excitation.

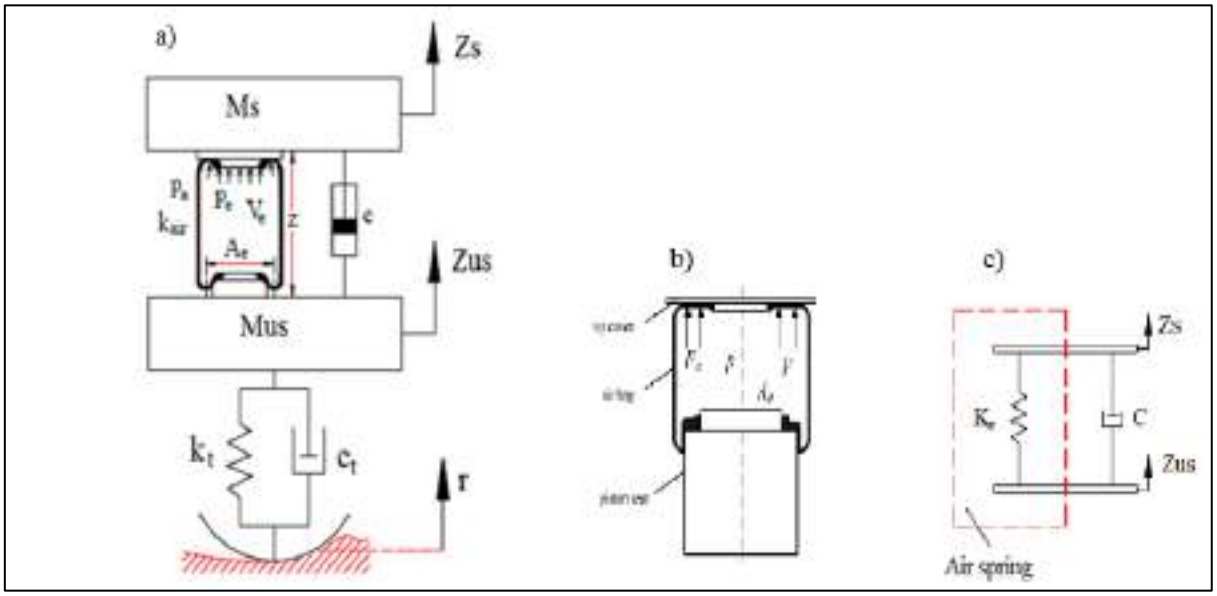

Figure (4-2) a) Suspension air system for quarter car. b) The schematic of the structure for air bag. c) Equivalent air spring.

The following equations of motion are derived using a mathematical model based on Newton's second law [88]:

$$M_{us}\ddot{Z}_{us} = K_{air}(Z_{us} - Z_s) + c(\dot{Z}_{us} - \dot{Z}_S) - K_t(Z_S - r) - c_t(\dot{Z}_{us} - \dot{r}) \quad (4.1)$$

$$M_S\ddot{Z}_S = -K_{air}(Z_{us} - Z_s) - c(\dot{Z}_{us} - \dot{Z}_S) \quad (4.2)$$

Where:

M_s and M_{us} are sprung mass and unsprung mass of the body;

C_t and k_t are the coefficient of damping and the stiffness for the tire;

K_{air} :is the stiffness coefficient of airbag;

C: is the coefficient of damping;

Z_s and Z_{us} are the displacements of sprung and unsprung masses;
and r is road surface roughness;
$Z = Z_s - Z_{us}$ is the distance between the unsprung and the sprung mass mass of a vehicle.

In order to calculate the stiffness of an air bag. The schematic of the structure as seen in Figure (4.2). Where p absolute pressure (pa), p_g is gauge pressure, p_a is atmospheric pressure. F_a elastic force of air bag, air spring can be expressed by equation

$$p = p_g + p_a \tag{4.3}$$

The derivative of the air spring's elastic force-to-displacement ratio may be used to determine the stiffness of the air spring.

$$F_a = (p - p_a)A_e \tag{4.4}$$

To determine the air bag of a suspension system's stiffness coefficient, according to Hooke's law[88] and insert equation (4.4), The derivative of the ratio elastic force and displacement of the air spring may be used to determine the stiffness of the air spring.

$$k_{air} = \frac{dF_a}{dz} = (p - p_a)\frac{dA_e}{dz} + \frac{dp}{dz}A_e \tag{4.5}$$

where $z = (z_s - z_{us})$ is the vertical displacement difference between the sprung mass and unsprung mass, A_e effective area.

There is no air exchange between the out and the air spring, according to equation for the ideal gas state and the thermodynamics law:

$$PV_e^n = \text{const} \tag{4.6}$$

When equation(4.6) is differentiated with respect to z, the result is

$$\frac{d}{dz}(p_e V_e^n) = np_e V_e^{n-1}\frac{dV_e}{dz} + V_e^n\frac{dp}{dz} = 0 \tag{4.7}$$

$$\frac{dP}{dz} = \frac{p.n}{V^n{}_e}\frac{dV_e}{dz} \tag{4.8}$$

$$A_e = -\frac{dV_e}{dz} \tag{4.9}$$

$$\frac{dP}{dz} = \frac{P.n.A_e}{V^n{}_e} \tag{4.10}$$

The equivalent stiffness may be calculated using the equations above:

$$K_{air} = (p_g + p_a)\frac{n\,A^2{}_e}{V_e} + p_g\frac{dA_e}{dz} \tag{4.11}$$

It can be considered an adiabatic process If the expansion stroke or compression is fast enough. An air state can therefore be defined as follows [89]

$$(p+p_a)V^n = (p_a + p_o){V_o}^n \tag{4.12}$$

Where P_o: is the initial air pressure, V_o : is the air spring's initial effective volume, n:is ratio of specific heat.

$$p = (P_o + P_a)\left(\frac{V_o}{V}\right)^n - p_a \tag{4.13}$$

The effective volume and area of an air spring change linearly as the height of the air spring changes.

$$V_e = V_O - \alpha(Z_s - Z_{us}) \tag{4.14}$$

$$A_e = A_o - \beta(Z_s - Z_{us}) \tag{4.15}$$

Where A_o: is the air spring's initial effective area. α and β are the changes in effective volume and area as a function of z.

$$K_{air} = \frac{n{A_e}^2}{V_e}\left[p_a + (p_o + p_a)\left(\frac{V_o}{V_e}\right)^n - p_a\right] + \frac{dA_e}{dz}\left[(p_o + p_a)\left(\frac{V_o}{V_e}\right)^n - p_a\right] \tag{4.16}$$

And at standard height (when displacement z=0), the stiffness of an air spring is defined as

$$K_{air} = \frac{n{A_e}^2}{V_e}\left[p_a + (p_o + p_a)\left(\frac{V_o}{V_e}\right)^n - p_a\right] + \left[(p_o + p_a)\left(\frac{V_O}{V_E}\right)^n - p_a\right]\left.\frac{dA_e}{dz}\right|_{z=0} \tag{4.17}$$

Substituting equation (4.17) in equations (4.1) and (4.2), this equations are a second-order differential equations, and we can utilize the Matlab Simulation program to solve these systems of equations because they are difficult to solve.

The system will be resolved and verified by one of the methods which are(using Simulink to construct the equations in Matlab) and the parameters of Table (4-1).

Table (4-1) parameters of the tradition air spring [90, 91].

No	**Parameters**	**Values**
1	m_{us} (Kg)	40
2	m_s (Kg)	400
3	c (N. s/m)	1000
4	k_s(N/m)	16000
5	k_t(N/m)	160000
6	c_t (N. s/m)	750
7	P_a (Pa)	1×10^5
8	V_O (m^3)	0.00298
9	A_o (m^2)	0.01667
10	P_o (Pa)	2.682×10^5
11	n	1.4
12	α	0.0169
13	β	-0.1122

The size of the air spring and the effective area are the most important factors for the design of the air spring for a city car, as well as changes in the effective volume(α)and the effective area (β)are sourced from [90, 91].

4.3 Design of PID Controller with GA for Nonlinear Pneumatic Quarter Car Integrated with Hydraulic Actuator Model

To raise the level of performance of the dynamic characteristics of the system without changing its specifications, there must be an external force that gives external energy to the system, forcing it to act as intended without manipulating those specifications. Therefore, a controlling projection after comparing the actual output with the desired input, and there will be an error. The controller's primary purpose is to create a control law that will allow the system to accomplish the desired results.

4.3.1 Proportional Integral Derivative (PID) Controller of Design System

PID controllers are well-known controllers used in industry. In addition, this controller can control nonlinear systems. The controls are made to automatically get eliminate of steady-state errors and adapt to what the system needs. In equation, a "PIDC" is described in equation(4.18).

$$u(t) = K_p\, e + K_i \int e\, dt + K_d \frac{de}{dt} \qquad (4.18)$$

The signal will proceed via the controller, which will compute the error signal's derivative and integral. The total of proportional gain (K_p) multiplied by the magnitude of the error, integral gain (K_i) time by the integral of the error, and derivative gain (K_d) multiplied by the derivative of the error is the signal (u)after passing through the controller as shown in figure (4-3), There will be a signal (u) delivered to the system, and as a result, output will be obtained [93].

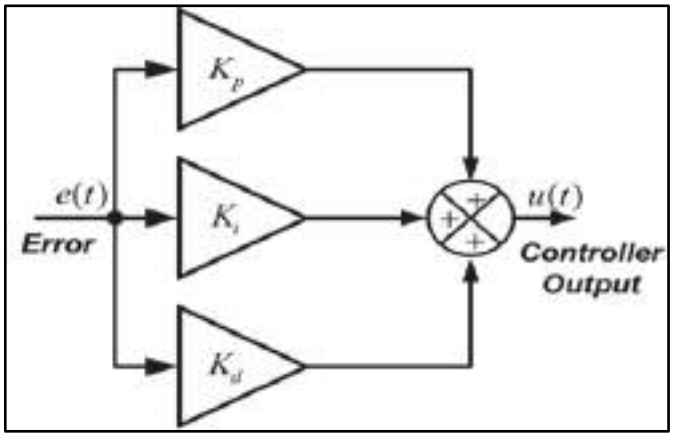

Figure (4-3) Structure of "PID" controller

Proportional *Kp*, integral *Ki*, and derivative *Ki* are the three types of gains. It can quickly modify or tune an applications to offer it fine control. For the purpose of fine-tuning the controller, Table 2 displays the variance in gain with various relevant factors.

Table (4-2) Gains fluctuation with a specific factor [94].

Response	Rise time	Over shoot	Settling time	SS error
K_p	Degrease	Increase	Small change	Degrease
K_d	Degrease	Increase	Increase	Eliminate
K_i	Small change	Degrease	Degrease	Small change

4.3.2 Tuning of The PID Parameters by GA

Finding the correct set of adjusted parameters within the controller is the key to controller design. Because the selection of these parameters is based on the trial and error which takes a lot of time and traditional techniques such as the Zeigler-Nichols method do not provide an optimum value for PID controller parameters, the tuning method in this study is structured as an optimization problem to address the limitations of employing trial and error and the selection process.

In this section, the Genetic Algorithm is used to optimize the PID controller settings for active pneumatic suspension-quarter cars simulation as depicted in the figure (4-4).

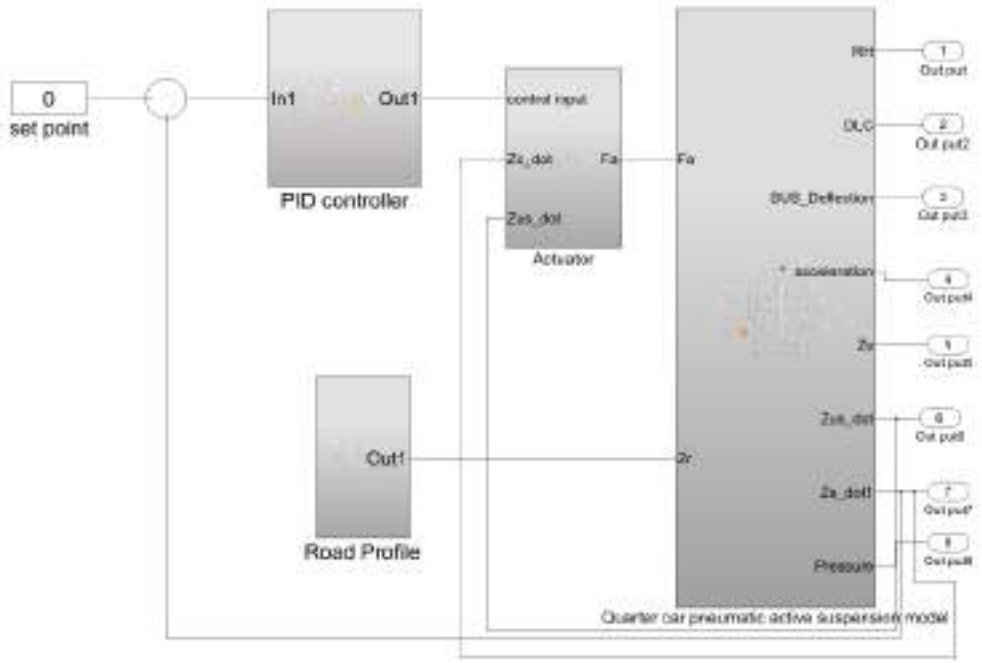

Figure(4-4) Block layout of PID-controlled active pneumatic suspension system

Figure (4-4) show the pneumatic active suspension system's control loop. The PID controller controls the actuator system according to the output from the velocity sensor for sprung mass, this will create a force proportional to the velocity sensor, this force will oppose the unsprung mass force so it will supress the oscillations immediately and improve the ride comfort and road holding. The PID controller was designed by optimized proportional– integral–derivative gains to provide a proper control orders to the actuator and entered desired force for suspension system, utilizing Genetic algorithm to tune the gains and to minimize the error via fitness function (the time integral times the absolute error criterion). A genetic algorithm is a type of random search strategy that may be used to find a solution to a problem. It is used to enhance complicated issues and solve systems of nonlinear equations. GA works with a set of alternative

solutions known as individuals or chromosomes that evolve repeatedly and employs probabilistic transition rules rather than deterministic principles. A generation is the name given to each iteration of the algorithm, a generation is a unit of measurement for each iteration of the algorithm [95]. Fitness-related behaviors and genetic components such as crossover and mutation are used to simulate the development of solutions [96].

4.3.3 An Optimization Terminologies

- The performance indices (objective function) which are used to evaluate the response by reducing the error, Time Integral Absolute Error (TIAE)

$$J_{ITAE} = \int_0^\infty t \cdot |e(t)| dt \quad (4.19)$$

- Variable of choice which contains (*Kp, Ki, Kd*).
- Search space, the limits which the parameters operate must be within a given range

The MATLAB platform was used to simulate the pneumatic active suspension model. Simulations were ran numerous times to achieve the optimal value for the algorithm's parameters so that examine performance of the suggested model. parameters of genetic algorithm for proposed model are recorded in the shown table(4-3) below:

Table (4-3) lists the parameters for the GA-based optimization method.

Parameter	Type/ Value
Population size	50
Scaling function	Rank
Crossover probability Mutation	0.5
probability	0.02
Maximum number of generations	50
Crossover	Arithmetic
Mutation	Uniform

The GA is set up and run for a total of 50 generations. The range of the PID inputs Ki, Kp, and Kd is ϵ [0,10].

After adjustment, the PID gains are documented in table (4-4), with two types of roads including a roughness road grade (B) and a road that includes two bumps in the simulation to test the proposed model of suspension system.

Table(4-4) Optimize Control gains for the proposed PID by GA.

Optimize Control gains	**Range**	**Obtain by GA**
Kp	3-5	4.001
Ki	0-1	0.3442
Kd	0-1	0.00001

Through the above table, the effect of Kp and Ki on improving steady state as shown, in contrast to Kd, which has no effect. As result, a GA-based PID controller tuning procedure has been created and implemented. Based on the simulation results, the optimal controller settings derived by combining this technique ITAE as cost indices have accomplished adequate set-point tracking and disturbance rejection in the proposed model.

4.4 Performance Analysis of the Proposed Fractional-Order-PID Controller

Many types of controllers have been used recently in an attempt to improve the ride comfort and road handling in vehicles, FOPID is one of those types that have been used in this field, which has been used by researchers in various fields. A proper fractional-I and fractional-D action setting can increase the PID controllers' performance even more, moreover setting the relative to (K_p, K_d, and K_i), two order parameters: the integral and the derivative order parameters need also be modified in partial order $PI^{\lambda}D^{\mu}$ controller, the

characteristics of "λ and μ" around (0,1), this gives the controller two extra degrees of freedom. A traditional PID is a subset of fractional controllers. So, if λ and δ are set to 1, a traditional PID controller is get, and if setting λ equal to 1 and μ equal to 0, a PI controller is get, this obtains by equation (4.20) the FOPID's continuous transfer function:

$$G_c(s) = \frac{U(s)}{E(s)} = K_p + \frac{K_i}{s^\lambda} + K_d s^\mu \qquad (4.20)$$

In the presence of a nonlinear actuator, the fractional controller's resilience is highlighted even more. Figure (4-8) portrays a block diagram that depicts the FOPID control framework.

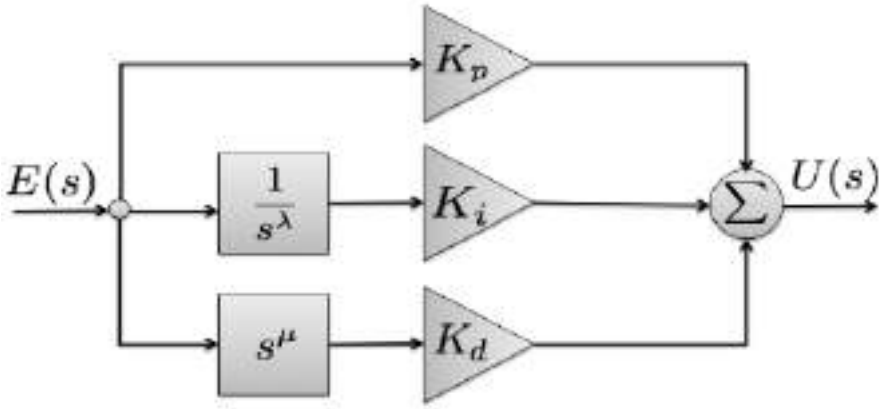

Figure (4-8) The schematic view of FOPID.

The fractional order controller's differential equation was written as [99]:

$$u(t) = K_p e(t) + K_i D_t^{-\lambda} e(t) + K_d D_t^{\mu} e(t) \qquad (4.21)$$

u(t) : the control signal in the time domain.

λ : is the integral part's order.

μ : is the derivative part's order.

Where K_p, K_i, and K_d are the controller's gains and e(t) denotes a difference between a process's single output that is measured and the desirable point. For "λ and μ" should be adjusted in order provide an precise controller with K_P, K_I, K_D. The most common definition in fractional-order calculus is the

Riemann–Liouville definition, which states that fractional order integration was defined as [100].

$$ {}_aD_t^{-\varphi} f(t) = \frac{1}{\Gamma(\varphi)} \int_a (t-\tau)^{\varphi-1} f(\tau) d\tau \qquad (4.22) $$

Where ϕ : indicates the difference integral's real order (0<ϕ<1).

a : is initial-time instance, which is commonly considered to be zero.

t : is the characteristic by which the differintegral was computed.

The problem, therefore, becomes how to keep the design process and structure of a controller as simple as possible (similar to that of a PID controller), at the same time delivering performance comparable to sophisticated controllers. One approach is to keep the PID controller's structure as shown in Eq. (4.21), but change the order of the integral and derivative terms to any non-integer number (1/s to $1/s^{\lambda}$ and s to s^{μ}), so that the controller's physical meaning remains the same. Still, the parametric search range is expanded [101], as illustrated in figure(4-9).

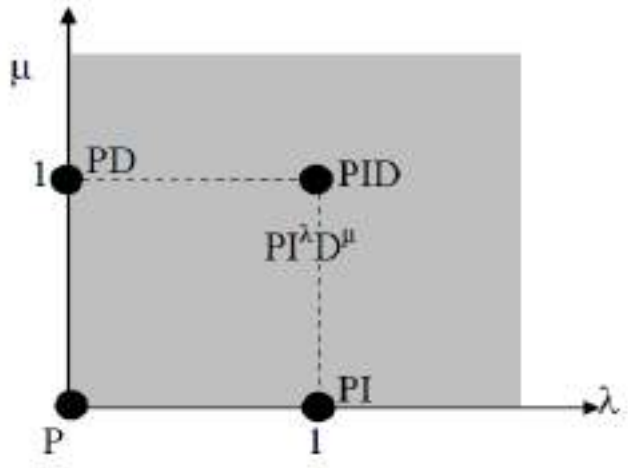

Figure (4-9) The parameters for "FOPIDC".

By fine-tuning all the parameters of the FOPID control, a superior outcome may be obtained via the Genetic Algorithm that has been proposed to design the pneumatic active suspension using the FOPID controller.

The pneumatic active suspension system's design includes the integrated of a hydraulic actuator that is electrically controlled by a controllable servo valve. The actuator is built by linking it to both sprung and unsprung masses. As the wheel is deflected owing to road disturbances, the actuator controls the displacement between the sprung mass and the wheel when the signal from the sensor is sent to a controller, which measures the acceleration of sprung mass and then the signal is amplified by controller (FOPID) and transmitted to the actuator, which generates the necessary force to absorb vibrations from the road , forming a closed loop system as apparent graphically in Figure (4-10).

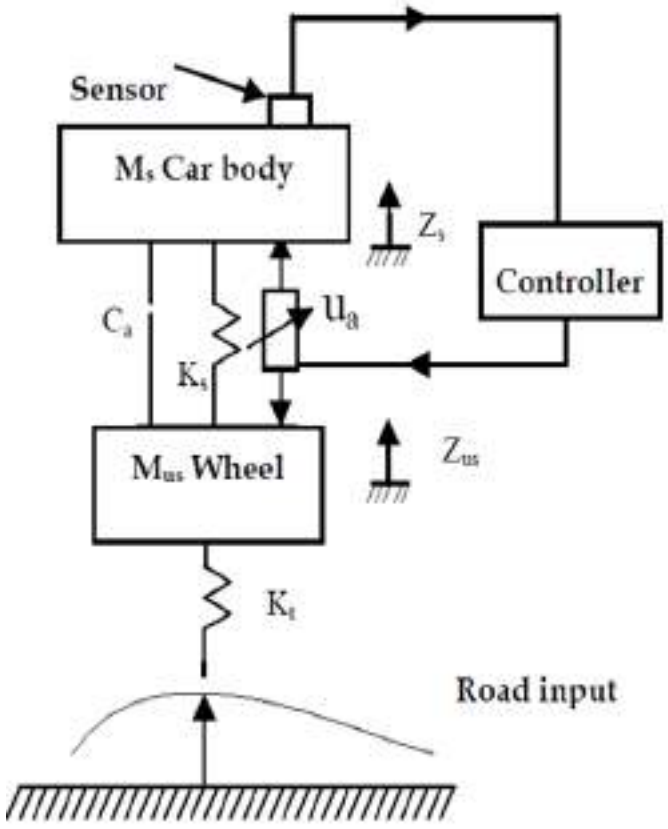

Fig. (4-10) Active suspension system [1].

To achieve the goal of obtaining the least vertical distance and vertical acceleration, the proposed control approach has been schematically presented in figure (4-10) with the desired signal is set to zero, since the controlled system's

desired outputs should be closed to zero. The two road profile model are the supply for the model of nonlinear quarter-car suspension. (two bump and random roughness road).

In this work, a simulation to verify the validity of the effect of the control strategy (FOPID) was presented, MATLAB Simulink was constructed on inserted hydraulic actuator in air suspension as depicted in figure (4-11).

Design proposed "FOPID" controller for quarter vehicle nonlinear pneumatic suspension with hydraulic actuator.

The major goal of designing a suspension system's controller is to minimize the vibration that travelers felt as a result of road disturbance while also improving ride comfort and handling. By incorporating the scaling gains, the FOPID controller's performance has increased. To test the proposed controller's robustness, two different forms of disturbances will be investigated (roughness road and two bump). For the air suspension system with hydraulic actuator, the GA Algorithm was utilized to adjust the settings of the FOPID controller.

From equation (4.21), *KP, Kd, Ki,* λ and μ parameters are designed for proposed control by GA, after several attempts have been made to determine the ranges to obtain the gains to adjust the FOPID controller's parameters. FOPID parameter ranges are chosen as follows:

$K_P \in [15\ \ 20], K_d \in [0\ \ 5], K_i \in [0\ \ \ 5], \lambda \in [0\ \ \ 1]$ and $\mu \in [0\ \ \ 1]$.

Because the control system wants outputs should be close to zero, the reference inputs are set to zero. Occasionally, a single performance is all that is required for the system, the optimization procedure in this case is typically easy. If more than one, the performance is selected as the objective function, however, a conflict may arise during optimization, resulting in certain objectives being degraded. To cope with these conflicts, an indicator (ITAE) is used to measure this performance in terms of the accumulation error over time. Equation (4.19)

show the mathematical formulations of the used performance indicator (ITAE) [102].

ITAE involves combining rise time, settling time, and overshoot optimization. It is computed by multiplying the integral of the error through the clock signal and integrating the result across the trip time [58]. FO-PID controller settings are obtained using a genetic algorithm with (ITAE) as the objective function. As shown in the schematic of a block of the Genetic algorithm optimized "fraction order –PID" controller for plant as shown in figure(4-11).

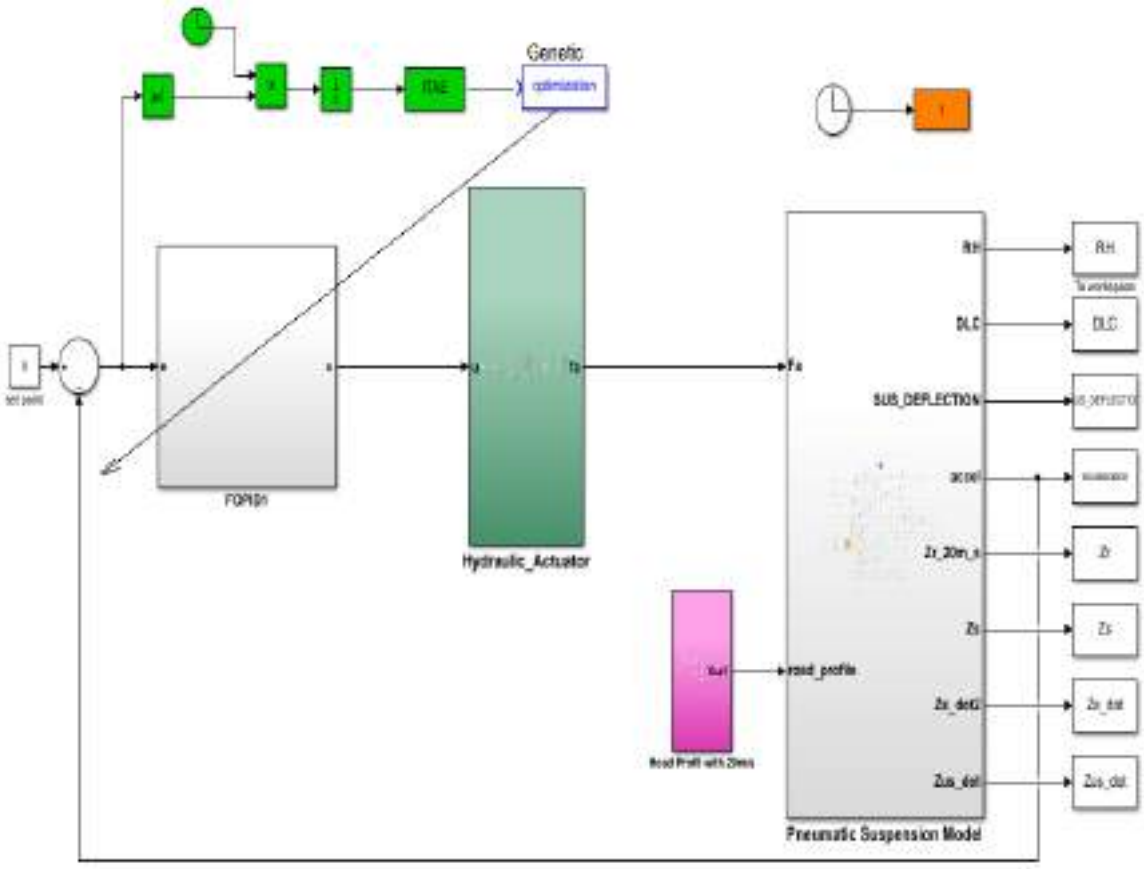

Figure (4-11) GA tuned FO-PID controller for the plant.

The error's absolute value is multiplied with the time of data and then integrated to get the "ITAE" to the global optimizer, GA which is passed. The FOPID characteristics are determined by the genetic algorithm, which is then passed on to the active pneumatic suspension system's closed loop control. This

method is run for the number of selected iterations. The genetic algorithm's parameters are as follows:

NO. of variable = 5

Number of generation = 100

Fitness scaling : Rank

Crossover technique: Arithmetic

Mutation : Uniform

The ranges of FOPID parameters are chosen as follows to shorten the optimization process as table(4-6).

Table(4-6) The range and optimal values of GA for FOPID control.

Parameters	Range values	Optimal value
Kp	15-20	18.011
Kd	0-5	0.487
Ki	0-5	0.001
λ	0-1	0.43
μ	0-1	0.9

4.5 Design of Slide Mode Controller with GA for Nonlinear Pneumatic Quarter Car integrated with Hydraulic Actuator Model

When the vehicle body is subjected to road roughness, oscillations may occur, in this case, the oscillations should be absorbed as quickly as possible. Slide mode control is one of the types of controllers that will be used to reduce the error in suspension system to obtain better stability and comfort when a vehicle travels over various disturbances, the impacts of such perturbations can be communicated from the road to the cabin's vehicle. This strategy, however, is more complex and sophisticated than using traditional linear methods.

From figure(4.15) can be illustrated the phase plane is divided into two semi-planes by the sliding surface (S_{slide} =0), one is (S_{slide} > 0) and the other is (S_{slide} <0). First, the SMC swap rules were used to construct the needed controller, resulting in sporadic control signals and, as a result, a chatter problem. To alleviate the problem of chatter, the control interruption of a narrow border near the sliding surface should be avoided in general [103].

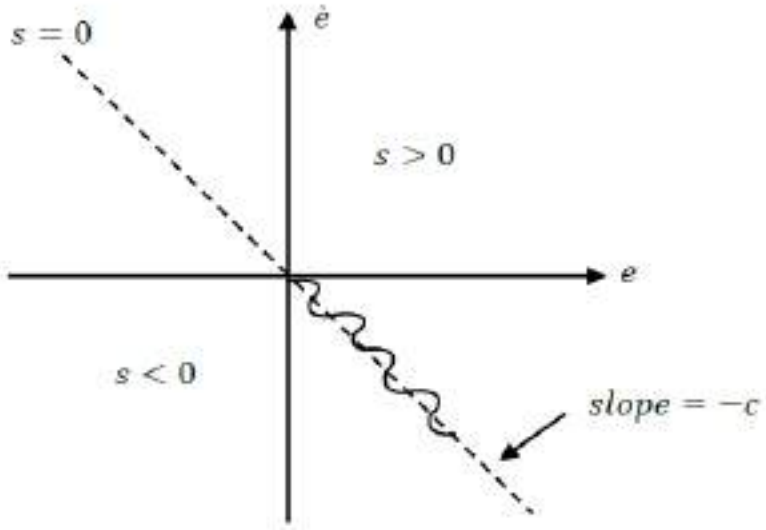

Figure (4-15) SMC phenomena phase-plane [103].

This section includes the SMC with pneumatic quarter car integrated with hydraulic actuator scheme, which is used to manage the suspension system using a random road as an external disturbance.

Let be the tracking of error as Figure (4-16).

$$e = x_d - x \tag{4.22}$$

Where variable x is velocity of sprung mass and x_d is desired signal which equal to zero.

The following is a description of the switching surface can be characterized as [104]:

$$s = \dot{e} + ce \tag{4.23}$$

Where (c) is positive convergence rate of x, we substitute equation (4.22) into equation (4.23)

$$s = (\ddot{x}_d - \ddot{x}) - c(\dot{x}_d - \ddot{x}) \quad (4.24)$$

The controller is designed using the proportional switch law to design the controller (u) as shown in the equation (4.25)[105].

$$u = (\alpha|e| + \beta|\dot{e}|)sgn(S) \quad (4.25)$$

$$u = (\alpha|\dot{x}| + \beta|\ddot{x}|)sgn(S) \quad (4.26)$$

Where α and β are positive constants.

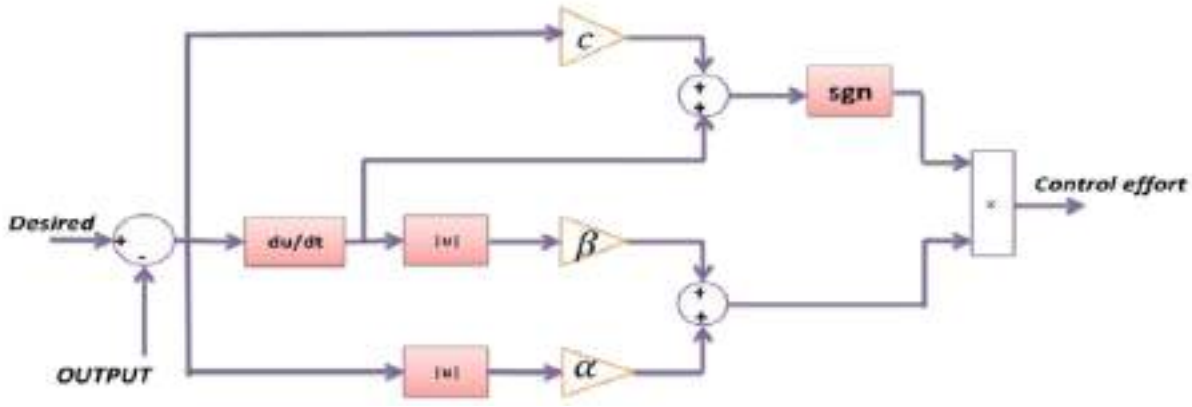

Figure (4-16) Detail of the sliding mode [105].

The Optimization of Proposed scheme Controller Parameters using Genetic Algorithm

Figure (4-17) shows a schematic description of the proposed control scheme. The controller (SMC) for a quarter vehicle of pneumatic with a hydraulic actuator is designed, this proposed control tries to estimate and approximate unknown parameters while reducing system nonlinearity. To fulfill the performance index, the controller variables are optimized. Genetic algorithm is utilized to adjust the optimal sliding mode controller parameters with (ITAE) as index of performance, it is computed by multiplying the error's integral with the clock signal then integrate it over time period. A controller will receive the

system's error signal as an input, and performance indices will be used as the objective function.

ITAE as objective function represented to minimize the error in the system's closed-loop control. The technique is repeated until the global optimal solution is found.

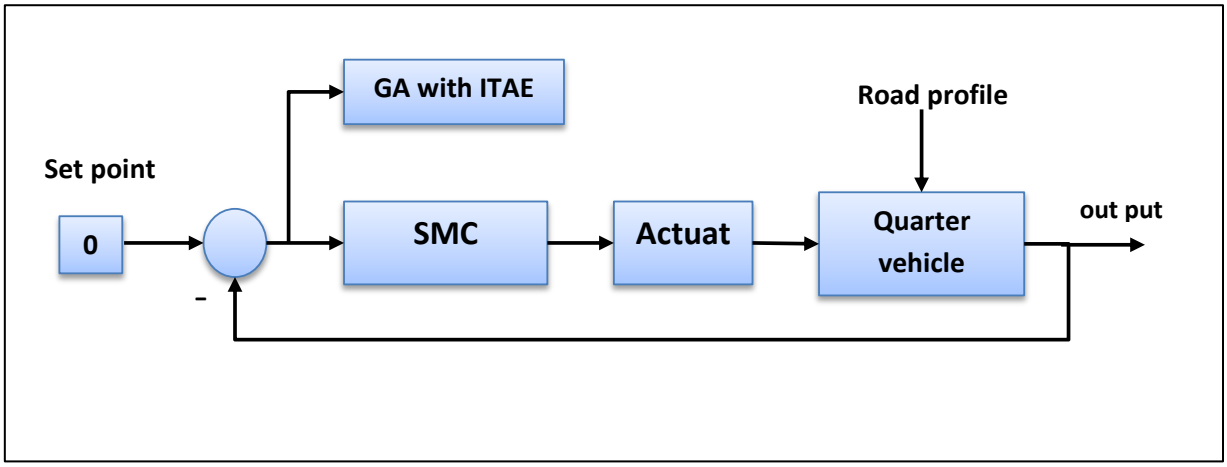

Figure (4-17) The Proposed Control Schematic Diagram.

The parameters selected for GA technique are given in table (4-9). To minimize the optimization time, The gains(c,α, and β) need to be adjusted the controller parameters for control scheme are chosen in the ranges listed below:

$C \in [10,30]$.

$\beta \in [0,3]$.

$\alpha \in [10,20]$.

Table (4-9) Optimizing input values for the best result.

GA parameters	Values
Maximum number of generations	100
Fitness scaling	Rank
Probability of crossover	0.8
Crossover technique	Heuristic
Mutation technique	Uniform
Object function accuracy	1×10^{-15}
Generation gap	0.9

After GA technique optimization, the parameters of controller are tuned as table shown:

Table (4-10) Optimal best values obtained by GA.

Parameters	Range values	Optimal value
C	10-30	25.02
β	0-3	0.180
α	10-20	13.49

In this section the control of sliding mode control is designed with genetic algorithm to test the quality of this control with the pneumatic active integrated the hydraulic actuator for two road profile input. The characteristic of the control scheme will be tested and compared with pneumatic suspension system to demonstrate the control technique, computer simulations using MATLAB/SIMULINK are provided. The outputs of Sliding Mode controller is used in order to get the desired hydraulic actuator force. The GA technique with objective function (ITEA) are used to find optimized values for the specified controller parameters.

4.6 The Proposed Controller of Fuzzy Logic Control with Genetic Algorithmic Optimization

Fuzzy logic controllers provide for the use of system expertise during the development of the rule base and can be used with systems that lack a defined mathematical model. The fuzzy logic control (FLC) method converts a language control technique and is commonly employed in suspension system [56]. The use of fuzzy logic to plan a controller an active pneumatic suspension to increase suspension system performance which is given in this section.

Figure (4-20) represents the block diagram of FLC active pneumatic suspension system to a 3-degree of freedom suspension system with hydraulic actuator. Dual inputs, error (e) with the error of change (ec) and one output (u) which has the desired force of the actuator, the output of FLC is the input to the actuator and the rule-base has been implemented. The sprung mass's velocity of error (e) and the acceleration of sprung mass change of error (ec) were employed as inputs, and the controlling of output (input to model). The rule bases of FLC are a linguistic-based rule set that takes into account previous human experience. Fuzzy controllers with forty-nine rules as shown in the table (4.10). The three stages to controlling the system itself are as follows [47]:

- Fuzzification : During the fuzzification stage, real-number (crisp) input values are converted to fuzzy values.
- Fuzzy inference : Based on the rule base and the data base, the fuzzy inference machine evaluates the input data and computes the controller outputs.
- Defuzzification : This stage converts the outputs, which are in fuzzy values, to real numbers.

The rule-based suspension system for three degrees of freedom is shown in the form of a lookup table (4.10), which was built from past experience

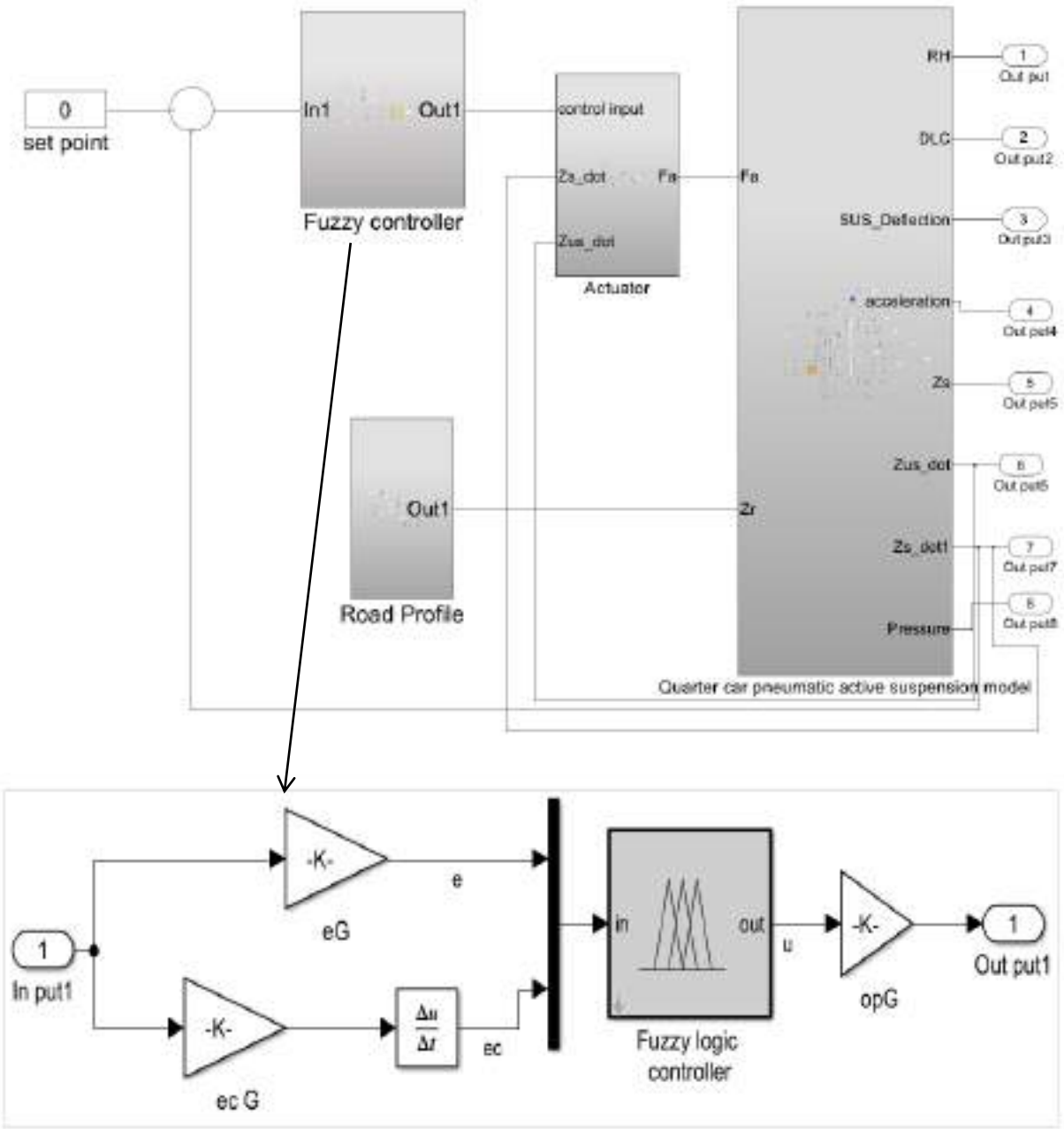

Figure (4-20) Block diagram of fuzzy logic-controlled active pneumatic suspension.

Table (4.10) Fuzzy logic rules table (3-DoF active pneumatic suspension system).

		Error change						
Error		*N-L*	*N-M*	*N-S*	*N-S*	*P-S*	*P-M*	*P-L*
	N-L	*P-L*	*P-L*	*N-B*	*-PM*	*P-S*	*P-S*	*Z-E*
	N-M	*P-L*	*P-M*	*N-B*	*P-S*	*P-S*	*Z-E*	*N-S*
	N-S	*P-M*	*P-S*	*N-M*	*Z-E*	*Z-E*	*N-S*	*N-M*
	Z-E	*P-M*	*P-S*	*N-S*	*Z-E*	*Z-E*	*N-S*	*N-M*
	P-S	*P-M*	*P-S*	*Z*	*Z-E*	*Z-E*	*N-S*	*N-M*
	P-M	*P-S*	*Z-E*	*Z-E*	*Z-E*	*Z-E*	*N-M*	*N-L*
	P-L	*Z-E*	*N-S*	*N-S*	*N-S*	*N-M*	*N-L*	*N-L*

Figure (4-21) depicts the surface plot rule base as indicated in table (4-10)

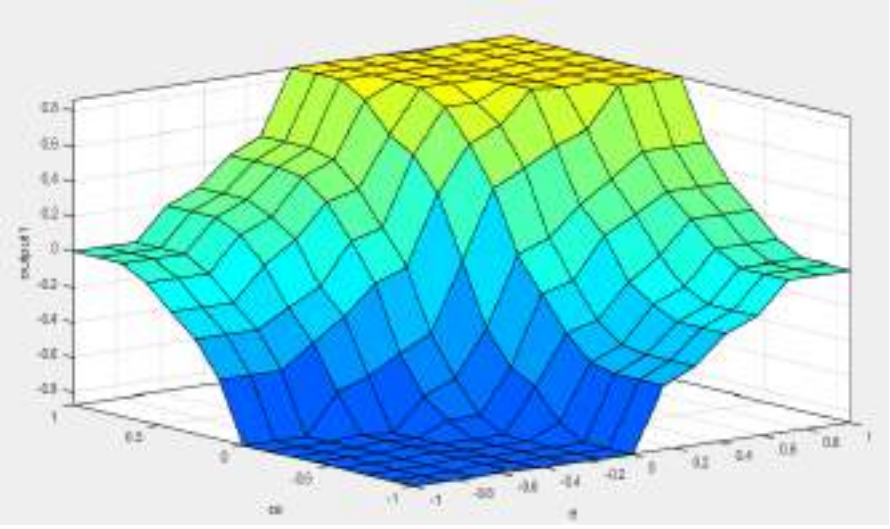

Figure (4-21) The surface plot rule for FLC

The proposed membership functions of FLC inputs and outputs; these membership functions were utilized to initiate system simulation; each

variable(input and output) consists of seven fuzzy sets (NL, NM, NS, ZE, PS, PM, PL), are there linguistic factors that suggest negative large, negative medium, negative small, zero, positive small, positive medium, and positive large, respectively and the fuzzy inference of system (FIS) of the Mamdani type.

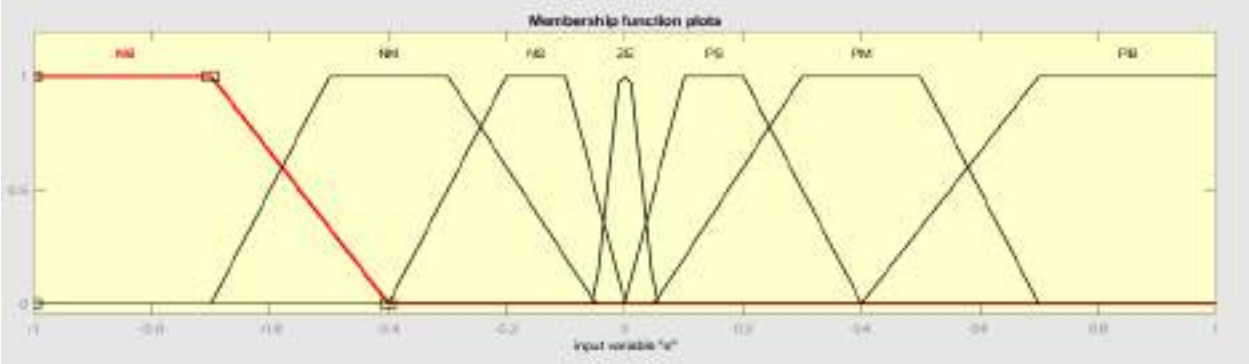

Figure (4-22) Input variable (e)

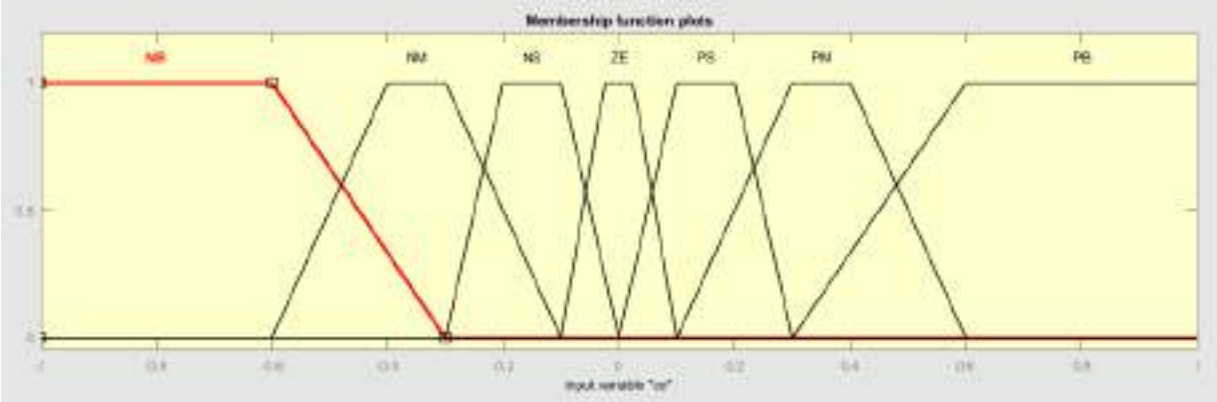

Figure (4-23) Input variable (ce)

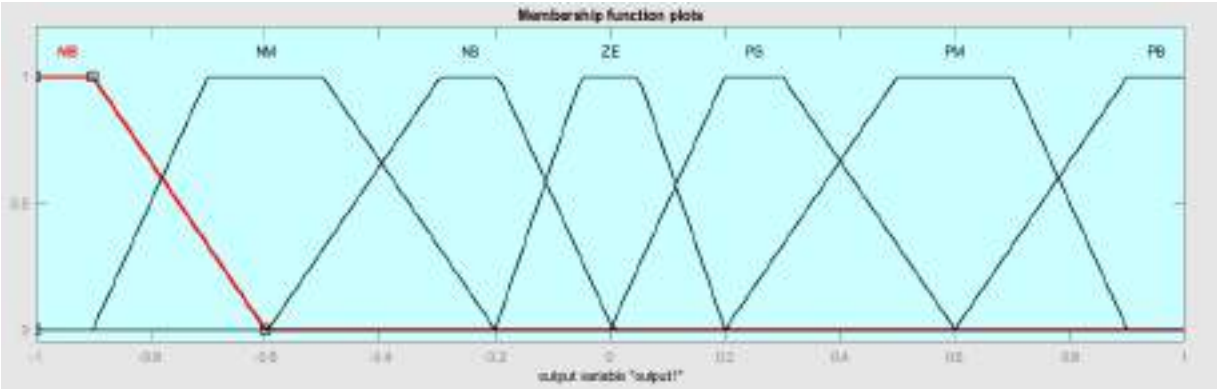

Figure (4-24) Output variable (u).

The inputs and outputs' discourse universes are normalized in the interval [-1, 1], for input and output variables, trapezoidal membership functions are utilized as shown in Figures(4-22,4-23,4-24).

In fuzzy parameters, the genetic intelligence method, which is trustworthy and resilient for exploring solution spaces, is used, to reach the optimal solution.

A random road excitation and two bump are used to demonstrate the effectiveness of the proposed by fuzzy logic with GA algorithm in this section. The tracking error *e(t)* and the differential tracking error *de(t)* are the fuzzy inference system inputs in the controller design in order to improve the scaling factor (SF) for Fuzzy controllers. It can automatically determine the optimal or near-optimal control gains based on the goal function's minimum, bringing performance of the system closer to the target. The overshoot and adjustment time are highlighted by ITAE, which shows the control system's speed and precision. As a result, the system responsiveness is estimated [60], and then the scaling factor (SF) for Fuzzy controllers are optimal as depicted in Figure (4-25).

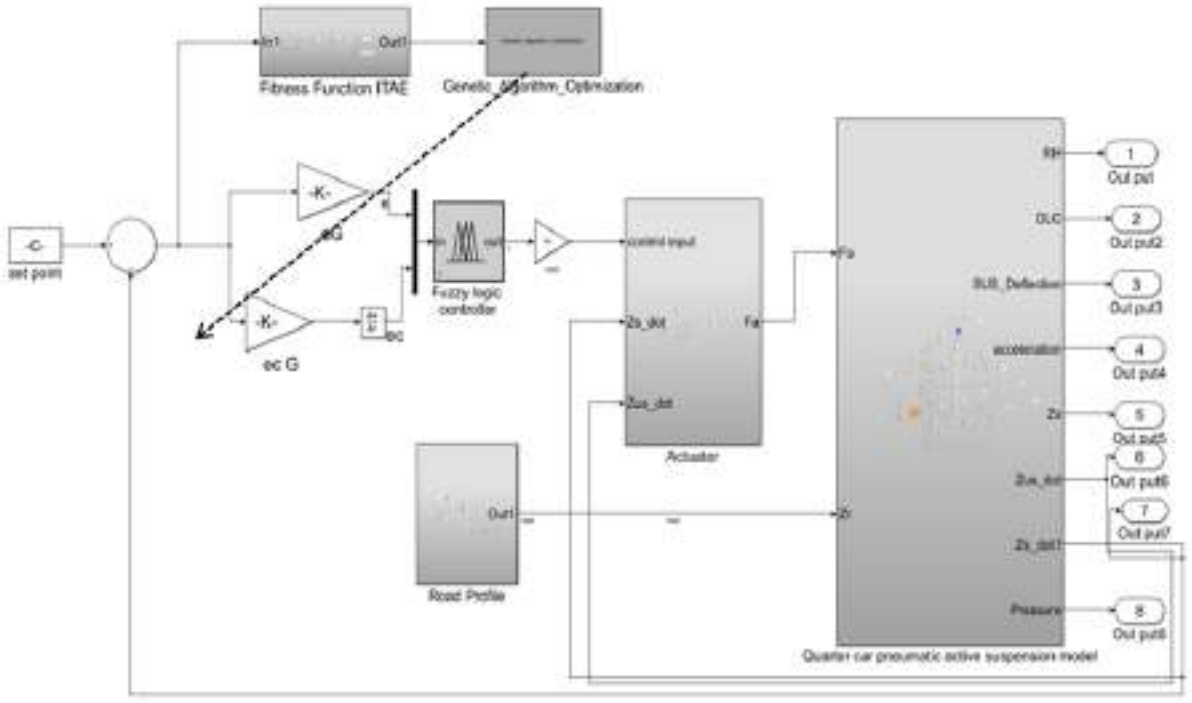

Figure (4-25) The FLC-GAO controller schematic.

For the goal of improving the scaling factor (SF) for Fuzzy controllers, as Figure(4.25) depicted the controller schematic.

Mathematically, the integral time absolute error (ITAE) performance used as index function as equation (4.19). The flow chart depicts the process for GA optimized scaling factors (SF) as Figure(4.26).

The parameters of genetic algorithms for proposed model are recorded in table shown below

Table (4-11) lists the parameters for the GA-based optimization method.

Parameter	**Type/ Value**
Population size	50
Crossover probability Mutation	0.5
Probability	0.02
Maximum number of generations	50
Creation function	Uniform
Crossover	Arithmetic
Selection	Tournament
Mutation	Uniform

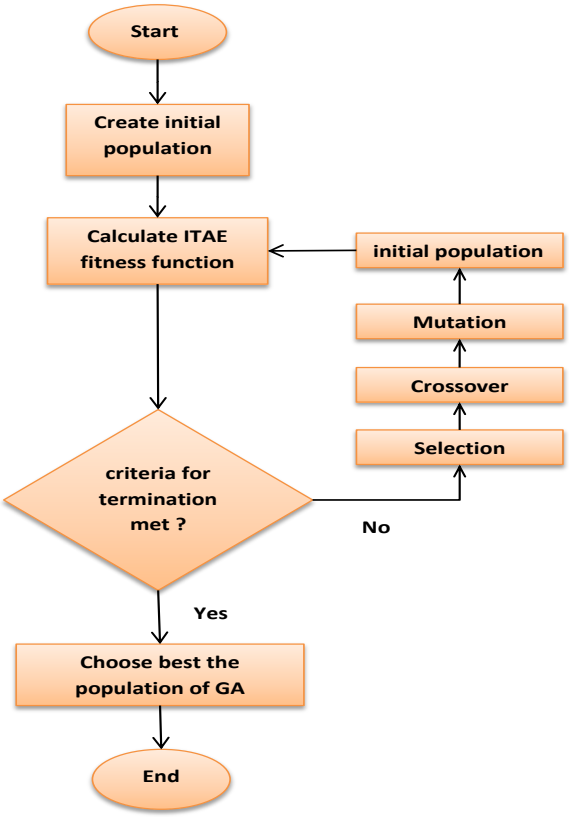

Figure (4-26) Flow chart of genetic algorithm optimized.

The ranges of FLC parameters are chosen as follows to shorten the optimization process as table(4.12).

Table (4.12) Range and optimal value for FLC.

Parameters	Range values	Optimal value
e	10-20	14.701
ec	0-5	1.351

4.7 Design of Proposed A Self-Tuning Fuzzy-PID Control for Active Pneumatic Quarter Vehicle

A self-tuning fuzzy PID controller is a hybrid of a tradition PID with a fuzzy controller. The traditional PID controller's parameters are frequently not properly adjusted for nonlinear plants with unexpected parameter fluctuations. As a result, automated tuning of the PID settings is required, this control approach is utilized to enhance the control effectiveness of nonlinear systems by adjusting the parameters of the PID controller, therefore combining fuzzy inference and providing a fuzzy adaptive "PIDC" [108]. The parameters Kp, Ki, and Kd of the "PIDC" adapted by simulation in Matlab utilizing appropriate fuzzy rules [109], coupled with optimization technique to overcome the appearance of uncertainties and nonlinearities and to control of nonlinear suspension system.

First and foremost, the fuzzy logic controller is built using rules to ensure that the system is stable. Each PID controller parameter has (three) rules for auto-tuning it, there are two input to the fuzzy logic controller (*e* and *ce*) and the output of the FLC is the parameters of the PID controller. In this system, the hydraulic actuator is controlled in order to control the system for nonlinear suspension.

To control system, PID-C was applied in the time domain, the control signal may be written as equation (4.18)

$$u(t) = K_p e(t) + K_i \int_0^t e(t)dt + K_d \frac{de(t)}{dt}$$

where e(t) is the difference in error between set point which equal to zero and the output, de(t) is the change of error, the control signal is u(t) for controlling force, the gain proportionately is K_P, the gain integral is K_i, and the gain derivative is K_d. A fuzzy controller transforms a linguistic control strategy into a control strategy, and the fuzzy rules are created using an expert's or database's expertise.

There are two inputs and three outputs in this FLC design, the goal of control and the type of controller both influence fuzzy rules. For equation(4.18) the fuzzy controller is used to tune the coefficients K_P, K_i, and K_d. The fuzzy logic outcomes of outputs are obtained by aggregating fuzzy sets of inputs and designing fuzzy rules using the MAX-MIN aggregation approach [110].To get the best solution for (K_P, K_i, and K_d), the Mamdani model is used as a fuzzy inference structure with some modifications. Figure(4.30) depicts the construction of the "Self-tuning FPIDC".

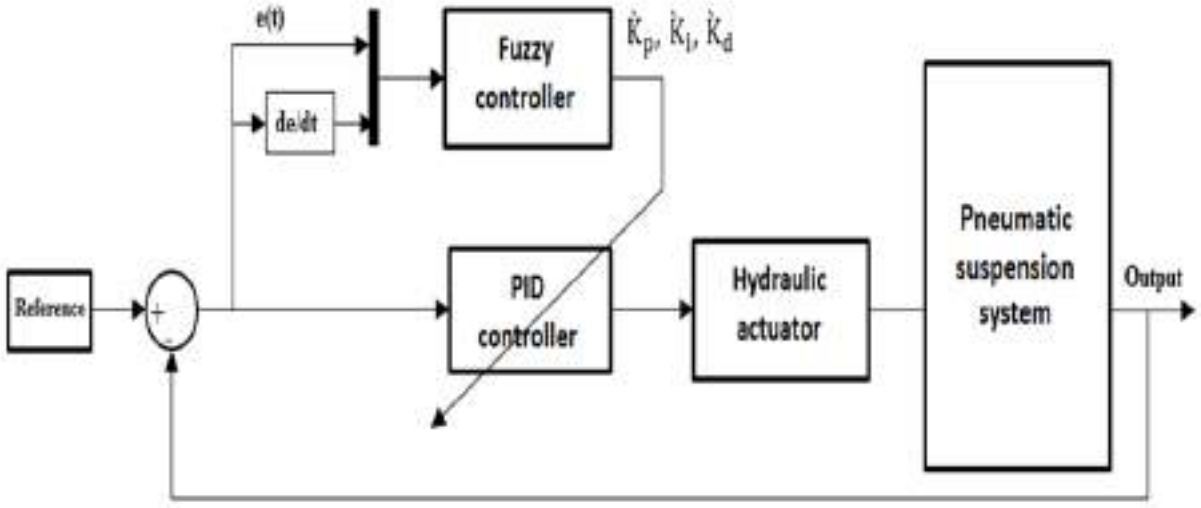

Figure (4-30) Block diagram of the pneumatic suspension model with "Self-tune PIDC".

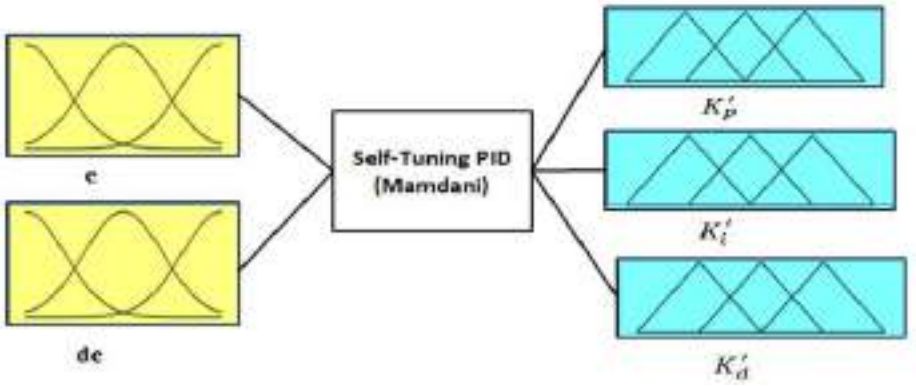

Figure (4-31). The Fuzzy Controller's Inputs and Outputs.

Figure (4-31) showed that the output of FLC are (K_P', K_i', and K_d') which are enhanced to tune PID gains (K_P, K_i, and K_d). The e(t) is the difference of the output the plant from its reference value (zero).

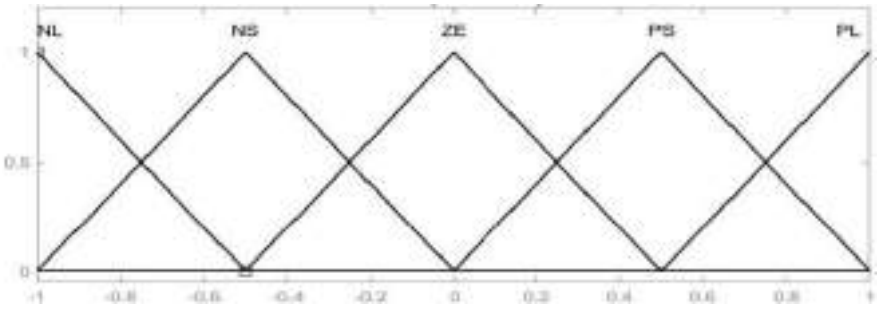

Figure (4-32) Fuzzy-Self PID for the membership of e(t) and de (t).

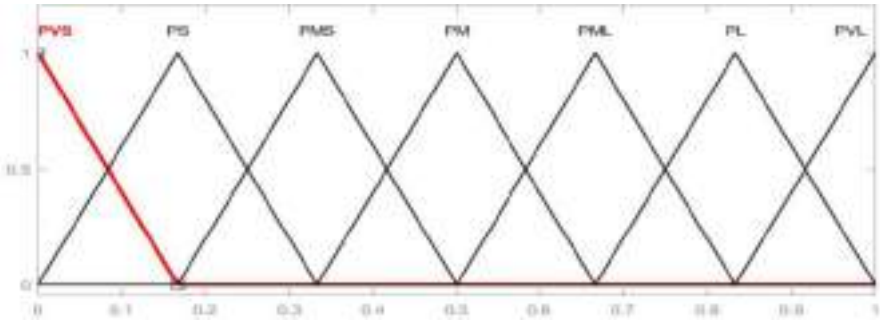

Figure (4-33) Fuzzy-Self PID membership functions of $\acute{k}_p$, $\acute{k}_i$, *and* $\acute{k}_d$.

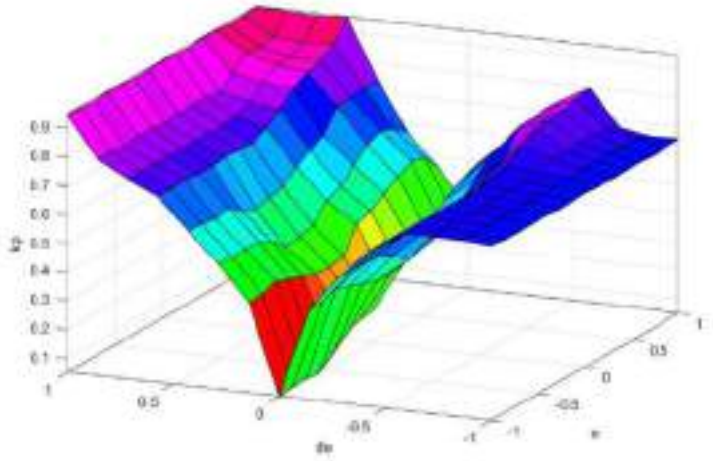

Fig. (4-34) K_P tunner.

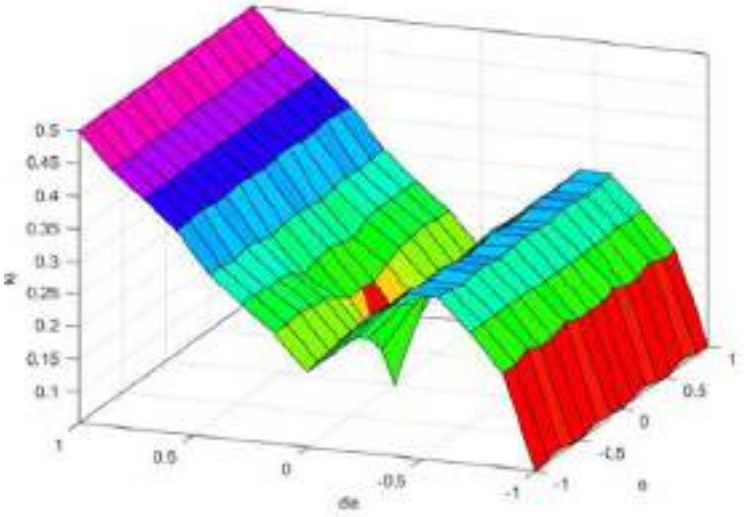

Fig. (4-35) K_i tuner.

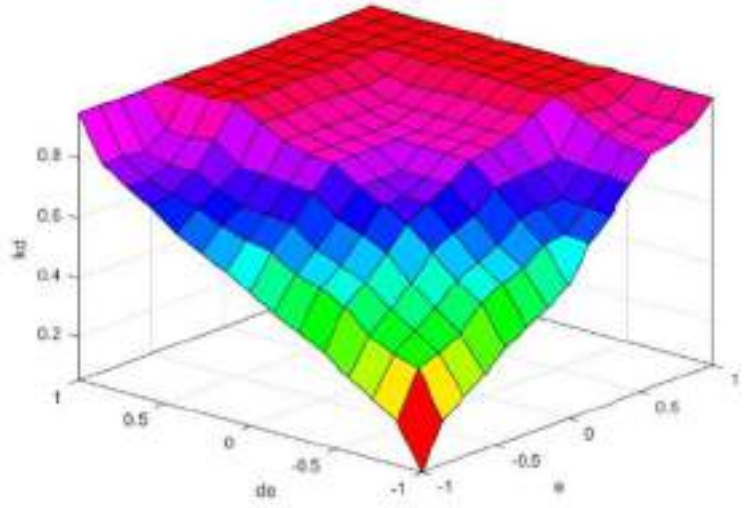

Fig. (4-36) K_d tuner.

Figure(4-31) shows that there are two inputs are connected to the controller, error and derived from error, these inputs have a range of (-1 to 1). Five membership functions are employed for each input variable (NL,NS ,ZERO, PL, PS) Negitive Large, Negative Small, Zero, Positive Large, Positive Small respectively. Figure(4-32) shows the functions of membership of the fuzzy inputs in detail. The fuzzy set has three outputs: K_P, K_i, and K_d. The outputs' ranges are from 0 to 1.

Here, "PVS, PS, PMS, PM, PML, PL, PVL, Positive Very Small, Positive Small, Positive Medium Small, Positive Medium, Positive Medium Large, Positive Large, Positive Very Large" respectively as shown in fig.(4-37).

For normalization, assume that K_P, K_i, and K_d have variable ranges$[K_{p(\min)}$, $K_{p(\max)}]$, $[K_{i(\min)}$, $K_{i(\max)}]$, and $[K_{d(\min)}$, $K_{d(\max)}]$, respectively. To generate a feasible rule base with good inference efficiency, the range of each parameter was established using a simulation of a PID controller [109].The parameters' ranges are as follows:

$K_p \in [1,6]$, $K_i \in [0.1,0.5]$, and $K_d \in [0,0.01]$

To obtain the coefficients K_P, K_i, and K_d, the above range with equation(4.19), when substitute into the equation(4.27) [111], as shown in Figure(4-37).

$$K_P' = \frac{K_P - K_{Pmin}}{K_{Pmax} - K_{Pmin}}$$
$$K_i' = \frac{K_i - K_{imin}}{K_{imax} - K_{imin}} \qquad (4.27)$$
$$K_d' = \frac{K_d - K_{dmin}}{K_{dmax} - K_{dmin}}$$

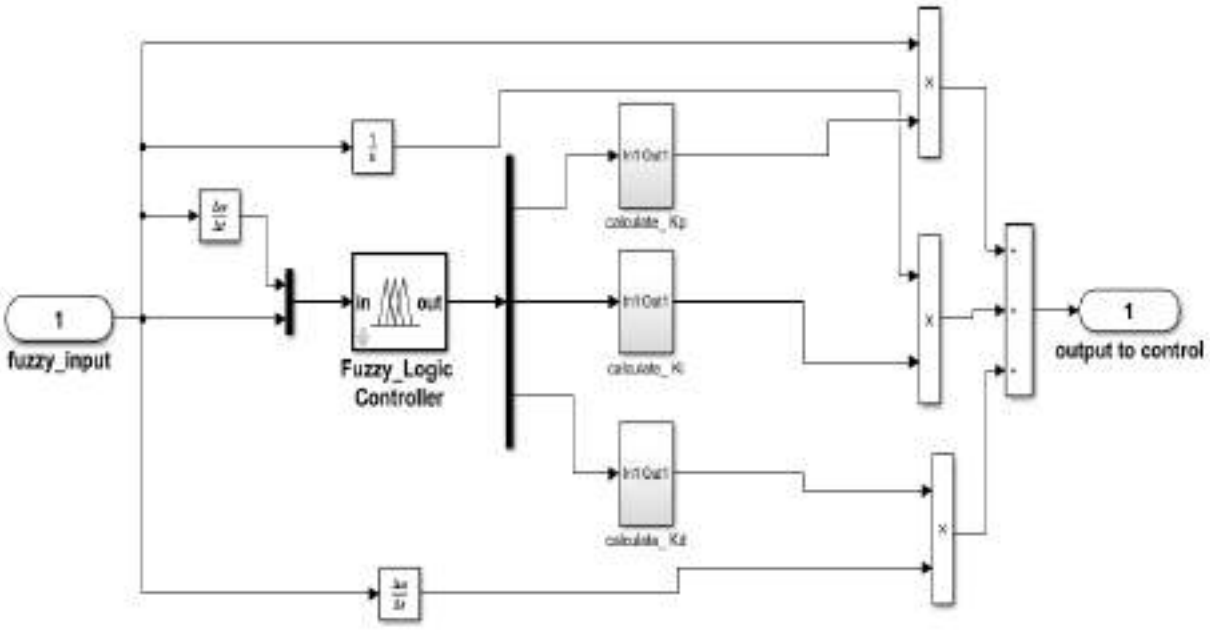

Figure (4-37) Block of Simulink fuzzy-self PID

The proposed controller of a Self-Tuning FPID controller is designed to obtain optimal parameters to reduce the vibration for non-linear active pneumatic suspension system with hydraulic actuator . The suspension system is controlled by a fuzzy logic controller with two inputs and three outputs, (K_P', K_i', and K_d') which are enhanced to tune PID gains (K_P, K_i, and K_d). The difference between the set point and the measured output parameter, as well as the sprung mass velocity, are two inputs and " K_P, K_i, and K_d " are three output parameters that determine the controllable force.

4.8 Design of Active Force Controller with GA for Nonlinear Pneumatic Quarter-Car Integrated with Hydraulic Actuator Model

A technique of active force control is proposed for a pneumatic suspension system of a quarter-car model with a hydraulic actuator utilizing an embedded fuzzy logic controller to govern a dynamic design and ensure the system's stability and robustness in the presence of unknown disturbances. To solve that problem of dynamic decoupling of the motion trajectories of a robotic arm, an active force control method is used. [112]. For controlling a robot arm, AFC has been proved to be superior than traditional methods when dealing with a range of disturbances and correcting for them [29]. AFC can be used under varying loading conditions and has a fast decoupling property. The origins of the AFC idea be linked back to Newton's second law of motion. The main element that affects how effectively the control strategy works is the estimation of the mass required by the AFC loop. Three loops make up the proposed controller structure and that two controllers systems were used, namely fuzzy control in outer loop and PID in inner loop. To reject road disturbances, the control of an outer loop is employed for calculating the target force. To maintain the real force near to the desired force, use is made of an inner force tracking loop which compensates the

disturbance force obtained from the error between the ideal and actual force vector. The suggested control strategy is robust owing to the implementation of a feedback loop for "Active Force Control" to determine the force caused by a disturbance.

Active force control operates by inferring the disturbance force from suitable actuator force measures via a force sensor and acceleration measurements via an accelerometer, simultaneously, an estimated mass should be calculated using an appropriate approach as illustrated in Figure (4-40).

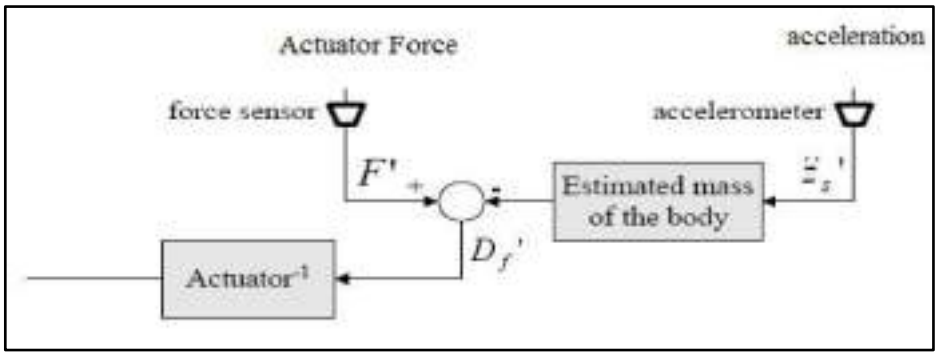

Figure (4-40) Active force control [51].

The design of the "Active Force Control" method implemented with a suspension dynamic system as displayed in Figure (4-41).

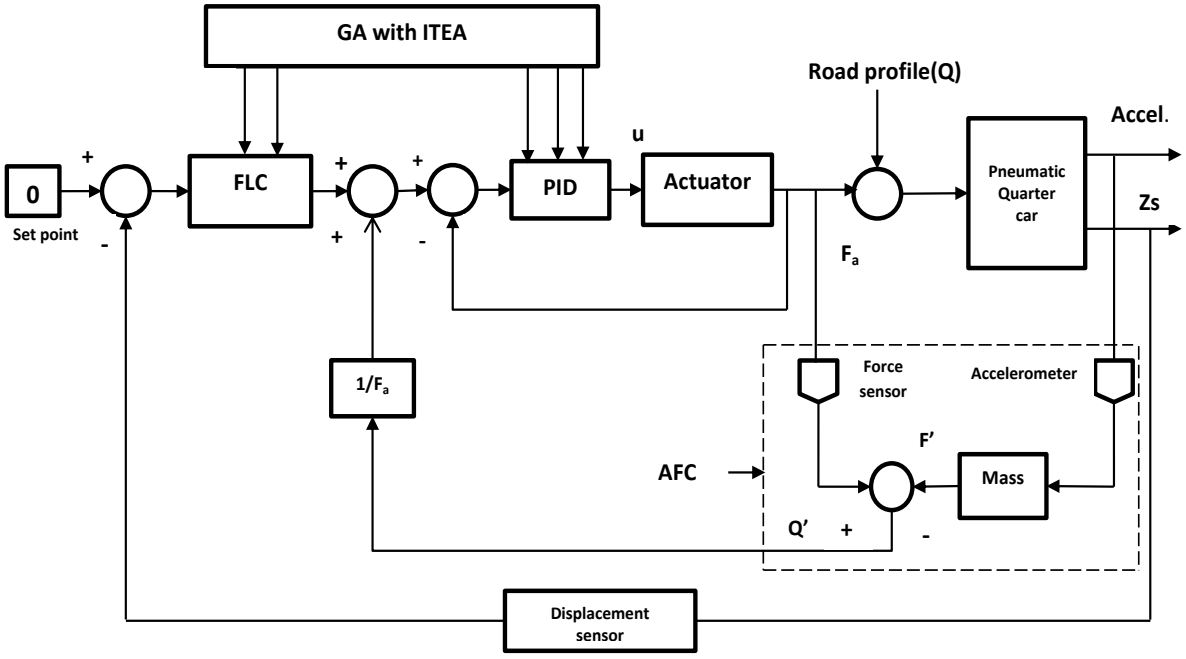

Figure(4-41) .The structure diagram of an AFC scheme

Figure (4-41) depicts the controller structure used in this investigation, which includes three controller loops. In the outer loop, FLC is employed to calculate the best target/commanded force. A traditional PID controller is used to track the force of the hydraulic actuator. The AFC loop is used to calculate the estimated force from the values obtained of the force and the dynamic system's acceleration.

The force that is created when the ideal and actual forces difference is known as the disturbance force is compensated by the AFC loop.

The key equation of motion driving the AFC algorithm is as follow [113] :

F_a + Q = m . a (4-28)

Where, F_a is the actuator force , Q is disturbance force, m is mass, and a is body's acceleration .

The estimated value of the disturbance force can be formulated as:

$$Q' = F_a' - m'a' \quad (4\text{-}29)$$

where, Q' is the disturbance or estimated force, physical sensing devices may be used to readily get F_a and acceleration (force sensor and accelerometer),

Intelligent processes can be used to obtain a mass(m), the key component that contributes to the control scheme's efficacy is the mass estimation required by the "AFC" loop. The estimated mass was obtained using a simple approximation approach in this simulation. The error sends a signal for the actuation system's adjustment equaling -Q', that may be utilized to decouple the real disturbance force Q, ensuring that the system remains steady despite changes in the external force [113]. "AFC" The loop is the primary component that improves the efficiency of the control strategy.

4.8.1 Controller for Fuzzy Logic (Force Computation)

The hydraulic actuator system with the pneumatic active suspension is extremely intricate and non-linear, and the suspension characteristics will alter as the vehicle ride through types different road conditions. Traditional control strategies are based on a fragile system paradigm and are incapable of adapting to changing environmental conditions. As a result, the suggested console employs Fuzzy Logic which was mentioned in the section 5.5.

4.8.2 Tracking Force

Figure (4-42) depicts the hydraulic actuator's inner loop of force tracking control. A PID controller is used to track the force of a hydraulic actuator. The gains of "PID" were tuned by genetic algorithm. The spool valve position and real-time piston speed are the two inputs to the hydraulic actuator model. Proportional Derivative control is then implemented with force tracking error as the input and control current as the output to drive the spool valve.

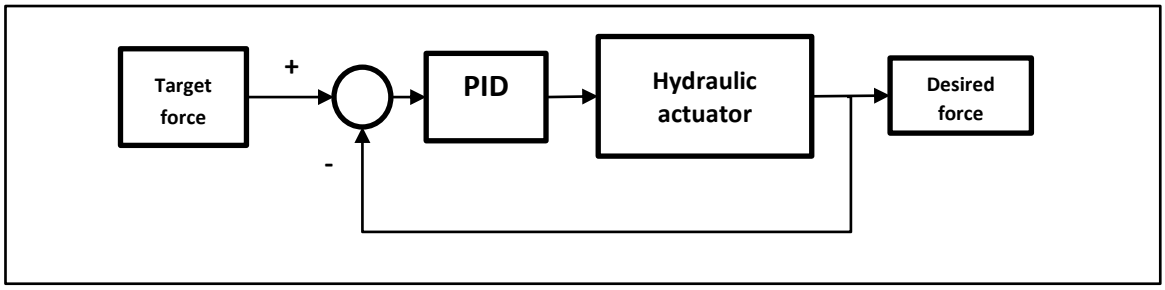

Figure (4-42) Tracking the hydraulic actuator's force.

To validate the controller's force tracking performance the sinusoidal, square, and arbitrary functions are used to express the targeted force. as shown in figures (4-43,4-44,and 4-45). These simulation models are consistent with [114].

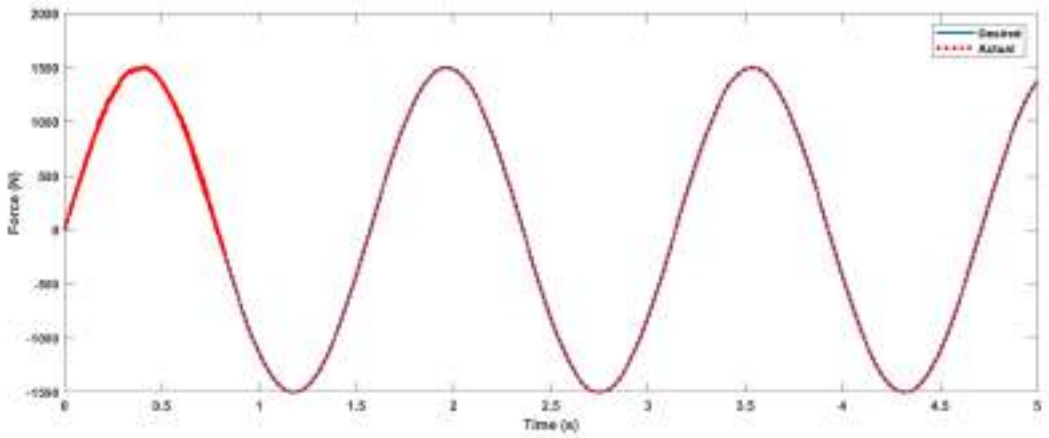

Figure (4.43) Sinusoidal signal for force tracking.

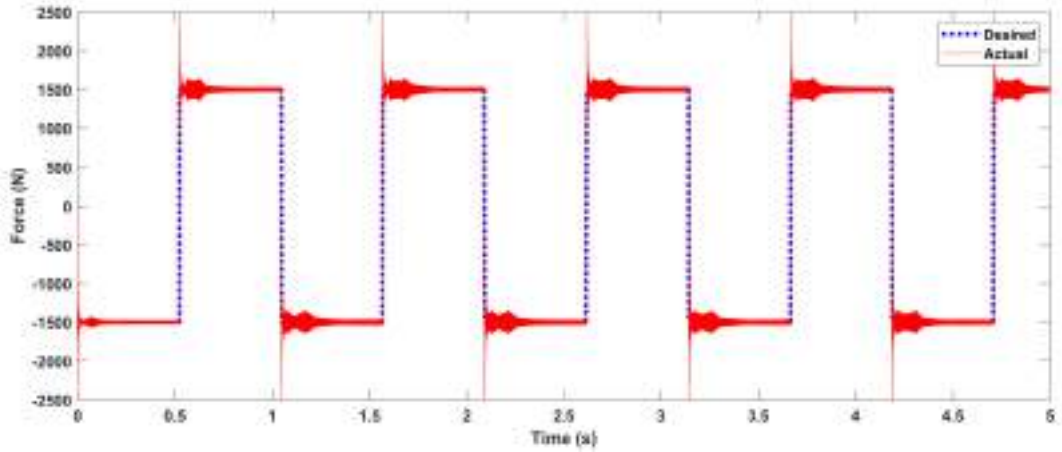

Figure(4-44) Square wave for force tracking.

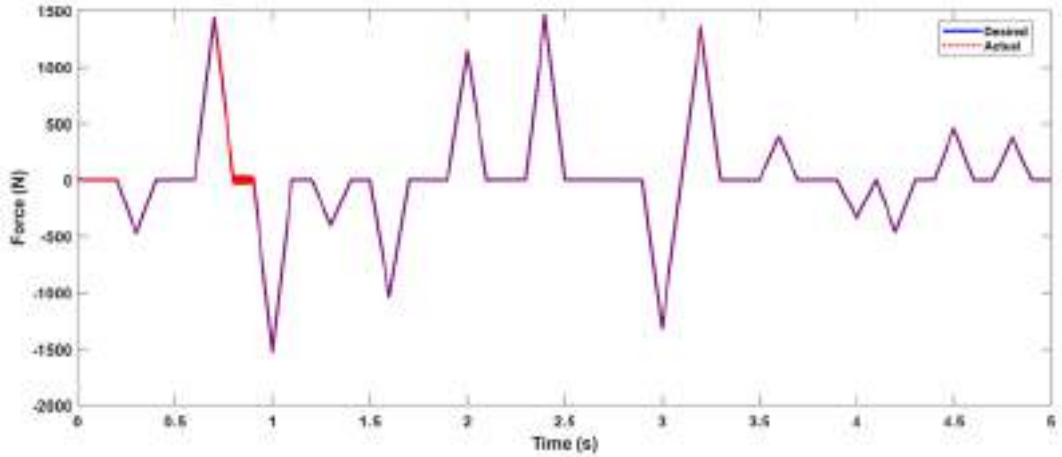

Figure(4-45) Random wave for force tracking.

4.8.3 The Optimization of Intelligent Active Force Control Parameters using GA algorithm

The proposed control is illustrated schematically in Figure(4-40). The AFC loop was created to recompense for dynamic disorders. The hydraulic actuator force tracking inner loop controller was designed to use the provided control mechanism to manage the actuator force and generate the needed force, it is utilized through combination with AFC scheme because it provides continuous, but not very robust performance. In accordance with what has been stated, the proposed controller is designed to reduce nonlinearity in the system.

The PID controller's main goal in this part is to regulate the actuator force and generate the needed force, which is calculated using the suggested control mechanism. The PID controller's equation in time domain is defined as equation(4.18)

$$u = K_p e_r + K_i \int_0^t e_r dt + K_d \frac{de_r}{dt}$$

where u: is the PID controller's output and The proportional, differential, and integral gains are represented by (K_p, K_i, and K_d).

A PID controller attempts to reduce error by adjusting the PID controller's three gains (k_p, k_i, k_d), GA approach and ITEA were used to reduce error and to optimize the parameters of each constructed controller to get the best values for gains (K_p, K_i, K_d, a, and b) in order to reduce the amount of suspension acceleration, and vehicle body displacement.

In this section, GA is utilized to tune the controller since it has the capability to identify uneven situations and has a propensity to whole-optimize [115]. The genetic algorithm's parameters are selected for adjusting as shown in table (4-17). The desired signal (velocity of sprung mass) set compared to zero, and the road profile is considered to be random, one bump, and two bump.

Table (4-17) Optimizing input values for the best result.

GA parameters	Values
No. of chromosomes in each generation	40
Fitness scaling	Rank
Probability of crossover	0.8
Crossover technique	Heuristic
Mutation technique	Uniform
Object function accuracy	1×10^{-15}
Generation gap	0.9

Through the process of optimization with the genetic algorithm, the gains were obtained for the controllers fuzzy logic and proportional-derivative present in the proposed system as shown in table:

Table (4.18) Range and optimal value for FLC.

Parameters	Range values	Optimal value
e	10-20	14.701
ec	0-5	1.351
K_p	0-1	0.000001
K_d	0-5	0.91

The idea from AFC technique, in the event that the forces of disturbance *Q'* are evaluated or measured accurately, then this value can be used to separate the actual forces *Q* of disturbance from the applied forces.

The AFC loop is designed in Figure (4-41) to compensate the system for a number of unknown disturbances, especially those related to the air system in order to remain robust and stable. The strategy's efficiency is based on the mass estimator when actuator force and the body acceleration are determined.

he body acceleration and the active force hydraulic actuator are both inputs to the AFC scheme. In outer loop, FLC is employed to calculate the best target commanded force and fuzzy controller is used to track the force of the hydraulic actuator. Its essential principle is for the actuator body's force and acceleration which are both measured and an estimation of the moving body's mass is made to compute the estimated force [116].

Chapter five

Results and Discussion

Chapter Five

Results and Discussion

5.1 Introduction

The vertical acceleration ($\ddot{Z}_s$) and vertical displacement (Z_s) for sprung mass are used to evaluate riding comfort while for tire deflection ($Z_{us} - Z_r$) and dynamic load coefficient(DLC) are utilized to evaluate road handling , respectively. The sprung mass's vertical displacement (Z_s) and the acceleration of the sprung mass ($\ddot{Z}_s$) shall be minimized by giving the control signal. When the vertical acceleration and vertical displacement of sprung mass decreased, the ride comfort will improved, while the performance of tire deflection and dynamic load coefficient are decreased, this mean the road holding and stability of vehicle. The capacity to respond to changes in road inputs allows an active suspension system to achieve a trade-off between road holding and ride comfort.

The control system is responsible for giving proper control orders the actuators, depending on the passive system's components and different types of controllers entering the required suspension force, the different types of controllers can be explained in this chapter.

5.2 Evaluating the Suspension System's Performance in Comparison to Two Air Suspension Systems (without control)

Non-linear air spring simulations (Gensys and traditional) are compared in terms of RMS of the sprung mass for vertical displacement, dynamic load coefficient, vertical acceleration, velocity, road holding, and vertical dynamic force. Road ISO Class B and one bump with a height of 0.1 m at a speed of (72 km/h) are taken into consideration in the evaluation of the ride comfort (RC), dynamic load coefficient (DLC), and road handling (RH) responses as objective

functions respectively. To find out which is better to use later with a specific controller to obtain better occupant comfort and vehicle stability.

The road profiles utilized in this section include road level B and one bump with height 0.1m as shown in figures (5-1 and 5-2).

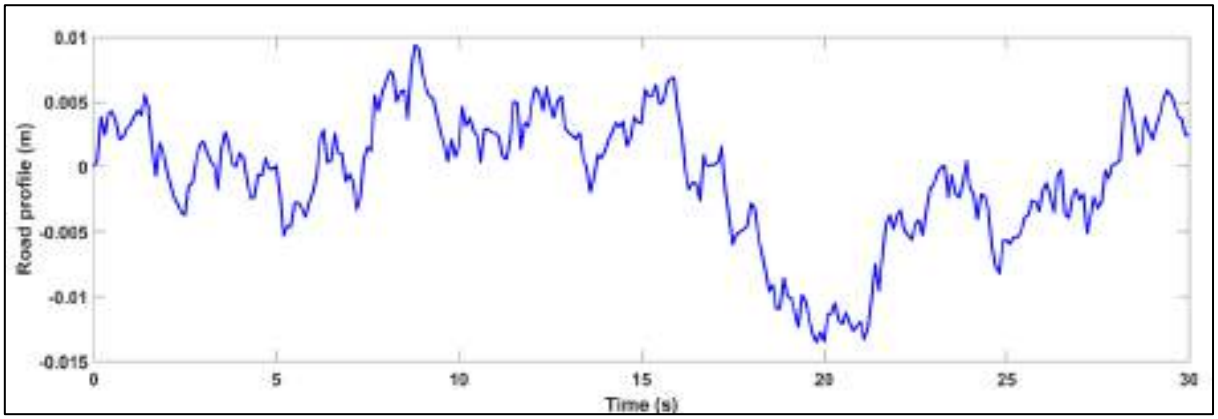

Figure (5-1) Road profile for roughness road ISO level B.

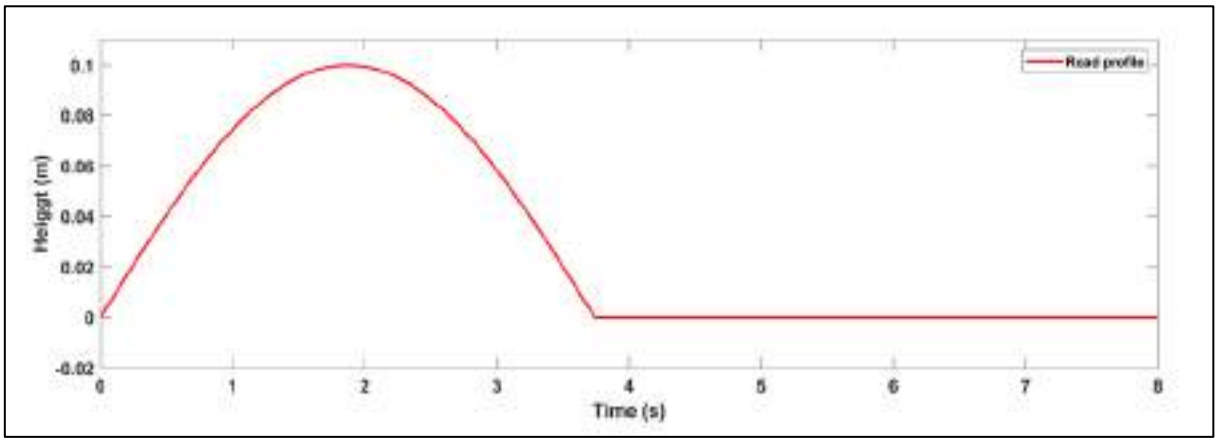

Figure (5-2) Road profile for one bump with height 0.1m.

Figures 5.3 to 5.9 show the comparison between the two air suspension between the air spring of the traditional type and the second type(Gensys) to assess the effectiveness of the air suspension utilizing the Simulink/MATLAB platform in the time domain for 10 second and an ISO level B random road and the figures 5.10 to 5.16 of for the same comparison for the road with one bump (0.1m) in the time domain for 5 seconds.

Table (5-1) The RMS value reduction for simulation (level B) road input.

No	Parameters(unit)	Traditional	(Gensys)	Reduction
1	Vertical acceleration(m/s^2)	1.567×10^{-1}	1.169×10^{-1}	25.4%
2	Vertical displacement(m)	5.902×10^{-3}	5.46×10^{-3}	8 %
3	Road holding(m)	1.206×10^{-3}	1.044×10^{-3}	23.5%
4	Dynamic load coefficient	1.756×10^{-2}	1.344×10^{-2}	23.46%
5	Suspension travel(m)	2.311×10^{-3}	2.266×10^{-3}	2 %
6	Dynamic tire load(N)	$7.579e\times 10^{+1}$	$5.796\times 10^{+1}$	23.5%

Table (5-2) The RMS value reduction for simulation bumpy road (0.1m) as input.

No	Parameters(unit)	Traditional	(Gensys)	Reduction
1	Vertical acceleration(m/s^2)	5.47×10^{-1}	3.09×10^{-1}	44 %
2	Vertical displacement(m)	2.684×10^{-2}	2.224×10^{-2}	17 %
3	Road holding(m)	1.477×10^{-3}	8.09×10^{-3}	45.22 %
4	Dynamic load coefficient	6.158×10^{-2}	3.377×10^{-2}	45.16 %
5	Suspension travel(m)	1.374×10^{-2}	1.145×10^{-2}	16.66 %
6	Dynamic tire load(N)	$2.658 \times 10^{+2}$	$1.456 \times 10^{+2}$	45.22 %

The simulation finding for the traditional air spring's with one bump road input, Figures 5-10 to 5-16 indicated vertical displacement, velocity, acceleration, road holding, suspension deflection, DLC, and vertical dynamic force of the suspension system take a longer time comparison with the Genesys type, resulting in the discomfort of the passengers and inadequate road handling capabilities.

In the two tables, 5-1 and 5-2 the vibration reduction in pneumatic suspension, Genesys air springs in comparison conventional air springs. For the same load and speed of the vehicle, the DLC value was consistently lower for Gensys spring for air suspension. Based on that, air suspension efficiency was clearly better for Gensys.

When a vehicle is traveling over a smooth surface, the DLC value is often very near zero.

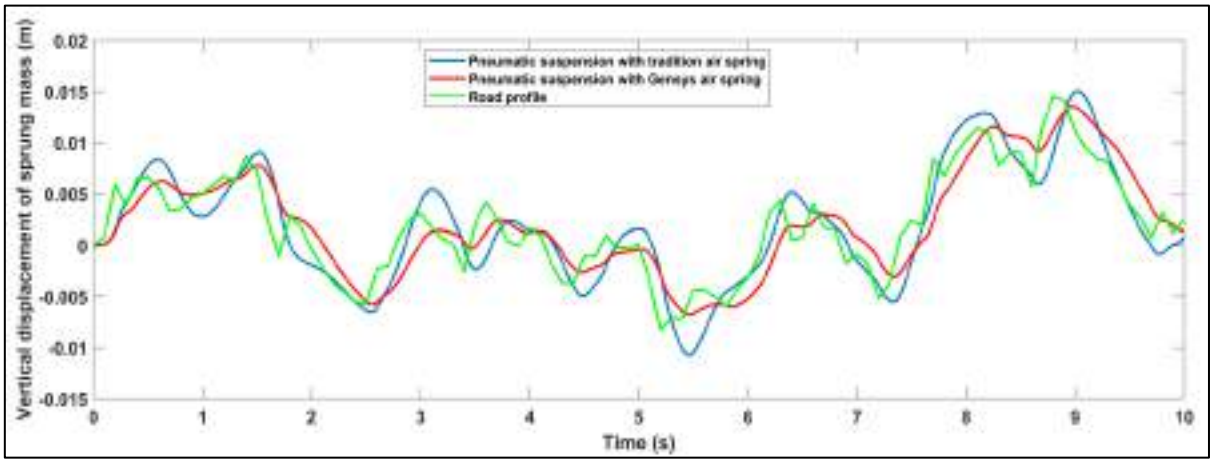

Figure (5-3) Comparison of vertical displacement of sprung mass.

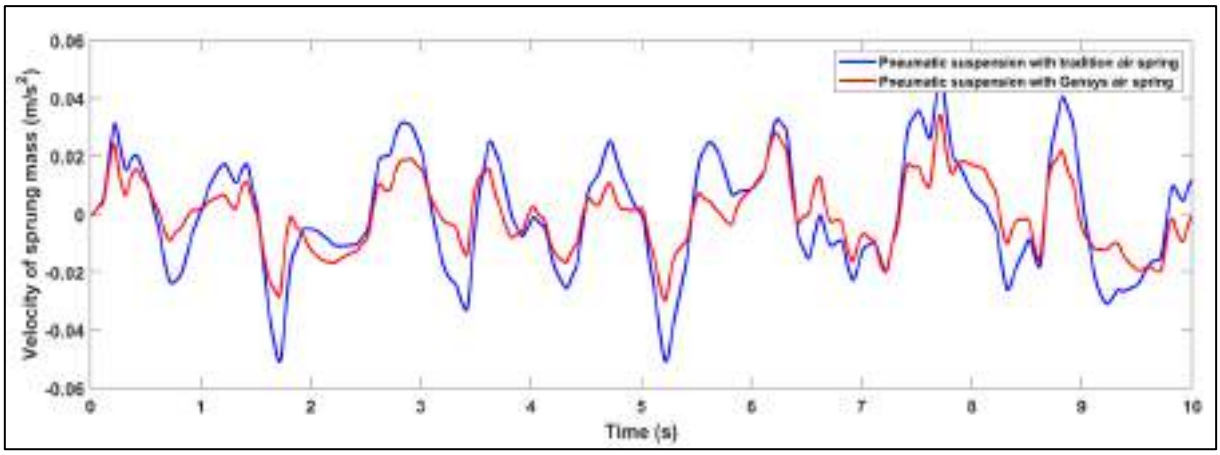

Figure (5-4) Comparison of vertical velocity of sprung mass.

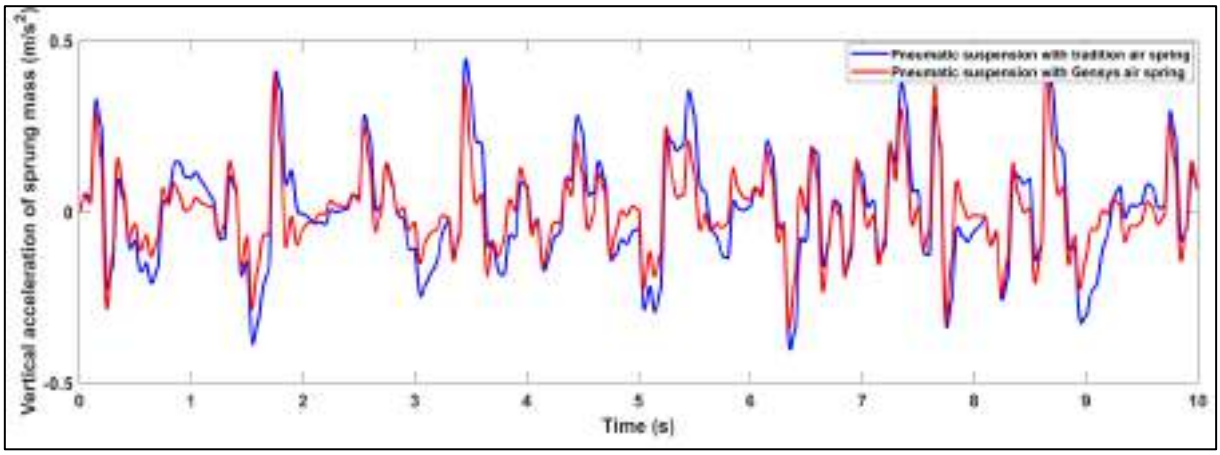

Figure (5-5) Comparison of vertical acceleration of sprung mass.

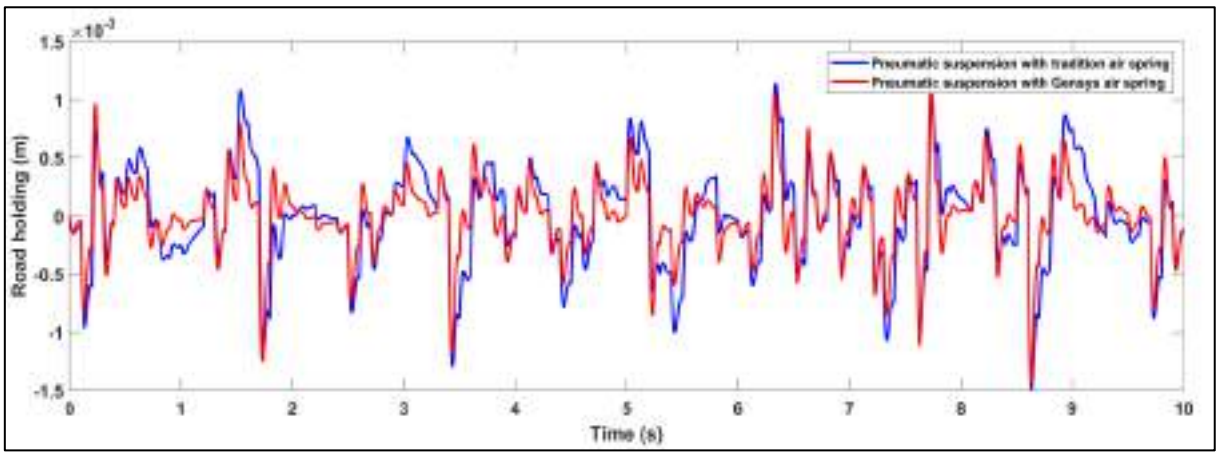

Figure (5-6) Comparison of road holding.

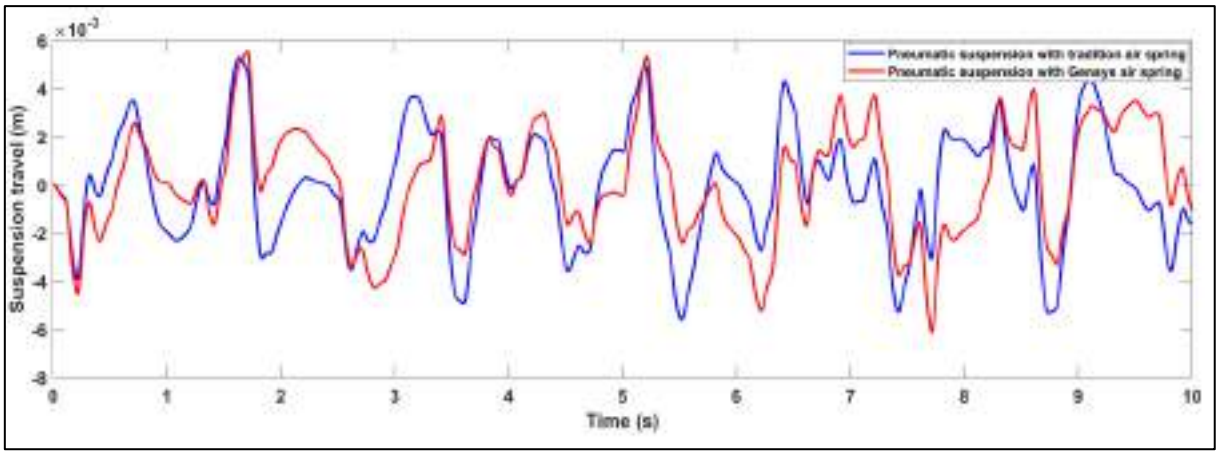

Figure (5-7) Comparison of suspension travel.

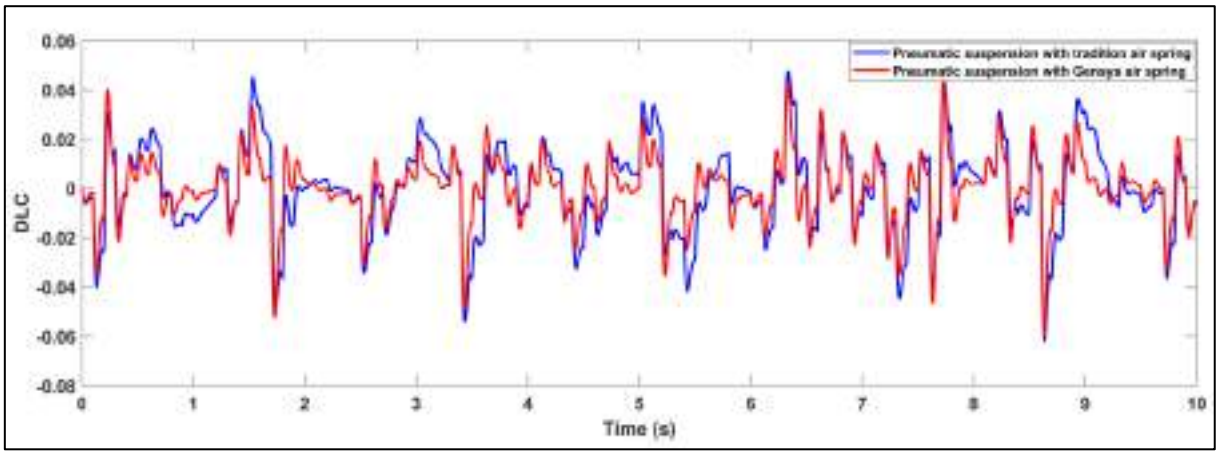

Figure (5-8) Comparison of dynamic load coefficient.

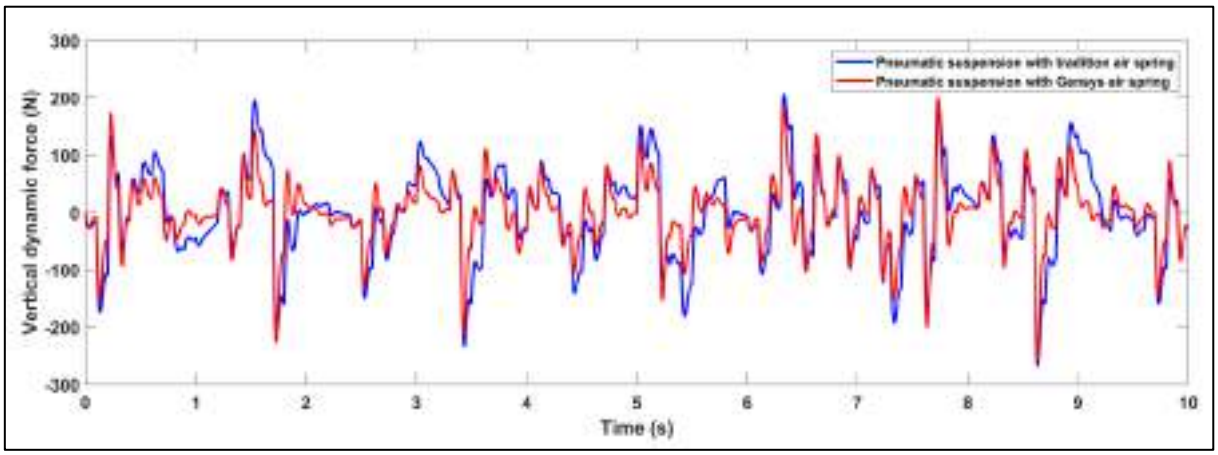

Figure (5-9) Comparison of the vertical dynamic force.

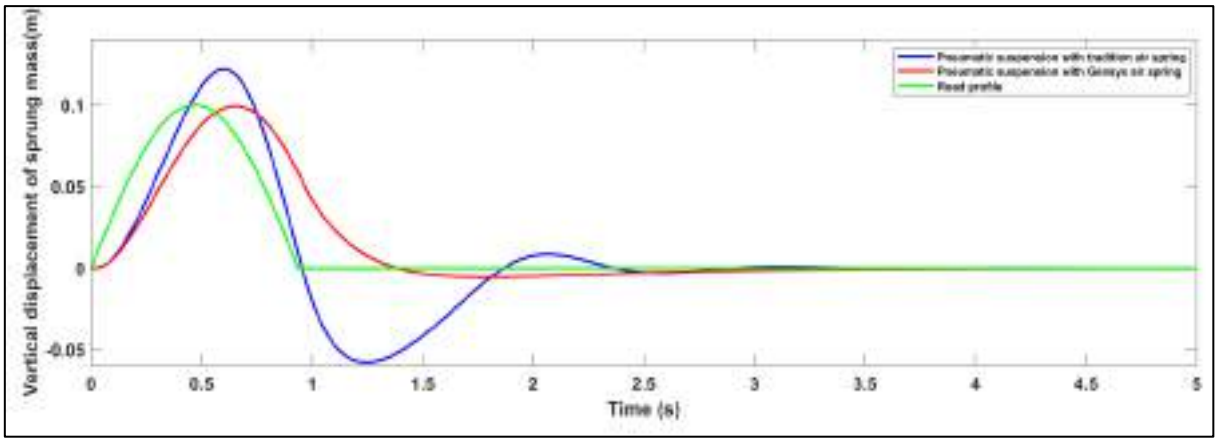

Figure (5-10) Comparison of the vertical displacement of sprung mass.

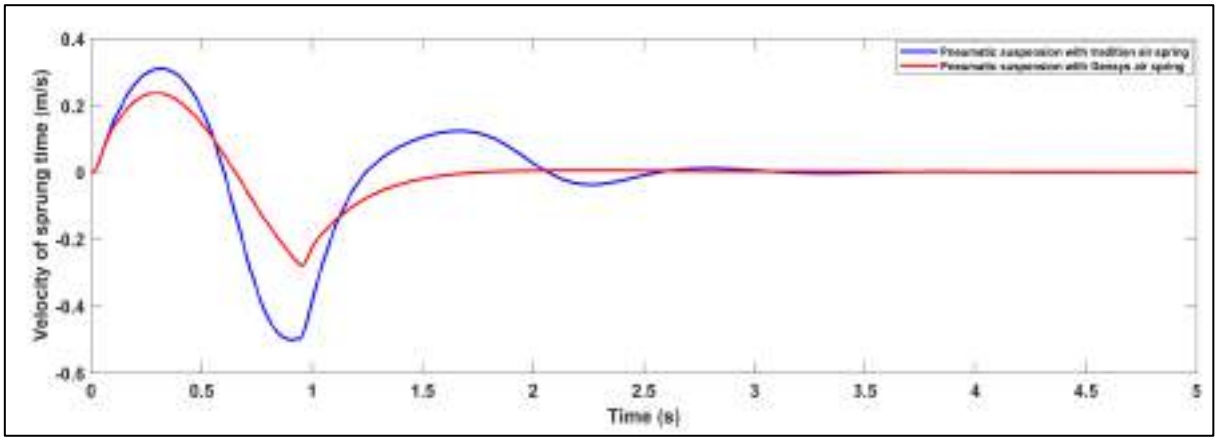

Figure (5-11) Comparison of vertical velocity of sprung mass.

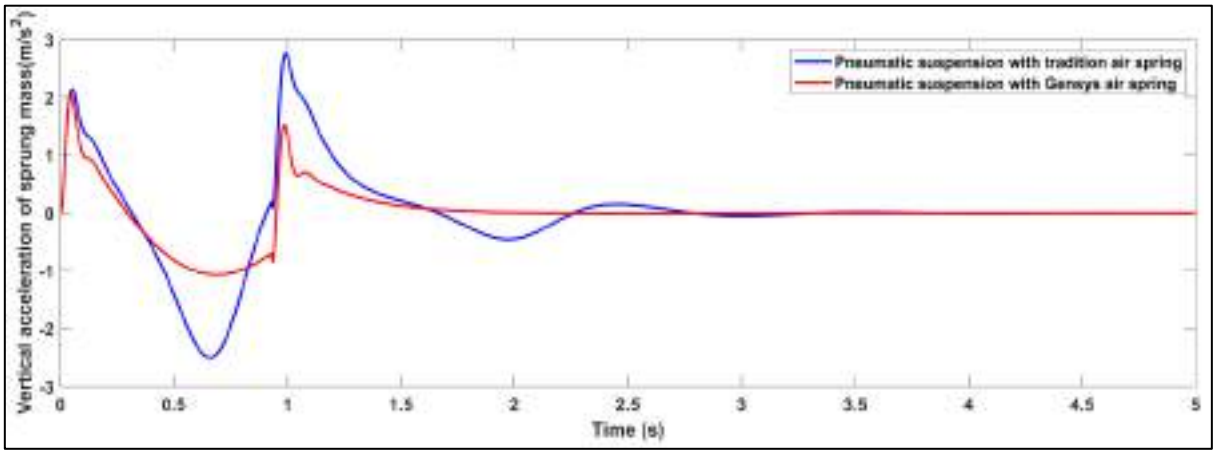

Figure (5-12) Comparison of vertical acceleration of sprung mass.

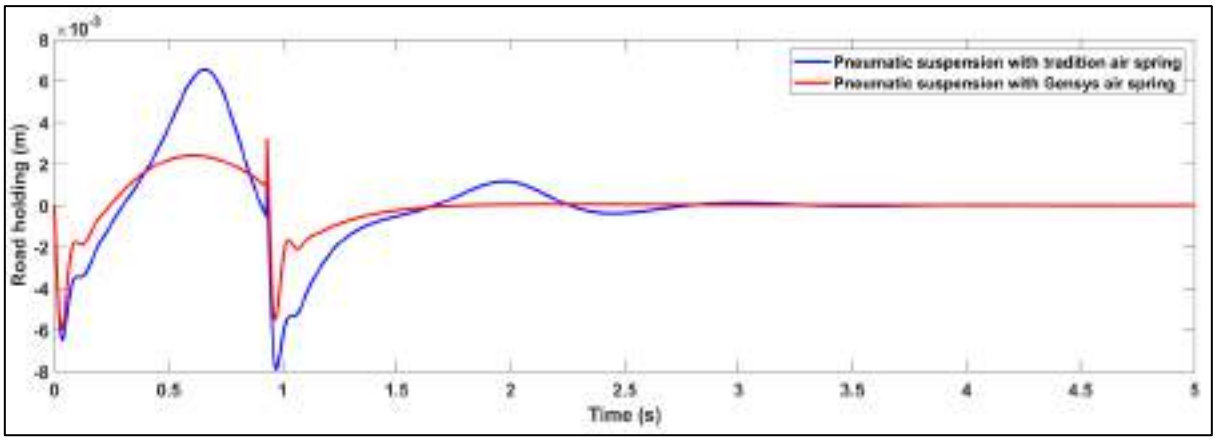

Figure (5-13) Comparison of road holding.

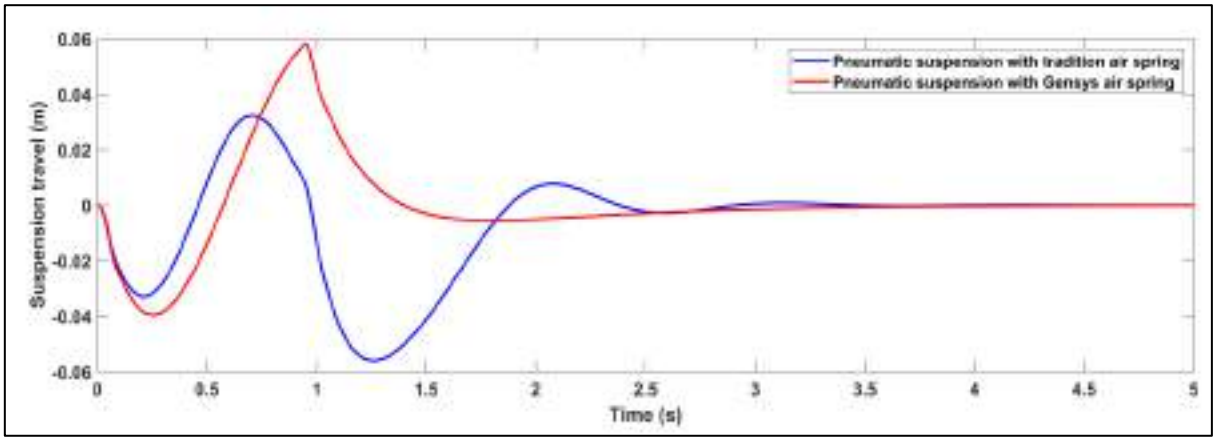

Figure (5-14) Comparison of suspension travel.

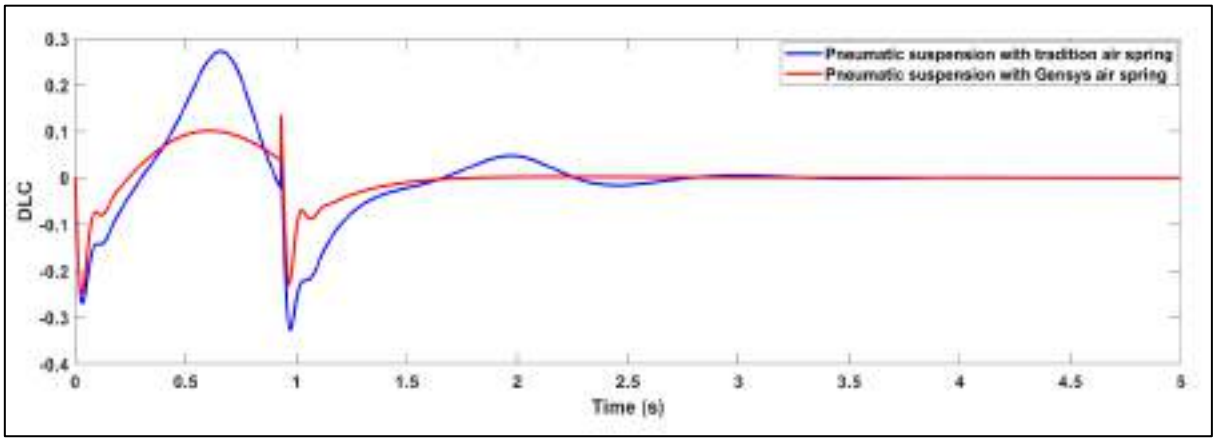

Figure (5-15) Comparison of dynamic load coefficient.

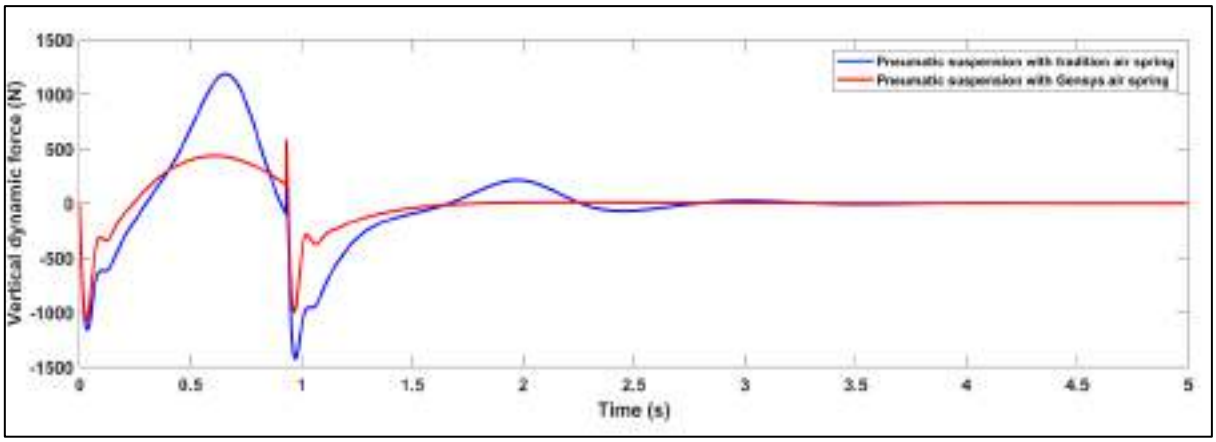

Figure (5-16) Comparison of vertical dynamic force.

Figures 5-17 to 5-22 presented a graph of the efficiency of two different air suspension systems to reduce negative impacts from a vehicle wheel traveling on a road with a bump of 0.1 m and an ISO B road surface when compared at speeds(5,10,15, 20, 25, 30, 40, 50, 60, and 72 m/s). The values of the vertical acceleration parameters (the lower the acceleration i.e the higher the ride comfort), the road stability, and the dynamic load coefficient of two different air suspension systems for two different roads were increased with the increase in vehicle speed.

The results showed that comfort of the ride, dynamic load coefficient, and road holding of air suspension of the quarter-car for Gensys air spring is superior to the traditional air spring as demonstrated by the results in the time domain response and this is in agreement with other studies [33, 92].

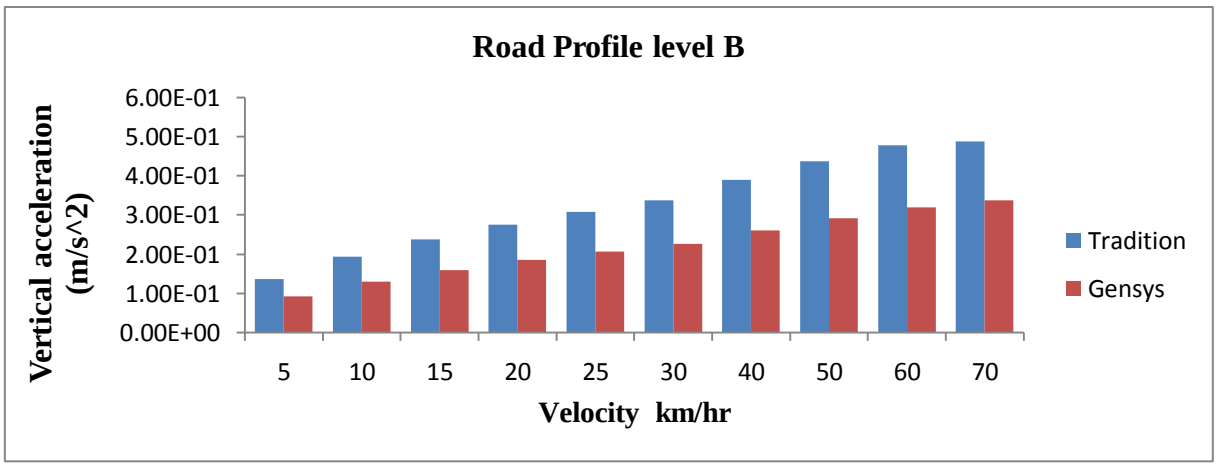

Figure (5-17) Ride Comfort with speed for Road Profile level B.

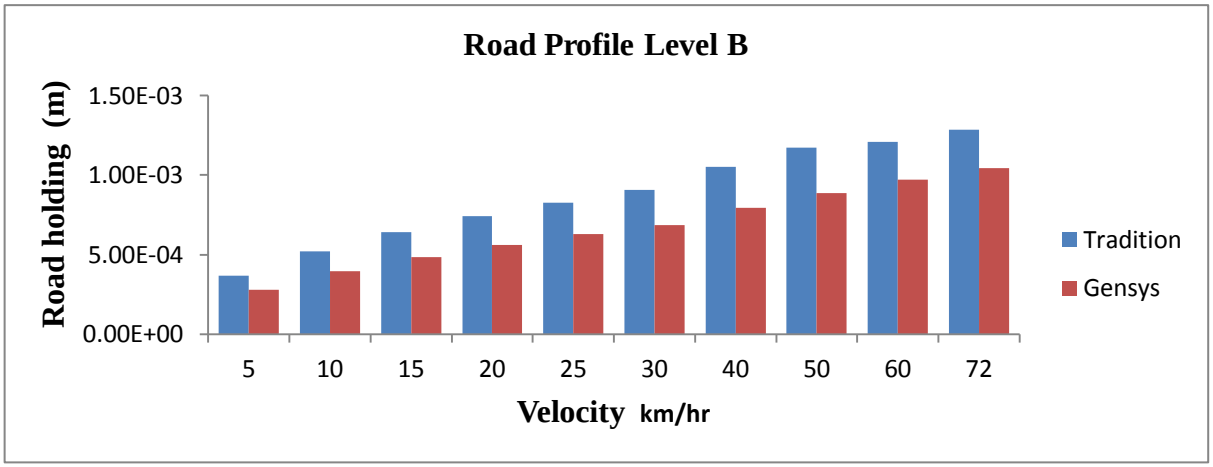

Figure (5-18) Road Holding with speed for Road Profile level B.

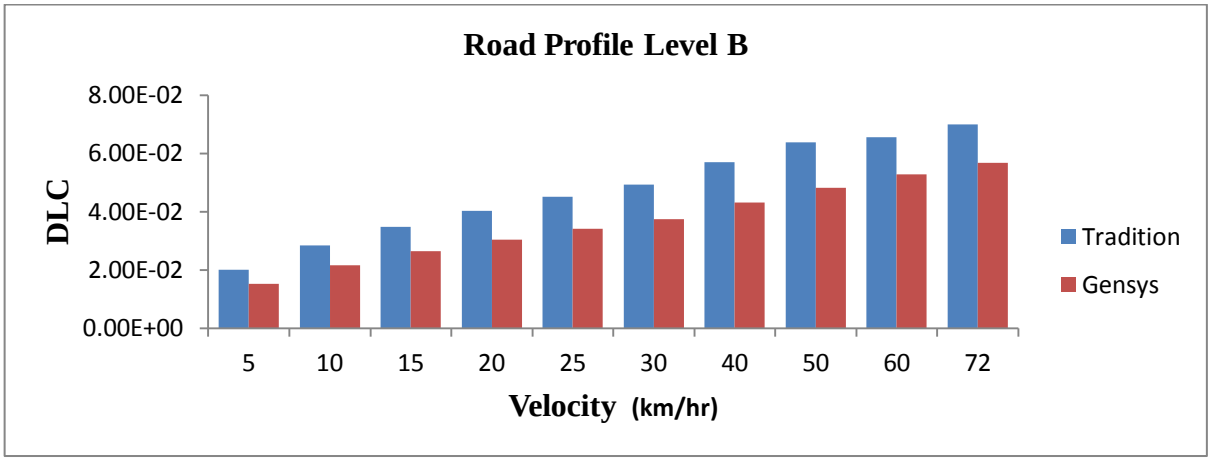

Figure (5-19) Dynamic Load Coefficient with speed for Road Profile level B.

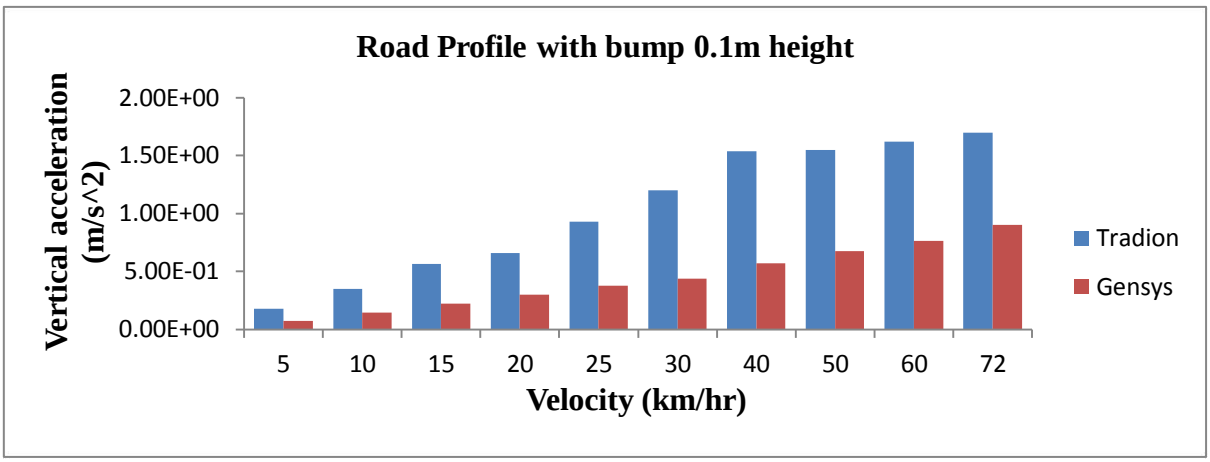

Figure (5-20) Vertical acceleration (ride Comfort) with speed bumpy road (0.1m).

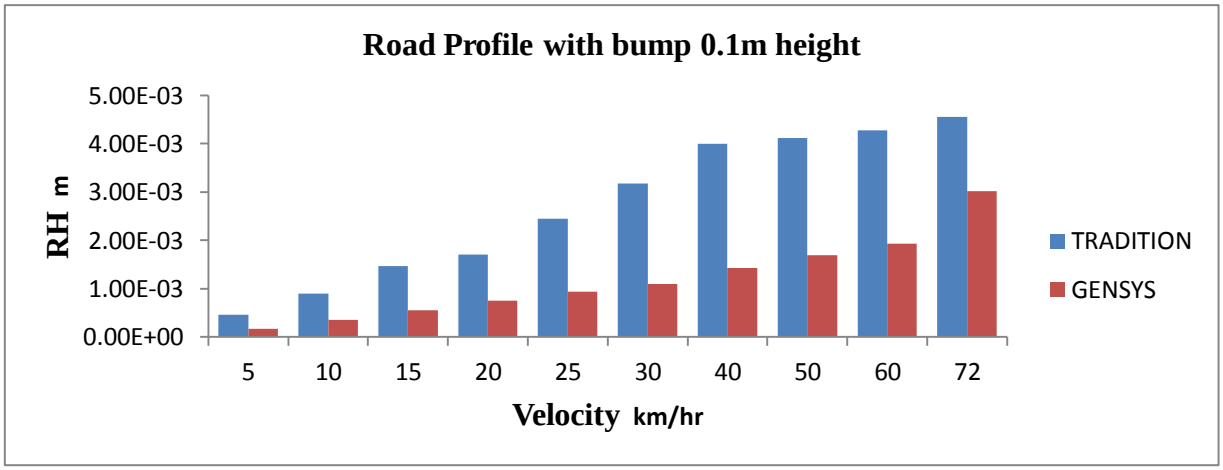

Figure (5-21) Road Holding with speed for bumpy road (0.1m).

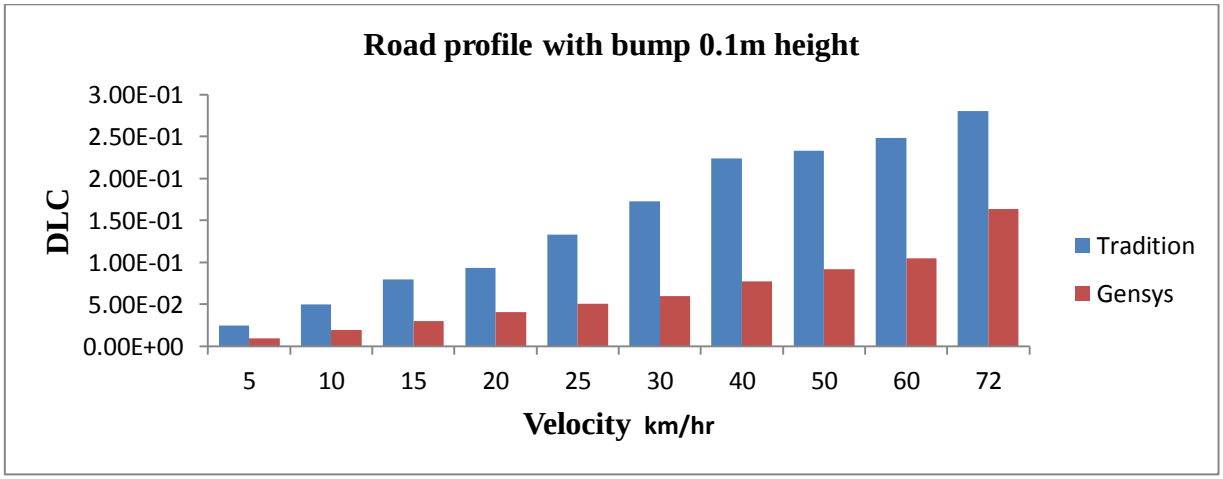

Figure (5-22) Dynamic Load Coefficient with speed for bumpy road (0.1m).

5.3 Results of PID Controller with GA for Nonlinear Pneumatic Quarter Car Integrated with Hydraulic Actuator Model

PID (proportional-integral-derivative) controller with genetic algorithm (GA) has been proposed for adjusting optimum PID parameters for better performance of the air suspension system integrated with a hydraulic actuator, using objective function integrated time absolute error(ITAE).

The objectives of this section is to optimize the PID controller to enhance road holding and ride comfort. Examining is done using MATLAB - Simulink the effect of the proposed controllers. Table (5-3) summarizes the results the road roughness.

Table: (5-3) Reduction in "RMS" values for roughness road input.

No	Parameters	Pneumatic	Optimal (PID)	Reduction
1	Vertical displacement of sprung mass (m)	5.192×10^{-3}	4.743×10^{-4}	89. 8%
2	The acceleration of sprung mass (m/s^2)	1.568×10^{-1}	5.058×10^{-3}	96.77%
3	Vertical dynamic force (N)	6.548	5.925	9.5%
4	DLC	2.223×10^{-2}	2.013×10^{-2}	9.44%
5	Road holding (m)	4.089×10^{-4}	3.703×10^{-4}	9.43%
6	Velocity of sprung mass (m/s^2)	1.351×10^{-2}	4.084×10^{-4}	96.97%

Uncontrolled (pneumatic system), PID controlled parameters of the ride comfort and road holding for the sprung mass are compared, for input road (roughness road class B, velocity 72 km/h)) are presented in Figures (5.3a-5.3h) in time domain.

Figure (5-23a) showed how the proposed controller reduces the peak amplitude from 1.34×10^{-2}at time 8.952s for pneumatic to 1.19×10^{-3}at time 9.84s for control PID of vertical displacement, this gives the passenger the feeling that he is walking in one level and Figure(5-23b) show the reduction

velocity from 1.35×10^{-2} to 4.084×10^{-4} for sprung mass. As shown in Figure(5-23c), the RMS of acceleration is decreased significantly and this reduction in body acceleration magnitude ensures greater ride comfort. Figures (5-23d), (5-23e), and (5-23f) illustrate the force dynamic, dynamic load coefficient, and road holding of unsprung mass for proposed control less than the force dynamic of unsprung mass when compared with pneumatic suspension, this leads to the improvement the handling of the vehicle with the road. Figure (5-23g) indicated that the fluctuations amplitude of the suspension travel signal is downward direction (negative direction). In response to a road bump, the suspension system's displacement needs to be continuously changed to make sure that the vehicle body's (sprung mass) displacement and acceleration are minimal.

Because of the time difference in the response between the actuator and the air spring, there is a difference in response suspension travel. Figure (5.23h) shows the actuator force with time. When the controller adjusts the initial oscillation, the maximum actuator force (F_a) equal to 329.3 (N) is reached. Figures (5.23a to 5.23e) illustrate that settling time and peak values have decreased by the proposed control in contrast to the pneumatic system for these sprung mass's characteristics are displacement, velocity of sprung mass acceleration (ride comfort), road holding, force dynamic, and dynamic load coefficient. As shown in the table(5-3) which provides the reduction's percentage in “Root Mean Square” among the different parameters for the roughness road.

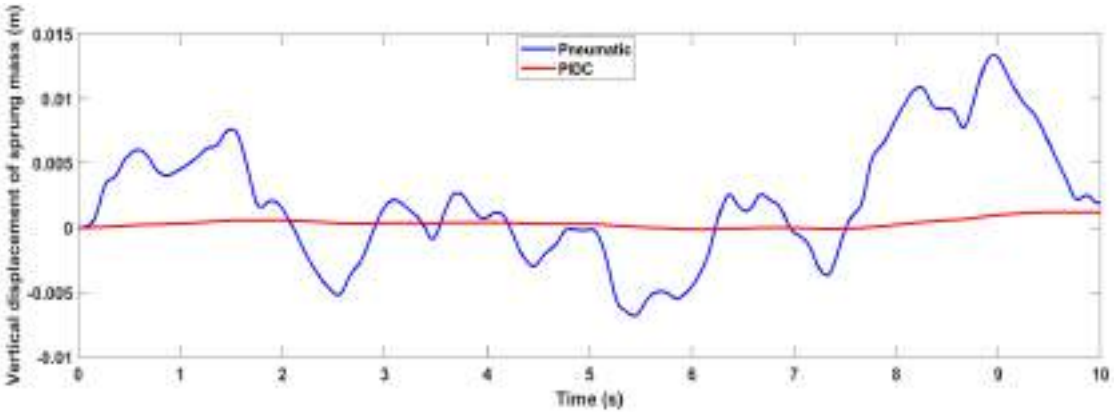
Pneumatic
PIDC
Vertical displacement of sprung mass (m)
Time (s)

(a)

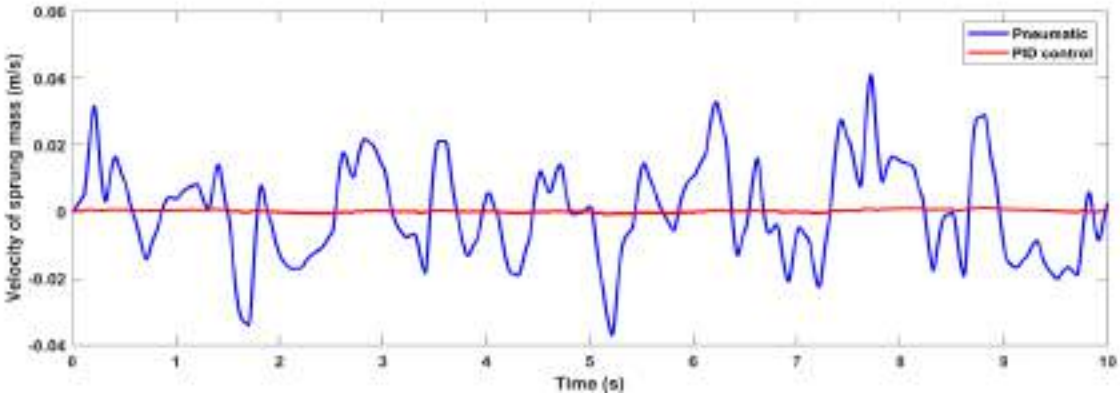
Pneumatic
PID control
Velocity of sprung mass (m/s)
Time (s)

(b)

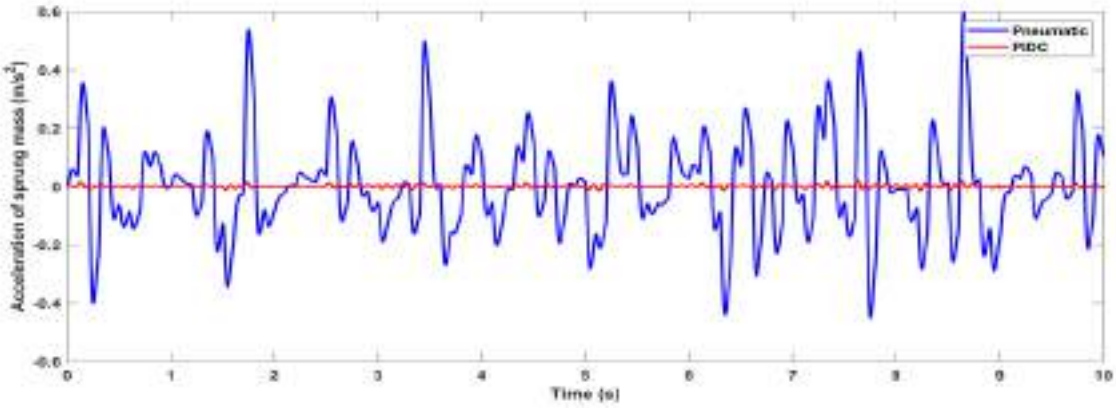
Pneumatic
PIDC
Time (s)

(c)

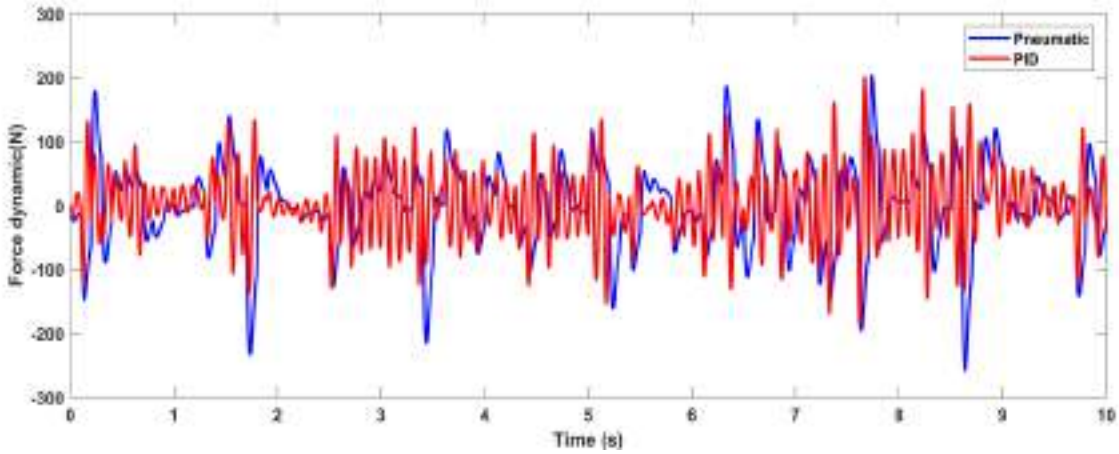
Pneumatic
PID
Force dynamic(N)
Time (s)

(d)

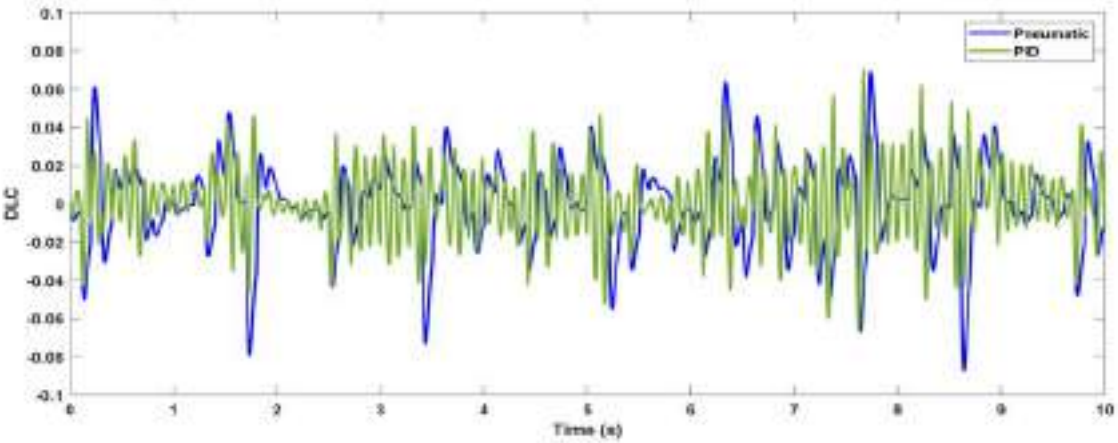
Pneumatic
PID
DLC
Time (s)

(e)

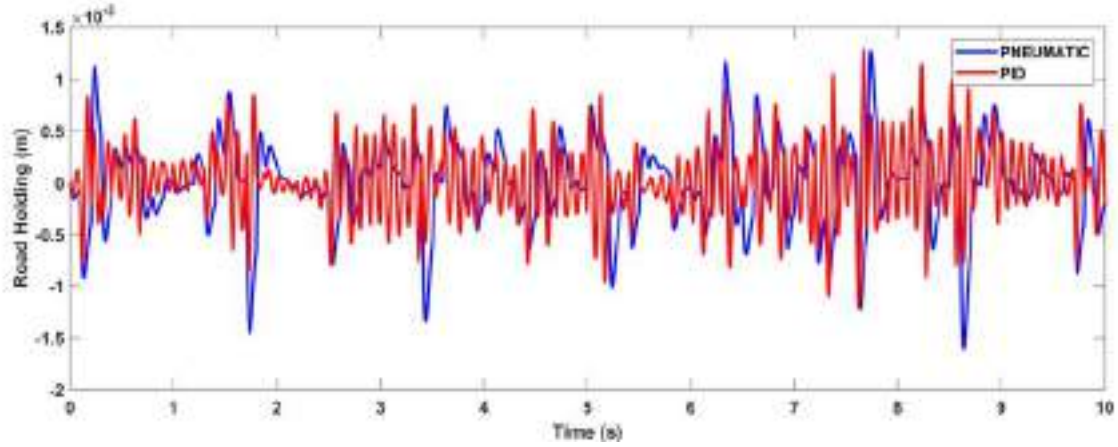
PNEUMATIC
PID
Road Holding (m)
Time (s)

(f)

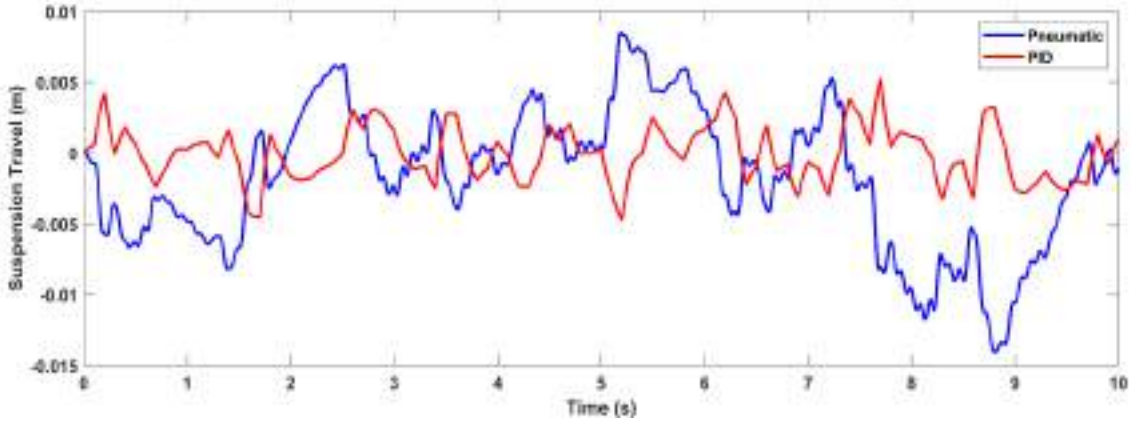

(g)

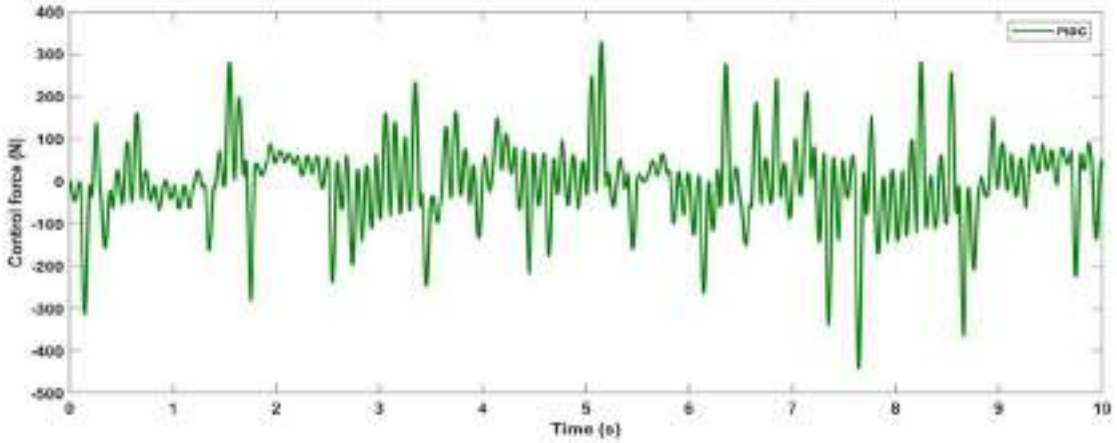

(h)

Figure (5-23) Performance Analysis of PID control for active pneumatic suspension (roughness road class B, velocity 72 km/h).

PID controller greatly minimize vibration of the quarter car system's sprung mass, as seen in the figures. Through the results, it can be shown PID is an effective controller compared to the air suspension system in simulations. PID controlled parameters, uncontrolled (pneumatic system) of the comfort of the ride and hold the road are compared, to the input road (two bump, velocity 36 km/h)) are presented in the following figures(5-24a to 5-24h) in the time domain.

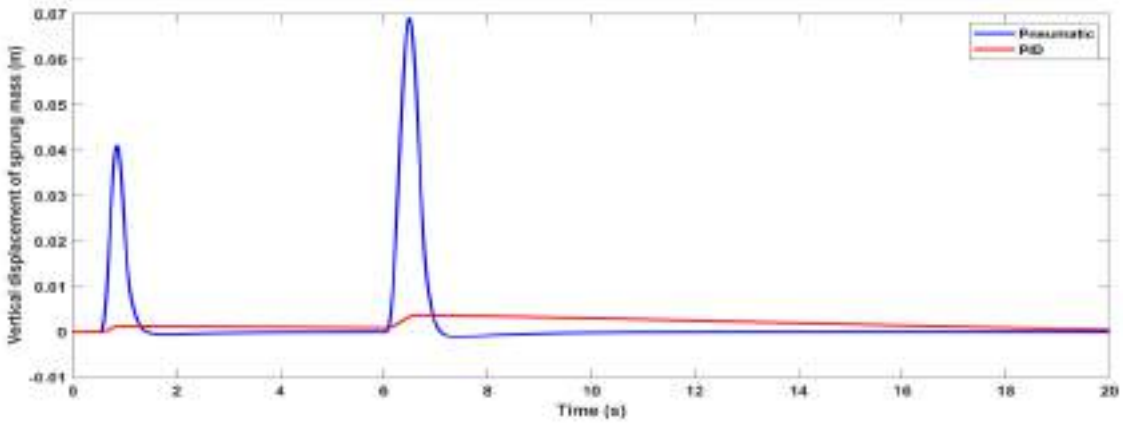

(a)

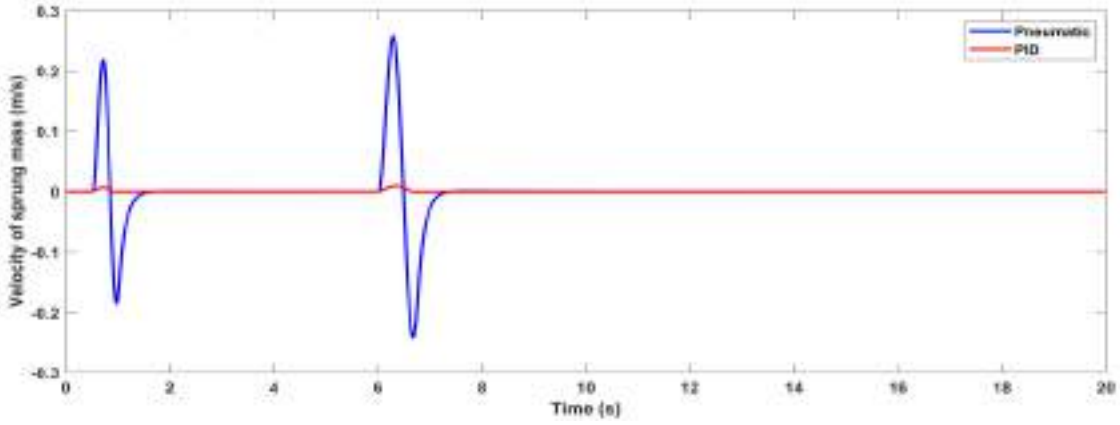

(b)

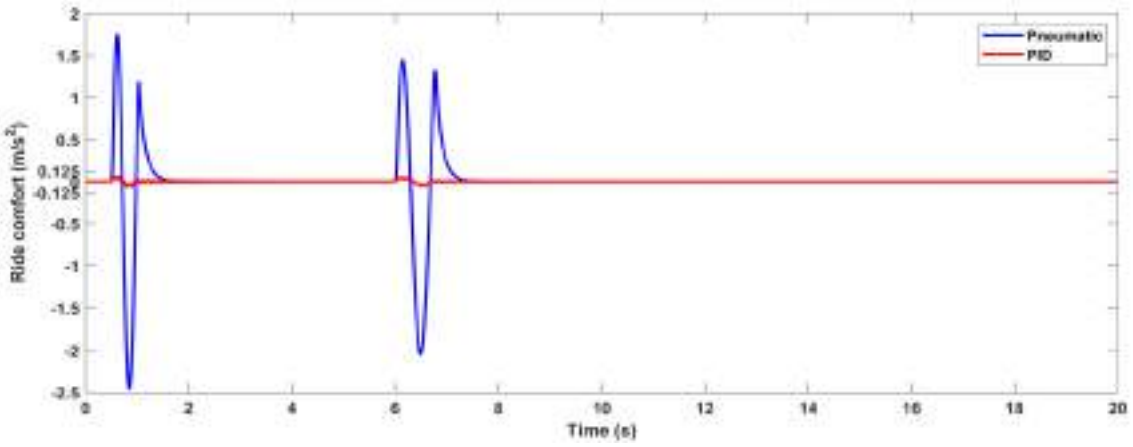
Pneumatic
PID
Ride comfort (m/s²)
Time (s)

(c)

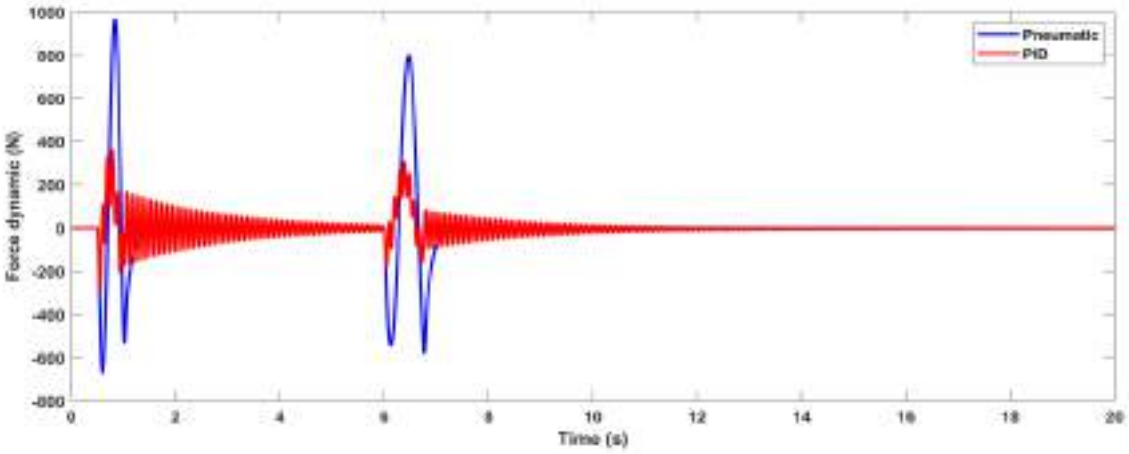
Pneumatic
PID
Force dynamic (N)
Time (s)

(d)

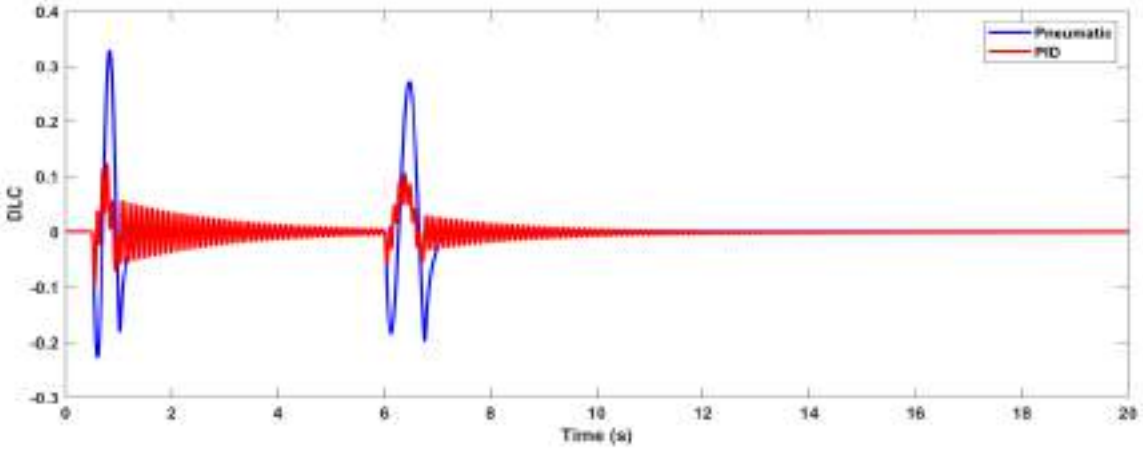
Pneumatic
PID
DLC
Time (s)

(e)

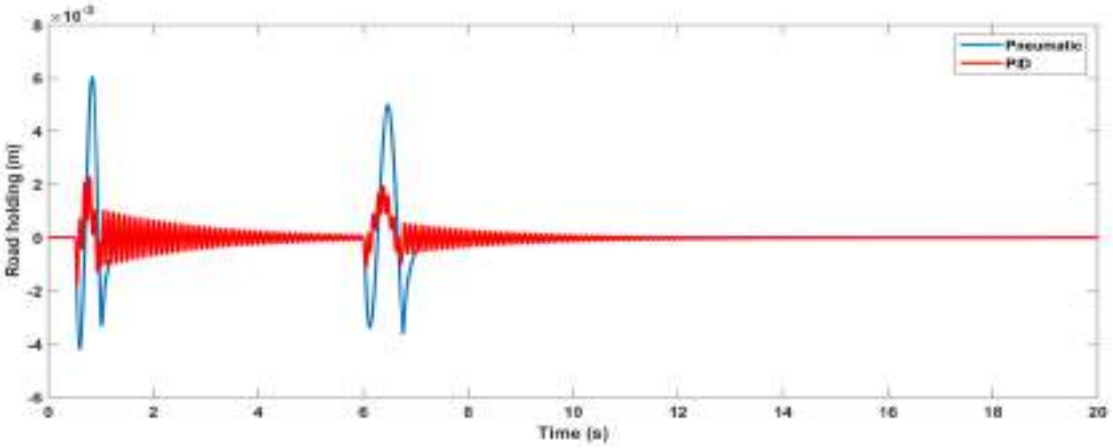

(f)

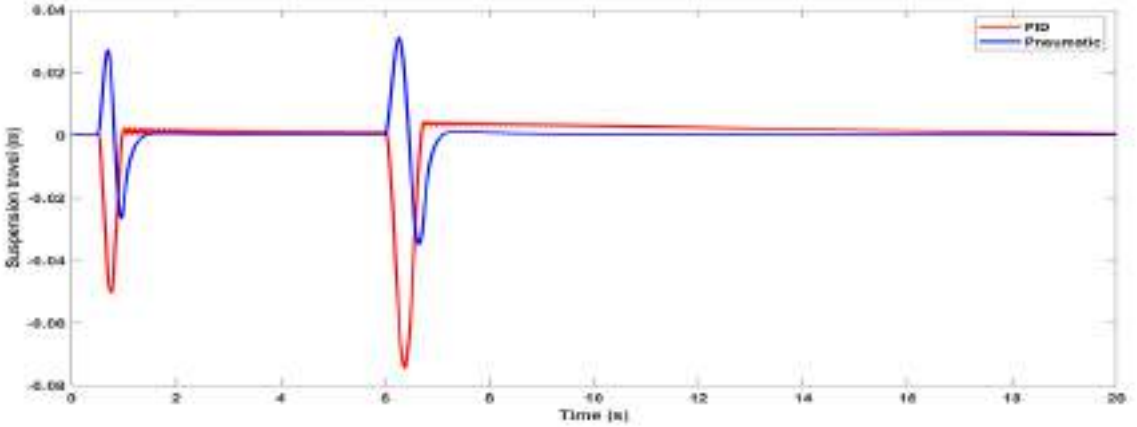

(g)

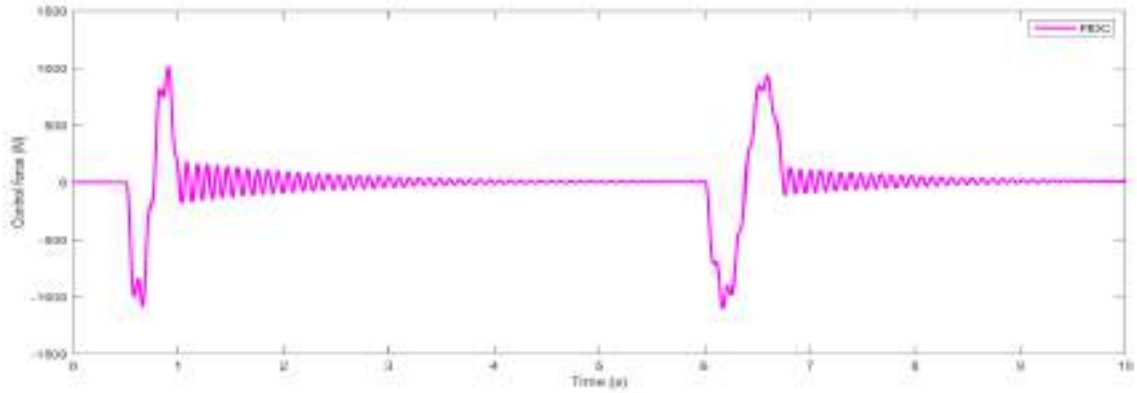

(h)

Figure (5-24) Performance Analysis of PID control for active pneumatic suspension (road two-bump, velocity 36 km/h).

The PID controller tuned by the GA is designed for the pneumatic active suspension system for two bump. The fitness functions for the best trial out of a total of 20 trials to get best results. Figure (5-25) represents the best and mean fitness with the number of generation, where the GA algorithm reduces the error until reaching the convergence stage. The proposed control in this section corresponds in improving response with [97] and [98].

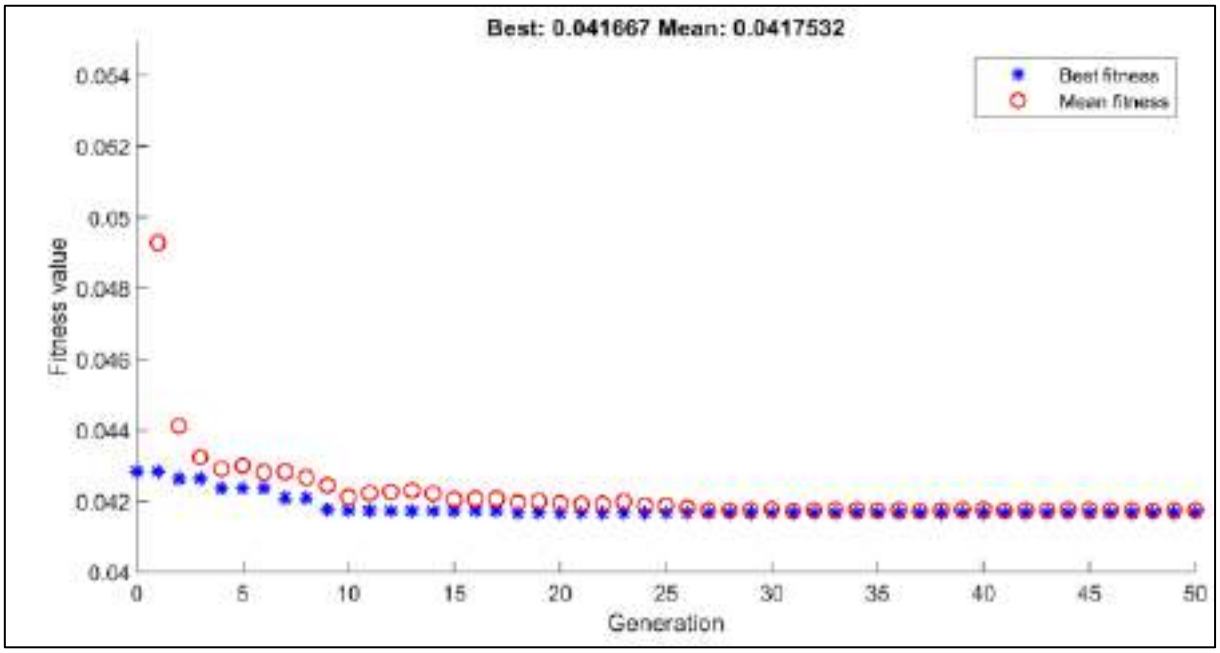

Figure (5-25) Fitness obtained by GA algorithm.

The reason why the displacement response does not return in the shortest possible time is that the processing of the PID controller(Lacks to settling time)when subjected to nonlinear systems modeling is ineffective when compared to the rest of the controllers in one domain and is effective in another, although there are impressive responses to vertical acceleration and the holding the road. Through the results the control PID was not adaptive with different bumpy roads.

5.4 Results of performance Analysis of the Proposed Fractional-Order-PID Controller

Roughness road (class B,72 km/h), the performance of pneumatic active none linear quarter vehicle suspension system for proposed control FOPID with Genetic algorithm

For roughness road class B, Figures (5.26a, 5.26b, and 5.26c) show "RMS" the vertical displacement of sprung mass FOPID controller decreased 96% compared the pneumatic system , or the system without a controller and for vertical acceleration of sprung mass decreased 97% compared to the pneumatic system and for vertical velocity of sprung mass decreased 98% , this means a high rate of passenger comfort, but at the expense of vehicle stability, meaning that the stability will be less compared to the pneumatic system through as shown in figures (5-26d) and (5-26e) illustrate that the value of road holding $6.938\times 10^{-4}$for FOPID controller and $4.573\times 10^{-4}$for the pneumatic system , which will increase from the pneumatic system to the FOPID controller, meaning that the stability of the vehicle will decrease, as well as the vertical dynamic wheel force will increase its value compared to the pneumatic system through the dynamic load coefficient (DLC) value that shows increase from 2.269×10^{-2} for the pneumatic system in comparison to 3.772×10^{-2} for the FOPID controller. Figure (5-26f) shows the vertical dynamic tire force that has deteriorated by the controller with an increase of 40%.

Figures (5-26i, 5-26j, and 5-26k) illustrated the change in the response for both K_p, K_i, and K_d with time. Table(5-4) summarizes the results performance parameters for rough road.

Table(5-4). Reduction in "RMS" values for roughness road input.

No	Parameters	Pneumatic	Optimal (FOPID)	Reduction (improvement)	Increase (no improvement)
1	Vertical displacement of sprung mass (m)	5.497×10^{-3}	1.282×10^{-5}	96.22%	-
2	The acceleration of sprung mass(m/s^2)	1.516×10^{-1}	1.974×10^{-3}	97.66%	-
3	Road holding (m)	4.573×10^{-4}	6.938×10^{-4}		34%
4	Velocity of sprung mass(m/s^2)	1.414×10^{-2}	3.576×10^{-5}	98.17%	-

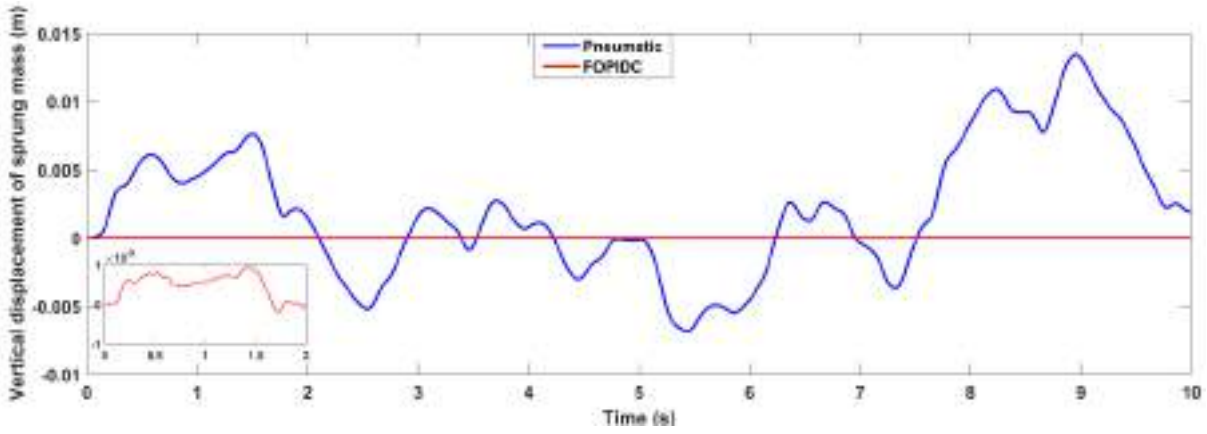

(a)

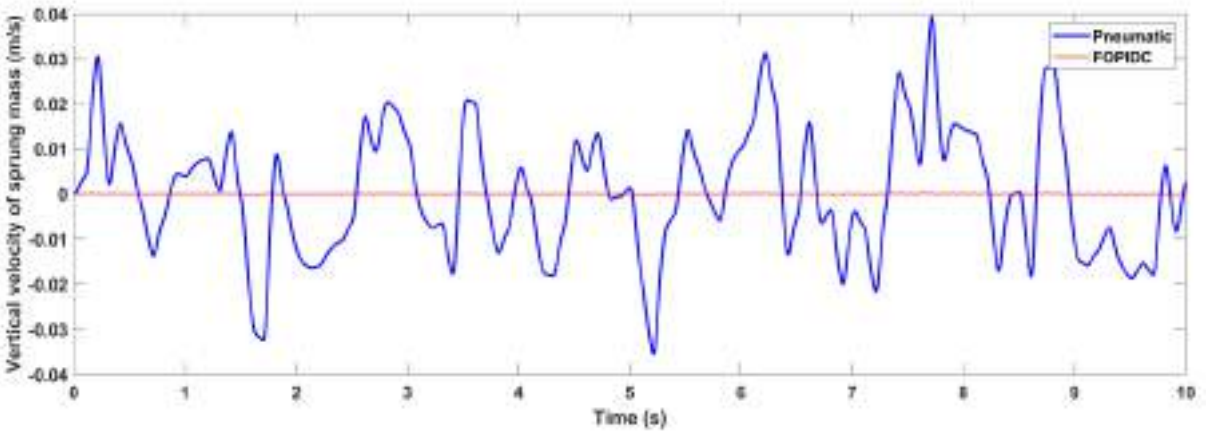

(b)

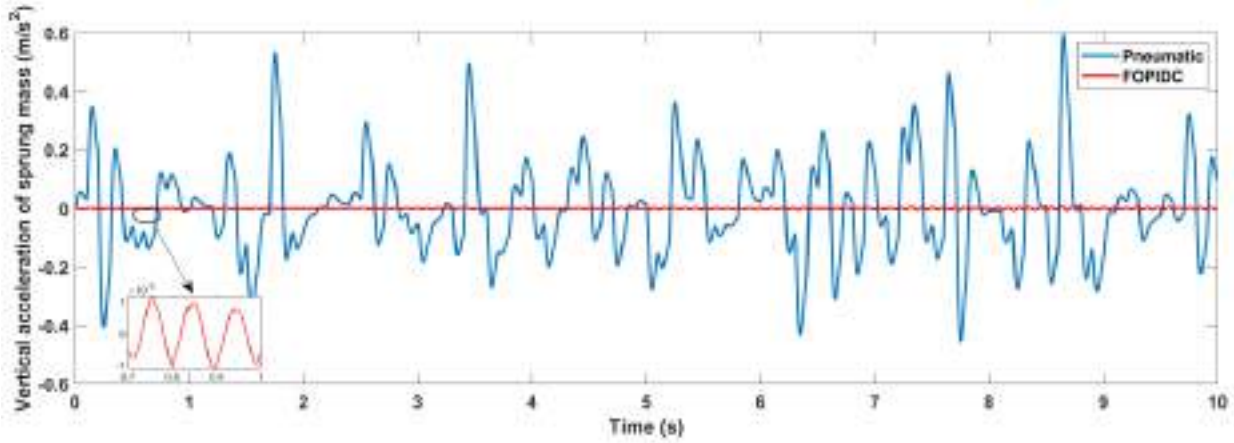
Vertical acceleration of sprung mass (m/s²)
Time (s)
Pneumatic
FOPIDC

(c)

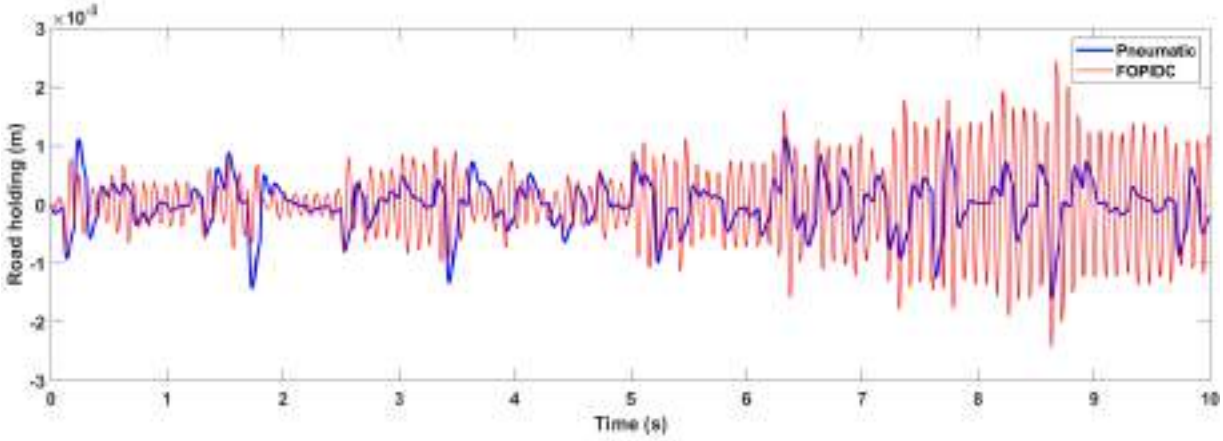
Road holding (m)
Time (s)
Pneumatic
FOPIDC

(d)

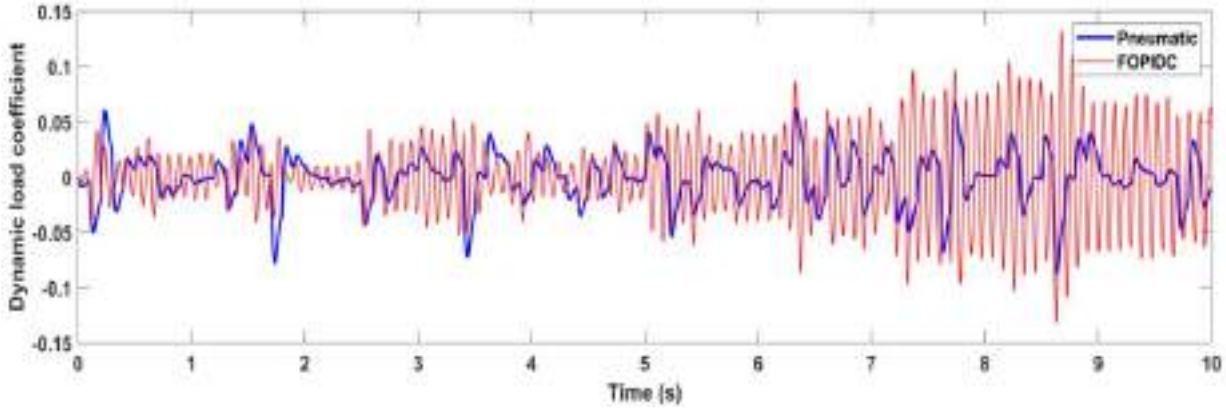
Dynamic load coefficient
Time (s)
Pneumatic
FOPIDC

(e)

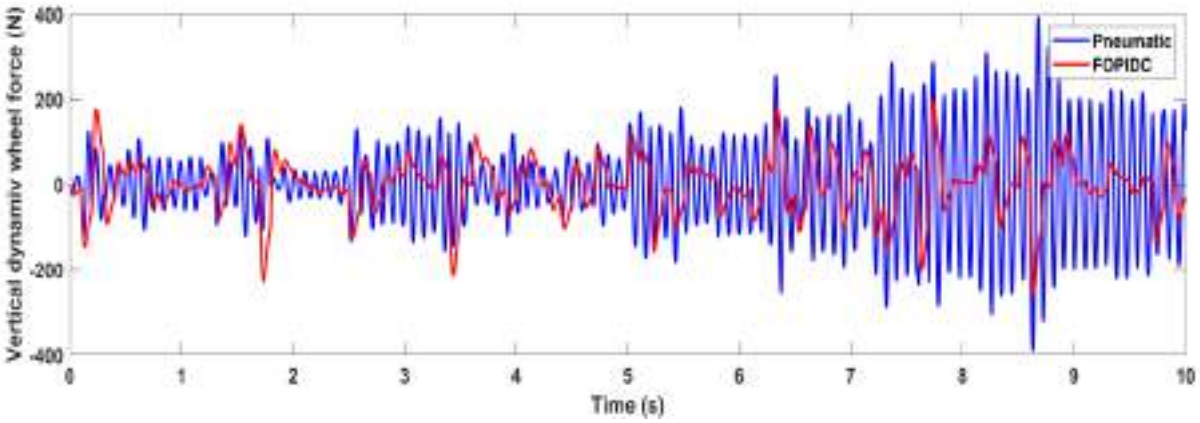
Vertical dynamiv wheel force (N)
Time (s)
Pneumatic
FOPIDC

(f)

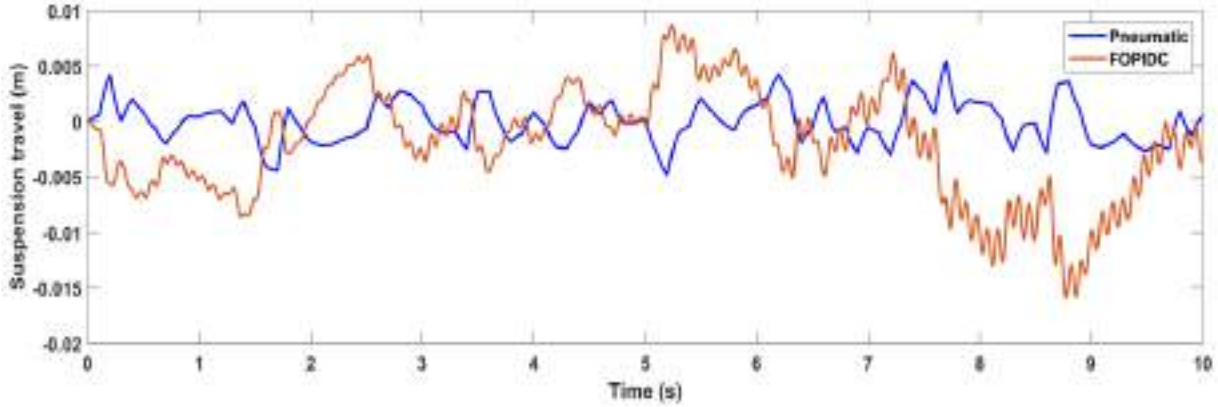
Suspension travel (m)
Time (s)
Pneumatic
FOPIDC

(g)

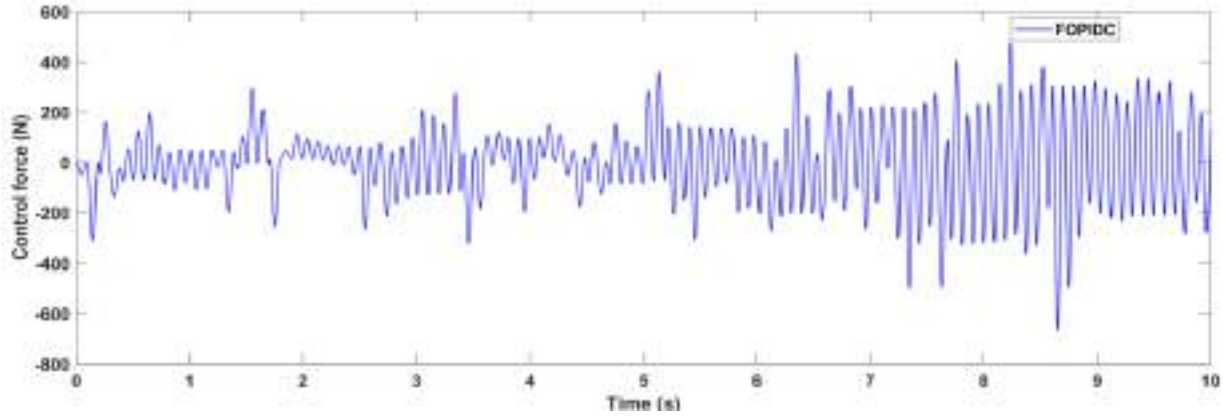
Control force (N)
Time (s)
FOPIDC

(h)

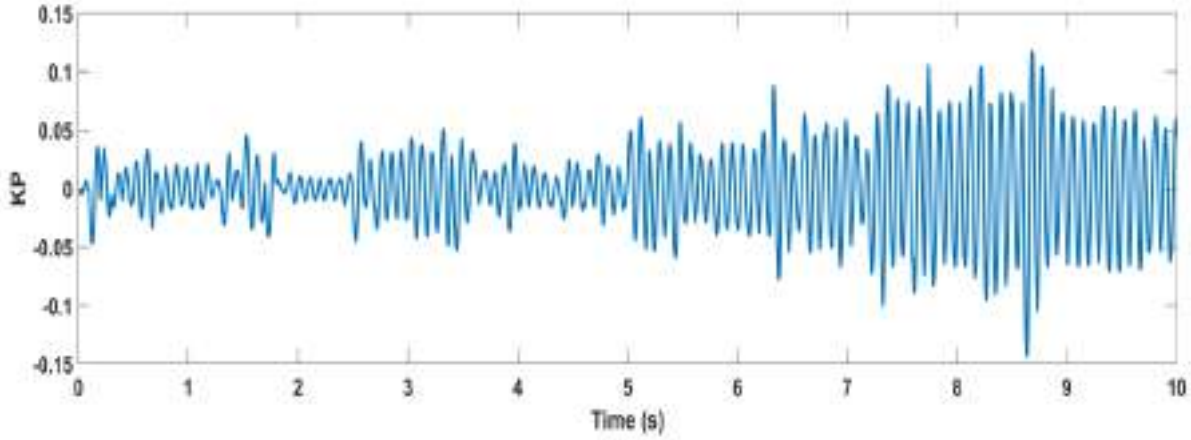

(i)

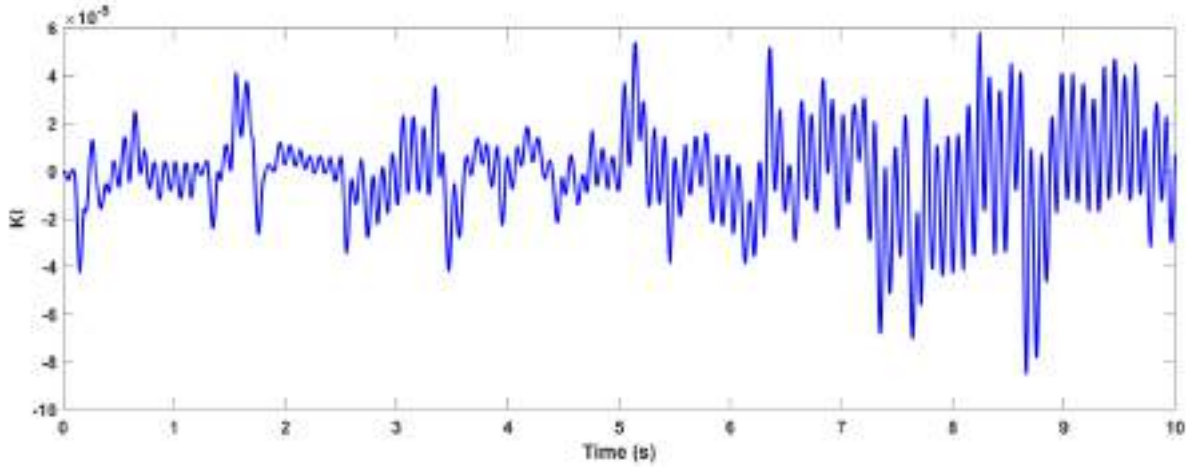

(j)

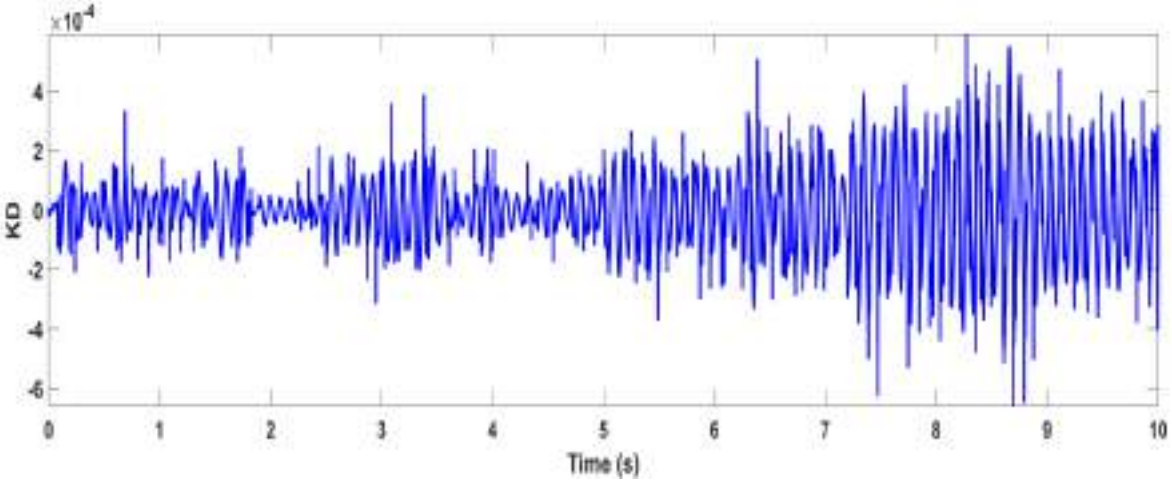

(k).

Figure (5-26) Performance Analysis of FOPID control for active pneumatic suspension (roughness road class B, velocity 72 km/h).

For bumpy road (two bump) and velocity of vehicle 36 km/h, the parameters of pneumatic active none linear quarter vehicle suspension system for proposed control FOPID with GA algorithm.

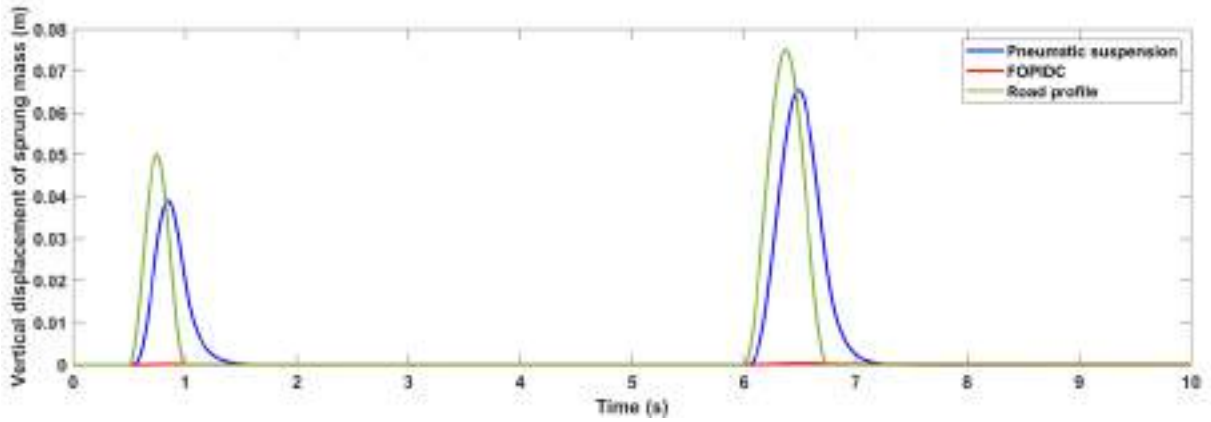

(a)

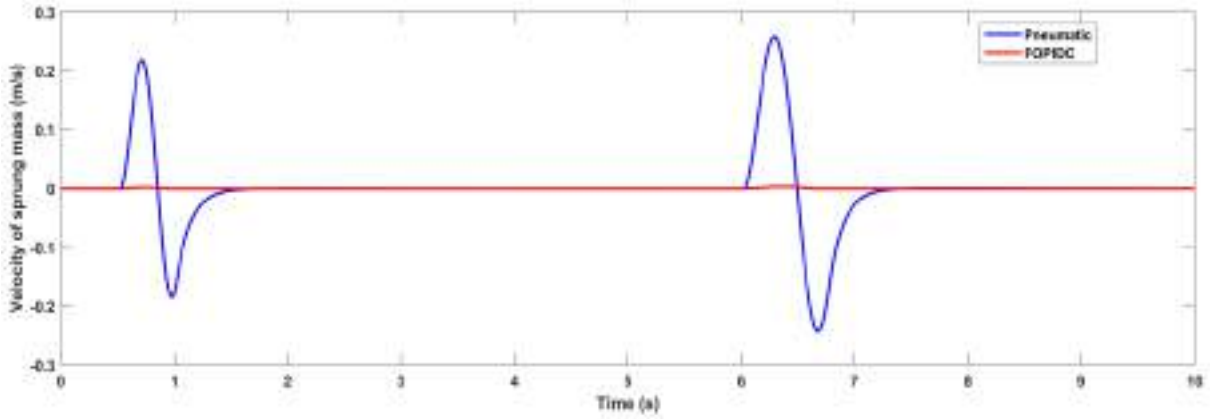

(b)

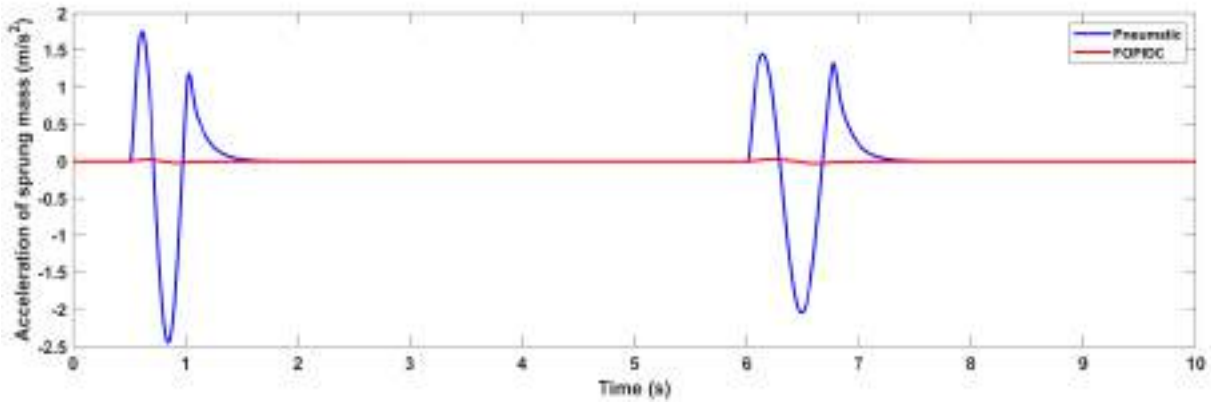

(c)

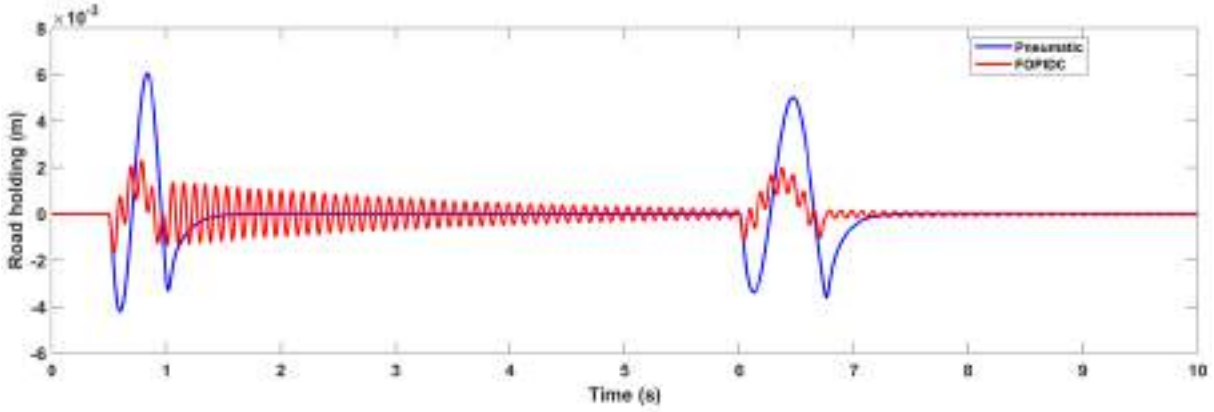
Road holding (m)
Time (s)
Passivo
FOPIDC

(d)

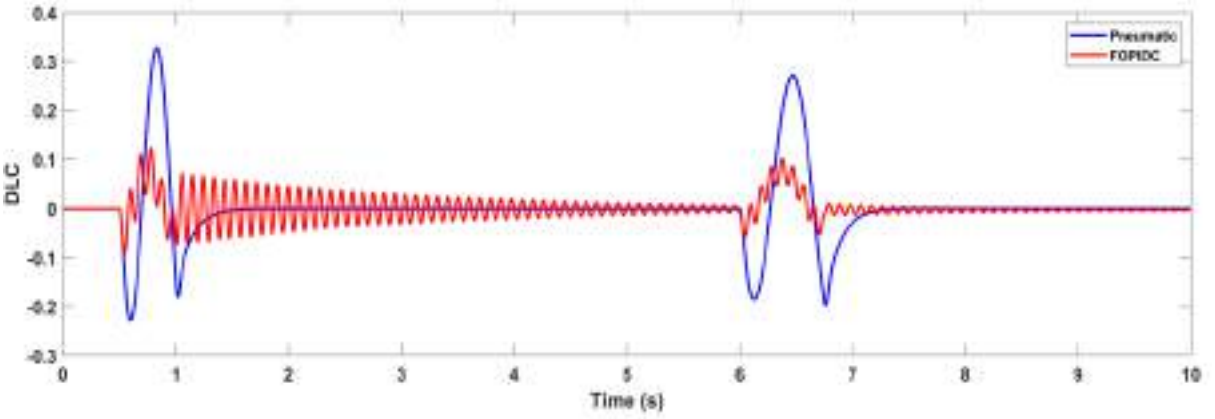
DLC
Time (s)
Passivo
FOPIDC

(e)

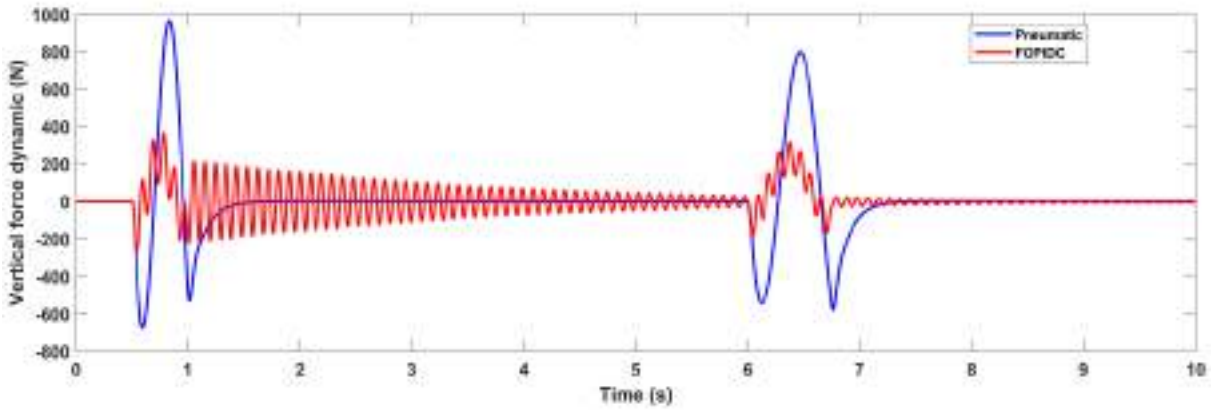
Vertical force dynamic (N)
Time (s)
Passivo
FOPIDC

(f)

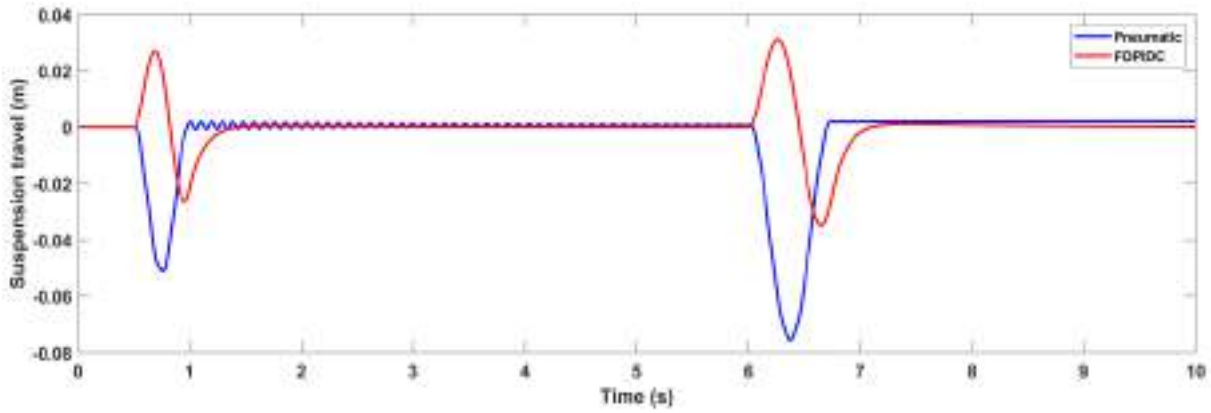

(g)

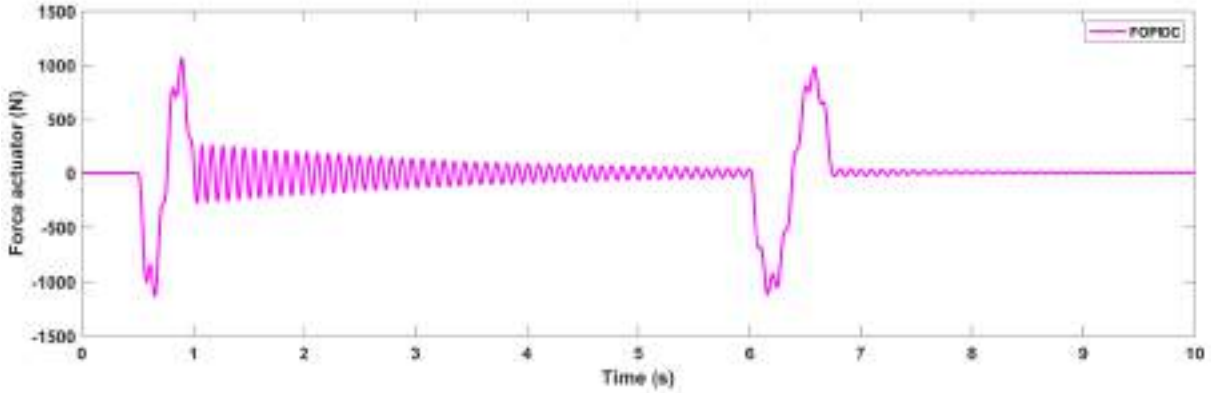

(h)

Figure (5-27) Performance Analysis of FOPID control for active pneumatic suspension (road (two-bump), velocity 36 km/h).

Figure (5-28) represents the best and mean fitness with the number of generations, where the GA algorithm reduces the error until reaching the convergence stage.

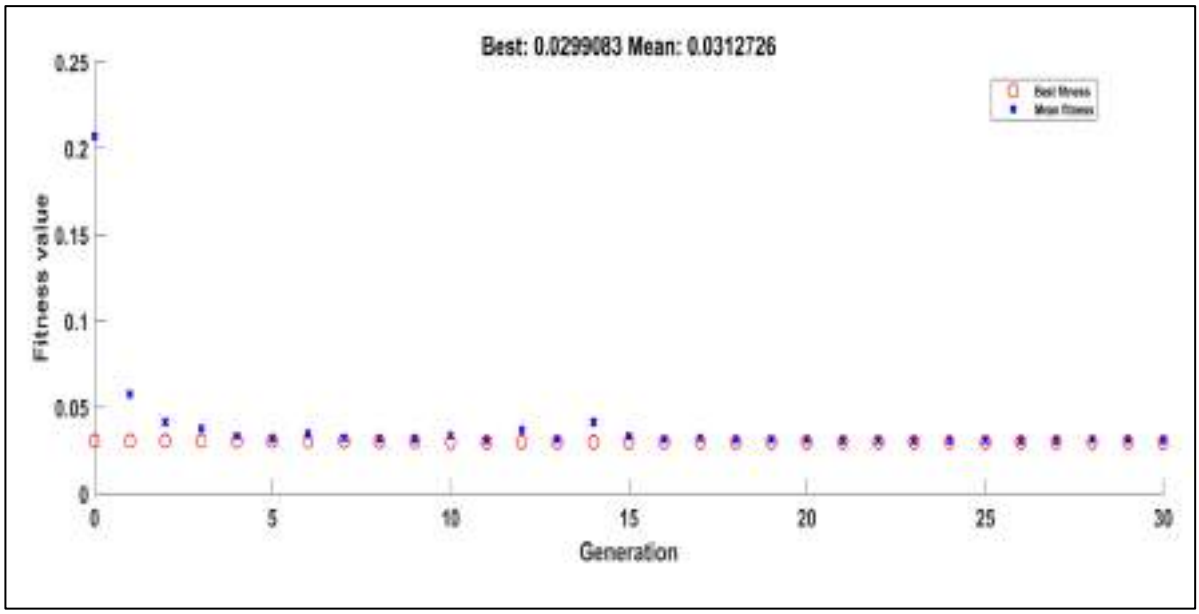

Figure (5-28) Fitness value obtained by GA

Table (5-5) Reduction in "RMS" values for (two-bump)road input.

No	Parameters	Pneumatic	Optimal (FOPIDC)	Reduction
1	the sprung mass's vertical displacement (m)	1.4×10^{-2}	1.285×10^{-4}	98%
2	sprung mass's acceleration ($m.s^{-2}$)	4.224×10^{-1}	1.995×10^{-3}	99.5%
3	Vertical dynamic wheel force (N)	1.668×10^{2}	8.968×10^{1}	46.12%
4	DLC	5.669×10^{-2}	3.053×10^{-2}	46%
5	Road holding (m)	1.043×10^{-3}	5.616×10^{-4}	46.15%
6	Velocity of sprung mass(m/s^2)	5.33×10^{-2}	1.854×10^{-4}	99.6%

According to Table (5-5) for disturbances input road (two bump), comfort (RC) and road holding (RH) are improved, but there is a clear fluctuation in the figures (5-26d, 5-26e, 5-26f) which show that the controller is not effective with this type of roughness road and Table (5-4), in addition to road holding (RH) is

not taken into account a significant improvement in ride comfort (RC)can be offered, as shown by the findings of ride comfort for FOPID controller when the road input is roughness class B.

Because of this, the FOPIDC is not adaptive with different road, it meaning cannot change its parameters in response to unforeseen disturbances.

5.5 Results of performance of Slide Mode Controller with GA for Nonlinear Pneumatic Quarter Car integrated with Hydraulic Actuator Model

Road roughness (grade B,72 km/h), the performance of pneumatic active non- linear quarter vehicle suspension system for proposed control SMC with Genetic algorithm.

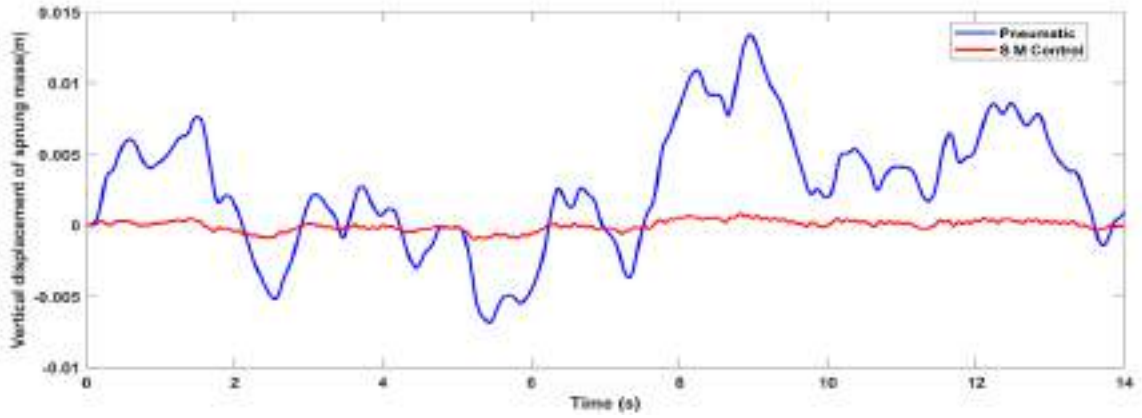

(a)

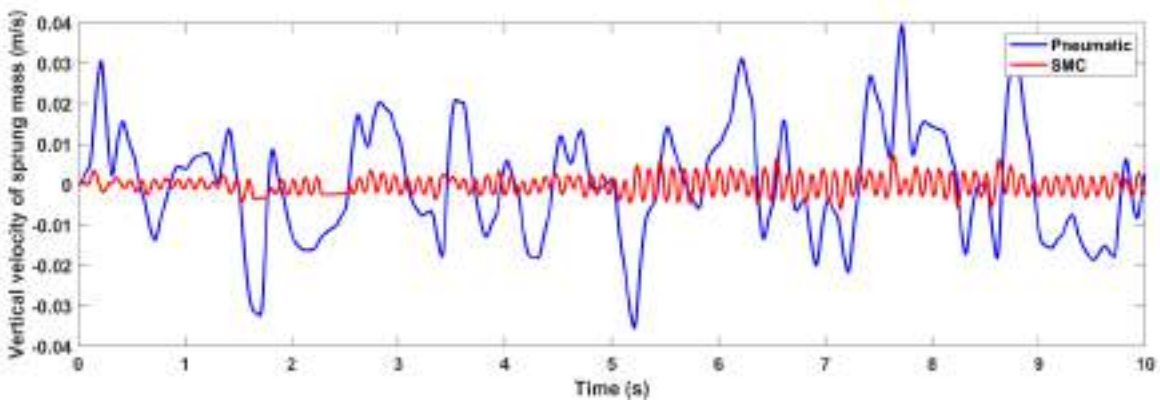
Vertical velocity of sprung mass (m/s)
Time (s)
Pneumatic
SMC

(b)

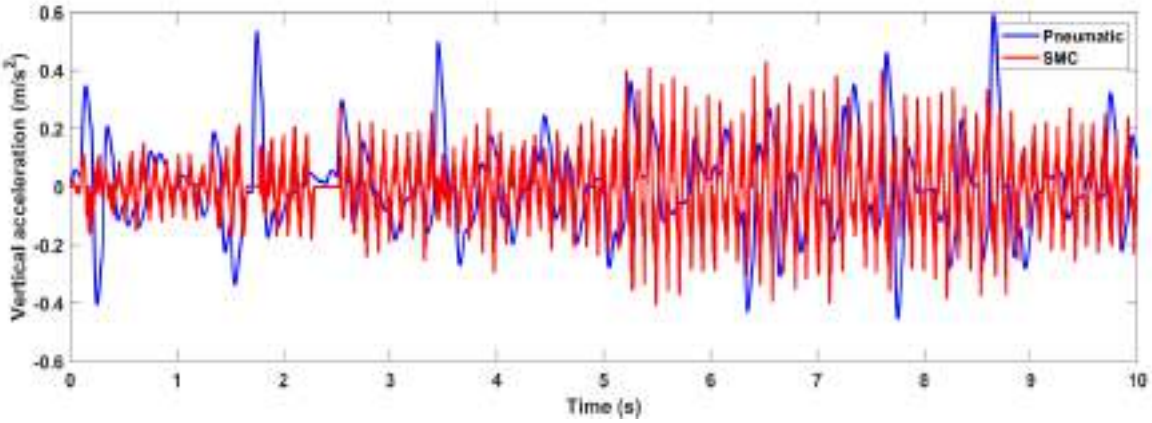
Vertical acceleration (m/s²)
Time (s)
Pneumatic
SMC

(c)

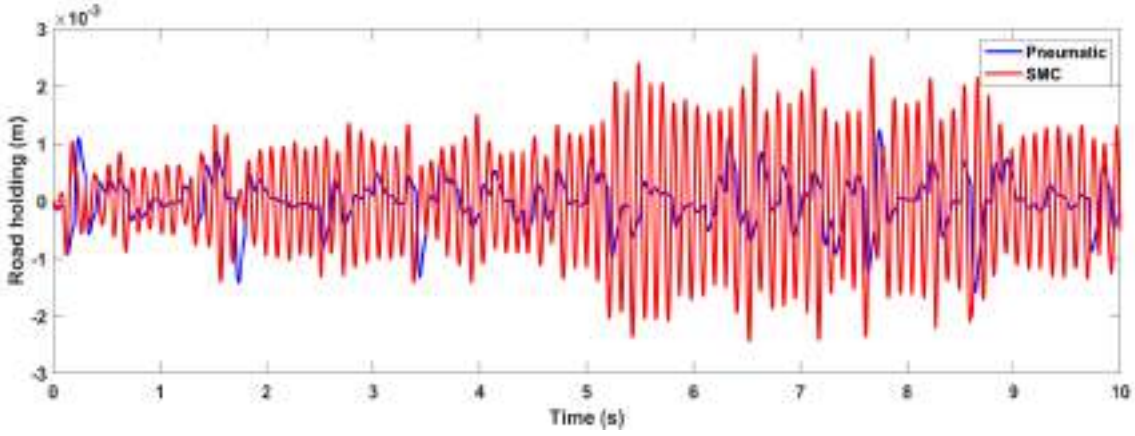
×10⁻³
Road holding (m)
Time (s)
Pneumatic
SMC

(d)

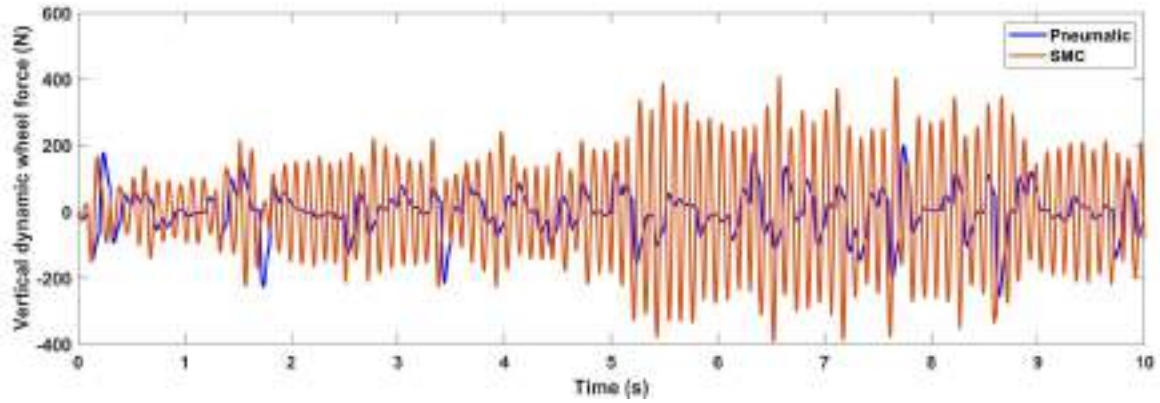
Vertical dynamic wheel force (N)
Time (s)
Pneumatic
SMC

(e)

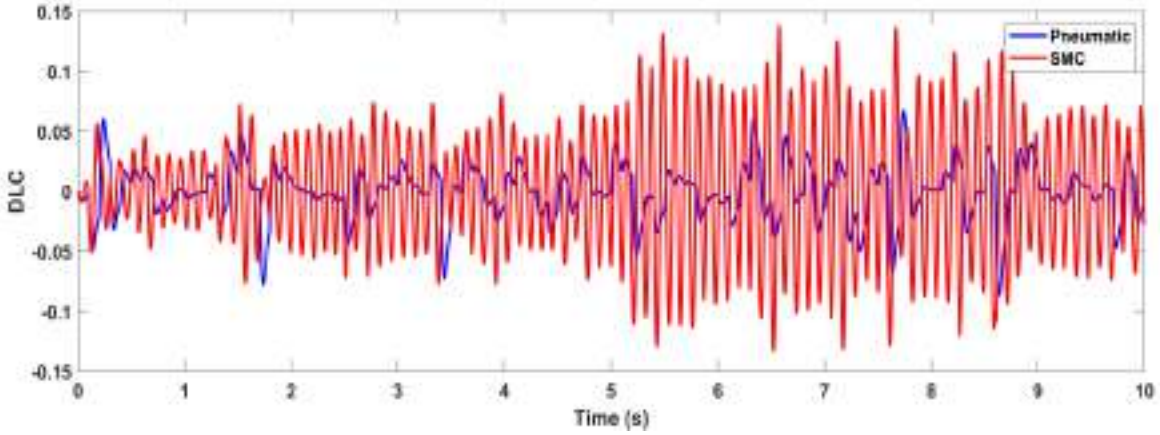
DLC
Time (s)
Pneumatic
SMC

(f)

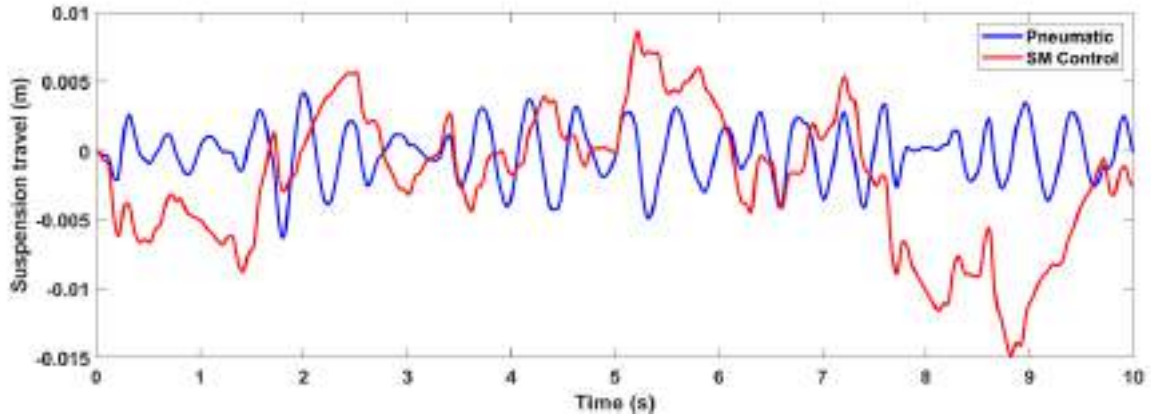
Suspension travel (m)
Time (s)
Pneumatic
SM Control

(g)

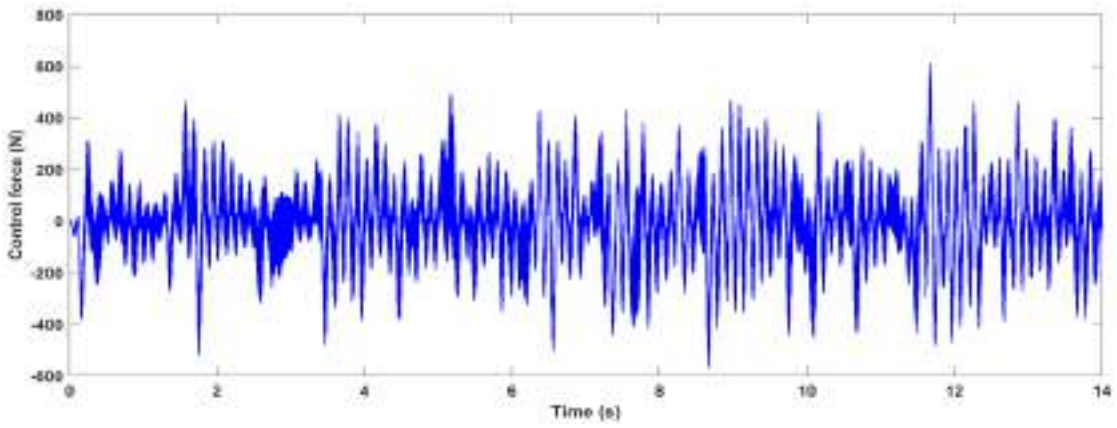

(h)

Figure (5-29) Performance Analysis of SMC control for active pneumatic suspension (roughness road level B, velocity 72 km/h).

Figure 5-30 show the best fitness value improves gradually in the generations, whose populations are closer to the optimal point.

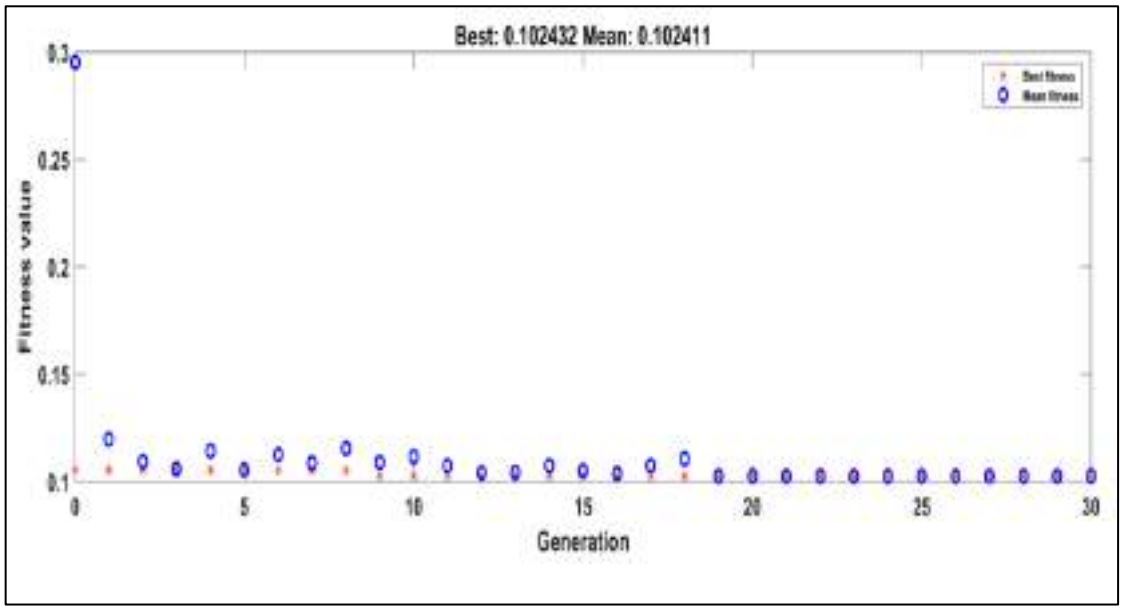

Figure (5-30) Convergence value obtained by GA.

Figures (5-29a, 5-29b, and 5-29c) the simulation results are shown the vertical displacement, vertical velocity, and vertical acceleration in the time

domain for the proposed system, the optimal SMC minimized these parameters compared to pneumatic suspension.

As shown in figures (5-29d, 5-29e, and 5-29f), where these figures explained that the transient responses amplitude of the sprung mass road holding, dynamic load coefficient, and vertical wheel force which have increase with time (no stability), meaning that the controller does not work effectively and this leads to the instability of the vehicle during the path on roads that have bumps, as a result, the effect of this controller is not adaptive to road bumps.

5.6 Results of performance of Fuzzy Logic Control with Genetic Algorithmic Optimization

Matlab Simulink for the proposed fuzzy logic control was used to analyze the suspension system's response. A fuzzy logic controller based on a genetic algorithm (GA) has been proposed to tune optimum FLC parameters for better performance of the air suspension system integrated with a hydraulic actuator, using an objective function (ITAE) integrated time absolute error. Optimal FLC for the pneumatic suspension system and pneumatic (passive) are compared in order to illustrate the comfort of the ride and the holding of the road for a passenger vehicle.

The input road (roughness road class B with velocity 72 km/h) and for input road (two bump with 50mm and 75mm amplitude, velocity 36 km/h)) are presented in the following figures in the time domain.

The parameters for sprung mass, vertical displacement, velocity, vertical acceleration, road holding, actuator force, vertical dynamic wheel load, suspension travel, and dynamic load coefficient are summarized in tables (5-6). The time response graphs of sprung mass's displacement are shown in the

figures, the FL controller designed produces a reduction in "RMS" the suspension system's active pneumatic suspension's sprung mass displacement reaction, as shown in the figures (5-31a and 5-32a), although there is a very small change from the transient vibration, the vibrations are quickly settled. The ability of FLGA to control the suspension system has been proven with 95.6 % and 95.2 % reduction in vertical displacement of sprung mass for the random disturbance and two bumps respectively. In the case of sprung mass velocity, the active system reduced both "RMS" when compared to the passive system for random and bumpy roads as shown in figures (5-31b and 5-32b).

These findings showed that the acceleration of the chassis against road irregularities and two bumps is a good improvement. Because of the applied suitable force from the actuator placed between sprung and unsprung masses would result in comfortable riding (minimize acceleration) for the passengers which is explained in figures(5-31c and 5-32c), for active system the acceleration values $(3.297\times 10^{-3}, 2.818\times 10^{-3})$ in compression with passive $(1.643\times 10^{-1}, 4.349\times 10^{-1})$ for random road and bumpy road respectively.

In case of the road holding, the active system for both the settling time and peak overshoot when comparison with the pneumatic system, the road holding in root-mean- square value has increased by 29% for random road and decreased 61% for bumpy road as shown in figures(5-31c and 5-32c) respectively. The increase in road holding by 29% compared to the pneumatic suspension system (without a controller) when the vehicle is traveling on a rough road is a bad indicator of the stability of the vehicle.

Figure (5-31g) showed the control force reaching about a value in RMS is 200N for the roughness road, which agree with [106], while the observed force in figure(5-32g) from the actuator controlled reaching about the value of 179N and the maximum value is 1054N at time 0.92s and in reverse direction so 1212N at time 6.166s, this agreement with [20].

Figures(5-31e and 5-32e) illustrate that the dynamic load coefficient for a road with two bumps is greater than for irregular road. The coefficient is generally lower for the air suspension system compared to the conventional spring suspension system.

Figures (5-31f and 5-32f) illustrate the vertical dynamic wheel load in the time domain, that the vehicle was excited by the rough road surfaces, resulting in continually varying tire forces and for the road with two bumps, this force decreases and fades until it reaches the tenth second, while on a rough road it increases with time, indicating that the vehicle is unstable while traveling.

In the case of suspension travel, the figure (5-31g) shows that the distance between the unsprung mass and sprung mass is oscillating, this means that when the vehicle is exposed to an irregular road, the distance of movement between the wheel group and the vehicle structure whenever it heads towards the negative or down gives more stability to the vehicle.

Figure (5-32g) can be shown that the active pneumatic suspension system with (FLGA) proposed controller exhibits greater negative deflection during the bumps disturbance intervals. A larger negative deflection means that the tire had good tire-road contact under the fluctuating conditions [32].

Figure (5-33) illustrates the convergence pattern between the best fitness with the average fitness values. The best fitness value not alter for many more generations after 25 generations. The best fitness and the average fitness are getting closer to one another, this indicates that the estimate could be optimal or close to optimal.

According to the simulation's outcome for road holding, it hasn't much improved during road holding analysis for fuzzy control strategy. This means that this controller (fuzzy logic) does not adapt itself to deal with irregular roads. Thus, the vehicle in terms of handling might not as better when the FL strategy only is used.

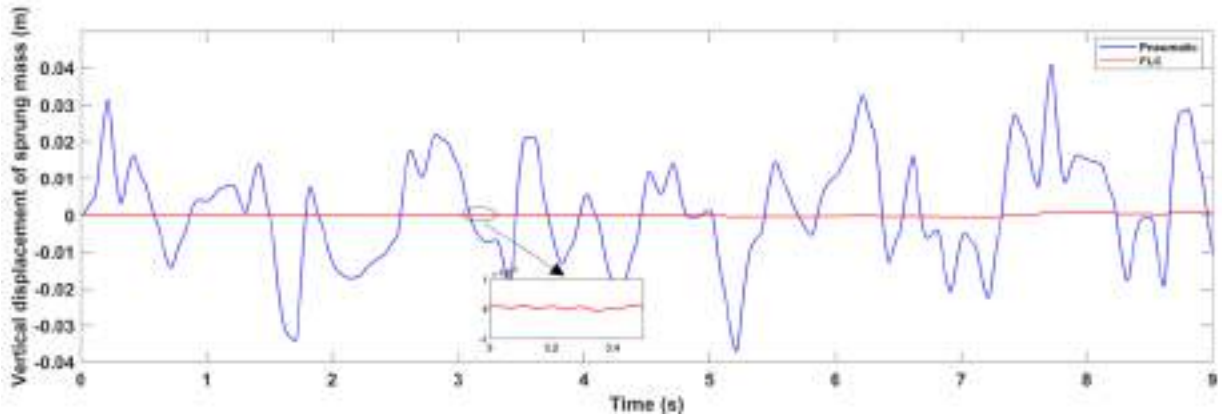
Vertical displacement of sprung mass (m)
Time (s)

(a)

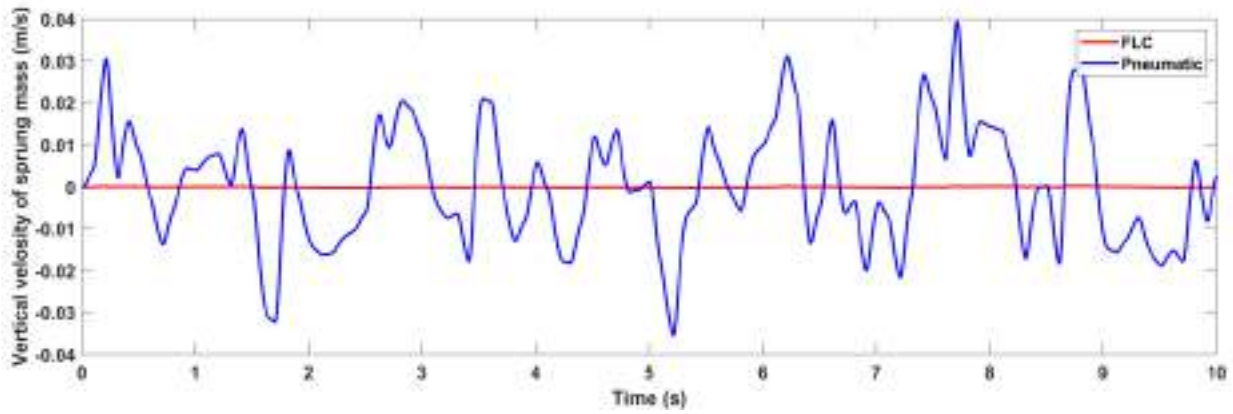
Vertical velocity of sprung mass (m/s)
Time (s)
FLC
Pneumatic

(b)

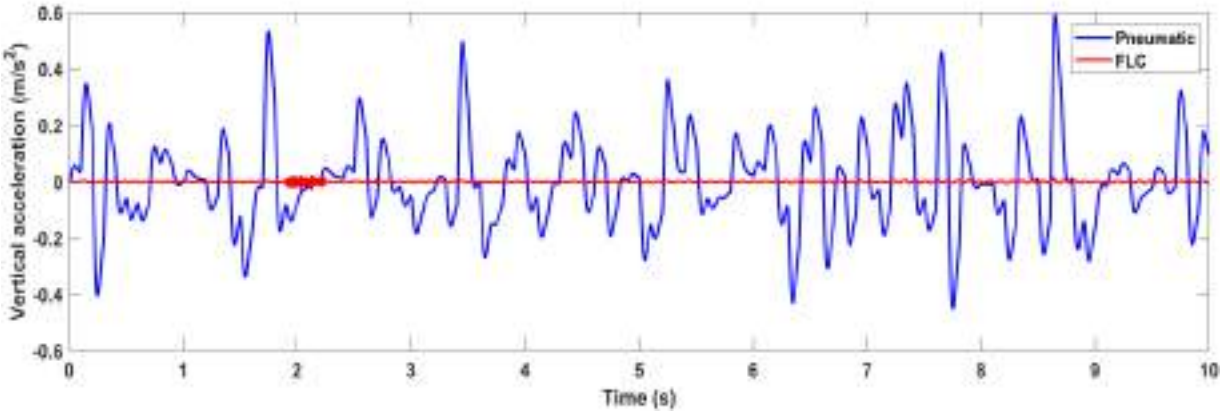
Vertical acceleration (m/s²)
Time (s)
Pneumatic
FLC

(c)

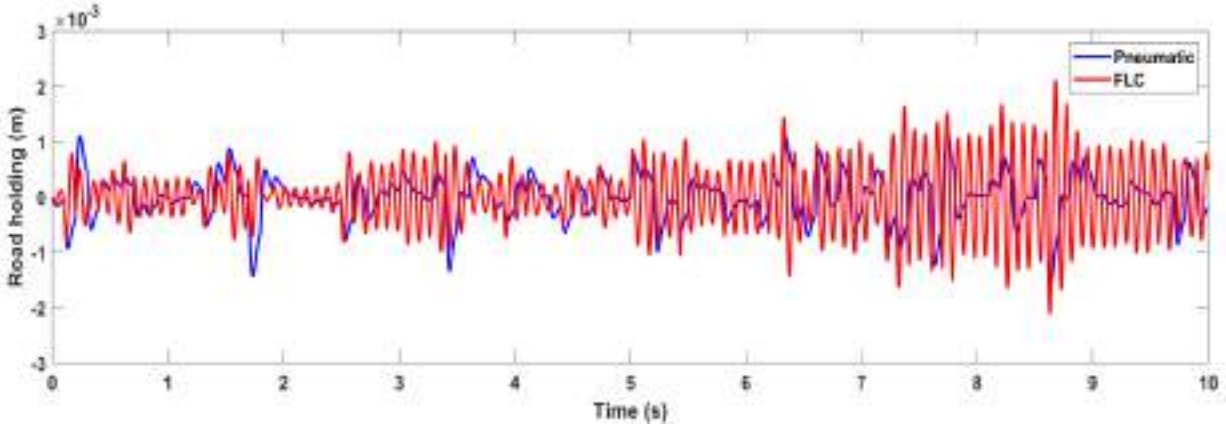
Road holding (m)
Time (s)
Pneumatic
FLC

(d)

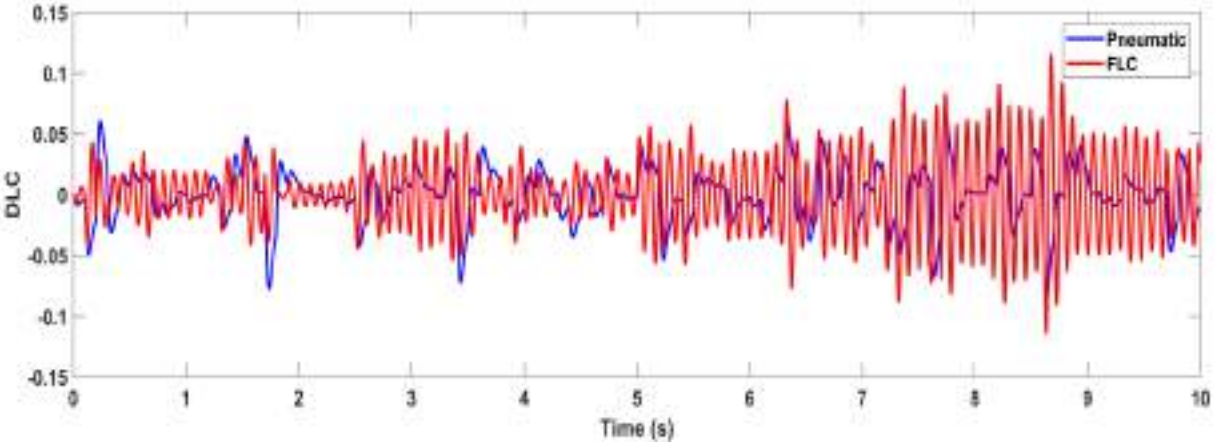
DLC
Time (s)
Pneumatic
FLC

(e)

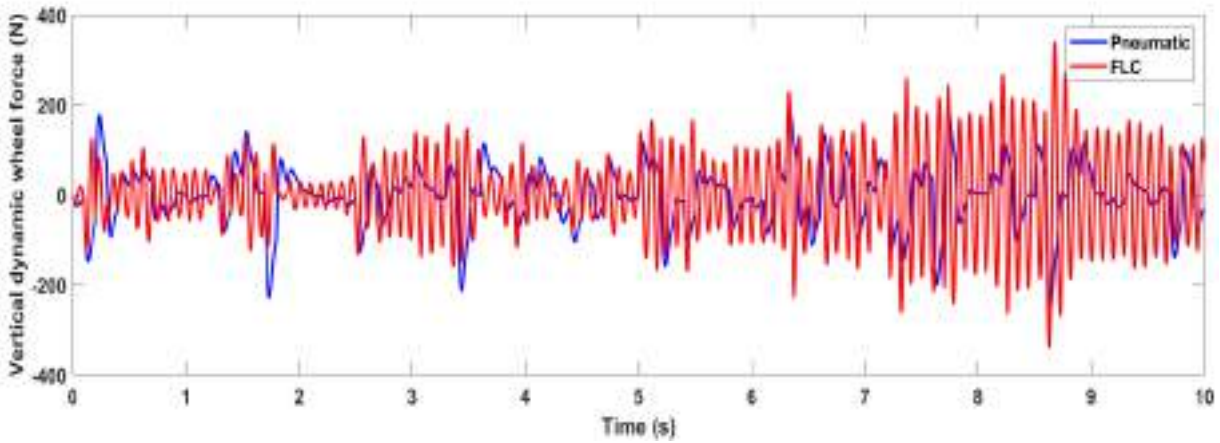
Vertical dynamic wheel force (N)
Time (s)
Pneumatic
FLC

(f)

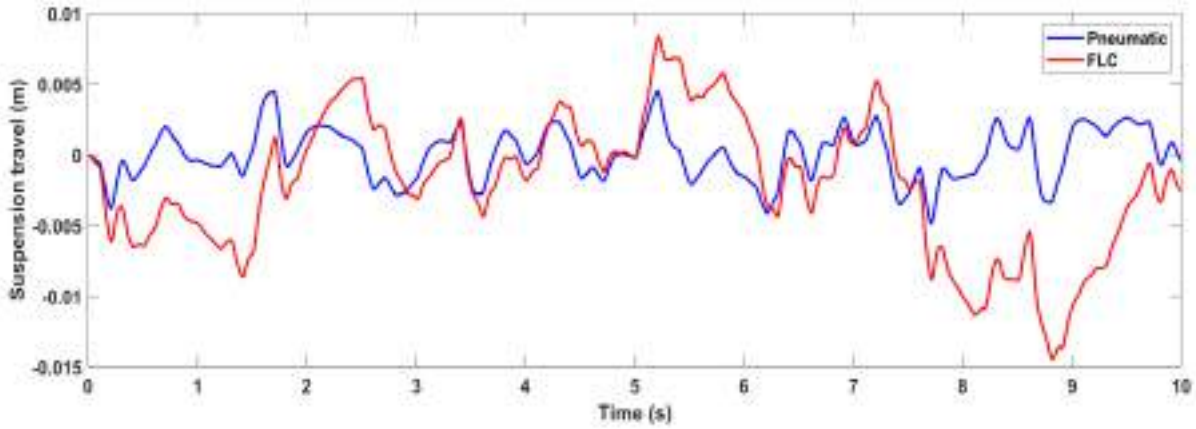

(g)

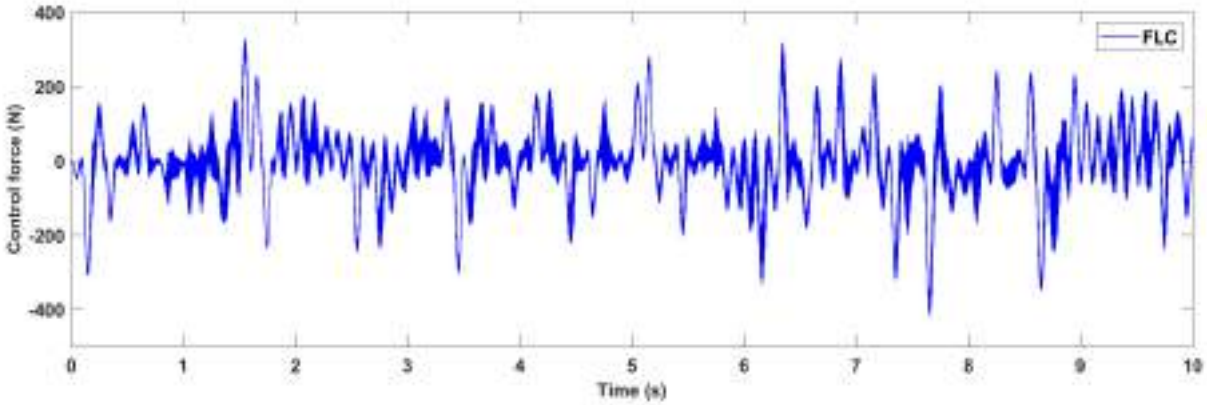

(h)

Figure (5-31) Performance analysis of FLC control for active pneumatic suspension (roughness road level B, velocity 72 km/h).

Table (5-6) Reduction in RMS values for roughness class B as road input

No	Parameters	Pneumatic	Optimal FLC	Reduction	Increase
1	sprung mass's displacement (m)	5.017×10^{-3}	1.750×10^{-4}	95.612%	-
2	sprung mass's acceleration (m/s^2)	1.643×10^{-1}	3.297×10^{-3}	97.999%	-

3	Force dynamic(N)	6.449×10^{1}	9.1249×10^{1}	-	29%
4	DLC	2.127×10^{-2}	3.161×10^{-2}	-	30.1%
5	Road holding (m)	4.032×10^{-4}	5.703×10^{-4}	-	29%
6	Velocity of sprung mass(m/s^2)	1.3×10^{-2}	6.28×10^{-4}	95.16%	-

For roughness road input, velocity 72 km/h are presented in the shown figures, the settling time and the peak value have decreased by the effect of a control system which was used a genetic algorithm against the pneumatic system.

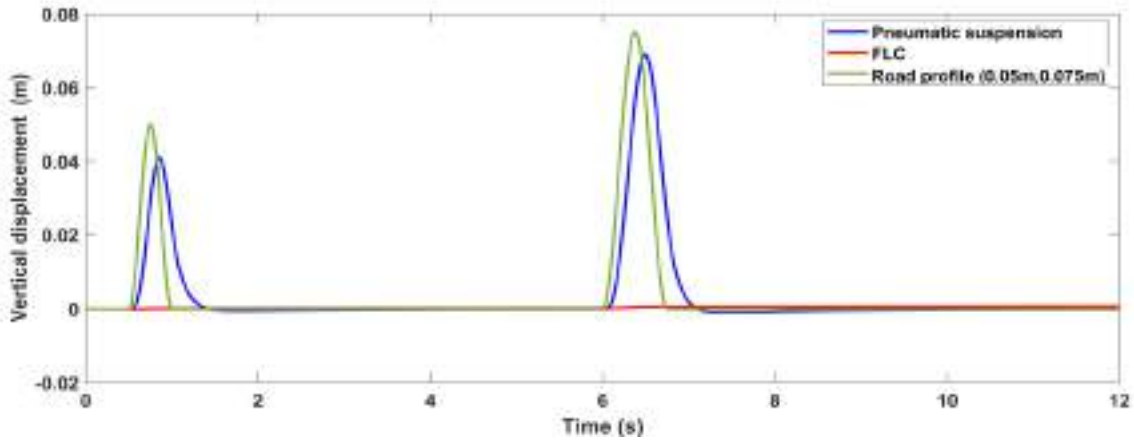

(a)

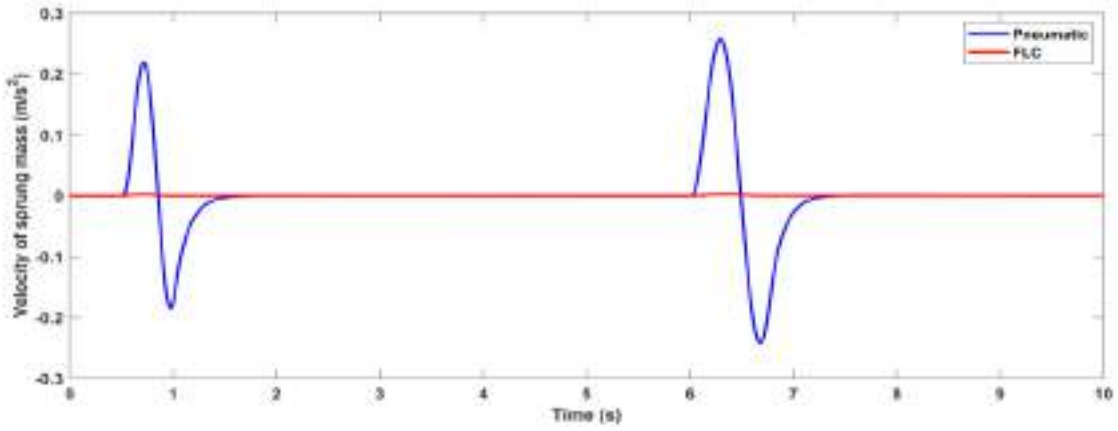

(b)

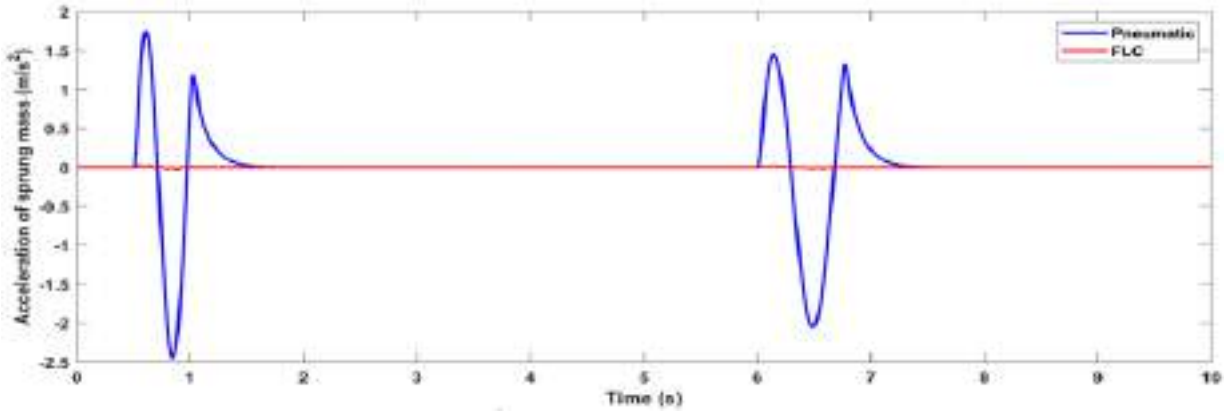
Pneumatic
FLC
Acceleration of sprung mass (m/s²)
Time (s)

(c)

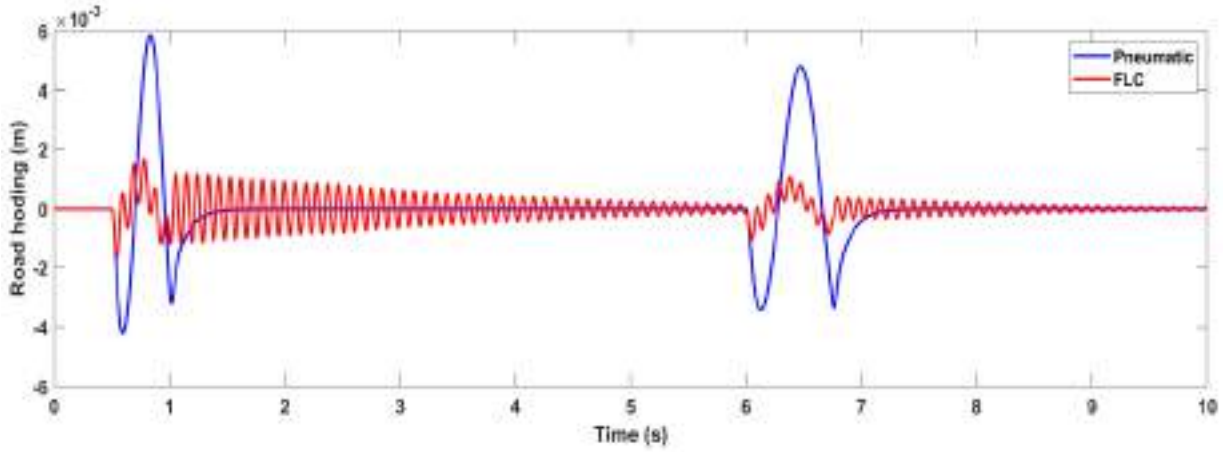
x 10⁻³
Pneumatic
FLC
Road hoding (m)
Time (s)

(d)

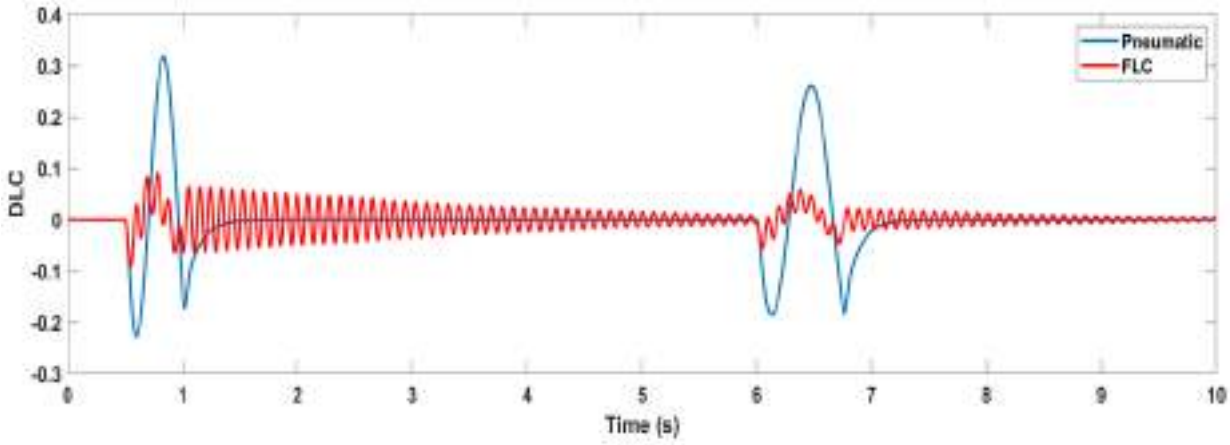
Pneumatic
FLC
DLC
Time (s)

(e)

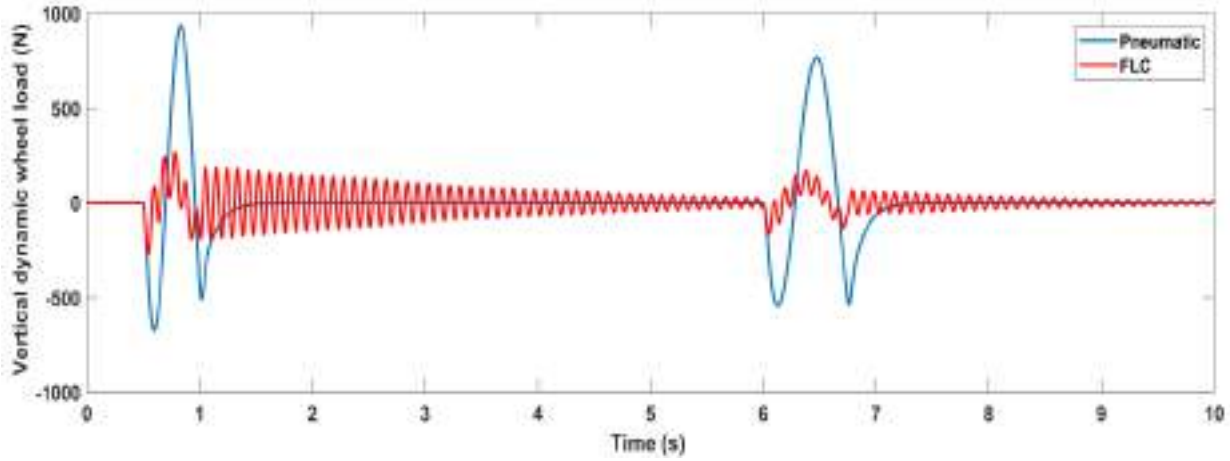
Pneumatic
FLC
Vertical dynamic wheel load (N)
Time (s)

(f)

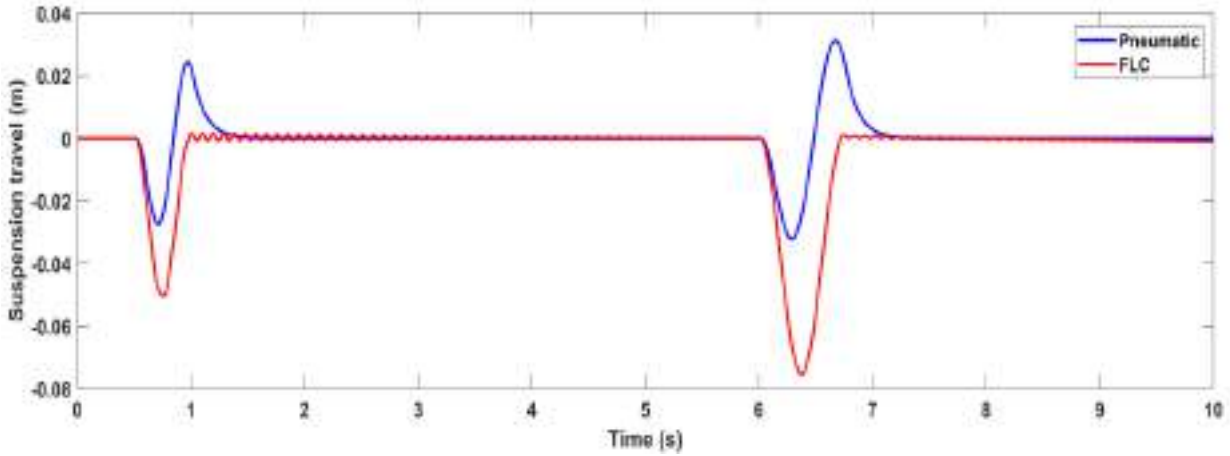
Pneumatic
FLC
Suspension travel (m)
Time (s)

(g)

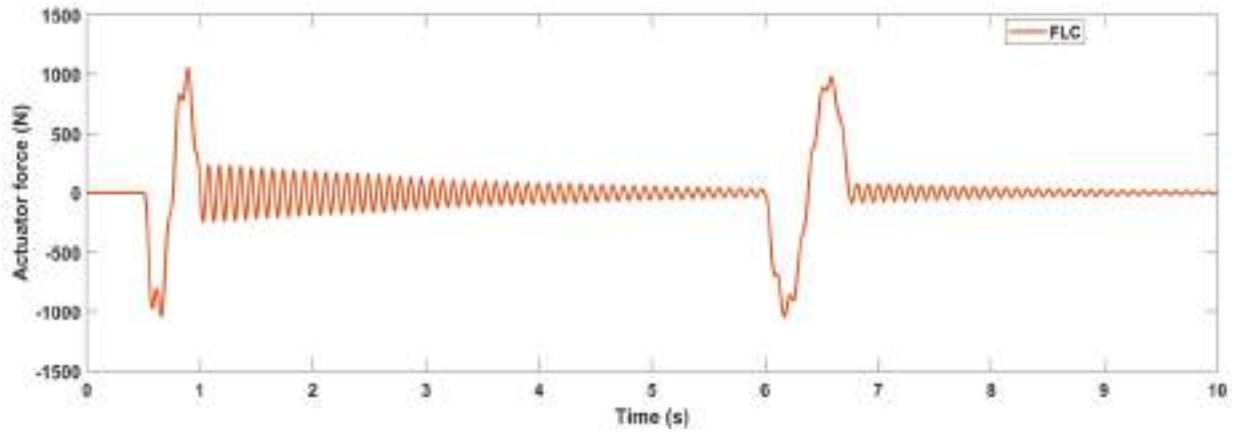

(h)

Figure (5-32) Performance Analysis of FLC control for active pneumatic suspension (road-two bump, velocity 36 km/h).

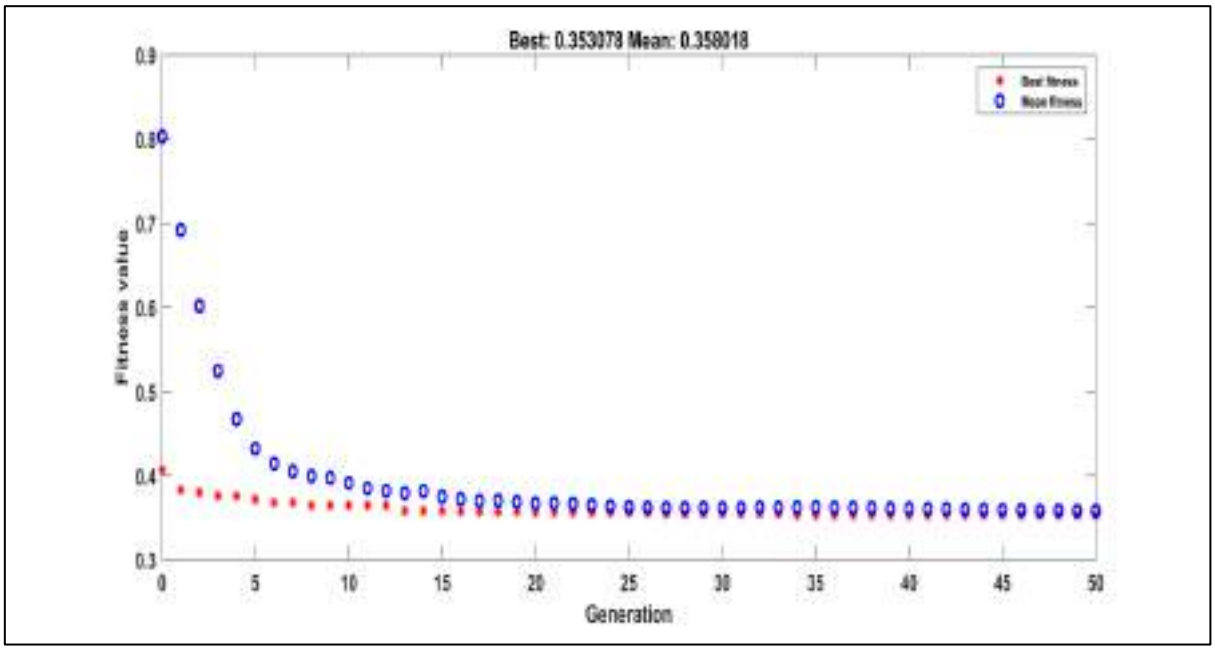

Figure (5-33) Convergence obtained by GA.

Table (5.7) Reduction in RMS values for two bump road input in RMS.

No	Parameters	Pneumatic	Optimal (FLC)	Reduction
1	sprung mass's displacement (m)	1.219×10^{-2}	5.851×10^{-4}	95.2%
2	sprung mass's acceleration in m/s^2	4.349×10^{-1}	2.818×10^{-3}	99.35%
3	DLC	5.937×10^{-2}	2.275×10^{-2}	61.6%
4	Road holding (m)	1.056×10^{-3}	4.148×10^{-4}	61.9%
5	Velocity of sprung mass(m/s^2)	5.581×10^{-2}	4.688×10^{-4}	99.16%

5.6 Analysis of Proposed A Self-Tuning Fuzzy-PID Control for Active Pneumatic Quarter Vehicle.

The results of active suspension with "Self-tuning FPID" controller are shown graphically by input roughness road at velocity with72 km/h and for input two bump with 50mm and 75mm amplitude with velocity 36 km/h.

From the tables (5-8 and 5-9) show a summary of results related to passenger comfort and vehicle road holding.

Figures (5-33a and 5-34a) showed the improvement in the vertical displacement of the sprung mass (This means a good improvement in passenger comfort) for both types of roads(roughness road and two bumps) after the obvious effect of the controller(self-tune FLPID). The controller minimized the road disturbance in "RMS" by 95.2% for a rough road (from 5.436×10^{-3} to 2.607×10^{-4}) and by 95.60% for a bumpy road (from 1.29×10^{-2} to 5.589×10^{-4}), Additionally, the simulations demonstrated stable convergence.

Figures (5-37b and 5-38b) showed the improvement in the vertical velocity of the sprung mass for both types of roads(roughness road and two bumps) after the obvious effect of the controller(self-tune FLPID).

Figures (5-33c and 5-34c) showed the improvement in the vertical acceleration of the sprung mass (This indicates a significant increase in passenger comfort) for both types of roads(roughness road and two bumps) after the obvious effect of the controller(self-tune FLPID). The controller reduced the road disturbance in "RMS" by 65.7% for a rough road (from 1.606 e-1 to 5.508-2) and by 91% for a bumpy road (from 5.058×10^{-1} to 4.468×10^{-2}). The simulations also revealed stable convergence.

Figures (5-33d) for a rough road the controller (self-tuning FLPID)was not effective in attenuating the response and therefore the vehicle's tires were not in contact with the road, which leads to the vehicle's instability while driving. While the effect of the controller itself is effective in holding the road when the road is two-fold, i.e. reducing the response from 1.247 * 10^-3 to 5.606 * 10^-4, i.e. by 55.1% as shown in figure(5-34d). Also for dynamic load coefficient with time and the vertical dynamic wheel load, the controller does not play a role in reducing the response to them , as in the figures (5-33e and 5-33f).

Based on the simulated outputs shown in the figures (5-33d, 5-33e, and 5-33f)for the roughness road, the controller (self-tuning FL-PID) does not play an effective role in adapting to the different road.

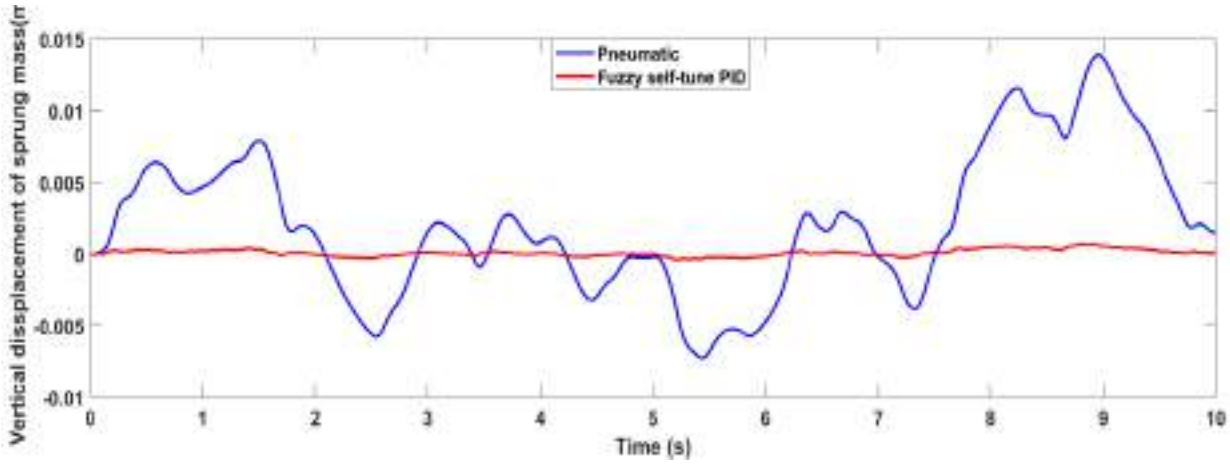
Pneumatic
Fuzzy self-tune PID
Vertical displacement of sprung mass(m
Time (s)

(a)

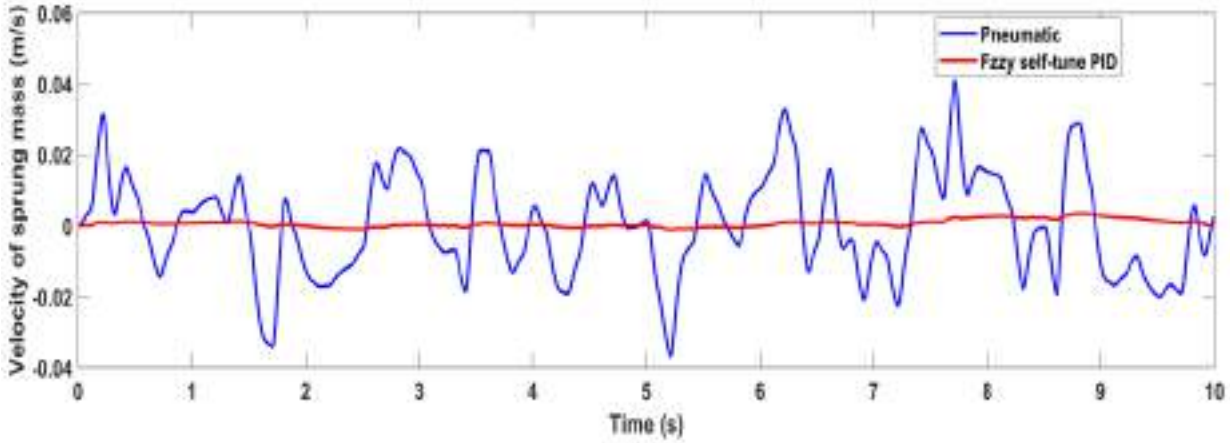
Pneumatic
Fzzy self-tune PID
Velocity of sprung mass (m/s)
Time (s)

(b)

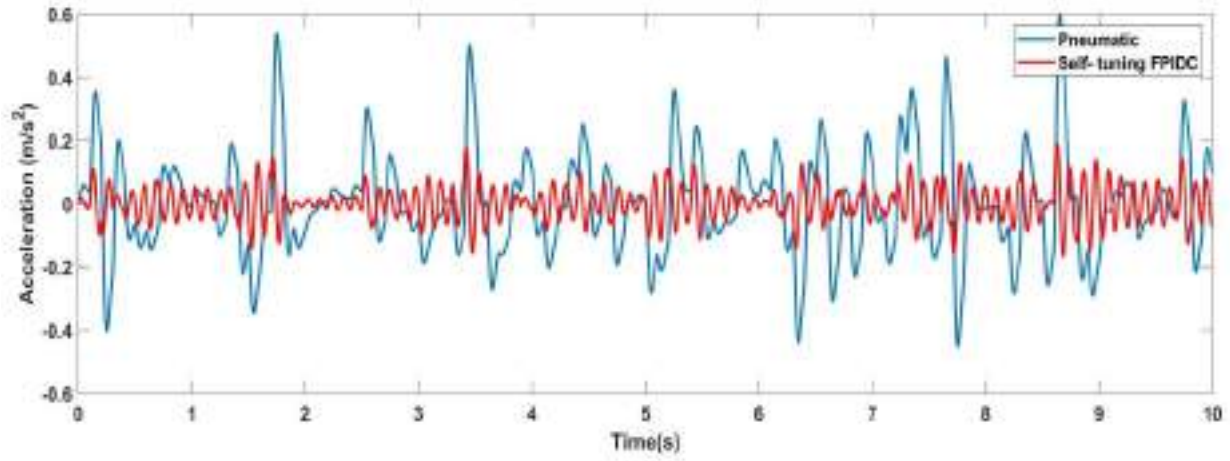
Pneumatic
Self- tuning FPIDC
Acceleration (m/s²)
Time(s)

(c)

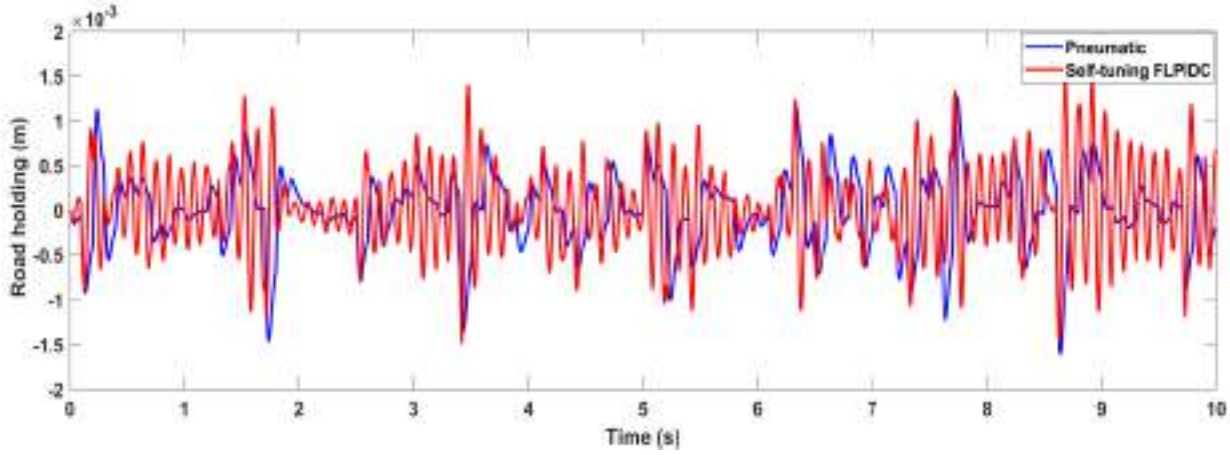
×10^-3
Road holding (m)
Time (s)
Pneumatic
Self-tuning FLPIDC

(d)

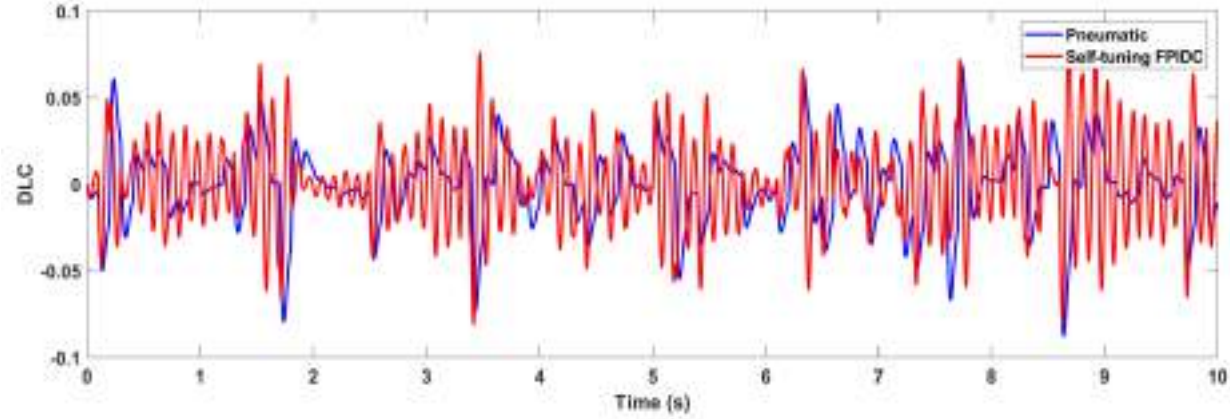
DLC
Time (s)
Pneumatic
Self-tuning FPIDC

(e).

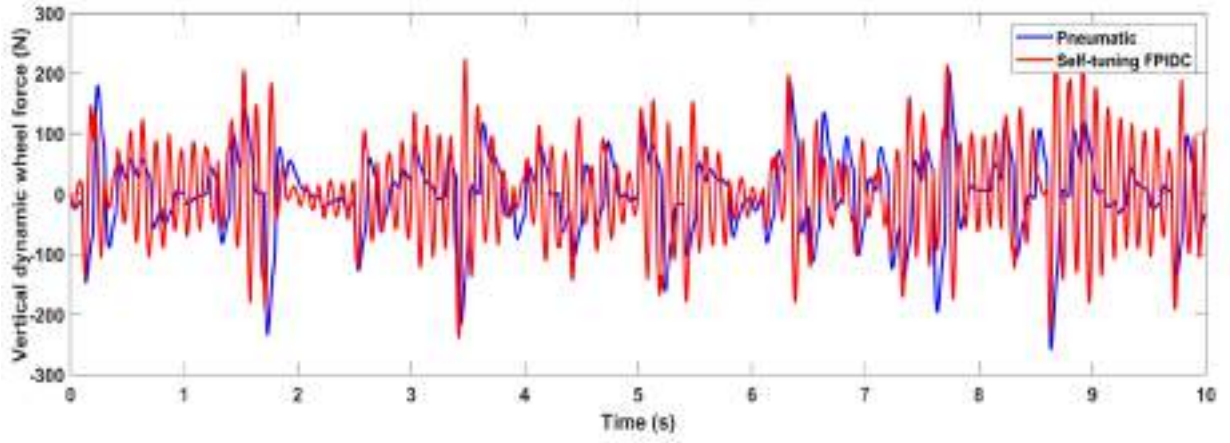
Vertical dynamic wheel force (N)
Time (s)
Pneumatic
Self-tuning FPIDC

(f).

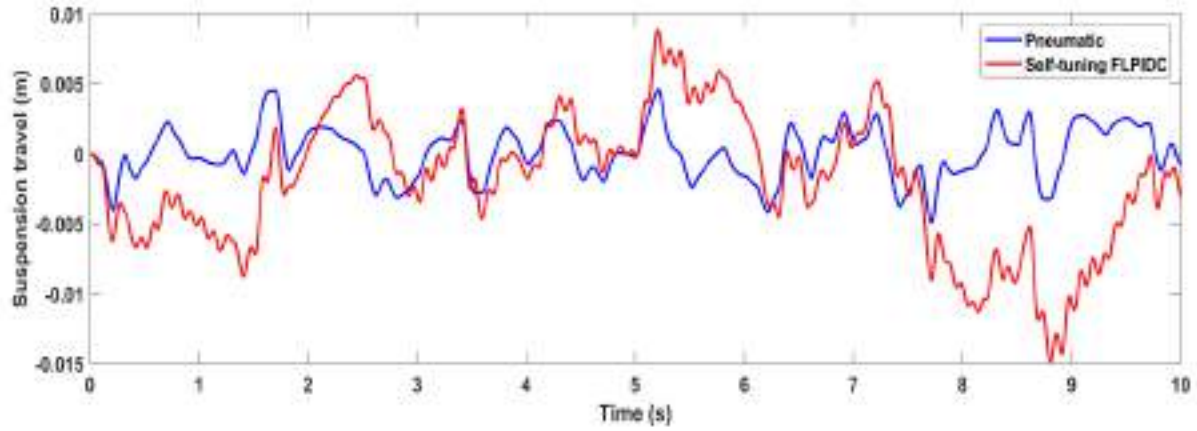

(g)

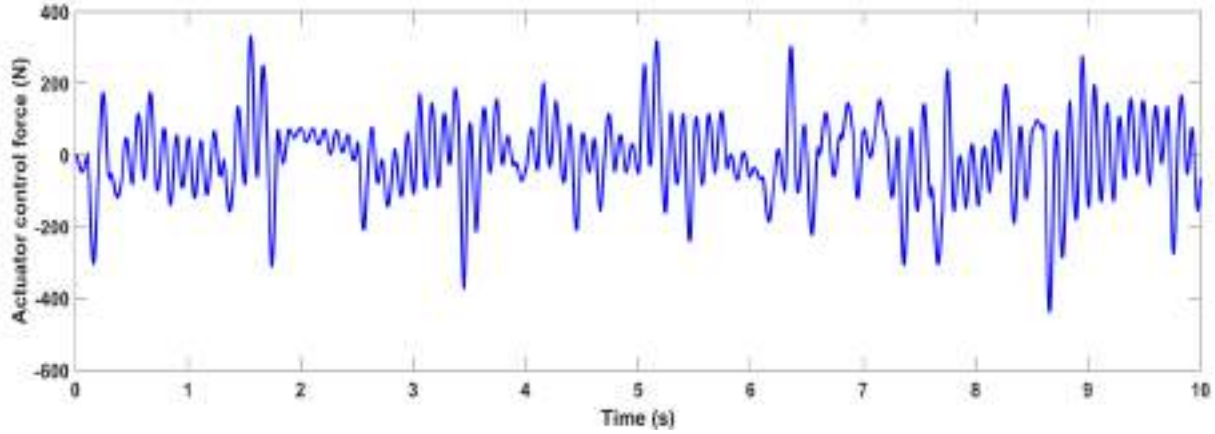

(h)

Figure (5-33) Performance Analysis of S-TFLPIDC control for active pneumatic suspension (rough road, level B, velocity 72 km/h).

Table (5-8) Reduction in overshoot values for roughness road input.

No	Parameters	Pneumatic	Optimal (FSTPID)	Reduction (improvement)	Increase
1	Vertical displacement of sprung mass (m)	5.436×10^{-3}	2.607×10^{-4}	95.2%	-
2	the sprung mas's acceleration(m/s^2)	1.606×10^{-1}	5.508×10^{-2}	65.7%	-
3	Force dynamic(N)	6.703×10^{1}	7.667×10^{1}	-	14.3%
4	DLC	2.2×10^{-2}	2.636×10^{-2}	-	16.5%
5	Road holding (m)	4.047×10^{-4}	4.772×10^{-4}	-	15.2%
6	Velocity of sprung mass(m/s^2)	1.392×10^{-2}	1.292×10^{-3}	90.7%	-

The results of active pneumatic suspension system with fuzzy self-tuning PID controller are presented graphically by input road of two bumps at velocity 36 km/h.

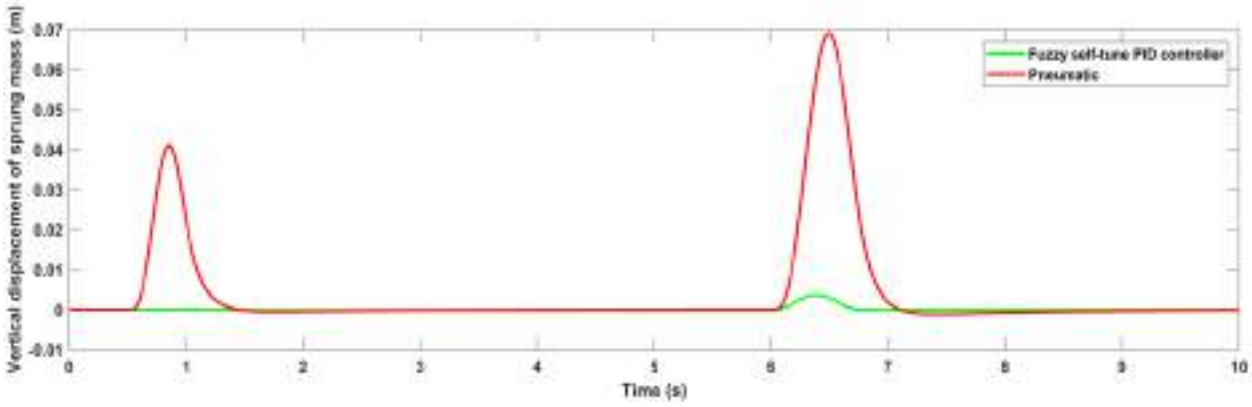

(a)

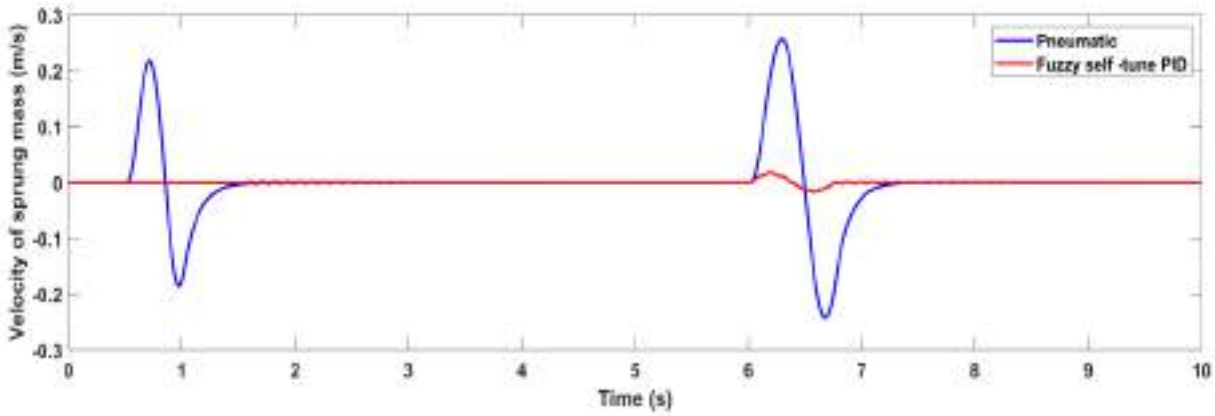
Pneumatic
Fuzzy self -tune PID
Velocity of sprung mass (m/s)
Time (s)

(b)

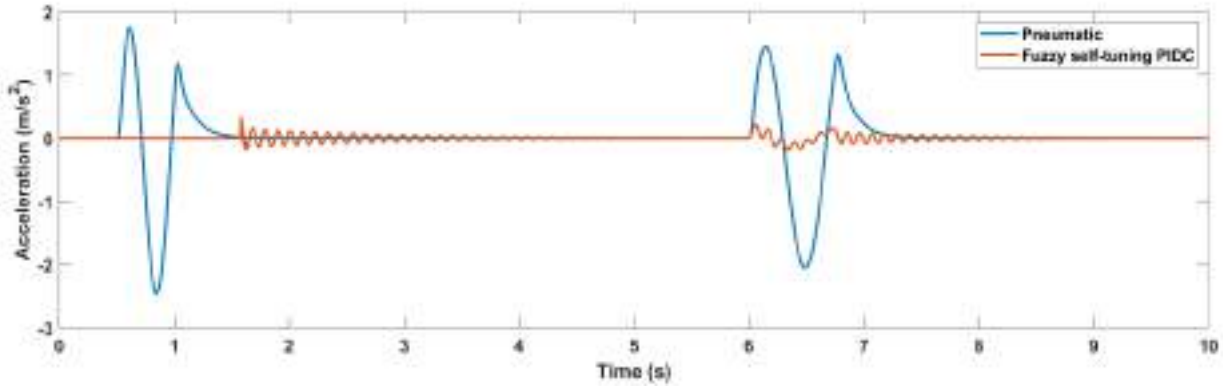
Pneumatic
Fuzzy self-tuning PIDC
Acceleration (m/s²)
Time (s)

(c)

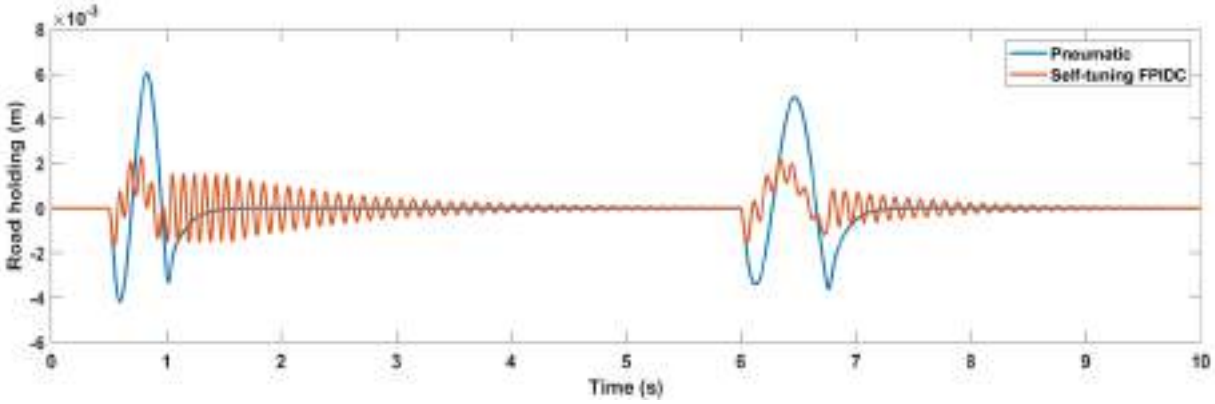
×10⁻³
Pneumatic
Self-tuning FPIDC
Road holding (m)
Time (s)

(d)

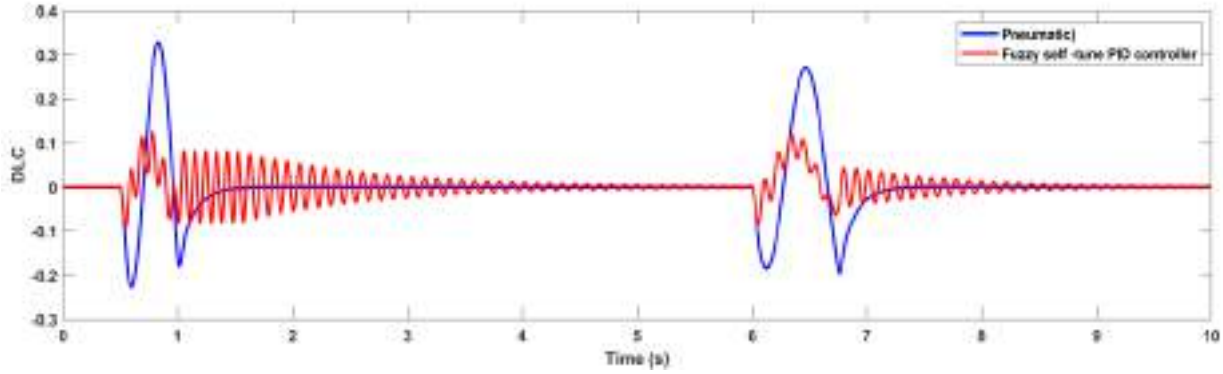
Pneumatic
Fuzzy self -tune PID controller
DLC
Time (s)

(e)

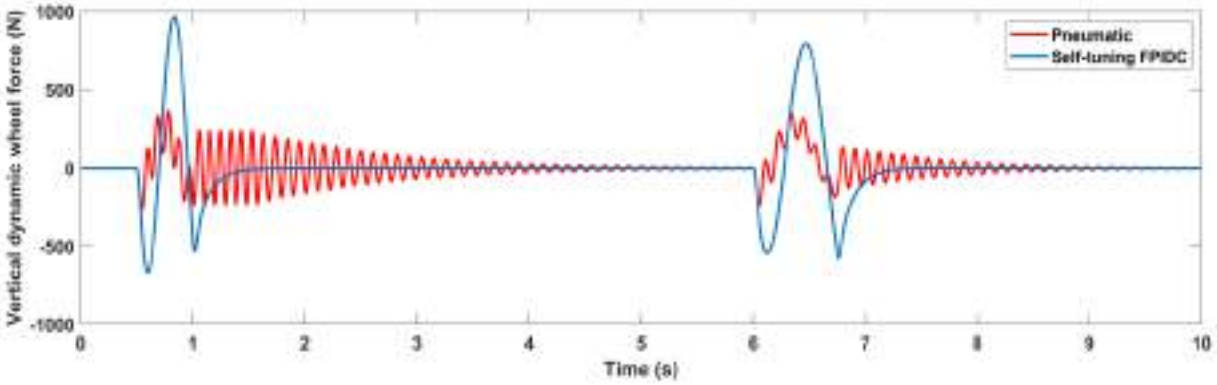
Pneumatic
Self-tuning FPIDC
Vertical dynamic wheel force (N)
Time (s)

(f)

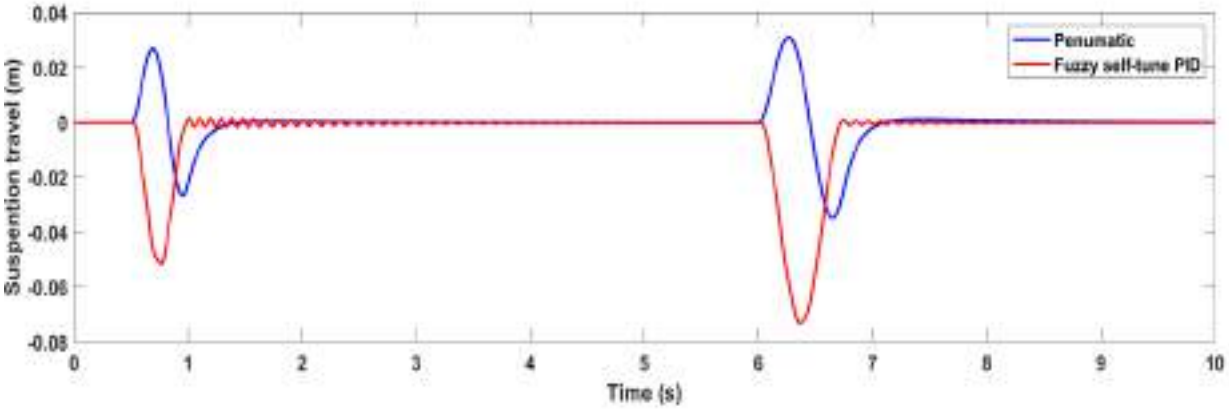
Penumatic
Fuzzy self-tune PID
Suspention travel (m)
Time (s)

(g)

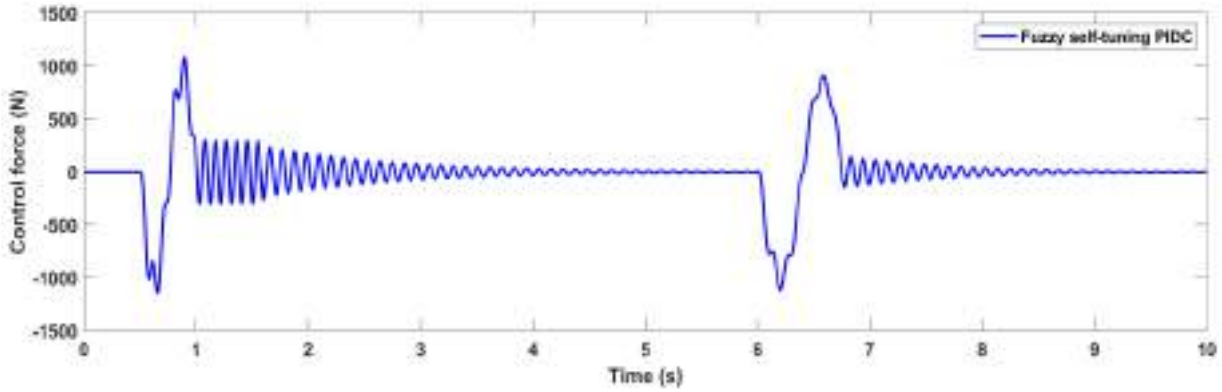

(h)

Figure (5-34) Performance Analysis of ST-FLPID control for active pneumatic suspension (road-two bump, velocity 36 km/h).

Table(5-9) Reduction in overshoot values for two bump road input in "RMS".

No	Parameters	Pneumatic	Control (FSTPIDC)	Reduction (improvement)	Increase
1	Vertical displacement of sprung mass (m)	1.29×10^{-2}	5.589×10^{-4}	95.61%	-
2	Acceleration of sprung mas(m/s^2)	5.058×10^{-1}	4.468×10^{-2}	91.15%	-
3	DLC	6.778×10^{-2}	3.048×10^{-2}	55%	-
4	Road holding (m)	1.247×10^{-3}	5.606×10^{-4}	55.1%	-
5	Force dynamic (N)	1.995×10^{2}	8.97×10^{1}	55%	-
6	Velocity of sprung mass(m/s^2)	5.67×10^{-2}	2.787×10^{-3}	95.07%	-

5.7 Results Analysis of Active Force-Fuzzy Logic Controller with GA for Nonlinear Pneumatic Quarter-Car Integrated with Hydraulic Actuator Model

From roughness road (ISO 8606 class B with velocity 72km/h) and for input road (two bump with 50mm and 75mm amplitude with velocity 36 km/h)) are presented in the following figures in the time domain.

The parameters of pneumatic active none linear quarter vehicle suspension system for proposed control FLAFC with Genetic algorithm in time domain.

Tables(5-10 and5-11) illustrate the percentage decrease in RMS of the different parameters for random and rough terrain input, due to the controller equipped pneumatic suspension with a hydraulic actuator to improve system ride comfort and road handling.

Figures (5-35a and 5-36a) are shown the car body displacement. It can be observed that the quarter car vertical displacement is much reduced and successfully reduced near zero approximately 88.5% for roughness road and 94.7% for the two-bumps road in the case of AFC method-based GA compared to the pneumatic suspension system. Good results were obtained in comparison with a coil spring for active suspension system [117].

Figures (5-35b and 5-36b) are illustrated the vertical velocity of the quarter car. It can be seen that the quarter car vertical velocity is significantly decreased and successfully lowered near zero in the case of AFC method-based GA, at around 95.3% for roughness road and 99% for the two-bumps road.

As shown in figures (5-35c and 5-36c) illustrate that both the "RMS" value of body acceleration which is a measure of ride quality is reduced from 1.593×10^{-1} to 7.971×10^{-3} for roughness road and from 4.731×10^{-1} to 7.006×10^{-3} for the two-bumps road and settling time has been reduced in the case of active force controller based GA algorithm. The simulation results and analyses above show that the suspension system provides a comfortable ride in compared to an active suspension system's coil spring [104].

Road holding has improved by AFC can be observed in figures (5-35d and 5-36d) and tables (5.10 and 5.11), compared to the pneumatic suspension in addition to controls previously described, AFC is the best strategy that offers excellent active control in terms of vehicle handling. It can be observed that the reduction of road holding (reduce the vibration) in "RMS" is 33.2% for rough roads and 63.49% for the two-bumps road. Figures (5-35e and 5-36e) show take into account the holding on the road measure, which describes the interaction between the tire and the road; the related principal performance indicator is " normalized tire deflection" dynamics, or dynamic load coefficient, as long as the normalized tire deflection is less than 1, there will be good road contact [117].

In the case of active pneumatic suspension (AFC), the suspension travel is increased from 1.821×10^{-3} (m) to 3.952×10^{-3} (m) for rough roads compared to pneumatic suspension system and from to give a more comfortable ride, this mean less displacement, while for 7.546×10^{-3} (m) to 1.346×10^{-2} (m) for the two-bumps road, the increase suspension travel for the two-bumps road to increase stability, active suspension systems have a larger possibility of enhancing road holding, this agreement with [118].

The suspension system's displacement must be continuously altered in reaction to a bump in the road to be able minimized acceleration and displacement of the vehicle's body. On the other hand, if a vehicle just employs a pneumatic only, the system of suspension won't nearly displace, as a result, this suspension system can be compared to a very solid block, and it has an immediate impact on the car's comfort with stability [119]. To improve ride comfort, or less the sprung mass's displacement, active suspension travel is increased compared to passive suspension [120].

Figures (5-35f and 5-36f) describe the vertical dynamic tire force for rough road reduction at "RMS" for time domain by 33.2% and for road bumps by 63.5% compared with pneumatic suspension(without actuator), this force is

related to road holding. Figures (5-35h and 5-36h) illustrate control force of the actuator which follows the path of the road and what it includes bumps and its limits between 300N and -400N.

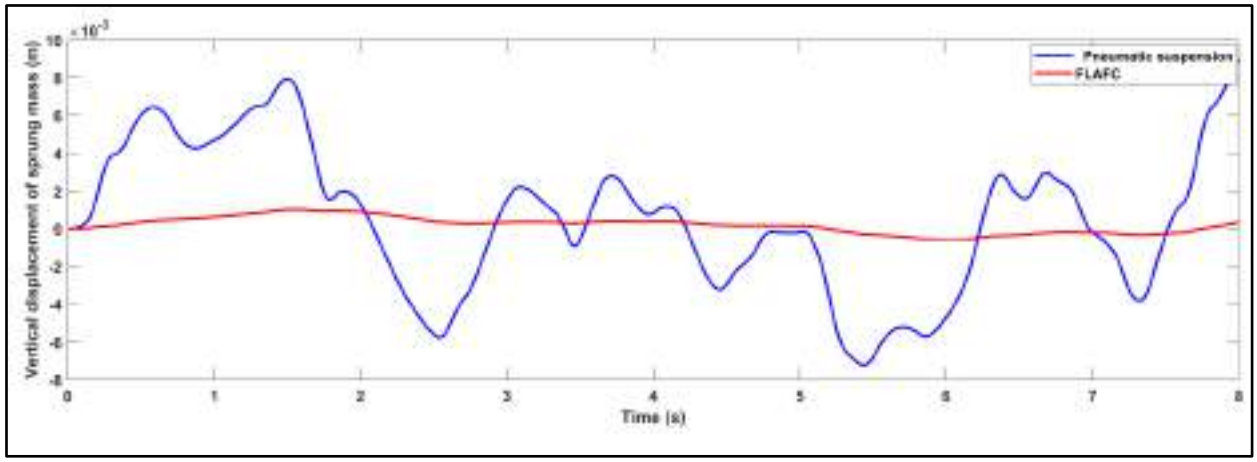

(a)

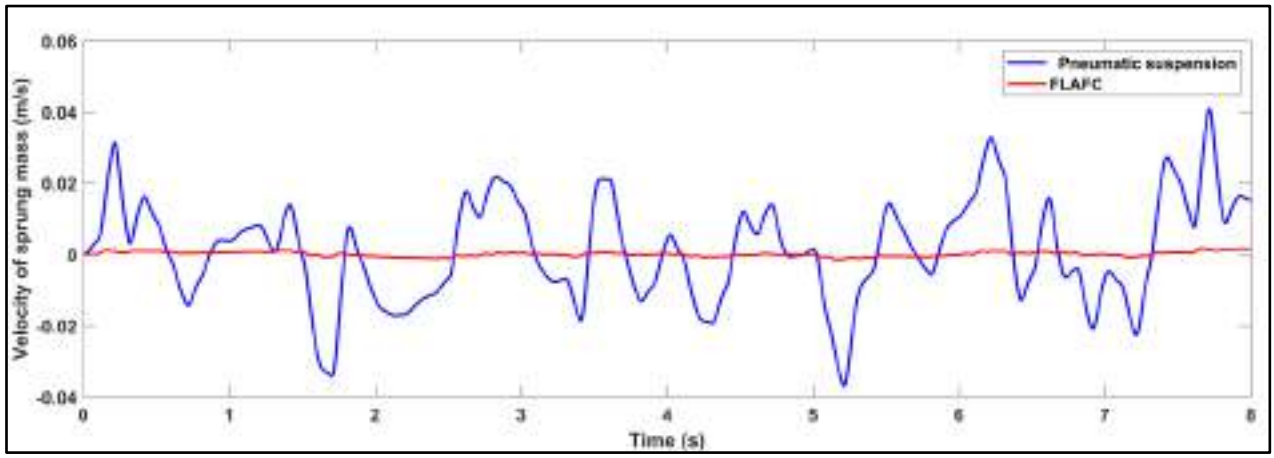

(b)

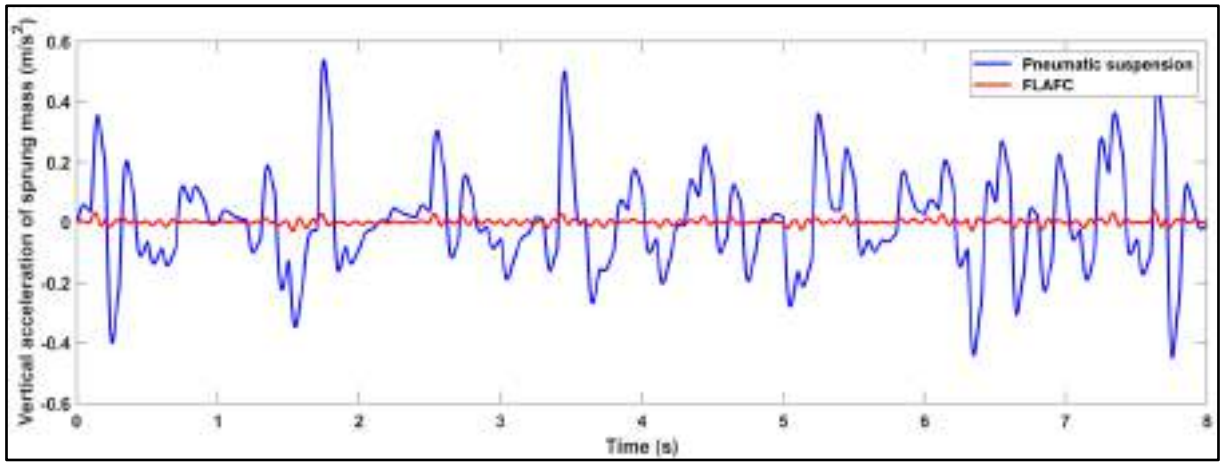
Vertical acceleration of sprung mass (m/s^2)
Time (s)
Pneumatic suspension
FLAFC

(c)

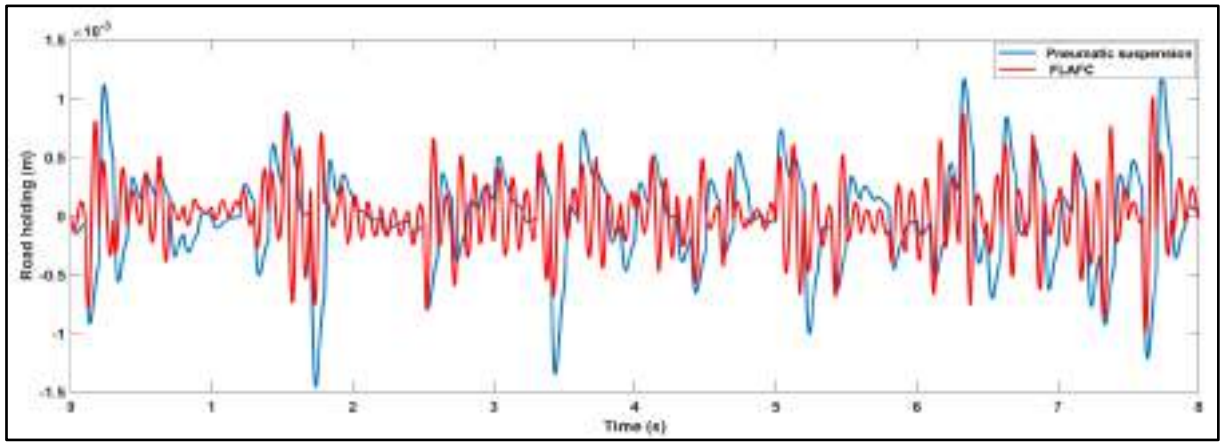
Road holding (m)
Time (s)
Pneumatic suspension
FLAFC

(d)

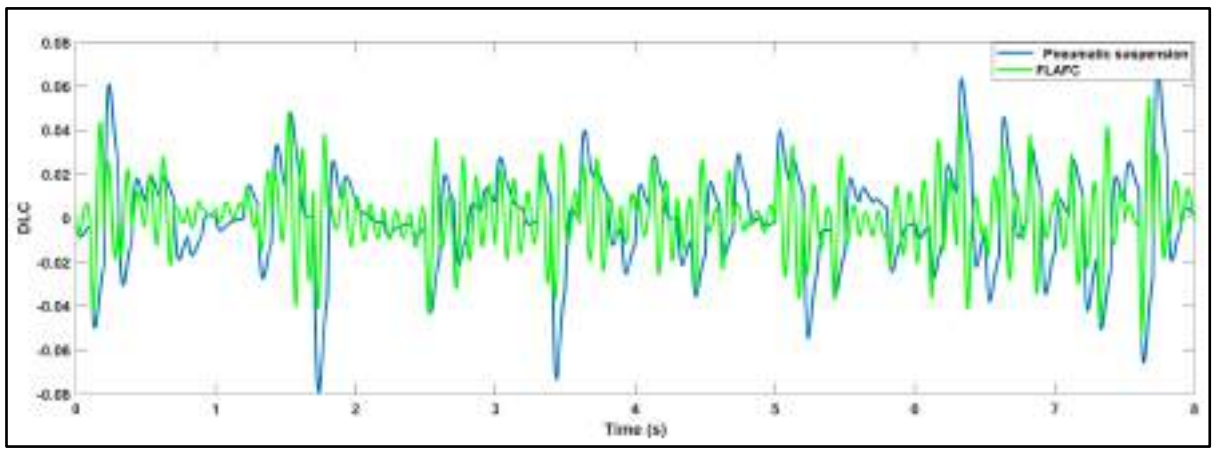
DLC
Time (s)
Pneumatic suspension
FLAFC

(e)

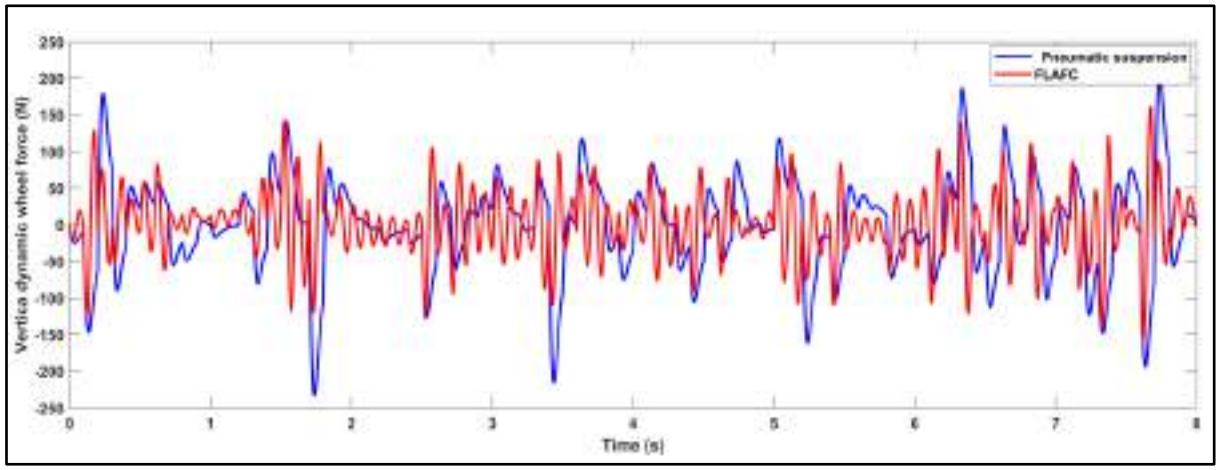

(f)

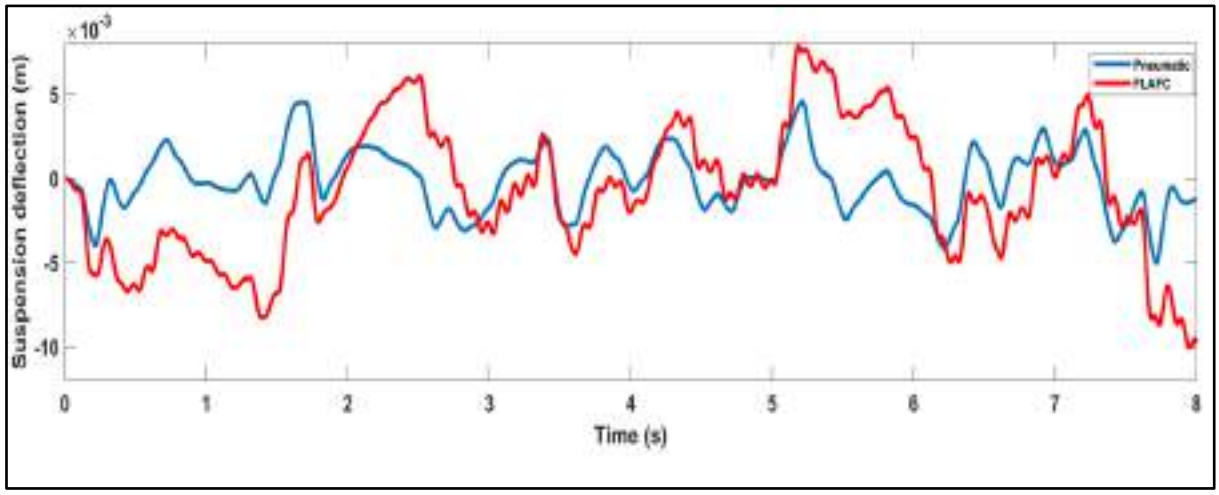

(g)

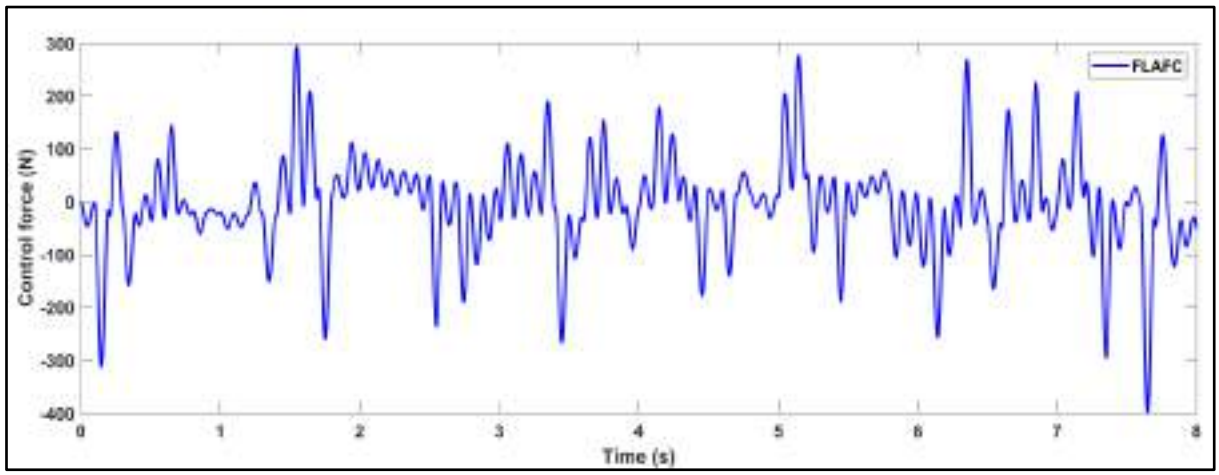

(h)

Figure (5-35) Performance Analysis of AFFLC control for active pneumatic suspension (rough road, level B , velocity 72 km/h).

Input road with two-bump,36 km/h, the parameters of pneumatic active none linear quarter vehicle suspension system for proposed control FLAFC with Genetic algorithm in time domain.

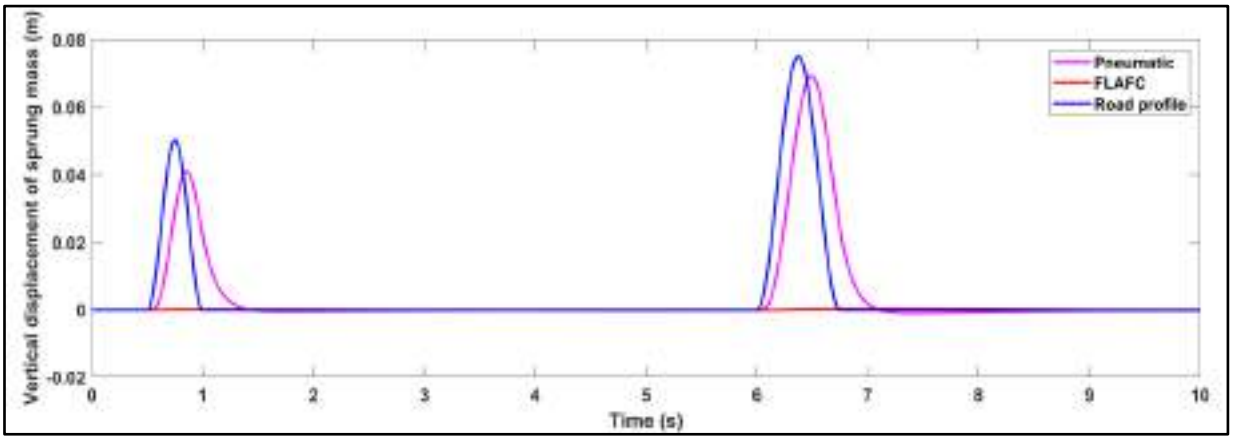

(a)

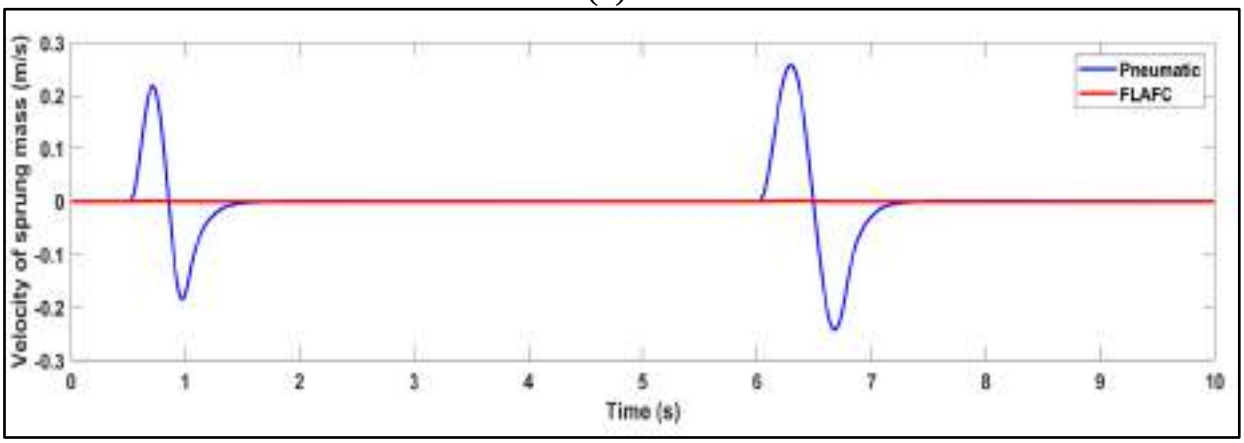

(b)

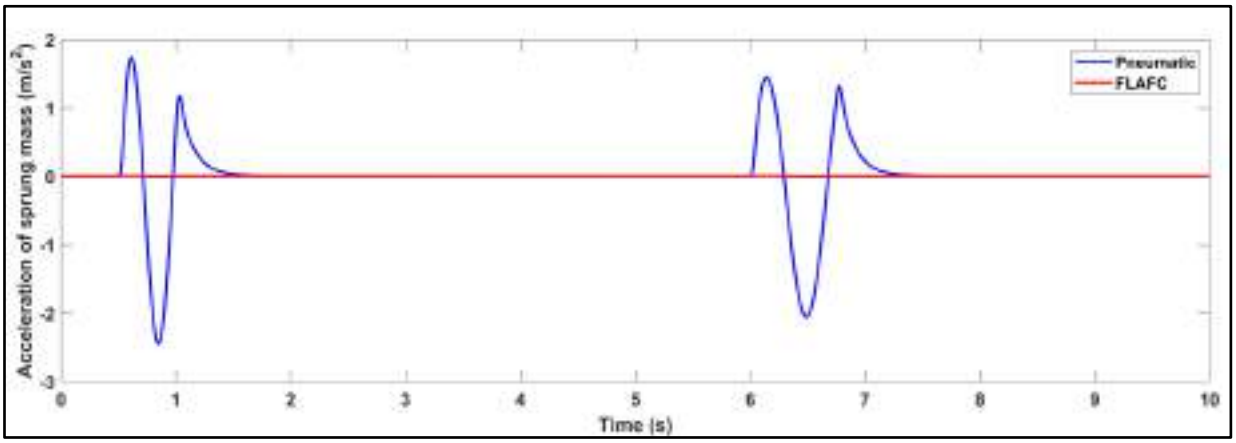

(c)

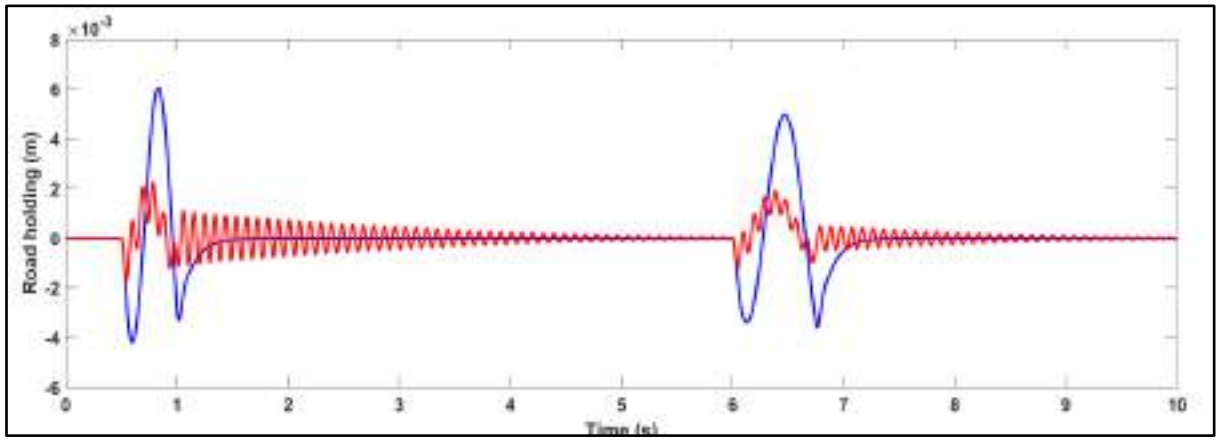
Road holding (m)
Time (s)

(d)

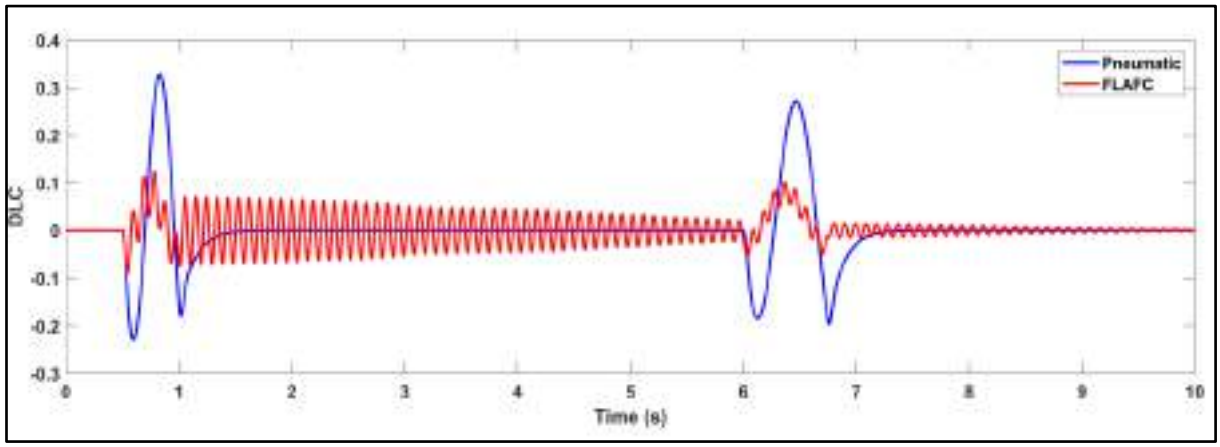
DLC
Time (s)
Pneumatic
FLAFC

(e)

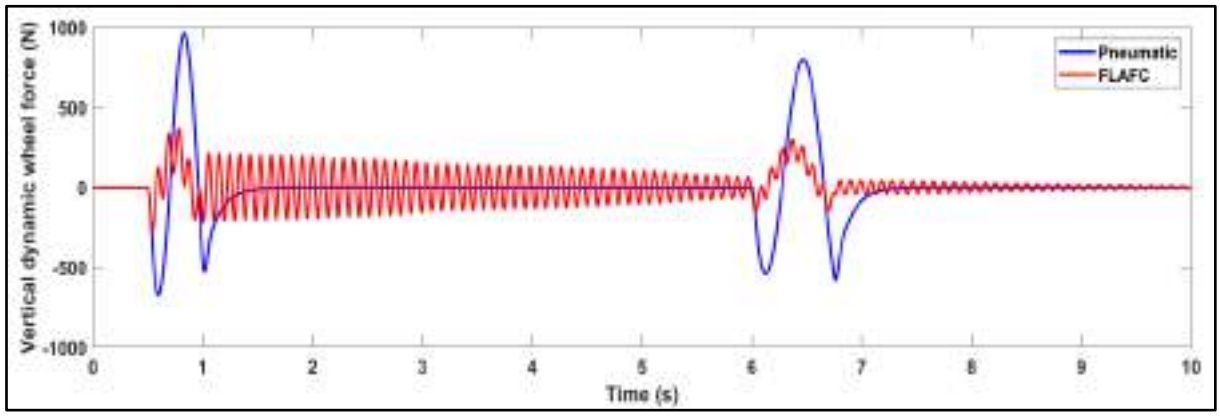
Vertical dynamic wheel force (N)
Time (s)
Pneumatic
FLAFC

(f)

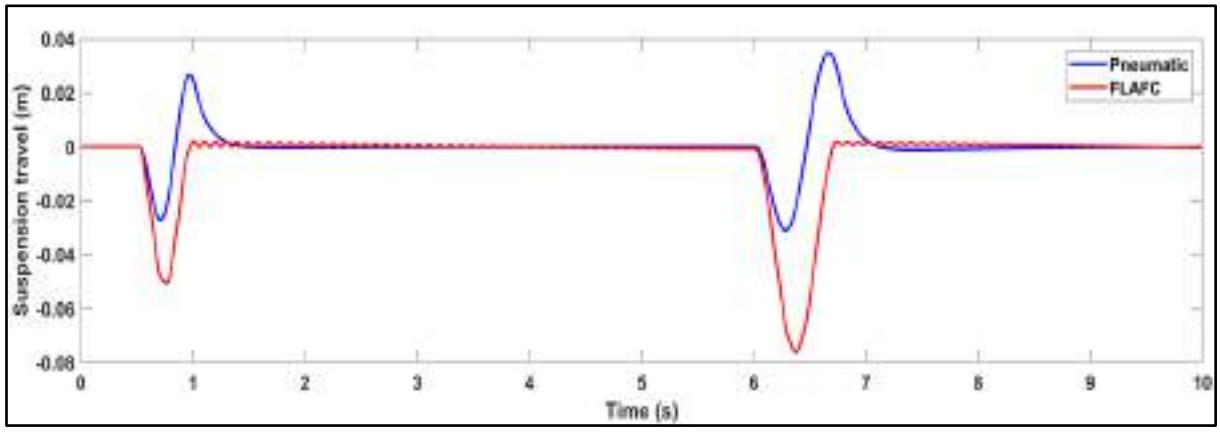

(g)

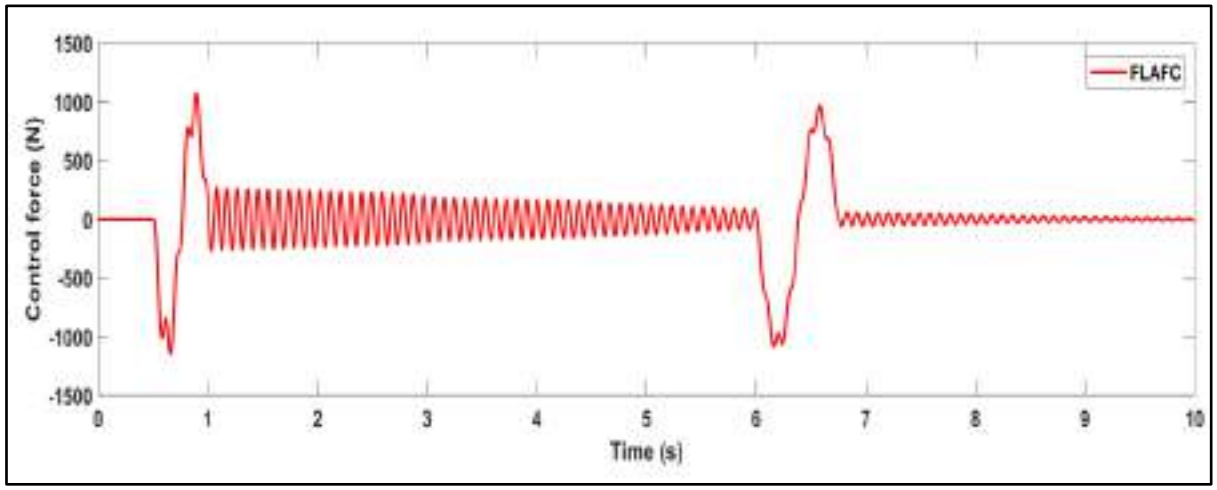

(h)

Figure (5-36) Performance Analysis of AFFLC control for active pneumatic suspension (road-two bump, velocity 36 km/h).

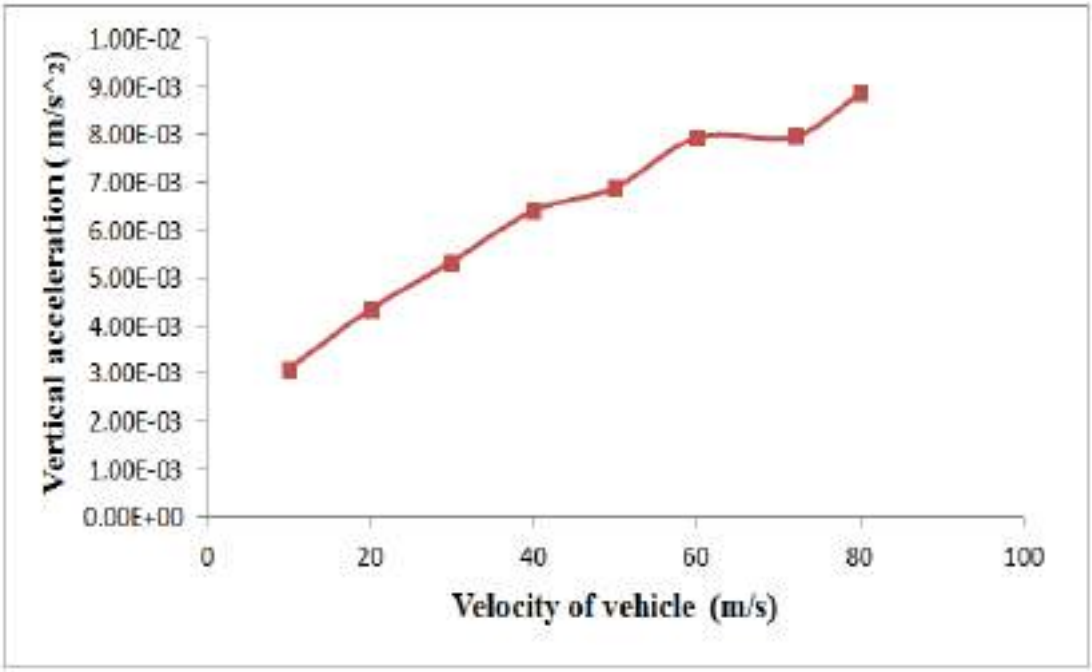
Vertical acceleration (m/s^2)
1.00E-02
9.00E-03
8.00E-03
7.00E-03
6.00E-03
5.00E-03
4.00E-03
3.00E-03
2.00E-03
1.00E-03
0.00E+00
0
20
40
60
80
100
Velocity of vehicle (m/s)

(a)

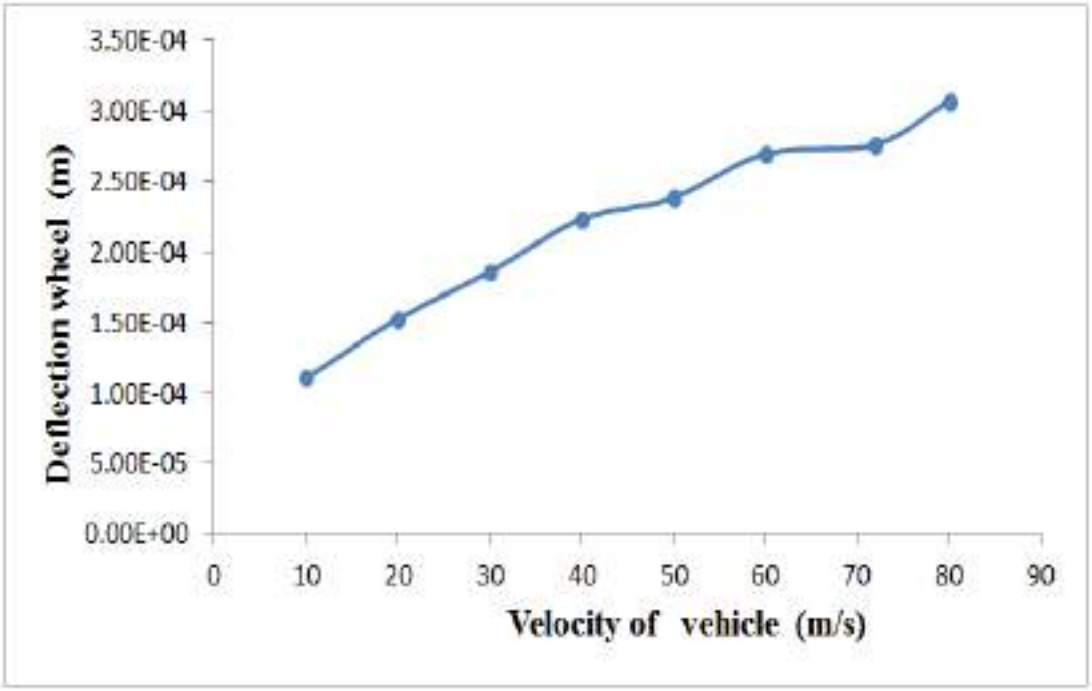
Deflection wheel (m)
3.50E-04
3.00E-04
2.50E-04
2.00E-04
1.50E-04
1.00E-04
5.00E-05
0.00E+00
0
10
20
30
40
50
60
70
80
90
Velocity of vehicle (m/s)

(b)

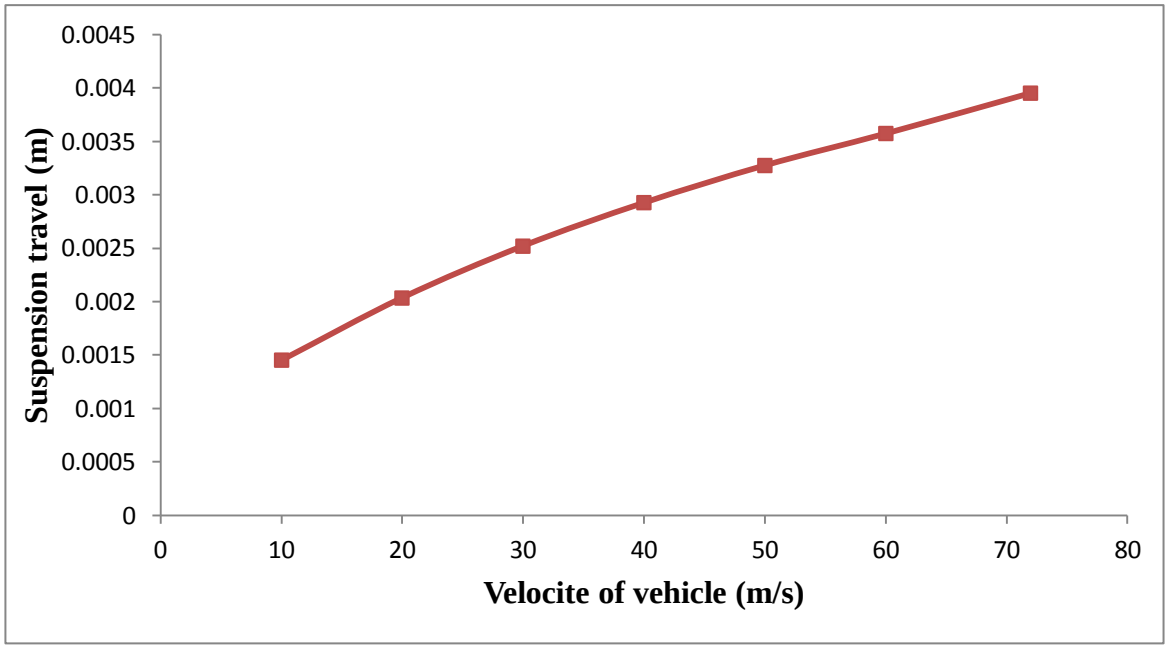
0.0045
0.004
0.0035
0.003
0.0025
0.002
0.0015
0.001
0.0005
0
Suspension travel (m)
0
10
20
30
40
50
60
70
80
Velocite of vehicle (m/s)

(c)

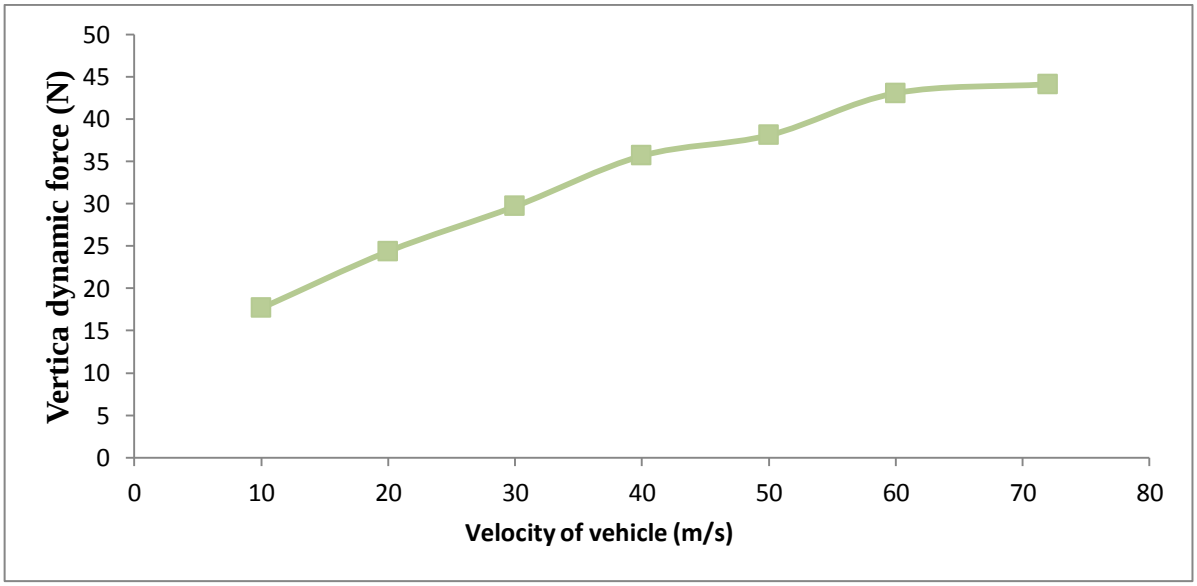
50
45
40
35
30
25
20
15
10
5
0
Vertica dynamic force (N)
0
10
20
30
40
50
60
70
80
Velocity of vehicle (m/s)

(d)

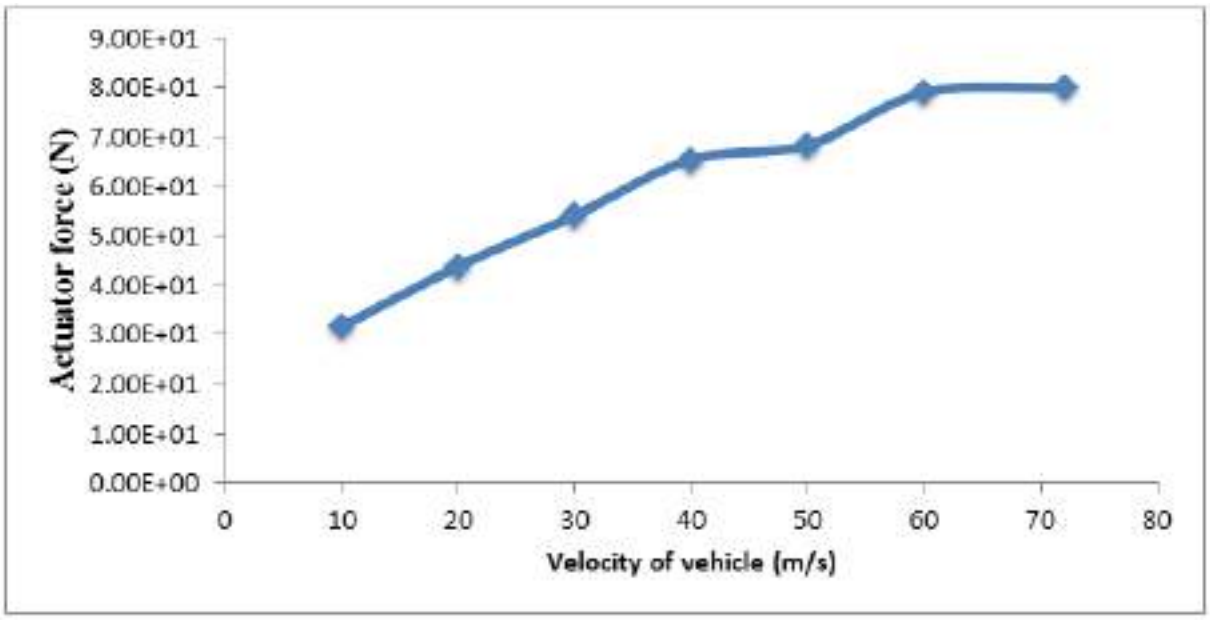

(e)

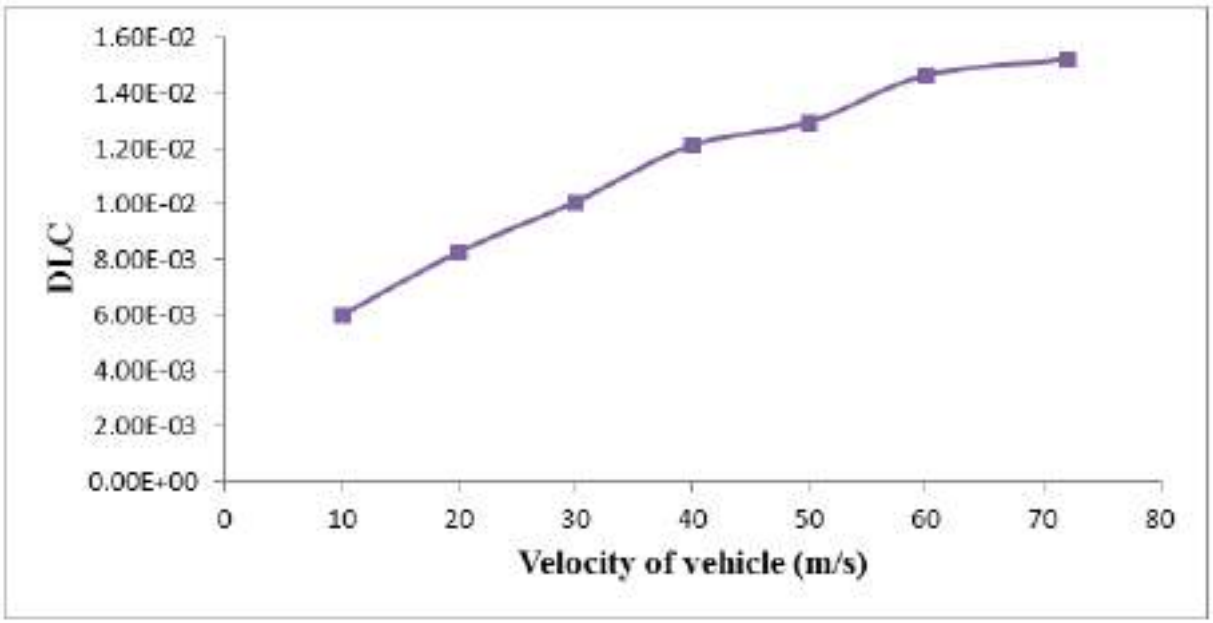

(f)

Figure (5-37) The behavior of ride comfort and road holding with the velocity of vehicle.

Figures (5-37a, 5-37b, 5-37c,5-37d, 5-37e and 5-37f) investigated is the effect of changing the dynamic responsiveness of vehicle speed for parameters of quarter-car. Figures show simulations performed with road level B for various vehicle speeds ranging from 10 m/s to 72 m/s. When the velocity of vehicle is increased, ride comfort for passenger decrease, as seen by the sprung mass acceleration "RMS" values plotted in Figure (5-37a). The deflection in “RMS” (Figure 5-37c), tire deflection in “RMS” (Figure 5-46b), vertical dynamic tire force (5-37d), and dynamic load coefficient(5-37f), which represent the stability of vehicle when increase velocity of vehicle the stability decrease. This analysis is agreement with [117]. Figure (5-37e) shows that the AFC suspension system outperforms the pneumatic suspension system in terms of the actuator's power demand.

Figure (5-38) depicts the point at which the best and average fitness levels converge. Both values nearly converge to each other in the eleventh generation and the average fitness has remained fairly near the best fitness, following twenty generations, the best fitness doesn't always alter as generations increase, i.e. providing the parameter values of an optimal or near-optimal solution.

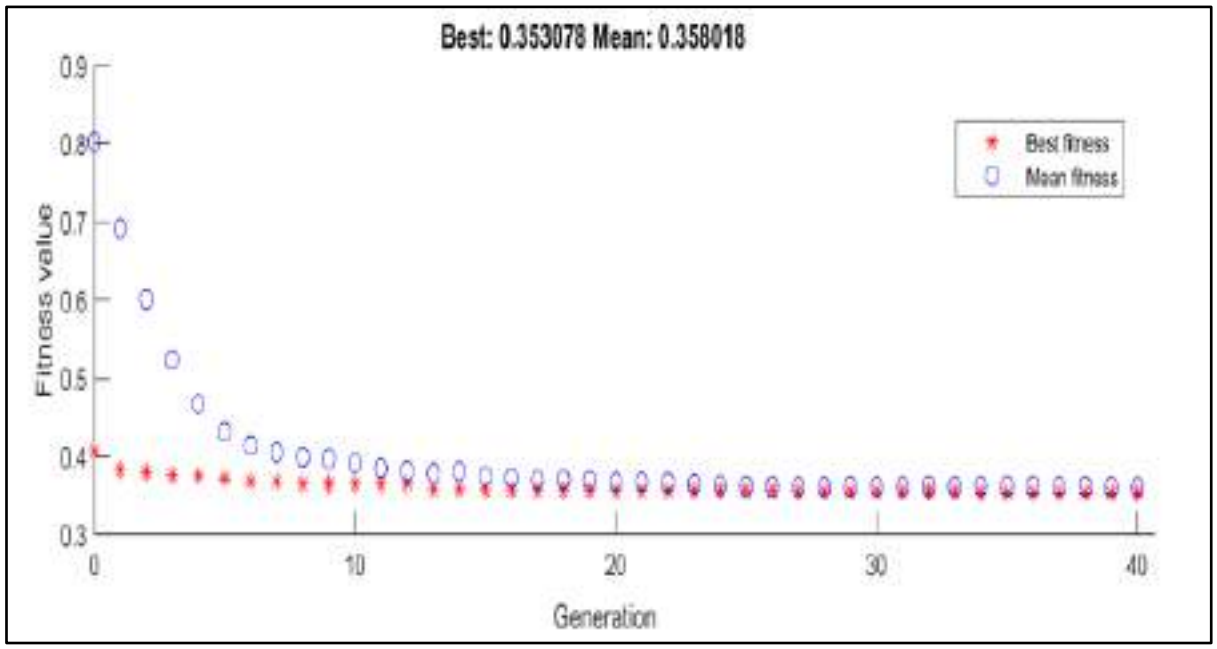

Figure (5-38) Convergence obtained by GA.

Table(5-10) Reduction in overshoot values for roughness road input.

No	Parameters	Pneumatic	Optimal(FL-AFC)	Reduction
1	VDSM (m)	3.859×10^{-3}	4.438×10^{-4}	88. 5%
2	ASM($m.s^{-2}$)	1.593×10^{-1}	7.971×10^{-3}	94.99%
3	VDWF (N)	6.6×10^{1}	4.411×10^{1}	33.2%
4	DLC	2.243×10^{-2}	1.499×10^{-2}	33.6%
5	RH (m)	4.125×10^{-4}	2.757×10^{-4}	33.2%
6	VSM (m/s)	1.409×10^{-2}	6.61×10^{-4}	95.3%

Table(5-11) Reduction in overshoot values for two bumps road input in RMS.

No	Parameters	Pneumatic	Optimal(FL-AFC)	Reduction
1	VDSM M (m)	5.017×10^{-3}	1.641×10^{-4}	94.735%
2	ASM (m.s-2)	4.731×10^{-1}	7.006×10^{-3}	98.35%
3	DLC	6.410×10^{-2}	2.34×10^{-2}	63.33%
4	RH (m)	1.179×10^{-3}	4.304×10^{-4}	63.49%
5	VDWF (N)	1.887×10^{2}	6.887×10^{1}	63.5%
6	VSM (m/s^2)	5.581×10^{-2}	4.688×10^{-4}	99.16%

Through the simulation results and analysis, it was shown that the Active Force Fuzzy Logic strategy is adaptive control and more robustness compared to the other of the types of controls which discussed in terms of comfort and handling road compared to the passive suspension system (pneumatic), it adapts to bumpy roads and gets good results.

5.8 Concluding Remarks

Characterization of the displacement and acceleration values of the sprung mass in the vehicle's suspension system, which play a part in stability and ride comfort through the vibrations brought on by the impact of the road. Control and Genetic algorithm optimization of an active nonlinear (3DOF) quarter car suspension system is presented in this section. The air suspension with a hydraulic actuator system provides a qualitative improvement in vehicle performance and ride comfort compared to traditional air suspension systems. The FLAFC simulation results have better performance in controlling and isolating the vibration from the road compared to other controllers for air suspension and for the same calculation time.

Chapter six

Conclusion and Recommendations

Chapter Six

Conclusions and Recommendations

6.1 The Conclusions

In this work, intelligent control design for quarter vehicle nonlinear pneumatic active suspension with hydraulic actuators has been investigated. Nonlinear hydraulic actuator and frictional forces' effects are taken into account. By simulating the pneumatic suspension alone, comparing the Gensys type with the traditional type, and obtaining the characteristics of the suspension, it was found that the first type is the best, and accordingly, it was chosen in the active control. It was connected to a hydraulic actuator and a control unit to control and optimize the control unit (A genetic Algorithm was used as a tool to tune the gains of the controller). The PID controller, Fractional order PID controller, Fuzzy controller, Fuzzy Control Active Force, A Self Tuning Fuzzy PID Controller, and Sliding Mode are implemented on a nonlinear pneumatic suspension with hydraulic actuator for the quarter car system and the controller scaling was tuned by optimization approach.

The air suspension-integrated hydraulic actuator's objective is to represent how the suspension system behaves with rough roads to evaluate the performance of the vehicle through simulations. The goal of this study was to improve the ride comfort of vehicles through the application of an air spring integrated with the hydraulic actuator of the suspension system.

- According to the findings, air suspension systems alone are unable to effectively reduce vibrations caused by bumpy roads.

- A benefit of the suggested air spring with extra volumes is the capability to control suspension stiffness through the orifice.
- AF-FLC was proven robustness controller with the integrated model is stable in terms of performance and has the ability to improve control targets better than other types of control used and the results show that the vertical displacement of sprung mass, vertical acceleration of sprung mass, road holding, and dynamic load coefficient is significantly reduced respectively by 88.5%, 95%, 33.2%, and 33.6% in comparison with other controllers for rough road class B. To design the best scaling factors of controllers for the vehicle's pneumatic active suspension system, the genetic algorithm was used because of its effective effect
- According to the simulation results, the proposed controller performs better at minimizing the body displacement's magnitude and settling time as well as its velocity and suspension travel.
- The hydraulic nonlinear actuators involving frictional forces are taken into consideration for their effects.
- Models that are the nonlinear and intricate can be handled by the controller using fuzzy logic (FLC). To deal with this problem, GA technic is used in this work to improve the performance of FLC-based PID controllers.
- The rough road inputs are of B-level approximately approximate to the road tested in practice to evaluate the car's ride and handling.

6.2 Recommendations for Further Work

Simulation model has demonstrated that it is successful to apply the preview information to model of a quarter-car, although this still needs to be tested experimentally. Below are a number of recommendations for future works.

- The double-integrated actuators with controllers can be used with each quarter in suspension system.
- Intelligent hybrid controller methods can be used to control the system to show behavior its performance in order to show the integrated air suspension system's efficacy, experimental work is required in advanced laboratories.
- It is suggested that experiments be performed on actual full suspension systems under actual operating circumstances.
- Other techniques for optimization can be utilized in future work, like the grey wolf algorithm.
- A comparison between two types of control over the suspension system, the electric pressure regulator and the control of the force of the integrated-actuator for the same road input.

References

Reference

[1] S. Mouleeswaran, “Design and Development of PID Controller-Based Active Suspension System for Automobiles”, controller design approaches-theory, tuning and application to frontier areas, pp.71-98 , 2012.

[2] H. Porumamilla, A. G. Kelkar, and J. M. Vogel, “Modeling and verification of an innovative active pneumatic vibration isolation system”, Journal of dynamic systems, measurement, and control, Vol. 130, No. 3, 2008.

[3] A. Masliiev, Y. Makarenko, and V. Masliiev, “Study of an air spring with improved damping of vibrations”, Vol. 4, No. 4, pp. 59–64, 2015.

[4] P. K. Eskandary, “Interconnected Air Suspensions with Independent Height and Stiffness Tuning”, MSc thesis, Waterloo, Ontario, Canada, 2014.

[5] J. G. Prada, A. Alonso, J. Vinolas, X. Carrera, K. Reybrouck, and J. G. Gimenez, “Gas dampers: Model development and potential ride performance evaluation” ,Veh. Syst. Dyn., vol. 49, no. 1–2, pp. 199–218, 2011.

[6] M. Biglarbegian, W. Melek, and F. Golnaraghi, “A novel neuro-fuzzy controller to enhance the performance of vehicle semi-active suspension systems”, Veh. Syst. Dyn., Vol. 46, No. 8, pp. 691–711, 2008.

[7] Z. Yin, A. Khajepour, D. Cao, B. Ebrahimi, and K. Guo, “A new pneumatic suspension system with independent stiffness and ride height tuning capabilities”, Vehicle system dynamics, Vol. 50, No. 12, pp. 1735–1746, 2012.

[8] L. X. Long et al., “Ride Performance Evaluation of Air and Hydro-Pneumatic Springs of Suspension System”, International Journal of Advanced Research in Engineering and Technology Vol. 12, No. 1, pp. 439–447, 2021.

[9] L. X. Long, L. Van Quynh, and B. Van Cuong, “Study on the influence of bus suspension parameters on ride comfort”, Vibroengineering Procedia, Vol. 21, pp. 77–82, 2018.

[10] S. Sarami, H. J. Meyer, and S. Hammes, “Development and investigation of a semi-active suspension system for full suspension tractors”, 16th International Conference of the International Society for Terrain Vehicle Systems 2008, ISTVS 2008, no. September. pp. 236–244, 2008.

[11] S. M. Savaresi, C. P.-V. C. Spelta, and O. S. L. Dugard, "Semi-Active Suspension Control Design for Vehicles", 1st editio. NEW YORK Butterworth-Heinemann, 2010.

[12] R. Buhari, M. Md Rohani, and M. E. Abdullah, “Dynamic Load Coefficient of tyre forces from truck axles”, Appl. Mech. Mater., Vol. 405–408, pp. 1900–1911, 2013.

[13] P. Hu, X. N. Zhang, and S. Tian, “Research on heavy truck dynamic load coefficient and influence factors”, MATEC Web Conf., Vol. 81, pp. 1–5, 2016.

[14] M. Presthus, “Derivation of Air Spring Model Parameters for Train Simulation”, MSc thesis, Lulea University of Technology, Sweden, 2002.

[15] H. J. Abid, “Air Suspension Control System for Passenger Vehicles Using PID and Fuzzy Controllers”, Ph.D.Thesis, Basrah University, 2015.

[16] M. Berg, “Three-dimensional airspring model with friction and orifice damping”, International Journal of Vehicle Mechanics and Mobility, Vol. 33, pp. 528–539, 2000.

[17] M. Bayraktar and R. Guclu, “Modelling of Air Springs in a Rail Vehicle”, 13th International Research/Expert Conference,Trends in the Development of Machinery and Associated Technology,, pp. 829–832, 2009.

[18] S. Das, "Functional Fractional Calculus for System Identification and Controls", 1st edition. Berlin, 2007.

[19] E. Elbeltagi, T. Hegazy, and D. Grierson, “Comparison among five

evolutionary-based optimization algorithms", Adv. Eng. Informatics, Vol. 19, no. 1, pp. 43–53, 2005.

[20] F. Van Den Bergh, "An Analysis of Particle Swarm Optimizers", University of Pretoria,South Africa, 2006.

[21] J. H. Holland, "Adaptation in Natural and Artificial Systems", 1 st. London: Bradford Books, 1992.

[22] J. Zhang, C. Xu, M. Yi, and Z. Jiang, "Prediction of the mechanical properties of ceramic die material with artificial neural network and genetic algorithm", Proc. IEEE Int. Conf. Intell. Comput. Intell. Syst. ICIS, Vol. 1, pp. 603–607, 2009.

[23] A. Alfadhli, "Active Seat Suspensions for Automotive Applications", Ph.D.Thesis, University of Bath, 2018.

[24] J. C. Cassa, G. Floridia, A. R. Souza, and R. T. Oliveira, "Prediction of cement paste mechanical behaviour from chemical compositon using genetic algorithms and artificial neural networks", Proc. 2nd Int. Conf. Intell. Process, Vol. 1 , pp. 291–298, 1999.

[25] W. Shouchun and D. Xiucheng, "Predicting China's energy consumption using artificial neural networks and genetic algorithms", International Conference on Business Intelligence and Financial Engineering Predicting, pp. 8–11, 2009.

[26] R. Hassan, B. Cohanim, O. De Weck, and G. Venter, "A comparison of particle swarm optimization and the genetic algorithm", American Institute of Aeronautics and Astronautics, Vol. 2, pp. 1138–1150, 2005.

[27] H. K. Tran, J. S. Chiou, and S. T. Peng, "Design Genetic Algorithm Optimization education software based fuzzy controller for a tricopter fly path planning," Eurasia Journal of Mathematics, Science & Technology Education, Vol. 12, No. 5, pp. 1303–1312, 2016.

[28] Y. P. Kuo and T. H. S. Li, "GA-based fuzzy PI/PD controller for automotive active suspension system", IEEE Trans. Ind. Electron., Vol.

46, No. 6, pp. 1051–1056, 1999.

[29] M. Tahmasebi, R. A. Rahman, M. Mailah, and M. Gohari, “Intelligent active force control of a robotic arm using genetic algorithm,” Jurnal Mekanikal, Vol. 6, No. 8, pp. 1277–1281, 2012.

[30] P. A. Weber and J. P. Braaksma, “Towards a North American geometric design standard for speed humps”, ITE journaL, Vol. 70, No. 1, pp. 30–34, 2000.

[31] G. A. Hassaan, “Car dynamics using quarter model and passive suspension, part i: Effect of suspension damping and car speed”, Inernational Journalof Computer Techniques, Vol. 1, No. 2, pp. 1–9, 2014.

[32] D. D. D. Das, M. S. Kumar, and S. R. Gampa, “Optimum PID Controller Design using PSO for Vehicle Active Suspension System Considering MATLAB Simulink Modeling based Road Profiles”, Journal of Electrical Engineering, 2017.

[33] M. M. Moheyeldein, A. M. Abd-El-Tawwab, K. A. Abd El-gwwad, and M. M. M. Salem, “An analytical study of the performance indices of air spring suspensions over the passive suspension”, Beni-Suef University Journal of Basic and Applied Sciences, Vol. 7, No. 4, pp. 525–534, 2018.

[34] T. A. Nguyen, “Advance the stability of the vehicle by using the pneumatic suspension system integrated with the hydraulic actuator”, Latin American Journal of Solids and Structures, vol. 18, no. 7, 2021.

[35] H. Kim and H. Lee, “Fault-tolerant control algorithm for a four-corner closed-loop air suspension system”, IEEE Transactions on industrial Electronics, vol. 58, no. 10, pp. 4866–4879, 2011.

[36] A. Kazemeini, H. Hacışevki, and N. Özada, “Improving Control Mechanism of an Active Air Suspension System”, MSc. Thesis, Eastern Mediterranean University, 2013.

[37] N. Khettou, M. Demic, S. Muzdeka, and M. Krsmanovic, “Contribution to

the modeling of a pneumatic semi-active control of vehicle suspension", University of Defense in Belgrade, Military Academy, Vol. 63, No. 4, pp. 99–115, 2015.

[38] H. J. Abid, J. Chen, and A. A. Nassar, "Equivalent Air Spring Suspension Model for Quarter-Passive Model of Passenger Vehicles", Hindawi Publishing Corporation International Scholarly Research Notices, Vol. pp. 1–6, 2015.

[39] P. Karimi , A. Khajepour, A. Wong and M. Anasar, "Analysis and optimization of air suspension system with independent height and stiffness tuning", International Journal of Automotive Technology, Vol. 17, No. 5, pp. 807–816, 2016.

[40] G. Dalvi, P. Chivkula, J. Trivedi, and A. B. I. Mathew, "Experimental and Simulation Study To Control", International Federation of Automatic Control, Papers On Line ,pp.166–172, 2018.

[41] W. Li, Y. Chen, S. Zhang, E. Mao, Y. Du, and H. Wen, "Damping Characteristic Analysis and Experiment of Air Suspension with Auxiliary Chamber," IFAC-Papers, Vol. 51, No. 17, pp. 166–172, 2018.

[42] M. Li, D. Wang, S. Zhang, S. Tan, and Y. Ji, "Study on FuzzPID control of Shared Chamber Air Suspension for ride comfort", MATEC Web Conf., vol. 293, no. 201 9, p. 01002, 2019.

[43] K. A. Abd El-gwwad, A. M. Abd-el-tawwab, M. M. Moheyeldein, and M. M. M. Salem, "Theoretical and Experimental Study of Semi-Active Four-State Switchable Damper Suspension System with Dynamic Air Spring", International Journal of Advanced Science and Technology,Vol. 29, No. 3, pp. 10–28, 2020.

[44] M. Mailah and G. Priyandoko, "Simulation of a suspension system with adaptive fuzzy active force control", Int. J. Simul. Model., vol. 6, no. 1, pp. 25–36, 2007.

[45] M. K. R. K. Pekgökgöz, M. A. Gürel, M. Bilgehan, "Active suspension of

cars using fuzzy logic controller optimized by genetic algorithm PID control quarter-car", International Journal of Engineering and Applied Sciences (IJEAS), Vol.2, Issue 4, pp.27-37 , 2010.

[46] J. Sun and Y. Sun, "Comparative study on control strategy of active suspension system", Proc. - 3rd Int. Conf. Meas. Technol. Mechatronics Autom., Vol. 1, pp. 729–732, 2011.

[47] G. Yang and Y. Zhao, "Fuzzy control of vehicle suspension system", Advanced Materials Research Mater. Res., Vol. 383–390, pp. 2012–2017.

[48] M. Jamil, A. A. Janjua, I. Rafique, S. I. Butt, Y. Ayaz, and S. O. Gilani, "Optimal control based intelligent controller for active suspension system", Life Science Journal, ISSN: 1097-8135,pp. 653-659, 2013.

[49] C. V. Reddy, S. R. Shankapal, and M. H. M. Gowda, "Modelling and simulation of hydropneumatic suspension for a car", SASTech - Technical Journal of RUAS,Vol. 13, No. 1, pp. 24–30, 2014.

[50] A. Çakan, F. M. Botsali, and M. Tinkir, "Modeling and controller comparison for quarter car suspension system by using PID and type-1 fuzzy logic", Applied Mechanics and Materials, Vol. 598 , pp. 524-528, 2014.2014.

[51] R. Rosli, M. Mailah, and G. Priyandoko, "Active suspension system for passenger vehicle using active force control with iterative learning algorithm", WSEAS Transactions on Systems and Control, Vol. 9, No. 1, pp. 120–129, 2014.

[52] A. M. Shirahatti, "Analysis and Simulation of Active Suspension System for Full Vehicle Model Subjected To Random Road Profile", International Journal of Innovative Research in Science, Engineering and Technology, Vol. 4, Issue 1, ,2015.

[53] S. Palanisamy and S. Karuppan, "Fuzzy control of active suspension system", Journal of Vibroengineering, Vol. 18, Issue 5, pp. 3197-3204, 2016.

[54] X. Dong, D. Zhao, B. Yang, and C. Han, “Fractional-order control of active suspension actuator based on parallel adaptive clonal selection algorithm”, Journal of Mechanical Science and Technology, Vol. 30, No. 6, pp. 2769–2781, 2016.

[55] M. H. Ab. Talib, “Intelligent controllers for vechicle suspension system using magnetorheological damper”, PhD. Thesis, Universiti Teknologi Malaysia, 2017.

[56] Y. Taskin, Y. Hacioglu, and N. Yagiz, “Experimental evaluation of a fuzzy logic controller on a quarter car test rig”, Journal Brazilian Soc. Mech. Sci. Eng., Vol. 39, No. 7, pp. 2433–2445, 2017.

[57] Z. Ding, F. Zhao, Y. Qin, and C. Tan, “Adaptive neural network control for semi-active vehicle suspensions”, Journal of Vibroengineering, Vol. 19, No. 4, pp. 2654–2669, 2017.

[58] U. Durairaj, V. Murugananthan, N. M. Yusoff, and B. Balasubramanian, “Automation of hydraulic active suspension system using harmony search algorithm tuned FOPID”, International Journal of Simulation: Systems, Science & Technology, Vol. 19, No. 6, pp. 1.1-1.7, 2018.

[59] Mahmoud H. Salem ,“Investigation of a non-linear suspension in a quarter car model",PhD. Thesis, Aston University, 2018.

[60] H. K. Tran and T. N. Nguyen, “Flight Motion Controller Design using Genetic Algorithm for a Quadcopter”, Journal of Measurement and Contro, Vol. 51, No. 3–4, pp. 59–64, 2018.

[61] A. A. Nassar and A. M. H. Al-Ghanim, “Modeling, simulation, and control of half car sduspension system using matlab/simulink”, International Journal of Science and Research, Vol. 7, No. 1, pp. 351–362, 2018.

[62] Ahmed A. Abougarair and Muawia M. A., “Design and Simulation Optimal Controller For Quarter Car Active Suspension System,” no. May, pp. 1–6, 2019.

[63] C. Zhou, X. Liu, F. Xu, and W. Chen, “Sliding mode switch control of

adjustable hydro-pneumatic suspension based on parallel adaptive clonal selection algorithm", Journal of Applied Science, Vol. 10, No. 5, 2020.

[64] Y. Shahid and M. Wei, "Comparative analysis of different model-based controllers using active vehicle suspension system", Journal Algorithms, vol. 13, no. 1, 2020.

[65] G. W. Kim, S. W. Kang, J. S. Kim, and J. S. Oh, "Simultaneous estimation of state and unknown road roughness input for vehicle suspension control system based on discrete Kalman filter", Journal of Automobile Engineering, Vol. 234, No. 6, pp. 1610–1622, 2020.

[66] Z. A. Karam and O. A. Awad, "Design of active fractional PID controller based on whale's optimization algorithm for stabilizing a quarter vehicle suspension system", Journl of Periodica Polytechnica Electrical Engineering and Computer Science, Vol. 64, No. 3, pp. 247–263, 2020.

[67] T. A. Nguyen, "Study on the sliding mode control method for the active suspension system", International Journal of Applied Science and Engineering, Vol. 18, No. 5, pp. 1–10, 2021.

[68] V. Gavriloski, "Dynamic Behaviour of an Air Spring Element", Journa of. Mechanical Engineering, 2005.

[69] V. Gavriloski, J. Jovanova, G. Tasevski, and M. Djidrov, "Development of new air spring dynamic model," Faculty of Mechanical Engineering, Belgrade Transactions, Vol. 42, No. 4, pp. 305–310, 2014.

[70] T. A. Nguyen, "Advance the stability of the vehicle by using the pneumatic suspension system integrated with the hydraulic actuator", Latin American Journal of Solids and Structures,Vol.18, No.7,2021.

[71] Pneumatic fluid power - Determination of flow-rate characteristics of components using compressible fluids — Part 3: Method for calculating steady-state flow-rate characteristics of systems)", ISO 6358-3.2014.

[72] Peter Beater," Pneumatic Drives", Springer, Germany, 1971.

[73] J. W. Baxter and J. R. Bumby, "Proceedings of the Institution of

Mechanical Engineers , Part I: Journal of Systems and Control Engineering" , Proceedings of the Institution of Mechanical Engineers, Published by SAGE,1955.

[74] V. Stojanovic and D. Prsic, "Robust identification for fault detection in the presence of non-Gaussian noises: application to hydraulic servo drives", Nonlinear Dynamic, Vol. 100, No. 3, pp. 2299–2313, 2020.

[75] R. Shimamune and K. Tanifuji, "Application of oil-hydraulic actuator for active suspension of railway vehicle: experimental study", Proceedings of the 34th SICE Annual Conference. International Session Papers. IEEE, pp. 1335–1340, 1995.

[76] Y. M. Sam and K. Hudha, "Modelling and force tracking control of hydraulic actuator for an active suspension system", In: 2006 1st IEEE conference on industrial electronics and applications, 2006.

[77] H. E. Merritt, Hydraulic Control Systems, John Wiley, New York.London, 1967.

[78] P. J. P. P.G. Howlett, Advances in Industrial Control, Springer-Verlag London Ltd ,2006.

[79] E. Truckenbrodt, Fluid Mechanics Volume 2: Elementary Flow Processes of Fluids of Variable Density Plus Potential Flows and Boundary Layer , German Edi. Munich Germany,Springer, 2008.

[80] Atheel Kadiem Abdul Zahra, "Fuzzy Sliding Mode Control Scheme for Full Vehicle Active Suspension Systems By",PhD.Thesis, Electrical Engineering, College of Engineering, University of Basrah, 2020.

[81] A. A. Aldair ,"Neurofuzzy Controller Based Full Vehicle Nonlinear Active Suspension Systems", PhD.Thesis, School of Engineering and Informatics, University of Sussex, 2012.

[82] A. A. Aldair and W. J. Wang, "Design an intelligent controller for full vehicle nonlinear active suspension systems", International Journal on Smart Sensing and Intelligent Systems, Vol. 4, No. 2, 2011.

[83] I. Fialho and G. J. Balas, “Road Adaptive Active Suspension Design Using Linear Parameter-Varying Gain-Scheduling”, IEEE Transactions on Control Systems Technology, vol. 10, no. 1, pp. 43–54, 2002.

[84] S. H. Hashemipour, M. Rezaei, and M. Khaliji, “A Study of the Performance of the PID Controller and Nonlinear Controllers in Vehicle Suspension Systems Considering Practical Constraints”, Research Journal of Recent Sciences, Vol. 3, No. 8, pp. 86–95, 2014.

[85] E.Venkateswarulu, N. Ramesh raju, and G.Seshadri, “The Active Suspension System With Hydraulic Actuator for Half Car Model Analysis and Self-Tuning With Pid Controllers”, International Journal of Research in Engineering and Technology, Vol. 03, No. 09, pp. 415–421, 2014.

[86] A. Al-zughaibi and H. Davies, “Controller Design for Active Suspension System of ¼ Car with Unknown Mass and Time-Delay”, International Journal of Mechanical, Aerospace, Industrial, Mechatronic and Manufacturing Engineering Vol:9, No:8, 2015.

[87] S. Razdan, “Comparison of Quarter Car Model of Active Pneumatic Suspensions using Mass Flow Control for a Small Car”, International Journal of Current Engineering and Technology, Vol. 2, No. 2, pp. 597–601, 2013.

[88] P. Xiao, H. Gao, P. Shi, and L. Niu, “Research on air suspension with novel dampers based on glowworm swarm optimization proportional–integral–derivative algorithm”, Advances in Mechanical Engineering, Vol. 10, No. 8, pp. 1–19, 2018.

[89] Z. Xie, P. K. Wong, J. Zhao, T. Xu, K. I. Wong, and H. C. Wong, “A noise-insensitive semi-active air suspension for heavy-duty vehicles with an integrated fuzzy-wheelbase preview control”, Hindawi Publishing Corporation, Mathematical Problems in Engineering, 2013.

[90] P. D. I. Torino, “Study and analysis of a pneumatic spring for city cars”, MSc.Thesis, Automotive Engineering , 2018.

[91] G. Quaglia and M. Sorli, “Air suspension dimensionless analysis and design procedure”, International Journal of Vehicle Mechanics and Mobility, Vol. 35, No. 6, pp. 443–475, 2001.

[92] V. Q. Le, “Comparing the performance of suspension system of semi-trailer truck with two air suspension systems”, Vibroengineering Procedia, Vol. 14, pp. 220–226, 2017.

[93] I. A. Daniyan, K. Mpofu, O. L. Daniyan, and A. O. Adeodu, “Modelling and simulation of a PID controlled active suspension system of a rail car”, Proceedings of the International Conference on Industrial Engineering and Operations Management, pp. 1470–1480, 2018.

[94] M. Avesh and R. Srivastava, “Modeling simulation and control of active suspension system in Matlab Simulink environment”, Students Conference on Engineering and Systems SCES, 2012.

[95] A. Jayachitra and R. Vinodha, “Genetic Algorithm Based PID Controller Tuning Approach for Continuous Stirred Tank Reactor”, Advances in Artificial Intelligence, pp. 1–8, 2014.

[96] K. F. Man, K. S. Tang, and S. Kwong, “Genetic algorithms: Concepts and applications”, IEEE transactions on Industrial Electronics, Vol. 43, No. 5, pp. 519–534, 1996.

[97] M. P. Nagarkar, Y. J. Bhalerao, G. J. Vikhe Patil, and R. N. Zaware Patil, “GA-based multi-objective optimization of active nonlinear quarter car suspension system—PID and fuzzy logic control”, International Journal of Mechanical and Materials Engineering, vol. 13, no. 1, 2018.

[98] N. M. Ghazaly, A. E. N. S. Ahmed, A. S. Ali, and G. T. A. El-Jaber, “H∞ control of active suspension system for a quarter car model”, International Journal of Vehicle Structures and Systems, Vol. 8, No. 1, pp. 35–40, 2016.

[99] D. Xue, C. Zhao, and Y. Q. Chen, “Fractional order PID control of A DC-motor with elastic shaft: A case study”, Proceedings of the American Control Conference, pp. 3182–3187, 2006.

[100] Chengbin Ma, “Fractional Order Control and Its Applications in Motion Control”, PhD.Thesis, Department of Electrical Engineering, University of Tokyo, 2004.

[101] F. V. Monje, C. A. M., Chen Y.Vinagre, B.M. Xue D., Fractiona-Order Systems and Controls. Verlag London: Springer, 2010.

[102] A. Science, “Fractional Order Control of Active Magnetic Bearing Systems”, PhD.Thesis, School of Engineering and Applied Science, University of Virginia 2015.

[103] V. Karaman and K. Kayisli, “Sliding Mode Control of Vehicle Suspension System Under Different Road Conditions”, International Journal of Engineering Science and Application, Vol. 1, No. 2, pp. 1–6, 2017.

[104] A. K. Abdulzahra and T. Y. Abdalla, “Fuzzy Sliding Mode Control Scheme for Vehicle Active Suspension System Optimized by ABC Algorithm”, Intelligent Systems and Applications, Vol. 11, No. 12, pp. 1–10, 2019.

[105] S. B. Aminreza Riahi, “Fuzzy and Sliding Mode Control Design for Vehicle Ride Performance”, International Journal of Automation and Power Engineering, pp. 37–41, 2012.

[106] J. Hurel, A. Mandow, and A. Garcia-Cerezo, “Tuning a fuzzy controller by particle swarm optimization for an active suspension system”, Annual Conference on IEEE Industrial Electronics Society, pp. 2524–2529, 2012.

[107] S. Rajendiran and P. Lakshmi, “Simulation of PID and fuzzy logic controller for integrated seat suspension of a quarter car with driver model for different road profiles”, Journal of Mechanical Science and Technology, Vol. 30, No. 10, pp. 4565–4570, 2016.

[108] B. K. Nguyen and K. A. Kyoung, “position control of shape memory alloy actuators by using self tuning fuzzy PID controller”, Conference Paper in International Journal of Control Automation and Systems, 2006.

[109] Zulfatman and M. F. Rahmat, “Application of Self-Tuning Fuzzy Pid

Controller on Industrial Hydraulic Actuator", The International Journal on Smart Sensing and Intelligent Systems,Vol. 2, No. 2, pp. 246–261, 2009.

[110] K. K. Ahn, D. Q. Truong, and Y. H. Soo, "Self tuning fuzzy PID control for hydraulic load simulator", International Conference on Control , Automation and Systems, pp. 345–349, 2007.

[111] H. Taghavifar and B. Li, "PSO-Fuzzy Gain Scheduling of PID Controllers for a Nonlinear Half-Vehicle Suspension System", SAE International Journal of Passenger Cars-Mechanical, Vol. 12, No. 1, pp. 5–20, 2018.

[112] J. R. Hewit and J. S. Burdess, "Fast dynamic decoupled control for robotics, using active force control", Mechanism and Machine Theory, Vol. 16, No. 5, pp. 535–542, 1981.

[113] K. Rajeswari and P. Lakshmi, "Simulation of Suspension System with Intelligent Active Force Control", International Conference on Advances in Recent Technologies in Communication and Computing, pp. 271–277, 2010.

[114] G. Priyandoko, M. Mailah, and H. Jamaluddin, "Vehicle active suspension system using skyhook adaptive neuro active force control", Mechanical systems and signal processing, Vol. 23, No. 3, pp. 855–868, 2009.

[115] S. Zeraati, "Designing fractional order PID for car suspension systems", International Journal of Scientific & Engineering Research, Vol. 6, No. 11, 2015.

[116] P. Sathishkumar, J. Jancirani, and J. Dennie, "Reduction of axis acceleration of quarter car suspension using pneumatic actuator and active force control technique", Journal of Vibroengineering, vol. 16, no. 3, pp. 1416–1423, 2014.

[117] M. Haddar, R. Chaari, S. C. Baslamisli, F. Chaari, and M. Haddar, "Intelligent PD controller design for active suspension system based on robust model-free control strategy Maroua", Journal of Mechanical Engineering Science, Vol. 233, No. 14, pp. 4863–4880, 2019.

[118] H. Chen, P.-Y. Sun, and K.-H. Guo, “Constrained H-infinity control of active suspensions: an lmi approach”, IEEE Transactions on Control Systems Technology,Vol.13,No.3, pp. 157–157, 2005.

[119] T. A. Nguyen, “Improving the Comfort of the Vehicle Based on Using the Active Suspension System Controlled by the Double-Integrated Controller”, Journal of Shock and Vibration, 2021.

[120] A. Shirahatt, P. S. S. Prasad, P. Panzade, and M. M. Kulkarni, “Optimal design of passenger car suspension for ride and road holding”, Joural of Brazilian Association of Engineering and Mechanical Sciences Brazilian., vol. 30, no. 1, pp. 66–76, 2008.

BJES Basrah Journal for Engineering Sciences

Basrah Journal for Engineering Sciences, Vol. 22, No. 2, (2022), 16-22

Original Article

Journal homepage: www.bjes.edu.iq
ISSN (Online): 23118385, ISSN (Print): 18146120

Analysis and Study Indicators for Quarter Car Model with Two Air Suspension System

Mahmood S. Mahmood [1,*], Ameen A. Nassar [2], Haider M. Mohammad [3]

[1,2] Department of Mechanical Engineering, College Engineering, University of Basrah, Basrah, Iraq
[3] Department of Material Engineering, College Engineering, University of Basrah, Basrah, Iraq
E-mail addresses: mahmood.shaeer@uomus.edu.iq , ameen.nassar@uobasrah.edu.iq , haider.mohammed@uobasrah.edu.iq
Received: 9 December 2021; Accepted: 20 April 2022; Published: 24 December 2022

Abstract

Modeling and simulation of non-linear quarter-car suspension system for two air spring models (traditional and dynamic new air spring) are contrasted in terms of (RMS) sprung mass acceleration, dynamic load coefficient, the vertical displacement, they are compared. Two and three (DOF) of the mathematical quarter models are implemented in MATLAB/Simulink platform. The Ride Comfort (RC), Dynamic Load Coefficient (DLC) and Road Handling (RH) responses are evaluated as objective functions respectively considering a vehicle speed at 72 km/h and road ISO Class B. The obtained results indicate that the vertical displacement, the (RMS) of the sprung mass acceleration, and dynamic load coefficient values with the new air model system decrease by 10.7 %, 30.6 %, and 13.49 % respectively, in comparison to a tradition suspension system, this one gives more comfort and effortless handling.

Keywords: Air suspension system, Ride comfort, Road holding, Dynamic load coefficient, and Vehicles used for commercial purposes.

https://doi.org/10.33971/bjes.22.2.3

1. Introduction

Because of the benefits in ride comfort and control of height, air suspension systems have become more popular in recent years. The key compromise is between ride quality and driving stability, because the suspension must be soft on one side to reach a high level of comfort while being stiff enough to retain good tire contact with the ground to ensure safety. However, an air spring suspension system can be developed to improve the vertical dynamics of vehicles. Air springs provide better comfort and handling performance because simple decrease of stiffness for obtaining soft suspension and constant suspension space, independently of load between the sprung and un sprung mass moreover, by supplying and strangling the air through an air circuit connected to the air spring it is possible to adjust air springs' heights. For analyzing the effects of suspension design parameters on vehicle ride comfort as well as friendliness of the road surface when vehicles travel on the road surface of ISO class B at velocity 20 m/s with a complete load for a half-vehicle model of a semi-trailer, the RC of the vehicle with the increase of the damping of the suspension was improved by Quynh et al. [1]. The simulation findings demonstrated that independent stiffness and the ride height control tuning can enable suspension that is more adaptable design for striking a better balance between a numerous conflicting requirements and obstacles was presented by Yin et al. [2]. The active pneumatic suspension with control strategy for a commercially manufactured small car which based on mass flow control with two different control strategies were presented, the first model mass flow to the air source has to be based on the differences of velocity between excitation and sprung mass and the mass flow rate in the second model is the sinusoidal function of the stimulation frequency from the base were presented by Randan et al. [3].

Gavriloski et al. [4] proposed a new air dynamic spring to develop the coefficient of damping for flow resistance when two volumes are linked together for analyzing the vertical dynamics of vehicle and the simulation and experimental results were analyzed. Masliiev et al. [5] studied the effect of system components parameters on the damping factor of vibrations and the development of the vibration amplitudes in a laminar and turbulent mode of airflow by an aperture that connects the air source with the supplementary reservoir was demonstrated in a pneumatic spring suspension, and gas-thermal and dynamic phenomena. Also, showed the damping coefficient dependent on the cross-section of the throttle orifice. Quynh et al. [6] evaluated the dynamic interaction between the road and heavy vehicle when the road surface roughness is random, by using impact factor of dynamic tire load, the minimal vertical dynamic load factor, and the maximal vertical dynamic load factor. Toyofuku et al. [7] investigated the relationship between the frequency of vibration and the air spring during the effect of the pipe diameter which connect air spring with auxiliary chamber and length on the dynamic air spring. Long et al. [8] analyzed the performance (the hydro pneumatic, the rubber and air system) for a fully dynamic model of a large vehicle operates under the different road surface roughness to assess the impact of suspension features on the dynamic load coefficient (DLC) and the obtained results. The hydro-pneumatic suspension system is much superior to the other suspension systems. Tang et al. [9] showed that the amplitude and frequency of the

Instrumentation Mesure Métrologie
Vol. 21, No. 4, August, 2022, pp. 151-158
Journal homepage: http://iieta.org/journals/i2m

Study of Performance of Incorporating Pneumatic Suspension System with the Hydraulic Actuator for Quarter Car and Using Controllers with Genetic Algorithm

Mahmood S. Mahmood[1,2*], Ameen A. Nassar[1], Haider M. Mohammad[3]

[1] Mechanical Engineering Department, Engineering College, University of Basrah, Basrah 61004, Iraq
[2] Electrical Engineering Department, Engineering College, University of Misan, Misan 62001, Iraq
[3] Materials Engineering Department, Engineering College, University of Basrah, Basrah 61004, Iraq

Corresponding Author Email: mahmoodshacker2020@gmail.com

https://doi.org/10.18280/i2m.210405

Received: 12 June 2022
Accepted: 13 August 2022

Keywords:
suspension system, hydraulic actuator, GA, FLC, FOPID

ABSTRACT

Suspension systems are one of the main parts of the vehicle that provide the passenger comfort and stability, while it is difficult for conventional passive suspension systems to cope with the vibrations to which the vehicle is exposed. Air suspension systems have a dynamic character that allows good handling of the road and a comfortable ride, but in a certain area for this reason the stiffness of the air suspension must be flexibly changed. The air suspension has been developed with the inclusion of a hydraulic actuator to create an additional force that withstands the incoming vibration from the road. The pneumatic suspension system parameters, such as vertical acceleration, road holding, and vertical displacement, are improved continuously based on the controllers that have been used for nonlinear pneumatic suspension systems, fractional order proportional integral derivative (FOPID), and fuzzy logic control (FLC). The genetic algorithm is utilized to tune the controller's parameters to the nonlinear active pneumatic system's 3-DOF. A model's simulation outcomes with controllers improved the suspension performance. The proposed active pneumatic system and pneumatic suspension systems are compared when a vehicle is traveling at a speed of 72 km/h on an ISO level B road to test the ability and efficiency of the system to suppress body vibration to enhance safety and provide a comfortable ride on rough roads. According to simulation results, the improved suspension substantially lowers vertical vibrations and enhances road adaptability.

1. INTRODUCTION

The damper, spring, and lever arm make up the standard suspension system. The spring and damper stiffness are both fixed in the traditional passive suspension system. As a result, the car's comfort and stability may suffer significantly. A quarter-car pneumatic suspension is a relatively shock system, but when the wheel is exposed to larger shocks, here comes the role of integrating the hydraulic actuator into the system as a better shock absorber. Active suspension systems are required in modern cars for a comfortable ride and the ability to hold on to the road. The suspension system's stiffness must be adjustable in real-time and the traditional pneumatic suspension system does not meet comfort and road holding requirements. For this reason, a nonlinear actuator is connected between the quarter-car model's sprung mass and unsprung mass and feeds energy into the system. The suspension of a car needs to be able to reduce vertical movement and acceleration of the body to make passengers more comfortable and to keep tire loads as low as possible for the best road handling.

The key to solving this problem is to change the spring, the damper, or both. These may help partially suppress vertical vibration without keeping the vehicle stable on the road. Alonso et al. [1] studied the effect of different parameters (variables in the tube that connects the air spring with the auxiliary tank, volume of the air chamber, volume of the auxiliary chamber) on the stiffness of the air spring to improve the comfort through the experimental results (design of the test machine to characterize the air suspension systems of railway vehicles) within the frequency range of the dynamics of the railway vehicle, which were compared and analyzed with the theoretical results. Yin et al. [2] proposed a pneumatic spring consisting of a double-acting pneumatic cylinder and two accumulators, and proved the theoretical model proposed and the experimental findings to be in great agreement.

By varying the air pressure in the two air chambers, Karimi Eskandary et al. [3] created a pneumatic suspension system model. In addition, by employing the optimized parameters, Abid et al. [4] were able to discover the corresponding air spring suspension model with the passive suspension system using the optimization technique offered using OptiY by SIMULINK simulation. A novel dynamic model is recommended by Gavriloski et al. [5] to look at how the air spring parameters affect the performance of the suspension system in passenger cars. In addition, Moheyeldein et al. [6] examined the efficacy of the GENSYS model in their investigation. In order to describe the nonlinear elastic properties at a substantial deformation, Zhu et al. [7] devised a nonlinear dynamic model of a pneumatic spring with a damper. In same regards, Nieto et al. [8] studied the three different kinds of active suspension actuators are pneumatic actuators. Nassar and Al-Ghanim [9] have used different control strategies in linear simulation models that compare

Appendix

Appendix-A

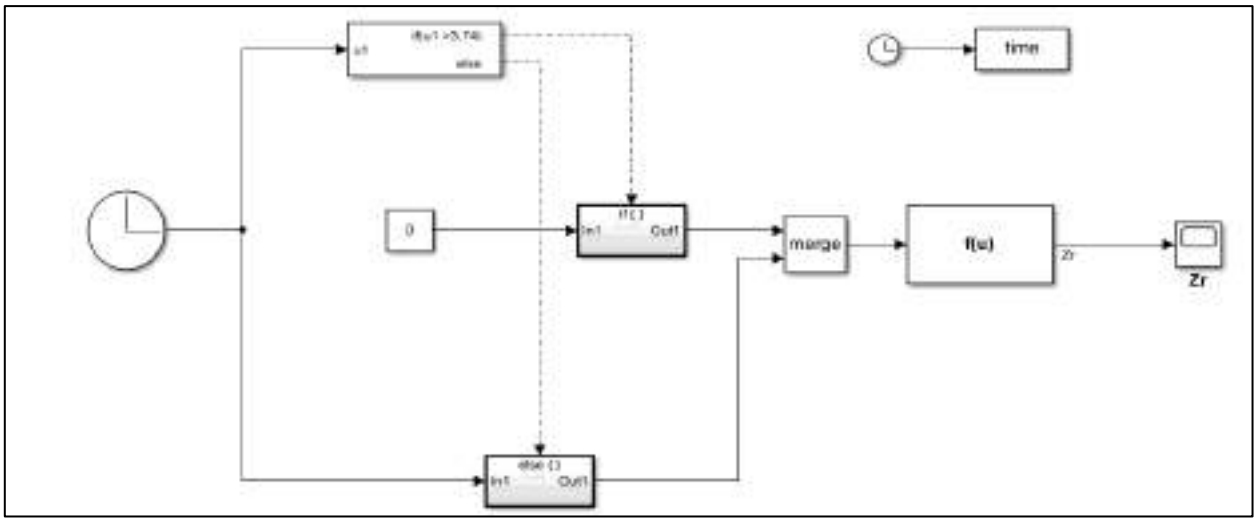

Figure (1.7A) Simple sine bump

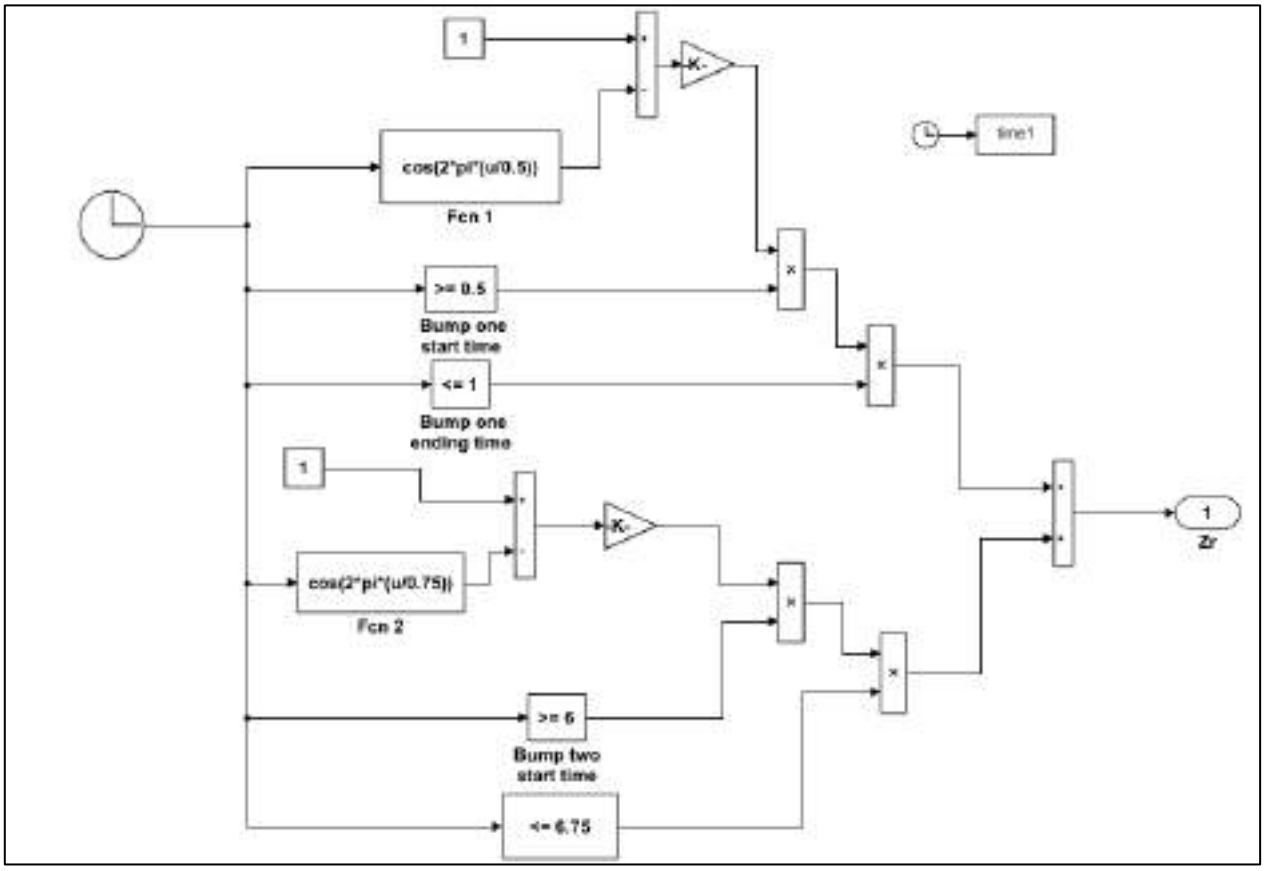

Figure (1-8A) Road profile with two bumps.

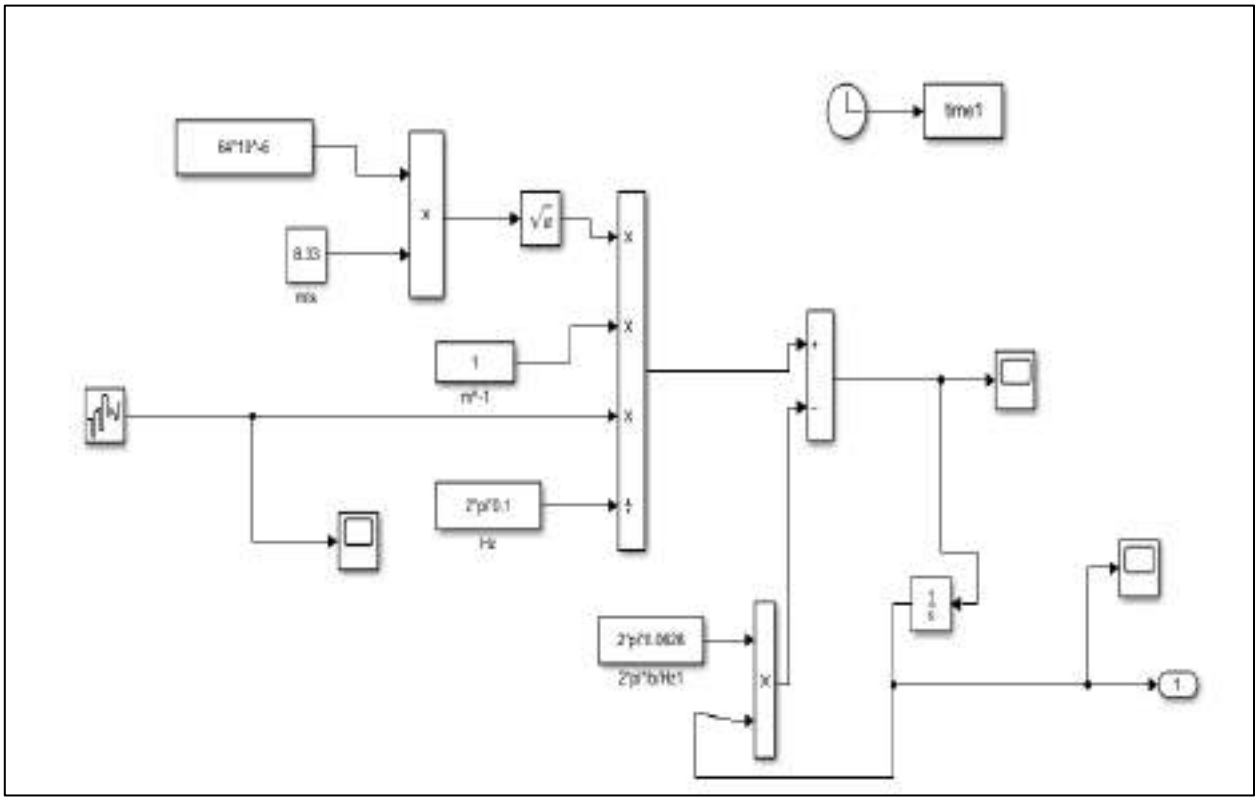

Figure (1-9A) Road input for roughness road ISO class B.

Experimental Study and Simulation of the Behavior of the Unsprung Mass of the Suspension System

Vibration Analyzer was used in this work to analyze the suspension system's vibrations. to record the component's acceleration, velocity, and displacement information. Accelerometer to measure the vibration on bumps at different speed conditions. This part, Data acquisition which designed by College of Engineering – University of Basrah, and accelerometer which used in this study are shown in Figures(A-1,A-2), which was conducted on a defined track as input university of Basrah road.

Figure(A-1) Data Acquisition.

Figure(A-2) Accelerometer.

Set-Up for an Experiment

The accelerometer is mounted on the suspension system (unspung mass) as shown in figure (A-3) to analyze the vibration caused by bumps under various speed conditions. The Data Acquisition Set up is placed in car and the accelerometer is mounted on suspension system and fixed it with tape. The accelerometer measure the vertical vibration to analyze the vibration caused by bumps under various speed conditions.

Figure(A-3) Placed the accelerometer on unsprung.

After linking the Data Acquisition with the accelerometer and the computer, analyzing the information and converting it by the Matlab/Simulink program into figures for acceleration and displacement for the purpose of analyzing the vibration behavior of the suspension system.

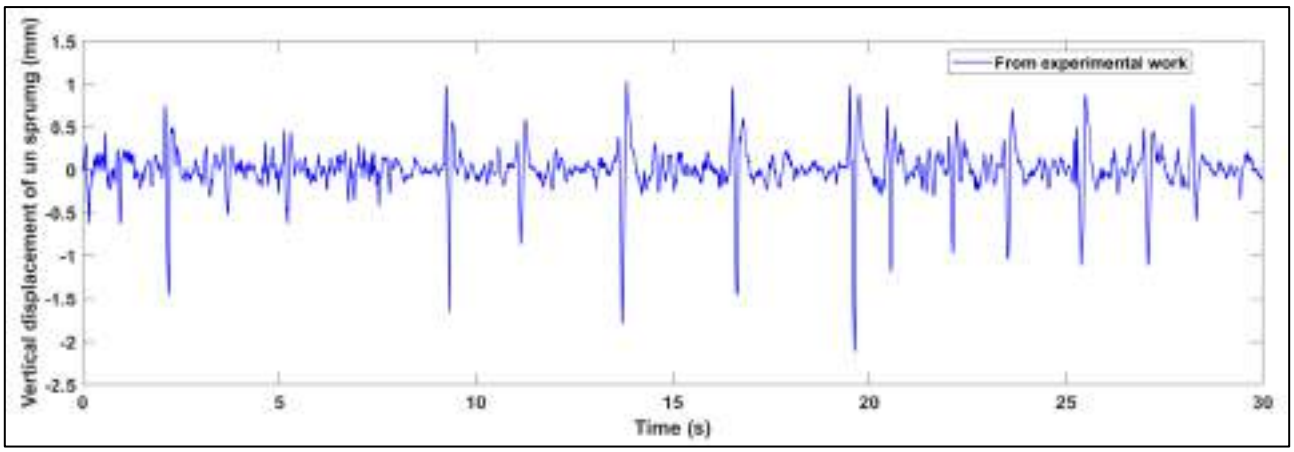

Figure (A-4) Vertical displacement of unsprung mass for velocity of car (10 km/h).

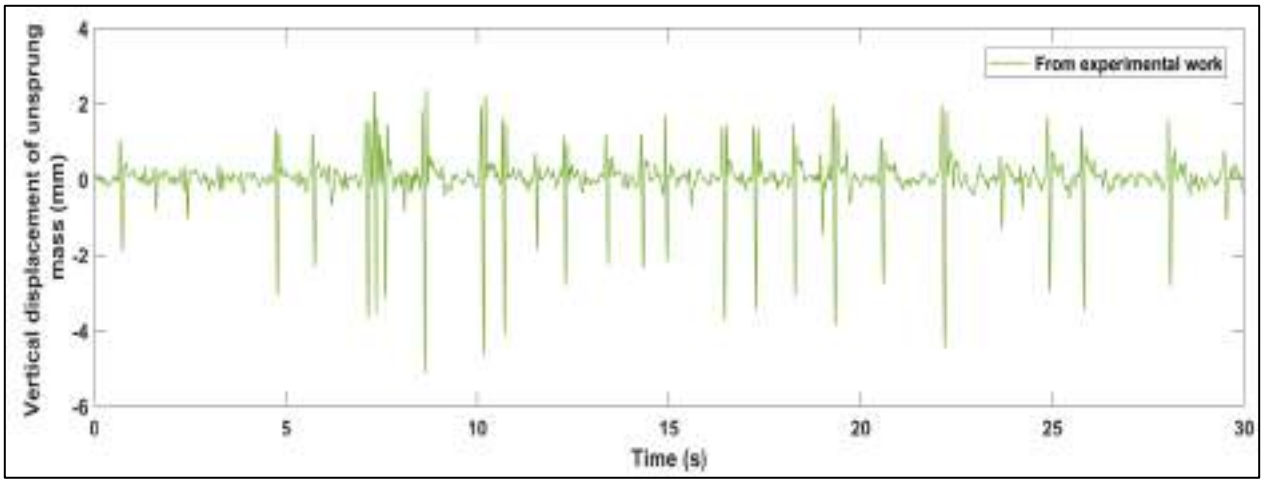

Figure (A-5) Vertical displacement of unsprung mass for velocity of car (20 km/h).

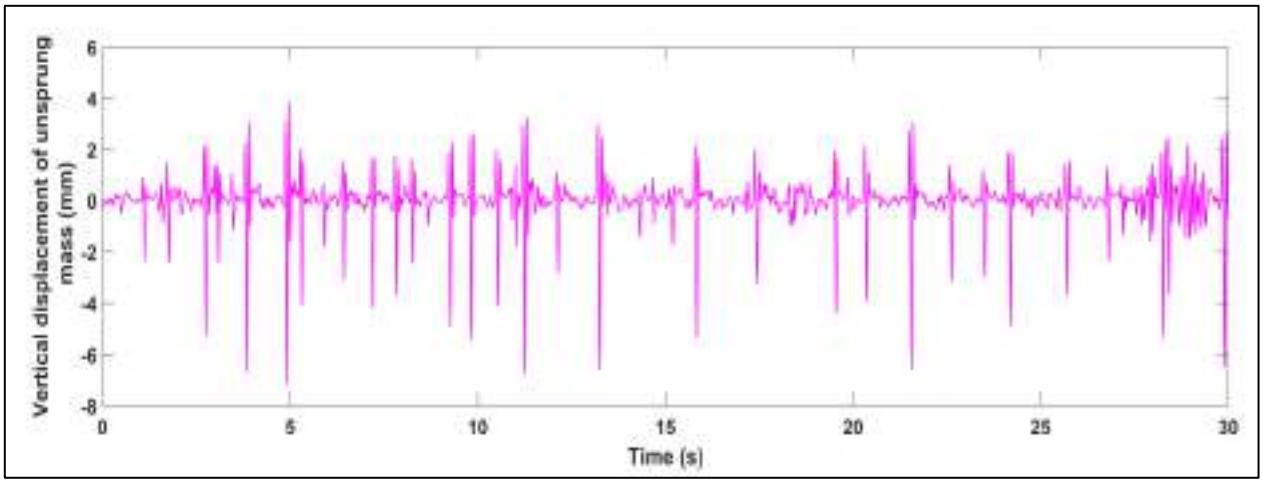

Figure (A-6) Vertical displacement of unsprung mass for velocity of car (30 km/h).

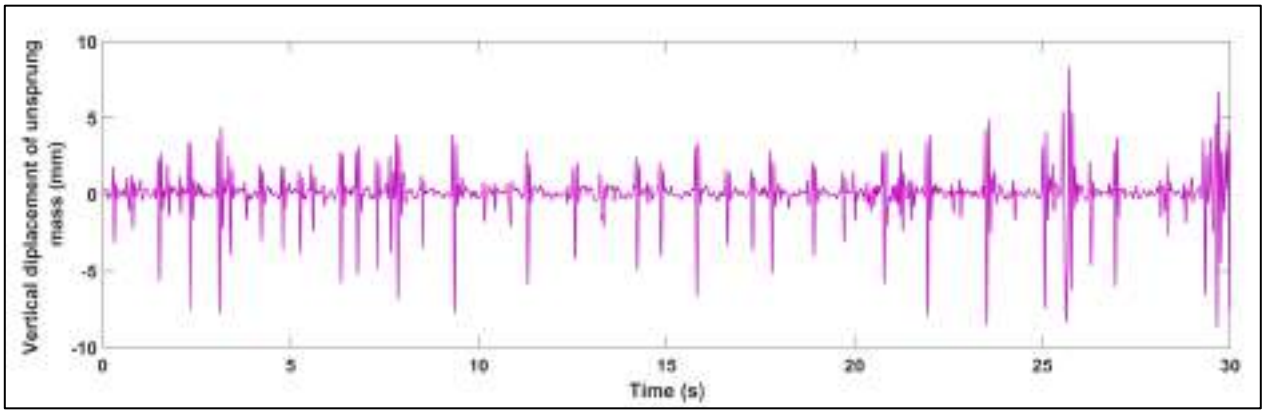

Figure (A-7) Vertical displacement of unsprung mass for velocity of car (40 km/h).

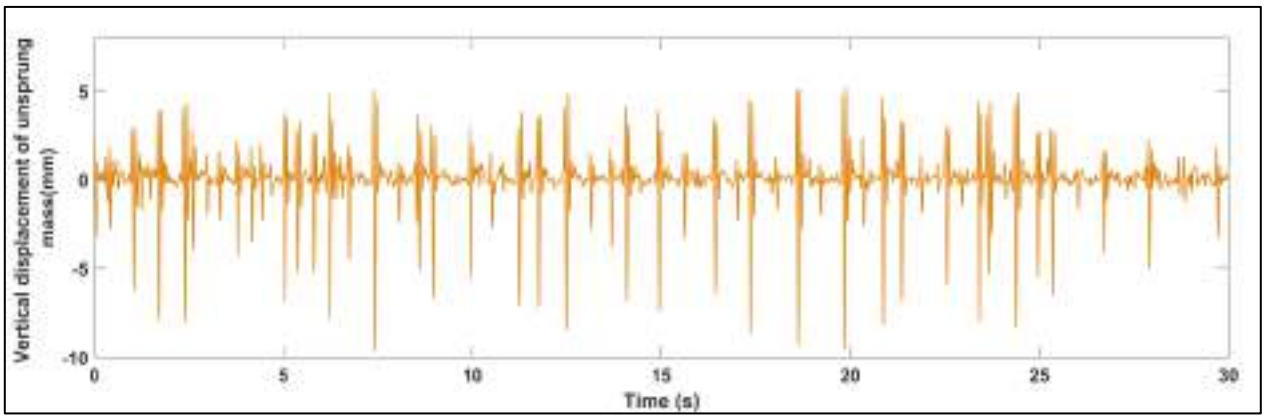

Figure (A-8) Vertical displacement of unsprung mass for velocity of car (50 km/h).

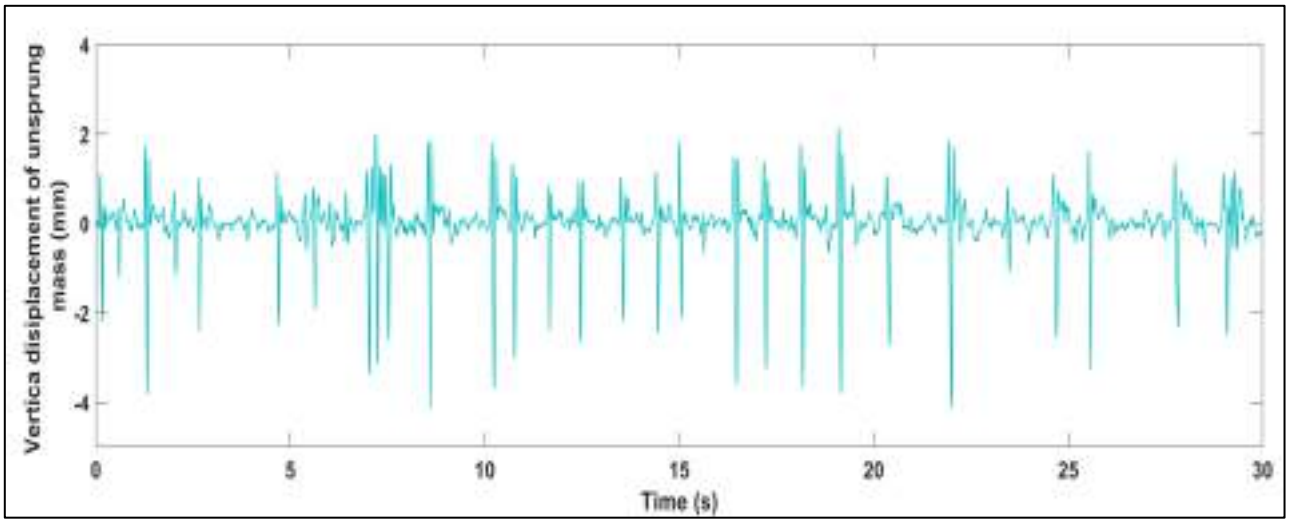

Figure (A-9) Vertical displacement of unsprung mass for velocity of car (60 km/h).

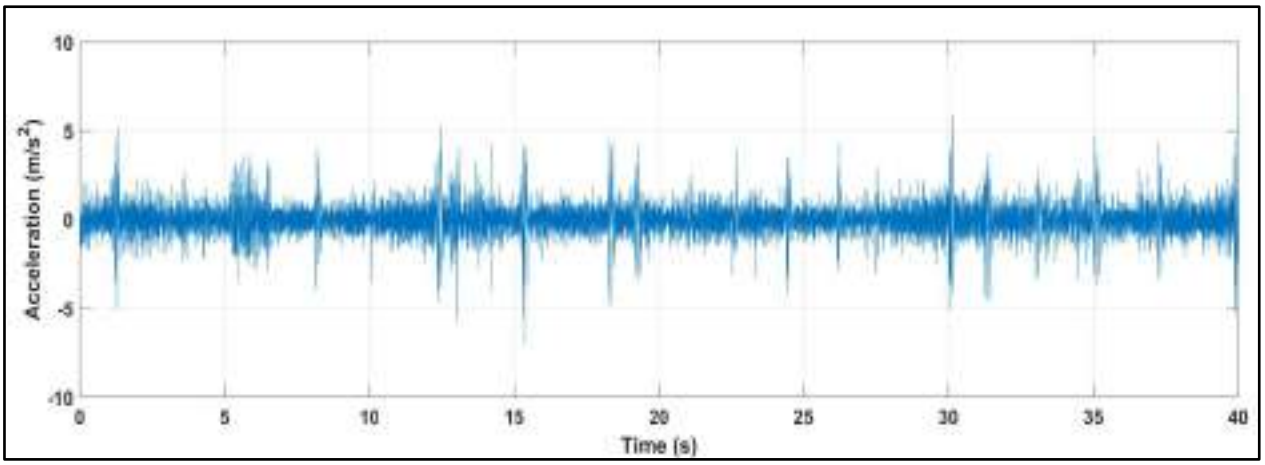

Figure (A-10) Vertical acceleration of unsprung mass for velocity of car (10 km/h).

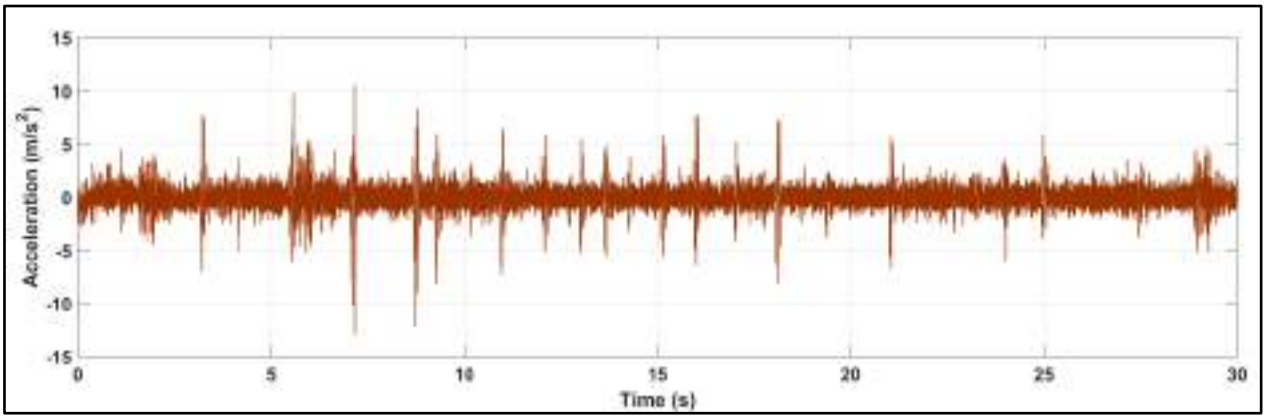

Figure (A-11) Vertical acceleration of unsprung mass for velocity of car (20 km/h).

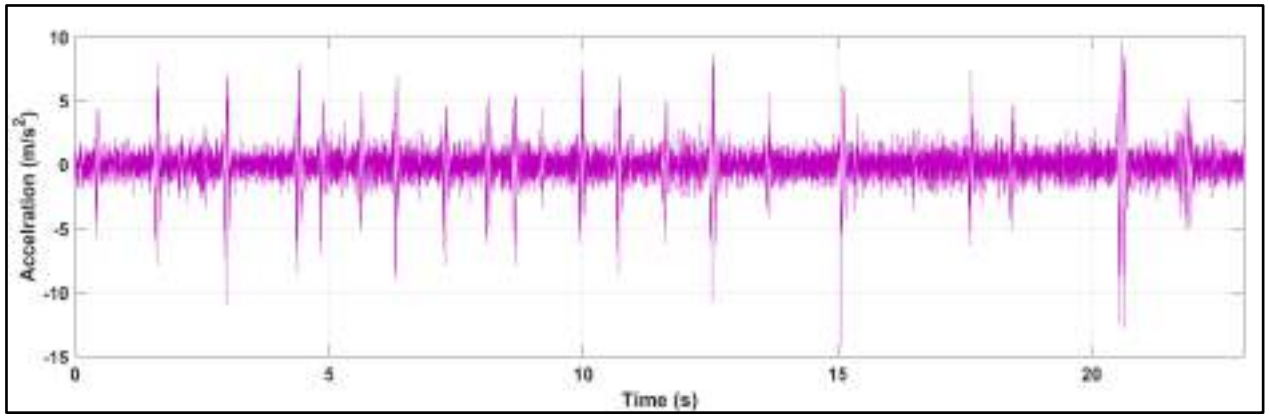

Figure (A-12) Vertical acceleration of unsprung mass for velocity of car (30 km/h).

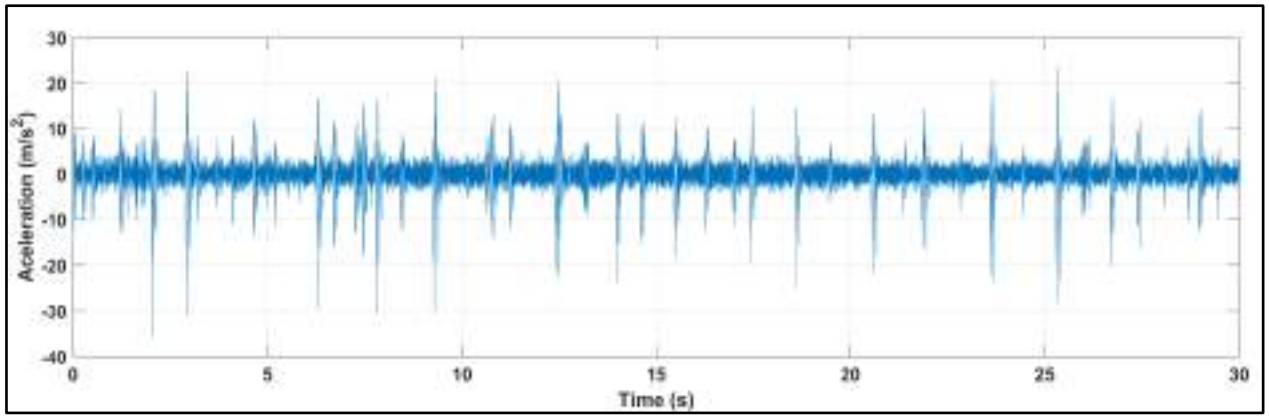

Figure (A-13) Vertical acceleration of unsprung mass for velocity of car (40 km/h).

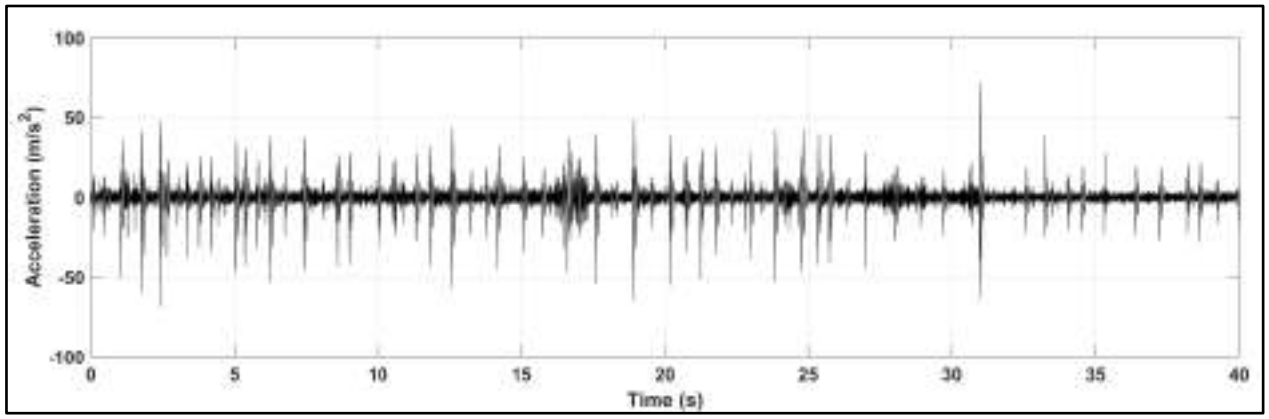

Figure (A-14) Vertical acceleration of unsprung mass for velocity of car (50 km/h).

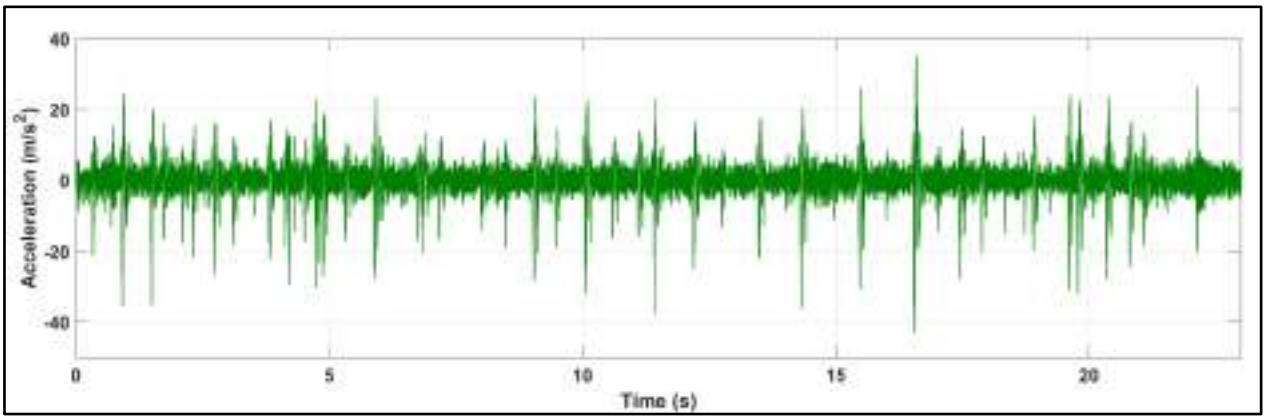

Figure (A-15) Vertical acceleration of unsprung mass for velocity of car (60 km/h).

Appendix-B

Calculation of the Damping in GENSYS Model[14].

```
close all, clear all, clc
%effecgive area
Ae=;
% Diameter of surge pipe
ds=;
% Surge pipe length
ls=
% Surge pipe area
As=(pi*ds^2)/4;
% REservoir volume
Vres=;
% Air bag volume
Vbag=;
%SCale factor
kwz=((Ae/As)*Vres/(Vres+Vbag));
% Ordinary rms acceleratons for an air spring
arms=[0.2:0.05:0.4]
% Frequencies
f=[0.5:0.5:20]
%Calculation of rms velocity and rms deflection
for j=1:length(f)
fj=f(j);
for i=1:length(arms)
vrms(i,j)=arms(i)/(2*pi*fj);
zrms(i,j)=arms(i)/(2*pi*fj)^2;
end
end
zsrms=(Ae/As)*zrms; %RMS displacement of the air in surge pipe
wsrms=zsrms/kwz; %RMS displacement over the model damper
wsmax=sqrt(2)*wsrms; %Calculation of maximal displacement over damper
vsrms=(Ae/As)*vrms; %Calculation of rms velocity in surge pipe
wsdotrms=vsrms/kwz; %Calculation of rms velocity over damper
p= ; %Calculation of pressure
ro=p/(287*288); %Calculation of density
Re=ro*ds*vsrms/1.789e-5; %Calculation of REynolds number for flow
%in surege pipe. 1.789e-5 kg/ms is the value of
%dynamic viscosity for viscosity for air.
k1=0.025; %Roughness for a new steel pipe
k2=0.00004; % Roughness for a smoothe pipe
e=Re.^0.9;
for l=1:max(size(e))
for m=1:min(size(e))
e2(m,l)=(5.74/e(m,l));
e3(m,l)=(log10(k1/(3.7*40)+e2(m,l)))^2;
e31(m,l)=(log10(k2/(3.7*40)+e2(m,l)))^2;
e4(m,l)=0.25/e3(m,l);
e41(m,l)=0.25/e31(m,l);
end
end
% Friction coefficent
```

```
fr=e4;
%Caculation of average friction coefficient
medelfr=sum(sum(fr))/(max(size(fr))*min(size(fr)));
% Correction factors for bend losses

frsmooth=e41;
medelfrsmooth=sum(sum(frsmooth))/(max(size(frsmooth))*min(size(frsmooth)));
Cf=medelfr/medelfrsmooth;% Cf=frough/fsmooth
Co=1; % from Appendix D
CRe=1.1;% from Appendix D
Kbstar=0.24;% from Appendix D
%Loss coefficients
Kb=Kbstar*CRe*Cf*Co;
Kfr=medelfr*ls/ds;% Kfr=(ls*f)/ds
Kc=0.5;% from Appendix D
Ken=1;% from Appendix D
%Total loss coefficient
Ktot=Kb+Kfr+Kc+Ken;
```

The Fluid Diagrams

The contraction coefficient can be found from Figure B- 1 below:

Contraction

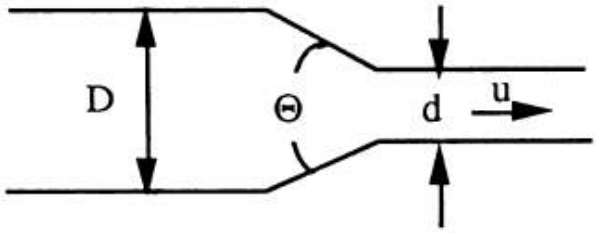

d/D	ζ(θ=60°)	ζ(θ=180°)
0.0	0.08	0.50
0.20	0.08	0.49
0.40	0.07	0.42
0.60	0.06	0.32
0.80	0.05	0.18
0.90	0.04	0.10

Expansion

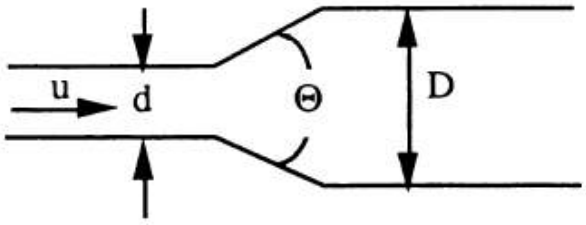

d/D	ζ(θ=10°)	ζ(θ=180°)
0.0		1.00
0.20	0.13	0.92
0.40	0.11	0.72
0.60	0.06	0.42
0.80	0.03	0.16

Figure B- 1 Values of the loss coefficients due to enlargement and contraction [14].

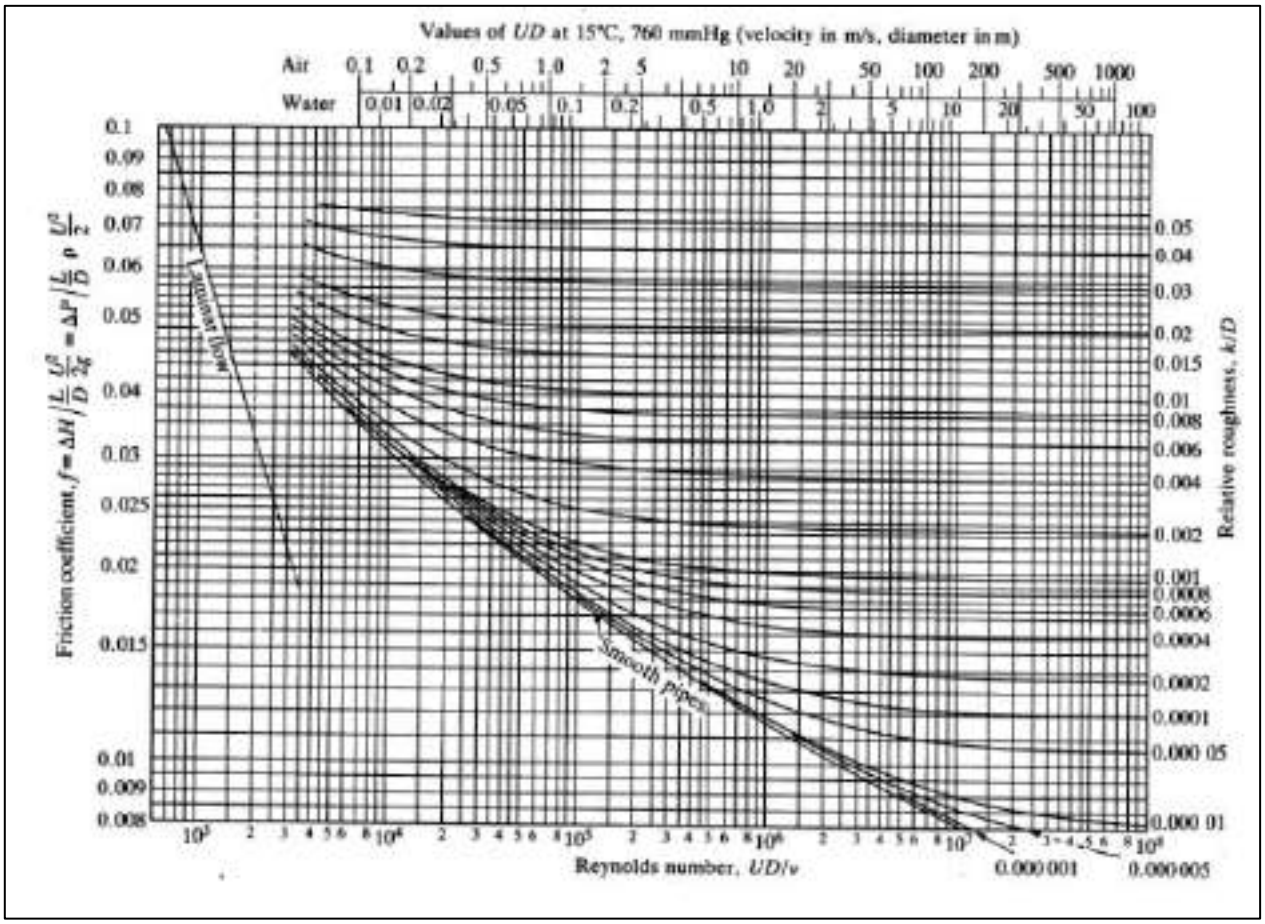

Figure B- 2 Moody diagram U is the mean velocity, D is the diameter, ν is the kinematic viscosity and k is the roughness value [15].

الخلاصة

اهتزازات المركبة وتذبذباتها غير ملائمة للغاية لأنها تزعج الركاب وتزيد من خطر انهيار المركبة. تتأثر سلامة وراحة الركاب واستقرار المركبة من خلال اهتزازها ، الهدف الرئيسي لتصميم الية التحكم في منظومة التعليق للمركبة هو تقليل الانزعاج الذي يشعر به الركاب بسبب الطرق الوعرة. العديد من الدراسات استخدمت جزء من المركبة(ربع مركبة) لدراسة وتحديد اهتزازات المركبات. تدرس هذه الأطروحة خصائص وفعالية نوع جديد من التعليق النشط للمركبة (دمج تعليق هوائي مع مشغل هيدروليكي لإنشاء قوة إضافية تقاوم الاهتزازات القادمة من الطريق) من خلال الية النمذجة والمحاكاة وتصميم وحدة التحكم .

في هذه الدراسة ، تم إنشاء نموذج رياضي لنظام التعليق الهوائي غير الخطي لربع مركبة ودمجه مع المشغل الهيدروليكي وتصميم وحدة التحكم والحصول على متغيرات نظام التعليق الهوائي ، تقيل التسارع العمودي ، وثبات الطريق ، وتقليل الإزاحة الرأسية بشكل مستمر بناءًا على وحدات التحكم التي تم استخدامها لأنظمة التعليق الهوائي غير الخطي.

ستة أنواع مختلفة من التحكم تم تصميمها ، ولاختيار أفضل الية تحكم فيما بينها اجريت المقارنات فيما بينها مقابل أنواع الطرق المختلفة. تم استخدام الخوارزمية الجينية لضبط معلمات وحدة التحكم لنظام التعليق الهوائي الغير الخطي النشط ذي(DOF). محاكاة وحدات التحكم المقترحة تمت باستخدام برنامج MATLAB/SIMULINK ، واظهرت استجابات المتغيرات للنماذج الخاضعة للتحكم مقابل الاضطرابات المختلفة ضمن النطاق الزمني.

استخدمت وحدات التحكم للسيطرة على قوة المشغل الهيدروليكي المدمج مع منظومة التعليق. بينت النتائج أن Fuzzy Logic Active Force Controller يتفوق على أنواع وحدات التحكم الأخرى من حيث الكفاءة والمتانة لتوفير الراحة و الاستقرار على الطريق من خلال تقليل كل من الإزاحة الرأسية لكتلة النابض والتسارع العمودي لكتلة النابض ، وثبات الطريق ، ومعامل الحمل الديناميكي على التوالي بنسبة 88.5٪ ، و 95٪ ، و 33.2٪ ، و 33.6٪ مقارنةً بوحدات التحكم الأخرى لفئة الطريق الوعر B. كما تمت مقارنة نماذج التعليق غير الخطي للمركبة الربعية ومحاكاتها دون تسليط الية تحكم (الزنبرك الهوائي التقليدي ونوع Gensys) من حيث تسريع الكتلة المعلقة ،عامل الحمل الديناميكي والإزاحة الرأسية من خلال (RMS). النتائج التي تم الحصول عليها من خلال مقارنتها تشير إلى أن نوع Gensys أكثر كفاءة من النوع التقليدي.

دراسة لمنظومة تعليق فعال لربع سيارة قابلة للتكيف مع ظروف الطريق

أطروحة مقدمة إلى

كلية الهندسة في- جامعة البصرة

كجزء من متطلبات نيل شهادة الدكتوراه

في الهندسة الميكانيكية

تقدم بها

محمود شاكر محمود

ماجستير علوم في الهندسة الميكانيكية

كانون الثاني / 2023